INL/EXT-13-30427

Status Report on Efforts to Enhance Instrumentation to Support Advanced Test Reactor Irradiations

J. Rempe
D. Knudson
J. Daw
T. Unruh
B. Chase
K. Davis
R. Schley
J. Palmer
C. White
K. Condie

January 2014

The INL is a U.S. Department of Energy National Laboratory
operated by Battelle Energy Alliance

Idaho National Laboratory

INL/EXT-13-30427

Status Report on Efforts to Enhance Instrumentation to Support Advanced Test Reactor Irradiations

J. Rempe
D. Knudson
J. Daw
T. Unruh
B. Chase
K. Davis
R. Schley
J. Palmer
C. White
K. Condie

January 2014

Idaho National Laboratory
Idaho Falls, Idaho 83415

http://www.inl.gov

Prepared for the
U.S. Department of Energy
Office of Nuclear Energy
and Through the INL LDRD Program
Under DOE Idaho Operations Office
Contract DE-AC07-05ID14517

ABSTRACT

The Department of Energy (DOE) designated the Advanced Test Reactor (ATR) a National Scientific User Facility (NSUF) in April 2007 to support the growth of nuclear science and technology in the United States (US). By attracting new researchers, from the university, national laboratory, and industry sectors, the ATR NSUF facilitates basic and applied nuclear research and development required to meet and advance the nation's energy needs. A key component of the ATR NSUF effort at the Idaho National Laboratory (INL) is to design, develop, and deploy new in-pile instrumentation that is capable of providing real-time measurements of key parameters during irradiation. To address this need, an assessment of instrumentation available and under-development at other test reactors was completed. Based on this initial review, recommendations were made with respect to what instrumentation is needed at the ATR, and a strategy was developed for obtaining these sensors. In 2009, a report was issued documenting this program's strategy and initial progress toward accomplishing program objectives. Since 2009, annual reports have been issued to provide updates on the program status. This report provides an update reflecting progress as of January 2014.

As reported in this document, significant accomplishments occurred in several instrumentation development and deployment areas during 2013. Specialized INL-developed sensors for real-time detection of temperature and thermal conductivity were provided to the Commissariat à l'Énergie Atomique et aux Energies Alternatives (CEA) in France and are being provided to the Institute for Energy Technology/Halden Reactor Project (IFE/HRP) in Norway for evaluation. High Temperature Test Laboratory (HTTL) staff, who are responsible for most in-pile instrumentation development, fabrication, and evaluation efforts, are also involved in expanding user options for peak temperature sensors, such as melt wires and silicon carbide temperature monitors, and integral fluence sensors, such as activation foils and flux wires. On-going tasks to deploy real-time length and flux detection sensors are continuing. An enhanced test rig for evaluating creep specimens with controlled load capabilities is now ready for use in the newly reactivated ATR pressurized water loop and efforts are continuing to develop a crack growth test rig. In addition, several tasks evaluating 'advanced' technologies, such as fiber-optics based length detection and ultrasonic thermometers, have continued. In October 2013, a new effort for developing a real-time capability for measuring changes in fuel diameter during irradiation was initiated.

As noted within this document, INL has made extensive investments to support advanced in-pile instrumentation and test rigs. In 2009, INL completed construction of the Test Train Assembly Facility (TTAF), which is located near the ATR and in 2013, the HTTL was moved to the new Energy Innovation Laboratory (EIL) facility in Idaho Falls. Although INL has clearly invested significantly in this effort, it should be stressed that multiple funding sources (e.g., ATR NSUF, Fuel Cycle Research and Development, Nuclear Energy Enabling Technologies, and Next Generation Nuclear Plant) were required to achieve in-pile instrumentation accomplishments. Hence, having focussed and coordinated efforts to provide US Materials Testing Reactors (MTRs) advanced in-pile instrumentation and standardized test rigs incorporating such instrumentation is essential if the US is to reap the benefits of this DOE investment. It is important to emphasize that standardized test rigs, which are regularly used at facilities such as the Halden Boiling Water Reactor (HBWR) in Norway and are under development for the Jules Horowitz Reactor (JHR) in France, are essential components of world class irradiation facilities. With standardized test rigs with advanced instrumentation, US MTRs will be able to more readily meet US industry and regulator needs for sustainment of nuclear energy.

CONTENTS

FIGURES

TABLES

EXECUTIVE SUMMARY

The Department of Energy (DOE) designated the Advanced Test Reactor (ATR) at the Idaho National Laboratory (INL) as a National Scientific User Facility (NSUF) in April 2007 to support the growth of nuclear science and technology in the United States (US). By attracting new researchers, from the university, national laboratory, and industry sectors, the ATR NSUF facilitates basic and applied nuclear research and development required to meet and advance the nation's energy needs. A key component of the ATR NSUF effort is the design, development, and deployment of new in-pile instrumentation to support irradiation testing. In addition to ATR NSUF needs, it is recognized that new in-pile instrumentation enhances the ability of NSUF facilities to attract new customers from the commercial power, defense, and manufacturing sectors. In 2008, a strategy was developed for obtaining these sensors. In 2009, a report was issued documenting this program's strategy and initial progress toward accomplishing program objectives. Since 2009, annual reports have been issued to provide updates on the program status. This report provides an update reflecting progress as of January 2014.

Background

As noted in Section 2 of this report, the ATR and other US Materials Testing Reactors (MTRs) are unique with respect to irradiation testing capabilities. For example, the test volumes and flux levels in each of the ATR irradiation locations [Static Capsules, the Hydraulic Shuttle Irradiation System (HSIS), Instrumented Lead Tests, and Pressurized Water Reactor (PWR) loops] are unsurpassed by few, if any, test reactors in the world. However, US instrumentation for in-pile testing lags behind instrumentation available at international MTRs. Despite its long history for developing highly specialized instrumentation to meet demands of customers conducting unique tests in one-of-a-kind test facilities, INL instrumentation research funding decreased significantly in the 1980s when large nuclear test facility programs ended.

To address this instrumentation need, the ATR NSUF initiated an effort that allowed INL to restart programs associated with the design and development of world class instrumentation. As part of this effort, a review was first completed to identify instrumentation available to users at other MTRs located in the US and abroad. Table ES-1 summarizes updated results from this review. The column labeled "Technology Available at ATR" indicates the types of sensors currently available to ATR users. The column "Proposed Advanced Technology" includes two categories: "Available at Other Reactors," which identifies several technologies employed at other test reactors that could be adapted to enhance ATR instrumentation capabilities; and "Developmental," which lists developmental or non-nuclear technologies that could be used in ATR irradiation tests. Technologies listed in this column are considered to be less "ready" for implementation. As noted in the footnotes for Table ES-1, blue text indicates current instrumentation research efforts, red text indicates demonstrated new or enhanced sensors now available to users as a result of recent instrumentation research, and magenta text indicates new sensors and capabilities that are now ready for deployment as a result of recent instrumentation research.

Instrumentation selected for investigation is based on anticipated user needs and "technology readiness" (to provide ATR NSUF users needed instrumentation as soon as possible). For example, other MTRs have sensors available for real-time detection of parameters such as neutron flux (thermal and fast) and geometry changes (length and diameter). As indicated by the blue text in Table ES-1, efforts are underway to explore these technologies. However, as discussed in Section 2, adapting instrumentation used at other test reactors often requires demonstrations because of ATR-specific irradiation conditions (e.g., higher neutron fluxes, higher temperatures, etc.) and test capsule geometries. As indicated by the red and magenta text in Table ES-1, several enhanced sensors are now available to ATR users as a result of this instrumentation development effort. The ultimate goal of this effort is to provide ATR NSUF users sensors for detecting all of the parameters listed in Table ES-1.

Table ES-1. Instrumentation available at ATR and proposed advanced technologies.

Parameter	Location			Available Technology at ATR	Proposed Advanced Technology	
	Static Capsule/ Shuttle	Instr. Lead	PWR Loop		Available at Other MTRs	Developmental
Temperature	✔	✔	✔	-Melt wires (peak)[a,b] -Silicon Carbide (SiC) temperature monitors (range)	-Paint spots (peak) -Thermal Expansion Devices (TEDs)	
		✔	✔	-Thermocouples (Type N, K, C[c], and HTIR-TCs[d])	-Expansion thermometer	-Fiber optics -Noise thermometry -Ultrasonic thermometers (UTs)
Thermal Conductivity		✔	✔	- Transient Hot Wire Method Needle Probe (THWM NP)	-Degradation using signal changes in thermocouples	
Flux/Fluence (neutron)	✔	✔	✔	-Flux wires and foils		
		✔	✔		-Self-Powered Neutron Detectors (SPNDs) -Subminiature / miniature fission chambers	- Moveable SPNDs - Micro-Pocket Fission Detectors (MPFDs)
Gamma Heating / Gamma Flux		✔	✔		-Calorimeters -Gamma thermometers (GTs) -Self-Powered Gamma Detectors (SPGDs)	
Dimensional		✔	✔	-LVDT-based elongation	-Diameter gauge	-Ultrasonic techniques -Fiber optics
Fission Gas (Amount, Composition)		✔	✔	-On-line sampling -Pressure gauge	-LVDT-based pressure monitors	-Acoustic measurements with high-frequency echography
Loop Pressure			✔	-Differential pressure transmitters -Pressure gauges with impulse lines		
Loop Flowrate			✔	-Flow venturis -Orifice plates	-Turbine flow meters (for individual fuel assemblies)	
Loop Water Chemistry			✔	-Off-line sampling / analysis	-Electrical chemical potential probes	
Crud Deposition			✔		- Diameter gauge with neutron detectors, and thermocouples	
Crack Growth Rate			✔		-Direct current potential drop (DCPD) technique	

a. Text color in Columns 5 through 7 designates:
Black - Sensors or capabilities existing at the ATR or existing or under development at other MTRs
Blue - New or enhanced sensors being investigated or for which investigations were initiated but deferred due to funding limitations
Magenta - New or enhanced sensors or capabilities for which laboratory investigations have been completed but require irradiation evaluation
Red - New or enhanced sensors or test rigs now deployed at the ATR because of recent instrumentation research
b. Although melt wires have been used at ATR, recent efforts have expanded the types offered to our users, allowing more accurate estimates of peak temperature with enhanced encapsulation methods.
c. Type C thermocouple use requires a "correction factor" to correct for decalibration during irradiation.
d. High Temperature Irradiation Resistant ThermoCouple (HTIR-TC)

Section 3 of this document provides detailed information about instrumentation available and under development at international MTRs. Several foreign test reactor programs, such as the Institute for Energy Technology at the Halden Reactor Program (IFE/HRP) have maintained their instrumentation development and evaluation research capability. Others, such as the Commissariat à l'Énergie Atomique et aux Energies Alternatives (CEA), not only offers users a suite of instrumentation, but is rapidly trying to increase their capabilities by developing and deploying new standardized test rigs. These standardized test rigs, which are regularly used at facilities such as the Halden Boiling Water Reactor (HBWR) in Norway and are under development for the Jules Horowitz Reactor (JHR) in France, are essential components of world class irradiation facilities. In order for the ATR and other US MTRs are to be competitive, enhanced instrumentation and standardized test rigs must be made available to their users.

INL Program Overview

The ultimate goal of recent INL in-pile instrumentation development efforts is to provide the required sensors and test rigs to support ATR irradiation needs. There is a national need for US researchers to have domestic access to sensors and test rigs that are comparable to that available at other MTRs. As discussed within this document, higher flux MTRs require more robust sensors than needed at international MTRs. Figure ES-1 graphically illustrates current INL efforts for developing and demonstrating new sensors. This figure includes sensor development from various fund sources, including INL Laboratory Directed Research and Development (LDRD), ATR NSUF, Nuclear Energy Enabling Technology (NEET), Fuel Cycle Research and Development (FCRD), and Next Generation Nuclear Plant (NGNP). There are several major activities identified, "Near-Term Technologies," "Developmental," and "Expansion." Representative tasks identified in each area are also shown with qualitative judgments with respect to current ATR capabilities compared to other test reactors. If requested funding levels are provided, the ATR NSUF is expected to have comparable instrumentation for many parameters during FY14, and "world class" (e.g., comparable in many cases, and in some cases, superior) irradiation capabilities by FY15. Current efforts to meet this national need come from various sources, and the ability to meet this FY15 goal is dependent upon allocated funding levels and sensor irradiation schedules.

Table ES-2 summarizes the status of INL efforts to provide enhanced instrumentation to ATR. Similar to Table ES-1, blue text indicates current instrumentation research efforts, and red and magenta text indicates new sensors now available to users as a result of recent instrumentation research. As indicated in this table, considerable progress has been made in this program since its inception. Several new sensors are now available to users; and as indicated in Section 5, several additional sensors should soon be available. It is also encouraging to see that some level of research has been initiated on many of the sensor technologies identified in this table.

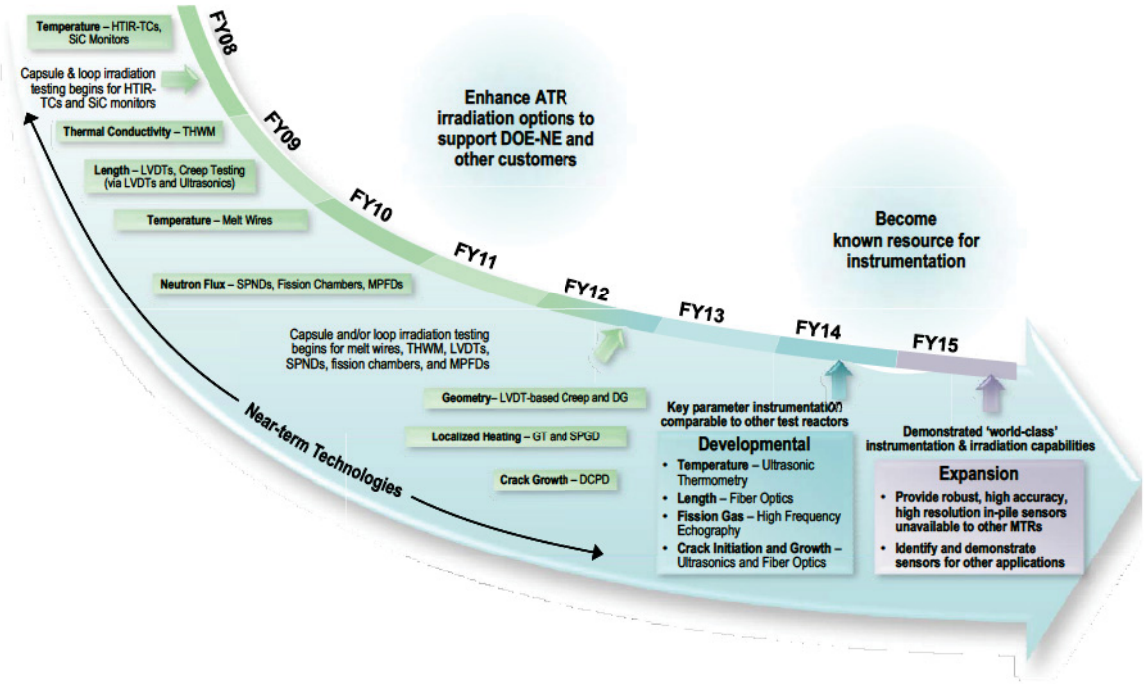

Figure ES-1. ATR instrumentation research and development (timing is dependent on funding availability).

Table ES-2. Status of ATR NSUF sensor development and enhancement efforts.

Parameter	Sensor	Status
Temperature	Melt Wires[a]	Currently used in several ATR NSUF irradiations. Both quartz and vanadium encapsulation available for wires with melting temperatures between 85 and 1455 °C.
	SiC Temperature Monitors	Currently used in several ATR NSUF irradiations.
	HTIR-TC	Initial out-of-pile testing completed. In-pile testing (in the first Advanced Gas Reactor (AGR-1) NGNP fuel irradiation test) and sensor enhancement evaluations completed; HTIR-TCs provided to MIT and IFE/HRP. Additional HTIR-TCs being fabricated for NGNP program in FY14.
	Ultrasonic Thermometers (UTs)	FCRD program funded first two years of a three year effort to develop and evaluate an enhanced prototype. Additional funding required to complete prototype evaluations and design optimization. Although prototype is focussed on use of magnetostrictive transducers, deployment will benefit from MITR test to compare irradiation-related survivability of piezoelectric and magnetostrictive transducers.
Thermal Conductivity	THWM NP	Prototype design developed and initial laboratory testing completed. Prototype THWM probe prepared and shipped to CEA and being prepared for shipment to IFE/HRP.

Table ES-2. Status of ATR NSUF sensor development and enhancement efforts.

Parameter	Sensor	Status
Elongation, Crud deposition, Corrosion	LVDTs	Out-of-pile testing completed on developmental LVDT that resists high temperature degradation and eliminates Curie temperature effects.
	Diameter gauge	Currently used in the Halden Boiling Water Reactor (HBWR) for detecting swelling, corrosion, and crud buildup. Three year LDRD initiated in FY14.
	Ultrasonic Techniques	Scoping tests completed on elongation prototype. Prior to deployment, additional prototype out-of-pile testing needed and results from NEET-funded MITR piezoelectric and magnetostrictive transducer irradiation test needed.
	Fiber Optic Techniques	FCRD funded first two years of a three year effort to develop and evaluate the accuracy of a candidate probe. Prior to deployment, an instrumented lead test needed to evaluate fiber optic survivability in radiation environments.
In-pile Creep Test Rig	LVDT-based rig with bellows	Design developed and prototype evaluated at PWR conditions in a laboratory autoclave. Enhanced design, with variable load capability, developed and evaluated in a laboratory autoclave. Both designs developed for future use in an ATR PWR loop.
Neutron Flux	Flux wires and foils	Various flux wires and foils available. Vanadium encapsulation available.
	SPNDs and fission chambers	Specially-developed fixturing designed, fabricated, and installed at ATRC. In FY13, additional evaluations of detectors completed. Additional ATRC evaluations planned for FY14. In addition, SPND will be included in NEET-funded MITR. Development of MPFDs for ATRC evaluations underway.
Gamma Heating	*Gamma thermometers and SPGDs*	Currently used at HBWR; SPGDs will be included in NEET-funded MITR irradiation in FY14.
Crack propagation	DCPD method with CT specimens	Currently used at HBWR; Investigations initiated in 2012.
	Ultrasonic techniques	Funding source needed for laboratory evaluations. Prior to deployment, results of piezoelectric and magnetostrictive transducer irradiation test at MITR needed.
	Fiber optics techniques	Funding source needed for laboratory evaluations. Prior to deployment, an instrumented lead test needed to evaluate fiber optic survivability in radiation environments.

a. Font in Column 2 designates:
Black - Sensors or capabilities existing at the ATR or existing or under development at other MTRs
Blue - New or enhanced sensors being investigated or if italics, for which investigations were initiated but deferred due to funding limitations
Magenta - New or enhanced sensors or capabilities for which laboratory investigations have been completed but require irradiation evaluation
Red - New or enhanced sensors or test rigs now deployed at the ATR because of recent instrumentation research

As discussed in Section 5, INL sensor development and evaluation activities rely heavily on collaborations with other research organizations, such as IFE/HRP and CEA, to maximize the benefit from research expenditures. For example, IFE/HRP and CEA will be evaluating the performance of INL-developed sensors during FY14. In addition, sensor development and deployment has been expedited by beneficial collaborations with selected universities possessing specialized capabilities, such as the Massachusetts Institute of Technology (MIT), Idaho State University (ISU), Utah State University (USU), Kansas State University (KSU), and Pennsylvania State University (PSU).

It should be noted that funding availability has delayed certain instrumentation deployment activities. For example, the FCRD program has been interested in (and funded development of) ultrasound-based and fiber optic-based instrumentation that can provide higher resolution/higher accuracy data than currently-available instrumentation. Unfortunately, decreases in FCRD funding for in-pile instrumentation has delayed deployment of such sensors. Blue italics text indicates instrumentation efforts in which activities have been delayed in FY14 due to such funding limitations.

Extensive investments to provide the facilities and equipment required for advanced in-pile instrumentation and test rigs development and deployment have been made by INL. In 2009, INL completed construction of the Test Train Assembly Facility (TTAF), which is located near the ATR. The TTAF is used for final assembly of experiments to be installed at the ATR. The TTAF was designed and furnished with

the equipment necessary to support the assembly of various configurations and design of test train experiments. The TTAF has various welding capabilities, including automated lathe and orbital gas tungsten arc welding, micro spot welding, and manual welding, that can be used to assemble various test train experiments. The TTAF also has the ability to perform induction brazes, an integral process in the assembly of test train experiments. Machining capabilities, such as a mill and a lathe, are also available at the TTAF. Experienced TTAF staff are available to support engineering and fabricate the experiment assemblies.

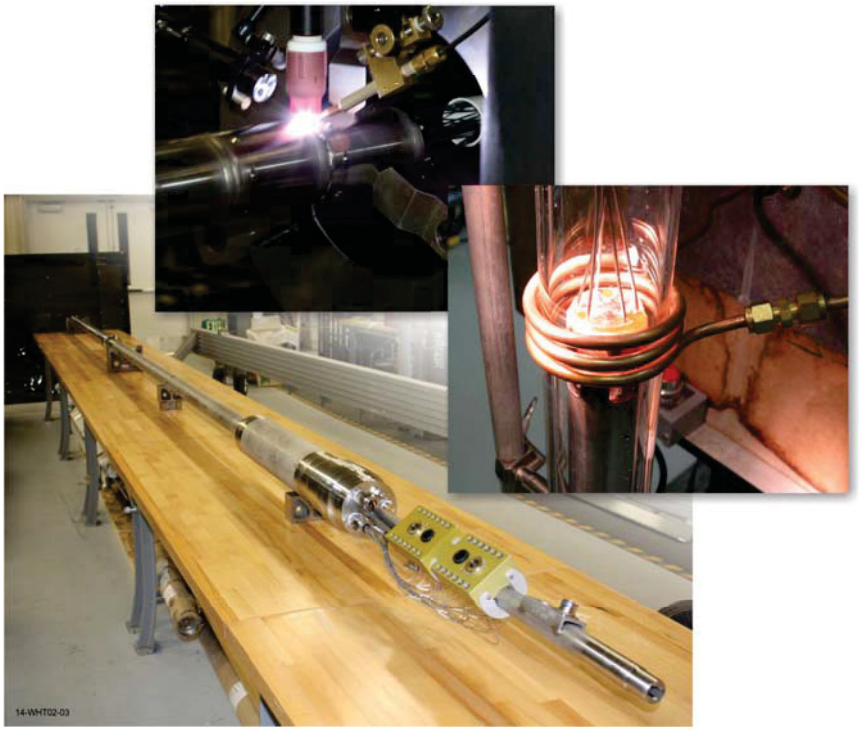

Figure ES-2. An irradiation experiment assembled using TTAF welding and brazing methods.

INL's existing High Temperature Test Laboratory (HTTL) is a unique facility for developing, fabricating, and performing laboratory demonstrations of proposed new in-core instrumentation. This facility features specialized sensor fabrication and evaluation equipment and trained staff with an established reputation for fabricating unique sensors. In December 2013, capabilities of the HTTL were relocated to INL's Research and Education Laboratory (REL), a newly constructed facility in Idaho Falls. As shown in Figure ES-3, the recently-relocated HTTL houses specialized sensor fabrication and evaluation equipment, including a laser welder, a real-time x-ray imaging system, a custom draw bench, several autoclaves, several tube furnaces (capable of temperatures up to 1800 °C), and a vacuum furnace (capable of temperatures up to approximately 2800 °C). In addition, a special area of the new facility houses systems for measuring thermal properties of materials such as a laser flash thermal property analyzer for thermal diffusivity measurements (and comparative specific heat and thermal conductivity measurements) up to 2800 °C, a push-rod dilatometer for comparison thermal elongation measurements up to 1600 °C, and a Differential Scanning Calorimeter (DSC) for obtaining specific heat capacity and melting temperature measurements up to 1600 °C. The new facility includes a specially-designed sensor fabrication room with locations for additional specialized equipment, such as an e-beam welder and a three dimensional computer tomography machine. Hence, the HTTL is anticipated to have an increased role in ensuring that required instrumentation is available to users of NSUF facilities and to address other DOE-NE program needs.

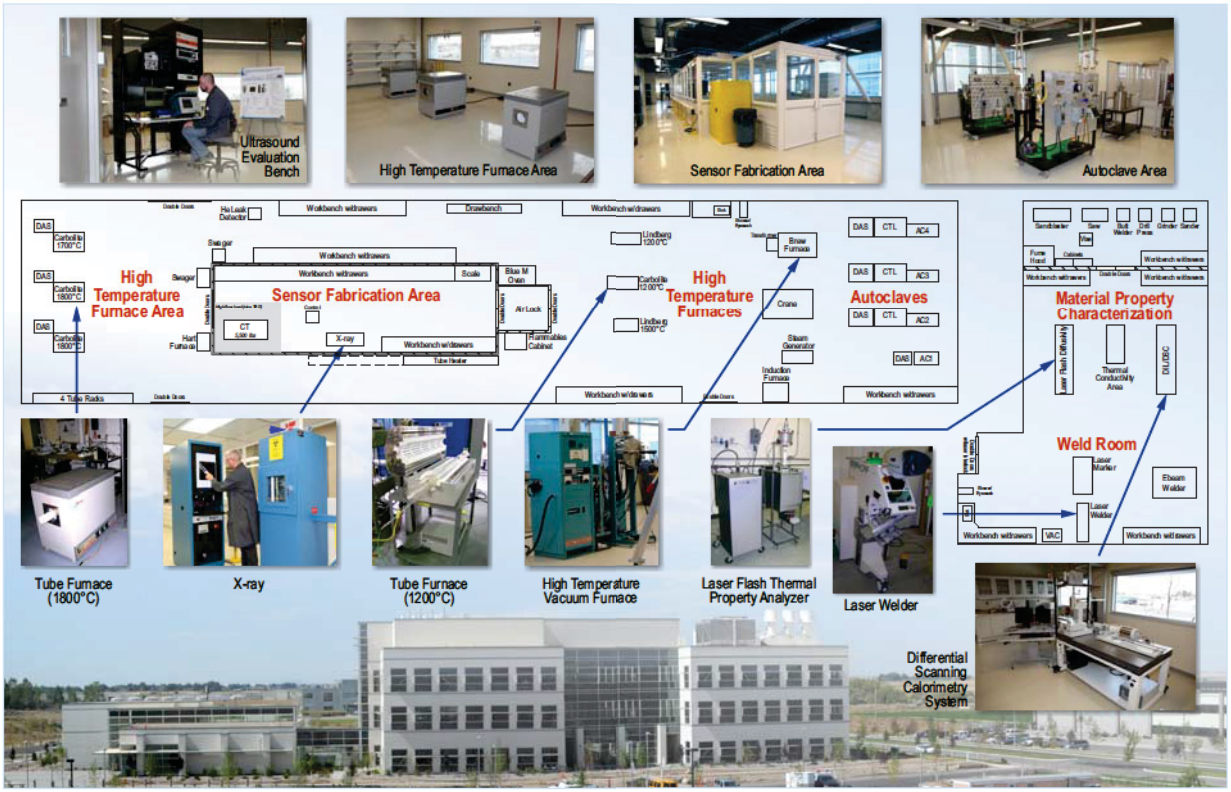

Figure ES-3. HTTL layout and equipment.

Although INL has clearly invested significantly in this effort, it should be stressed that multiple funding sources (e.g., ATR NSUF, FCRD, NEET, and NGNP) were required to achieve these accomplishments. Hence, having focussed and coordinated efforts to provide US MTRs advanced in-pile instrumentation and standardized test rigs incorporating such instrumentation are essential if the US is to reap the benefits of this DOE investment.

In-Pile Inpile Instrumentation Accomplishments

Significant HTTL accomplishments occurred in several instrumentation development and deployment areas during 2013. For example, HTTL staff:

- Continued expansion of a melt wire library while providing ATR NSUF users appropriate melt wires for their tests. INL has an established melt wire library with materials ranging from ~85 to 1455 °C that may be encapsulated in quartz or metal tubes (see Figure ES-4).
- Continued SiC temperature monitor support for ATR NSUF and FCRD users;
- Identified an appropriate IFE/HRP HBWR irradiation for ATR NSUF evaluation of four HTIR-TCs and a THWM NP. The HTIR-TCs were shipped to IFE/HRP in FY12 (see Figure ES-5), and preparations were initiated to fabricate a THWM NP for shipment to IFE/HRP in FY14;
- Completed FY13 FCRD feasibility evaluations of an ultrasonic thermometer for obtaining high resolution, high accuracy temperature profiles in FCRD irradiations (see Figure ES-6) and fabricated magnetostrictive transducers for ATNR NSUF ultrasonic transducer survivability irradiation in MITR;

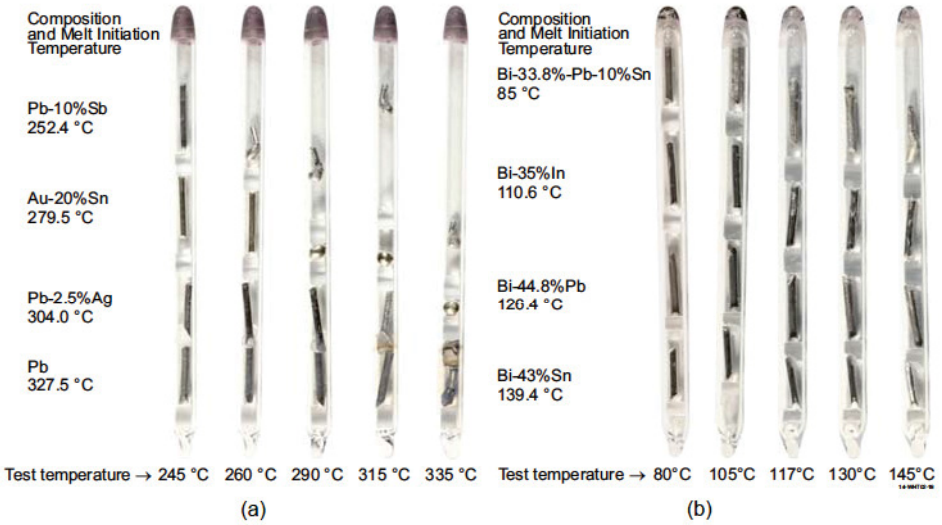

Figure ES-4. Quartz tube containing four melt wires in separated compartments: (a) Example of ideal indicator melt wires; (b) Example of non-ideal indicator melt wires.

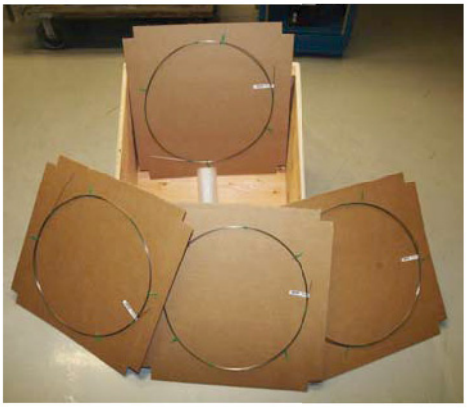

Figure ES-5. HTIR-TCs prior to shipment to IFE/HRP.

- Fabricated and shipped a THWM NP to CEA for evaluating fuel thermal conductivity (see Figure ES-7). The THWM NP was shipped to CEA in F13, and ATR NSUF evaluations are scheduled for FY14;
- Completed FCRD efforts to design and perform autoclave evaluations of enhanced and controlled load creep test rigs for future use in an ATR PWR loop (see Figure ES-8);
- Completed FY13 FCRD evaluations of fiber optics-based elongation probe;
- Completed FY13 ATR NSUF efforts to evaluate the need to reduce uncertainties associated with localized heating using sensors, such as gamma thermometers and SPGDs;
- Completed LDRD FY13 efforts to develop and evaluate the performance of a crack growth test rig (see Figure ES-9);
- Provided encapsulated flux wire sensors to ATR NSUF customers (see Figure ES-10);

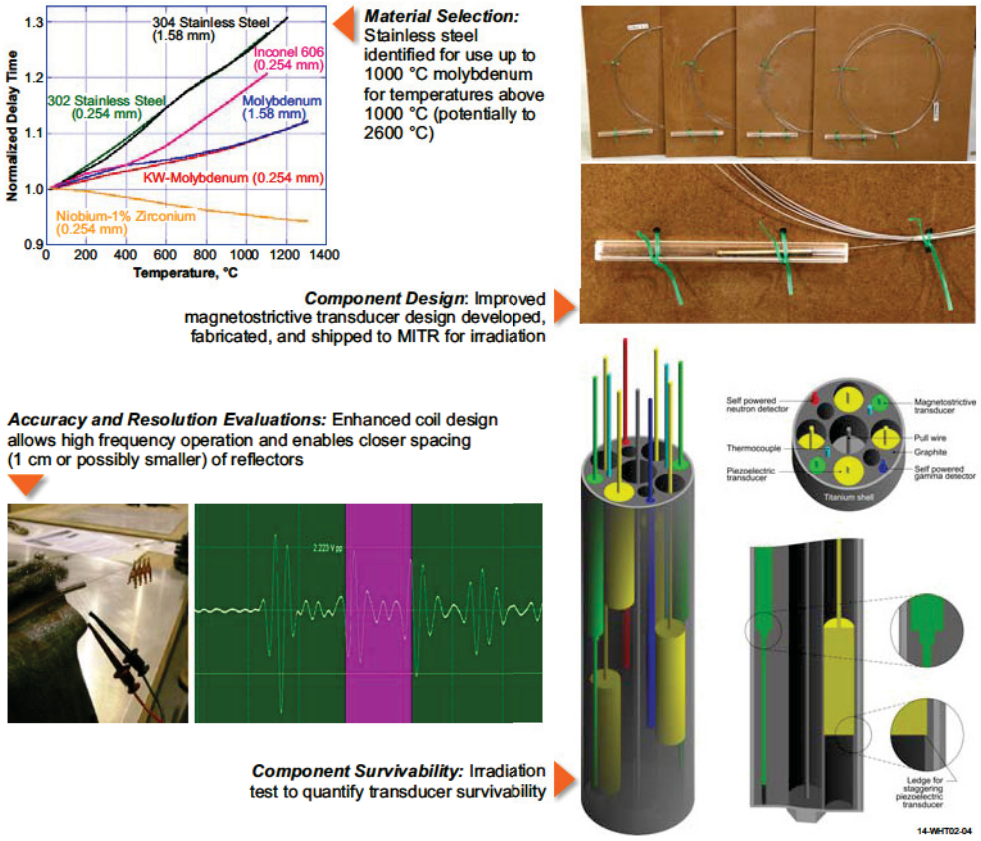

Figure ES-6. HTTL efforts to develop and deploy ultrasonic thermometer and support ultrasound transducer survivability irradiation.

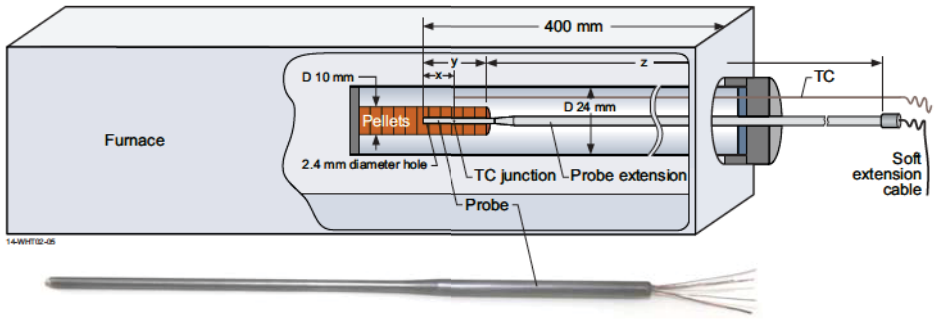

Figure ES-7. THWM NP fabricated for and shipped to CEA for fuel evaluations in a furnace.

- Completed ISU-led ATR NSUF project evaluating real-time flux sensors in the ATRC using specialized fixturing for flux detector evaluation (see Figure ES-11); and
- Continued FY13 NEET efforts to fabricate and evaluate MPFDs (see Figure ES-12).

Details about each of these achievements are reported in Section 5. In addition to providing ATR NSUF customers the instrumentation required for their irradiation tests, it should be noted that this effort has clearly added to the prestige and capabilities of the ATR NSUF and to the DOE. As noted previously, international collaborations have been established with leaders in the world of in-pile testing, such as IFE/HRP and CEA. Partnerships with universities have not only helped students successfully complete

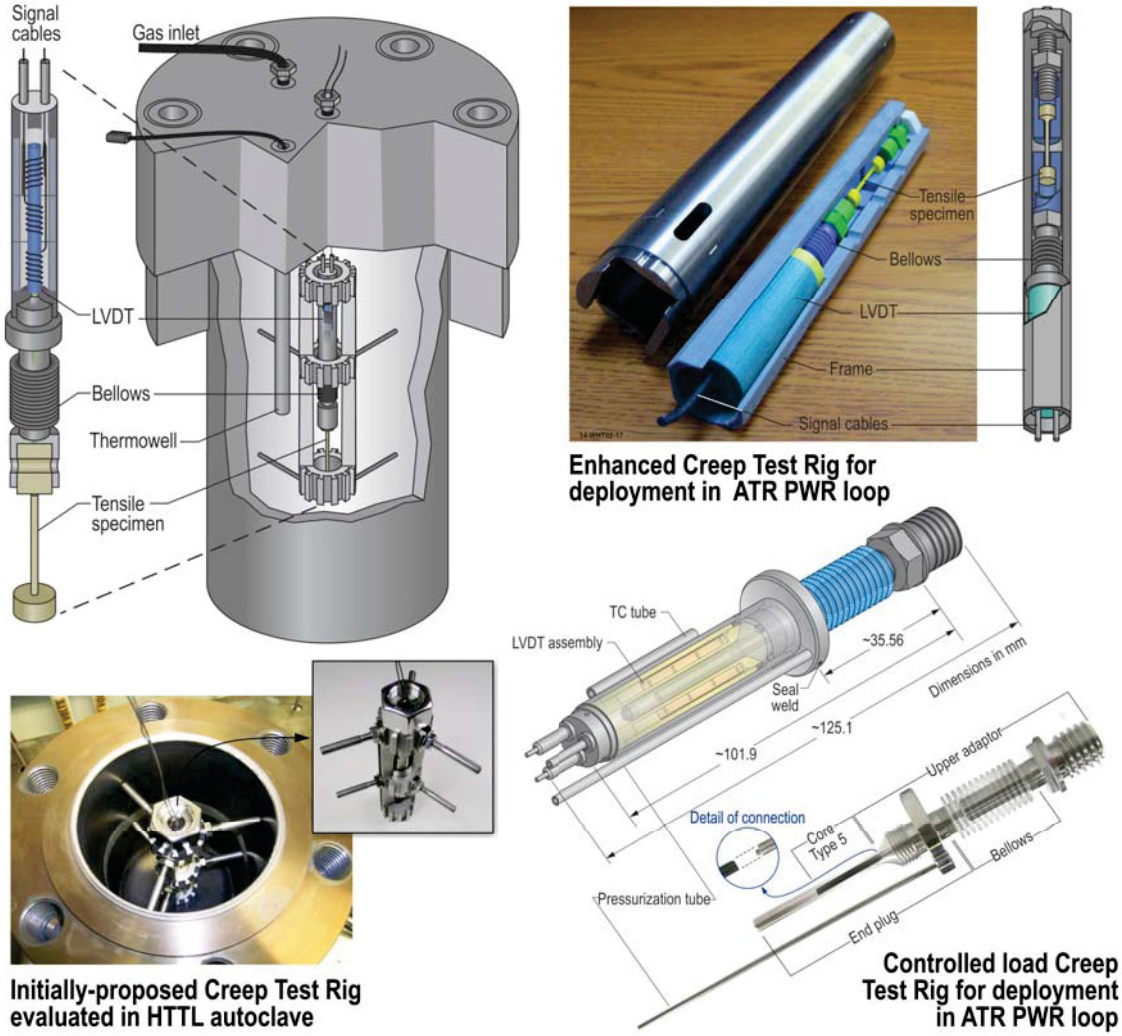

Figure ES-8. Enhanced and controlled-load creep test rig design and evaluation efforts completed.

their graduate level research, but have led to new INL employees. Over 29 peer-reviewed conference papers and 22 archival journal papers have been produced, and several patents have been awarded or are pending from this research.

Future Efforts

During FY14, several significant in-pile instrumentation activities are underway. For example, HTTL staff are funded to:

- Evaluate SiC temperature monitors from several ATR NSUF, EPRI, and FCRD irradiations
- Complete ATR NSUF flux monitor evaluations in ATRC
- Complete ATR NSUF activities to evaluate THWM NP performance in CEA fuel tests
- Complete ATR NSUF activities to evaluate HTIR-TC and THWM NP performance in HBWR irradiation

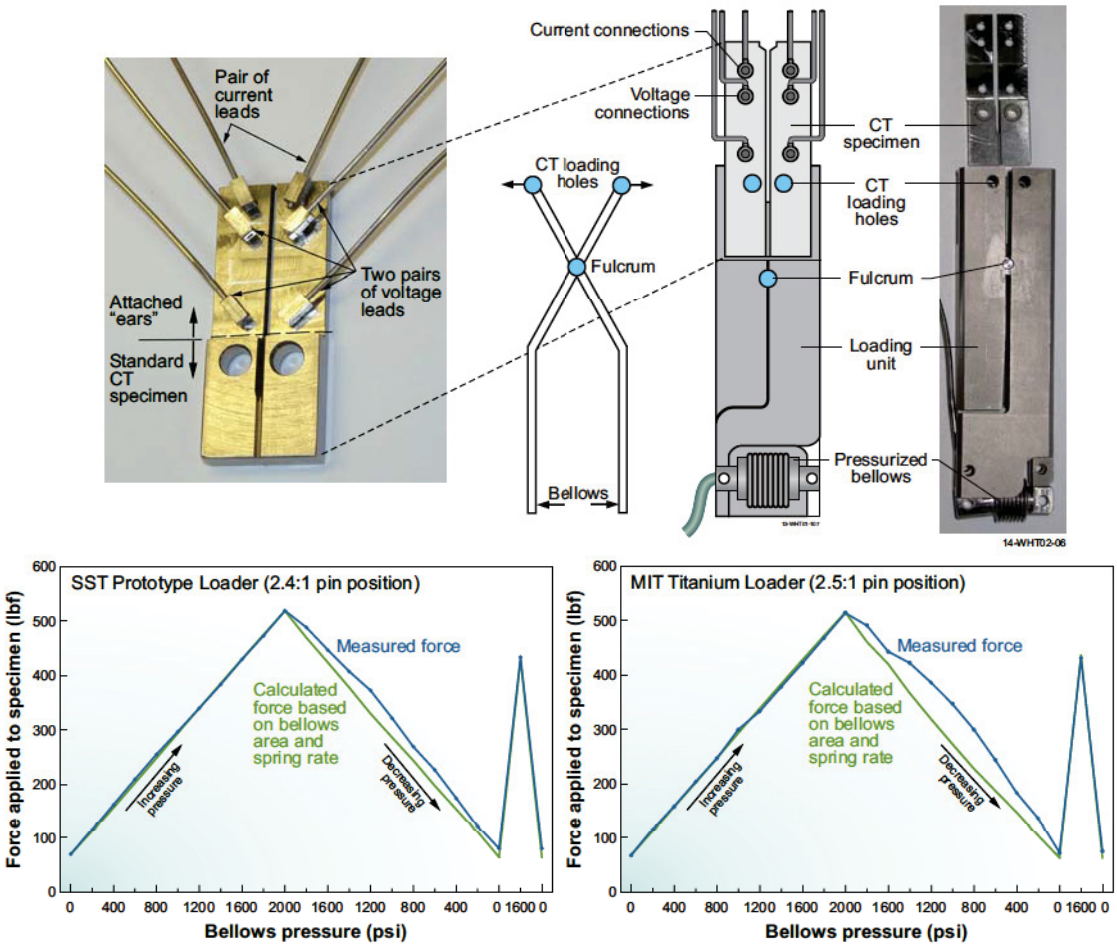

Figure ES-9. Design and fabricated components of the DCPD test rig.

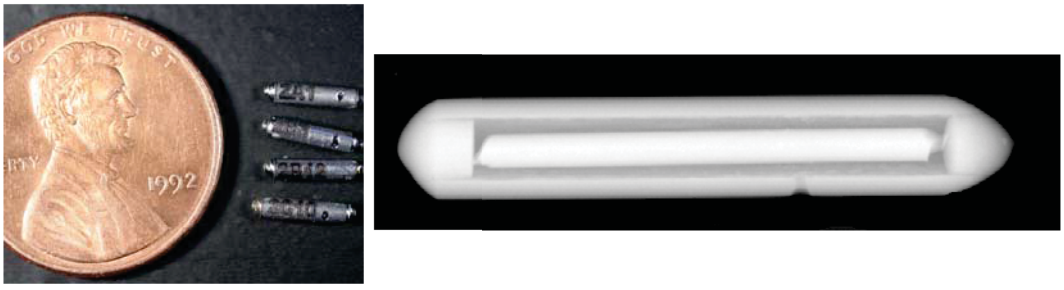

Figure ES-10. Encapsulated iron flux wires with radiograph.

- Assist MIT with installation and evaluation of ATR NSUF ultrasonic transducer irradiation and complete FY14 NEET efforts to support this irradiation
- Provide several HTIR-TCs for NGNP testing
- Provide encapsulated melt wires for FCRD accident tolerant fuel irradiation
- Complete FY14 NEET efforts to fabricate and evaluate the performance of MPFD prototypes

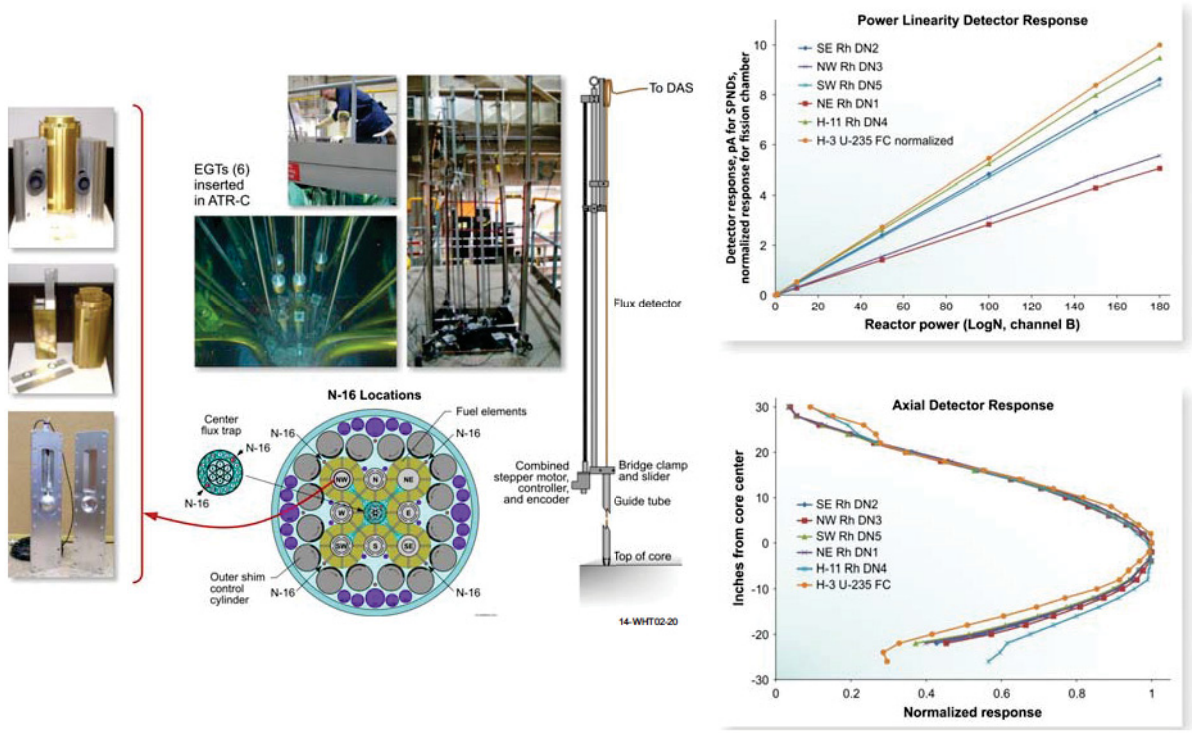

Figure ES-11. Completed ISU-led ATR NSUF project evaluating real-time flux sensors in the ATRC using specialized fixturing for flux detector evaluation.

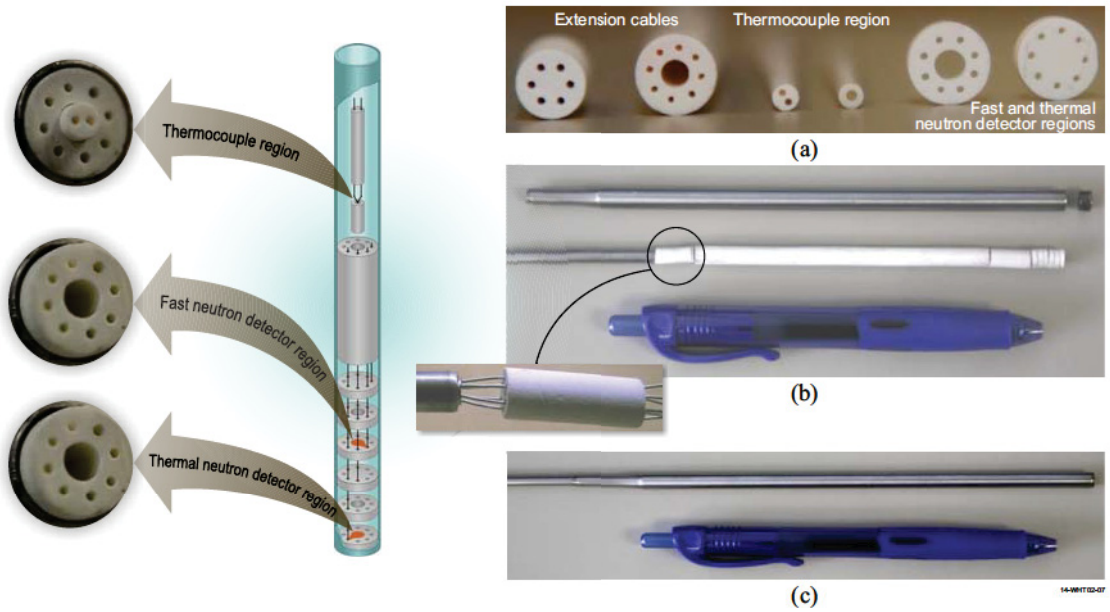

Figure ES-12. MPFDs offer unique miniature neutron detection options.

- Complete FY14 LDRD laboratory evaluations of a diameter gauge for use in ATR
- Complete FY14 LDRD autoclave evaluations and preparation for MITR irradiation of a crack growth test rig

As noted above, further efforts to further deploy sensors relying on ultrasound and fiber optic techniques have been deferred due to FCRD funding reductions. Likewise, efforts to evaluate sensors for localized heating have been reduced. In addition, no funding source has been identified to launch much-needed efforts to develop and deploy standardized test rigs for use in the ATR.

Standardized test rigs with state-of-the-art instrumentation, that are tailored to meet US industry needs for fuel irradiation testing and US regulatory requirements for data acceptance, are essential if US MTRs are to compete with international MTRs. Evaluations suggest that standardized test rigs have the potential to offer ATR users a one-third reduction in costs and long lead times associated with one-of-a-kind experiment designs. Participation from vendors, regulators and experienced ATR analysts and researchers in this effort are essential to ensure that test rigs are tailored to meet US industry needs and regulatory requirements for fuel development testing. Specially-developed instrumented standardized test rigs will allow DOE-NE programs [ATR NSUF, FCRD, Advanced Reactor Concepts (ARC), etc.] to obtain much-needed, high fidelity data for evaluating the performance of new fuels and will attract new users to ATR NSUF facilities.

Standardized test rigs will differ for specific irradiation facilities and locations. Figure ES-13 illustrates a preliminary conceptual design for a standardized test rig for use in ATR Loop 2A. Based on user specifications, the test rig could be instrumented with sensors capable of withstanding anticipated pressures, temperatures, and radiation levels in Loop 2A fuel tests and provide real-time data to address user needs. In addition to providing sensors within each test rig, supplemental sensors, such as flux wires, melt wires, and silicon carbide temperature monitors, will be included exterior to the test rig to increase confidence in the accuracy of obtained data.

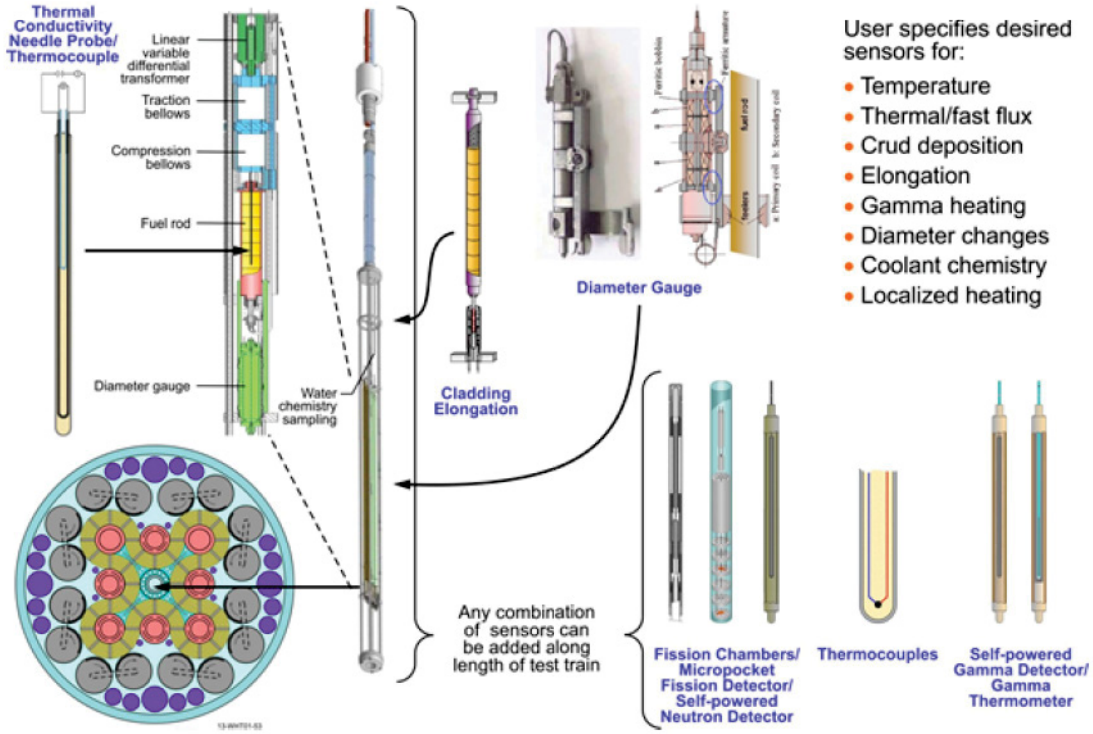

Figure ES-13. Candidate standardized test rig for evaluating fuel rod diameter changes, thermal conductivity, and fission gas release in a PWR loop.

A standardized test rig represents a much needed, final step in efforts to provide the US world class instrumentation and irradiation capabilities. In addition to increasing usage of the recently reactivated ATR Loop 2A, a standardized test rig will also provide a basis for testing at other ATR NSUF facilities, such as the High Flux Isotope Reactor (HFIR) and MITR, and the Transient Reactor Test (TREAT) facility (that DOE may restart). With standardized test rigs with advanced instrumentation, US MTRs will be able to more readily meet US industry and regulator needs for sustainment of nuclear energy. As discussed within this report, this domestic capability could assist in evaluating phenomena affecting US commercial nuclear power plants, such as fuel thermal conductivity degradation as a function of burnup and fuel dispersion and axial relocation during a Loss of Coolant Accident (LOCA).

ACRONYMS AND ABBREVIATIONS

ACRR	Annular Core Research Reactor
ADELINE	Advanced Device for Experimenting up to Limits Irradiated Nuclear fuel Elements
ARC	Advanced Reactor Concepts
ASTM	American Society for Testing and Materials
ATR	Advanced Test Reactor
ATRC	Advanced Test Reactor Critical
BR2	Belgium Reactor 2
BTB	Back-To-Back
BWR	Boiling Water Reactor
CALIPSO	In Core Advanced Loop for Irradiation in Potassium SOdium
CEA	Commissariat à l'Énergie Atomique et aux Energies Alternatives
CFD	Computational Fluid Dynamics
CGR	Crack Growth Rate
CNEA	Argentinean National Energy Commission
COD	Crack tip Opening Displacement
CT	Compact Tension
CVD	Chemical Vapor Deposition
DCPD	Direct Current Potential Drop
DG	Diameter Gauge
DOD	Department of Defense
DOE	Department of Energy
DOE-NE	Office of Nuclear Energy in the Department of Energy
DSC	Differential Scanning Calorimeter
ECN	Netherlands Energy Research Foundation
ECP	Electrochemical Corrosion Potential
EDL	Electronics Design Laboratory
EFDA	European Fusion Development Agreement
EFPI	Extrinsic Fabry-Perot Interferometer
EGT	Experimental Guide Tube
EPRI	Electric Power Research Institute
ETR	Engineering Test Reactor
FCRD	Fuel Cycle Research and Development
FP	Fabry-Perot
FNDS	Fast Neutron Detection System
HANARO	High Advanced Neutron Application Reactor
HBWR	Halden Boiling Water Reactor
HFIR	High Flux Isotope Reactor
HFR	High Flux Reactor

HRB	Hochtemperatur-Reaktorbau
HSIS	Hydraulic Shuttle Irradiation System
HTIR-TC	High Temperature Irradiation Resistant ThermoCouple
HTGR	High Temperature Gas Reactor
HTTR	High Temperature Test Reactor
HTTL	High Temperature Test Laboratory
IASCC	Irradiation Assisted Stress Corrosion Cracking
IAEA	International Atomic Energy Agency
ID	Inner Diameter
IDR	Invention Disclosure Record
IFE/HRP	Institutt for Energiteknikk (Institute for Energy Technology) at the Halden Reactor Project
INP NNP	Institute of Nuclear Physics at the National Nuclear Center
INTA	Instrumented Test Assembly
INL	Idaho National Laboratory
ISU	Idaho State University
JAEA	Japan Atomic Energy Agency
JAERI	Japan Atomic Energy Research Institute
JHR	Jules Horowitz Reactor
JMTR	Japan Materials Test Reactor
JRC	Joint Research Centre
JSI	Jozef Stefan Institute
KAERI	Korea Atomic Energy Research Institute
KSU	Kansas State University
LC	Lucent Connector
LDRD	Laboratory Directed Research and Development
LEP	Life Extension Project
LOCA	Loss of Coolant Accident
LOFT	Loss of Fluid Test
LORELEI	Light water One-Rod Equipment for LOCA Experimental Investigations
LWR	Light Water Reactor
LWRS	LWR Sustainability
LVDT	Linear Variable Differential Transformer
MADISON	Multirod Adaptable Device for Irradiations of LWR fuel Samples Operating in Normal conditions
MARICO	Material Testing Rig with Temperature Control
MCNP	Monte Carlo Neutron Particle
MELODIE	Mechanical Loading Device for Irradiation
MICA	Material Irradiation CApsule
MIT	Massachusetts Institute of Technology

MITR	Massachusetts Institute of Technology Nuclear Research Reactor
MIT-REL	MIT-Nuclear Reactor Laboratory
MM	MultiMode
MOU	Memo of Understanding
MPFD	Micro-Pocket Fission Detector
MSV	Mean Square Voltage
MTR	Materials Testing Reactor
NaK	Sodium-Potassium
NASA	National Aeronautics and Space Administration
NEET	Nuclear Energy Enabling Technologies
NGNP	Next Generation Nuclear Plant
NRG	Nuclear Research & Consultancy Group
NSUF	National Scientific User Facility
NW LIPT	NorthWest Large In-Pile Tube
OD	Outer Diameter
ODS	Oxide Dispersion Strengthened
OECD	Organization for Economic Cooperation and Development
OFS	Optical Fiber Sensors
OPD	Optical Path Difference
ORNL	Oak Ridge National Laboratory
PBF	Power Burst Facility
PCM	Power Cooling Mismatch
PHWR	Pressurized Heavy Water Reactor
PIE	Post Irradiation Examination
PSU	Pennsylvania State University
PWR	Pressurized Water Reactor
PZT	Lead Zirconate Titanate
RIA	Radiation-Induced Absorption
REL	Research and Education Laboratory
SCK•CEN	Studiecentrum voor Kernenergie • Centre d'Étude de l'énergie Nucléaire
SEM	Scanning Electronic Microscope
SE SIPT	Southeast Standard In-Pile Tube
SFR	Sodium Fast Reactor
SiC	Silicon Carbide
SM	Single Mode
SPERT	Special Power Excursion Reactor Test
SPGD	Self-Powered Gamma Detector
SPND	Self-Powered Neutron Detector
TC-NT	ThermoCouple Noise Thermometry

TED	Thermal Expansion Device
THWM	Transient Hot Wire Method
THWM NP	Transient Hot Wire Method Needle Probe
TOF	Time-Of-Flight
TRIGA	Training, Research, Isotopes, General Atomic
TREAT	TRansient REActor Test
TTAF	Test Train Assembly Facility
US	United States
US NRC	United States Nuclear Regulatory Commission
USU	Utah State University
UT	Ultrasonic Thermometer
UV	UltraViolet
VTT	Technical Research Centre of Finland
VVER	Vodo-Vodyanoi Energetichesky Reactor
ZPPR	Zero Power Physics Reactor

1. INTRODUCTION

The Department of Energy (DOE) designated the Advanced Test Reactor (ATR) as a National Scientific User Facility (NSUF) in April 2007 to support the growth of nuclear science and technology in the United States (US). By attracting new research users - universities, laboratories, and industry - the ATR NSUF facilitates basic and applied nuclear research and development, further advancing the nation's energy security needs. A key component of the ATR NSUF effort is to provide new in-pile sensors and test rigs that are capable of providing real-time measurements of key parameters during irradiation. To address this need, it is important to know what instrumentation is available and under development at other test reactors. In addition, alternate sensor technologies that aren't currently deployed in test reactors, but offer enhanced sensing capabilities, must be identified. Based on an initial instrumentation review completed in 2008, recommendations were made with respect to what instrumentation is needed at the ATR, and a strategy was developed for obtaining these sensors. In 2009, a report was issued documenting this instrumentation development strategy and initial progress toward accomplishing instrumentation development program objectives.[1] Since 2009, annual reports[2,3] have been issued to provide updates on this program strategy and the progress made toward implementing the strategy. This report provides an update reflecting progress as of January 2014 toward designing, developing, and deploying enhanced instrumentation.

1.1. Background

The ATR is a pressurized, light-water moderated, beryllium-reflected research reactor located at the Idaho National Laboratory (INL). Its ability to produce an extremely high neutron flux makes it possible to subject materials to the equivalent of years of radiation exposure in a commercial nuclear reactor in a matter of weeks or months. The ATR core design allows many experiments to run concurrently, with each experiment receiving a different and carefully controlled level of neutron irradiation. Originally commissioned in 1967 to evaluate fuels and materials performance for the Navy Nuclear Propulsion Program, the ATR is expected to continue operating until at least 2050.

As noted above, DOE's decision to designate the ATR as a NSUF is increasing the ATR's customer base from various nuclear science and technology programs. In addition, instrumentation efforts to support such irradiations are now derived from several DOE-sponsored nuclear research and development programs, including the Next Generation Nuclear Plant (NGNP), the Fuel Cycle Research and Development (FCRD), and the Nuclear Energy Enabling Technology (NEET) efforts. New in-pile instrumentation will further increase the ATR's ability to attract new customers from the commercial power, defense, and manufacturing sectors.

It is recognized that improved instrumentation techniques and standardized test rigs with advanced instrumentation are needed to support ATR in-pile irradiations. For decades, irradiation tests at international material test reactors (MTRs) have used in-pile instrumentation to measure parameters, such as temperature, dimensional changes, fission gas release, neutron fluence, and gamma heating. However, US instrumentation for in-pile testing lags behind instrumentation available at international MTRs. Hence, a key component of the ATR NSUF is to develop, fabricate, and demonstrate the performance of new real-time sensor technologies required to measure key parameters for irradiation testing and standardized test rigs incorporating such sensors to reduce irradiation costs and schedules.

INL's existing High Temperature Test Laboratory (HTTL) is a unique facility for developing, fabricating, and performing laboratory demonstrations of proposed new instrumentation. This facility features specialized sensor fabrication and evaluation equipment and trained staff with an established reputation for developing unique sensors. In December 2013, capabilities of the HTTL were relocated to INL's Research and Education Laboratory (REL), a newly constructed facility in Idaho Falls. As shown in Figure 1-1, the recently-relocated HTTL houses specialized sensor fabrication and evaluation equipment, including a laser welder, a real-time x-ray imaging system, a custom draw bench, several autoclaves, several tube furnaces (capable of temperature up to 1800 °C), and a vacuum furnace (capable of temperatures up to approximately 2800 °C). In addition, a special area of the new facility houses existing HTTL systems for measuring thermal properties of materials; such as a laser flash thermal property analyzer for thermal diffusivity measurements (and comparative specific heat and thermal conductivity measurements) up to 2800 °C, a pushrod dilatometer for comparison thermal elongation measurements up to 1600 °C, and a Differential Scanning Calorimeter (DSC) for obtaining specific heat capacity and melting temperature measurements up to 1600 °C. The new facility includes a specially-designed sensor fabrication room with locations for additional specialized equipment, such as an e-beam welder and a three-dimensional computer tomography machine. Hence, the HTTL is anticipated to have an increased role in ensuring that instrumentation is available to users of NSUF facilities and to address other DOE-NE program needs.

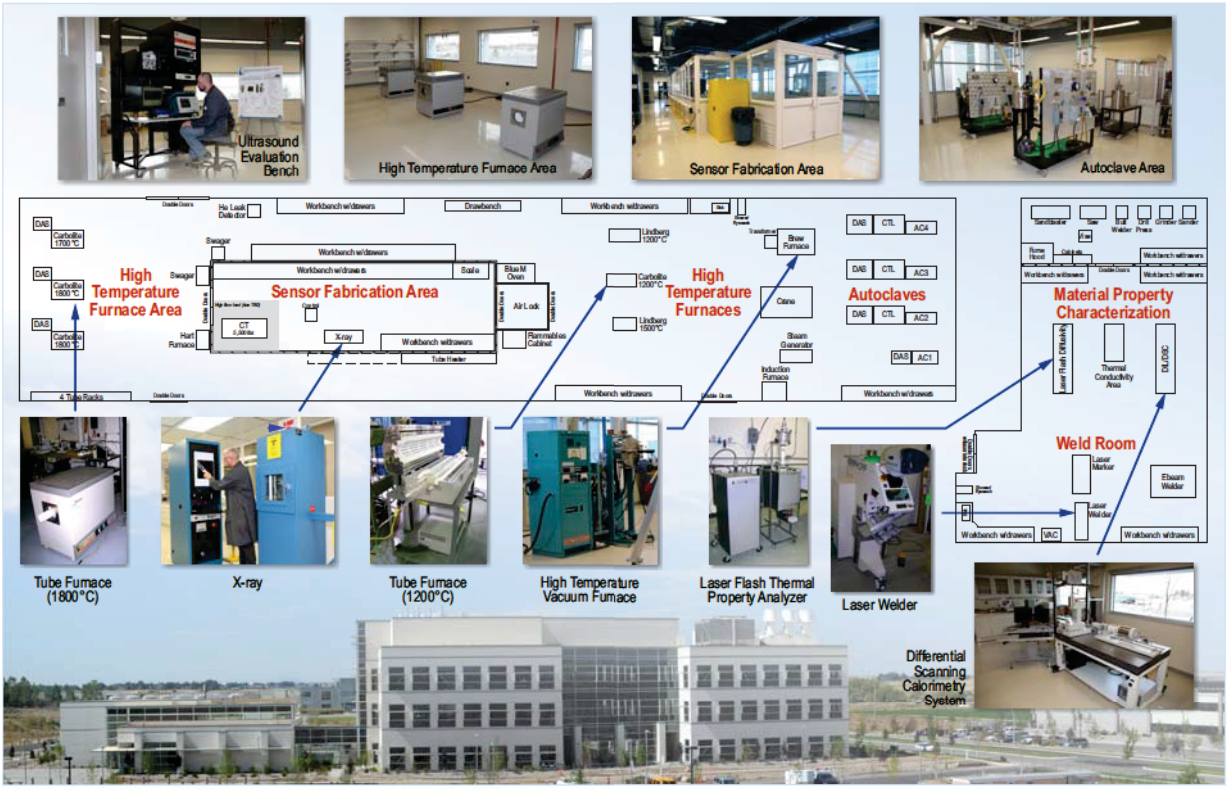

Figure 1-1. .HTTL layout and equipment.

To address the need for fabricating advanced test rigs, INL constructed and equipped the Test Train Assembly Facility (TTAF). The TTAF, which is located near the ATR, is used for final assembly of experiments to be installed at the ATR. The TTAF was designed and furnished with the equipment necessary to support the assembly of various configurations and design of test train experiments. The TTAF has varied

welding capabilities, included automated lathe and orbital gas tungsten arc welding (GTWAW), micro spot welding, and manual welding, that can be used to assemble various test train experiments. The TTAF also has the ability to perform induction brazes, an integral component in the assembly of test train experiments. Machining capabilities, such as a mill and a lathe, are also available at the TTAF. Experienced TTAF staff are available to support engineering and fabricate the experiment assemblies.

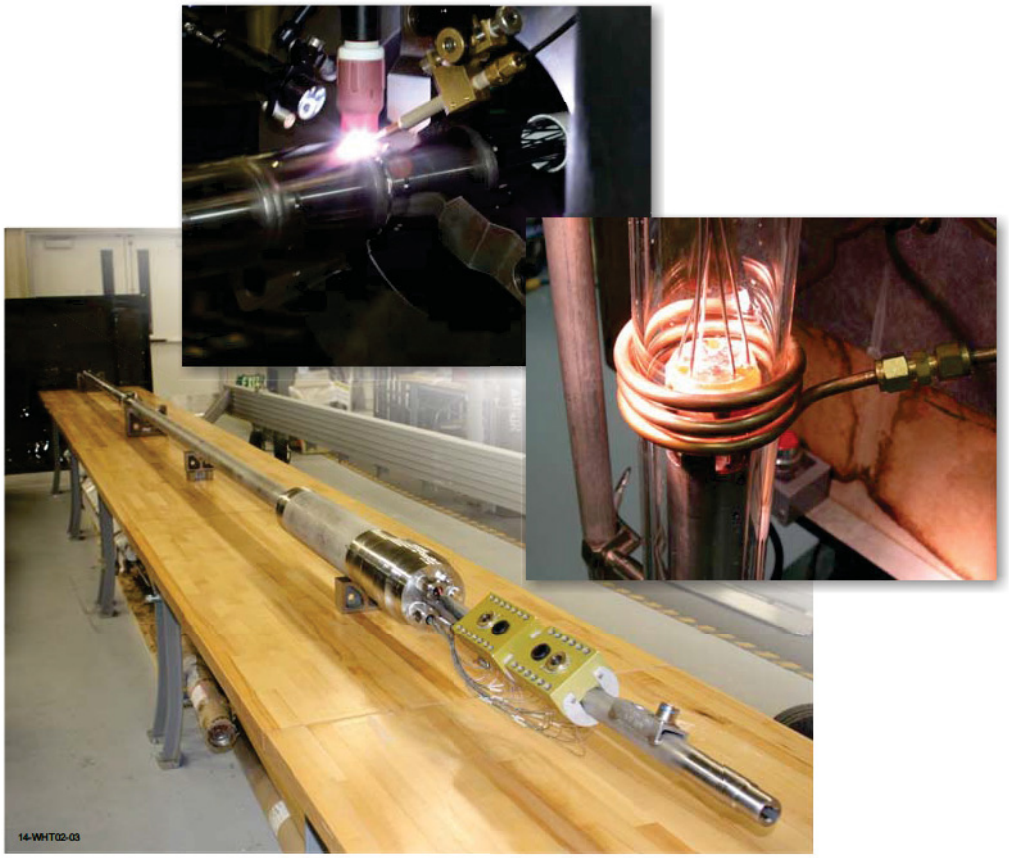

Figure 1-2. An irradiation experiment assembled using TTAF welding and brazing methods.

1.2. Report Content

As noted above, this effort began by completing a review to document what in-pile instrumentation is currently available at the ATR and other MTRs and what instrumentation could be developed or transferred from other applications to enhance in-pile irradiation testing. This report provides results from an updated review. Section 2 provides an overview of irradiation locations available in the ATR and the ATR Critical (ATRC) facility, what materials are typically irradiated in various experimental configurations, and what instrumentation is typically available for each configuration. Section 2 also highlights irradiation capabilities of other test reactors in the US and abroad. Section 3 summarizes instrumentation currently used to support test reactor programs and on-going efforts to provide instrumentation to facilities outside the INL. Section 4 outlines a program for obtaining all of the higher priority instrumentation, based on customer input, required for near-term and long-term irradiations at ATR and other test reactors. Where possible, potential collaborators are identified for obtaining this instrumentation. Section 5 summarizes INL

progress on accomplishing objectives in the plan presented in Section 4, identifying new in-pile instrumentation under development at INL to support ATR irradiations and reporting on the status of each research effort. References for this document are listed in Section 6.

2. BACKGROUND

As in prior status reports, this section provides an overview of irradiation locations available in the ATR and ATRC, what materials are typically irradiated in representative experimental configurations, and what instrumentation is typically available for each configuration. A brief overview of capabilities at other selected MTRs is also included.

2.1. ATR

The ATR is a unique facility for scientific investigation of the irradiation of nuclear fuels and materials.[4-8] Designed to allow simulation of high neutron radiation exposures in a short time period, the ATR has a maximum power rating of 250 MW_{th} with a maximum unperturbed thermal neutron flux of 1×10^{15} n/cm^2-s and a maximum fast neutron flux of 5×10^{14} n/cm^2-s. The ATR is cooled by pressurized (2.5 MPa) water that enters the reactor vessel bottom at an average temperature of 52 °C, flows up outside cylindrical tanks that support and contain the core, passes through concentric thermal shields into the open part of the vessel, then flows down through the core to a flow distribution tank below the core. When the reactor is operating at full power, the primary coolant exits the vessel at 71 °C.

2.1.1. Reactor Design and Characteristics

As shown in Figure 2-1, the ATR core consists of 40 curved plate fuel elements in a serpentine arrangement around a 3 x 3 array of primary testing locations, or nine large high-intensity neutron flux traps. The unique ATR control device design permits large power variations among its nine flux traps using a combination of control cylinders (drums) and neck shim rods. The beryllium control cylinders contain hafnium plates that can be rotated toward and away from the core. Hafnium shim rods, which withdraw vertically, are inserted or withdrawn for minor power adjustments. Within bounds, the power level in each corner lobe of the reactor can be controlled independently to allow for different power and flux levels in the four corner lobes during the same operating cycle. The ratio of fast to thermal flux can be varied from 0.1 to 1.0. In addition to the nine large volume (up to 48"/1.2 m long and up to 5.0"/13 cm diameter) high-intensity neutron flux traps, there are 66 irradiation positions inside the reactor core reflector tank, and there are two capsule irradiation tanks outside the core with 34 low-flux irradiation positions. A Hydraulic Shuttle Irradiation System (HSIS), more commonly referred to as the “Rabbit”, has also been installed in the ATR. The HSIS provides the ATR the capability to irradiate samples in small capsules (in the B-7 position) for materials research, rapid activations, and isotope production.[9]

2.1.2. Test Configurations and Conditions

Irradiated samples are enclosed in test capsules that are then typically placed in a basket to facilitate positioning within the reactor. This section provides summary information about the primary ATR test configurations, which are conceptually shown in Figure 2-2. More detailed information can be found in References 4 and 9.

- ***Static Capsule Experiments*** - These capsules may contain a number of small samples or engineered components. Static capsule experiments may be sealed or may contain material that can be in contact with the ATR primary coolant. Capsules may be any length, up to 122 cm and may be

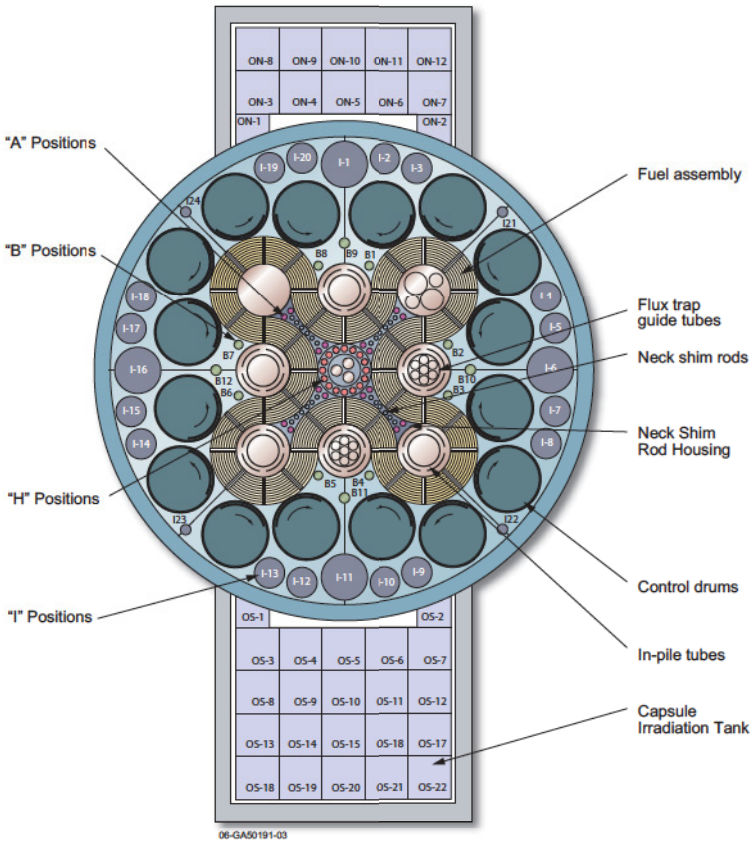

Figure 2-1. ATR core cross section showing irradiation locations.

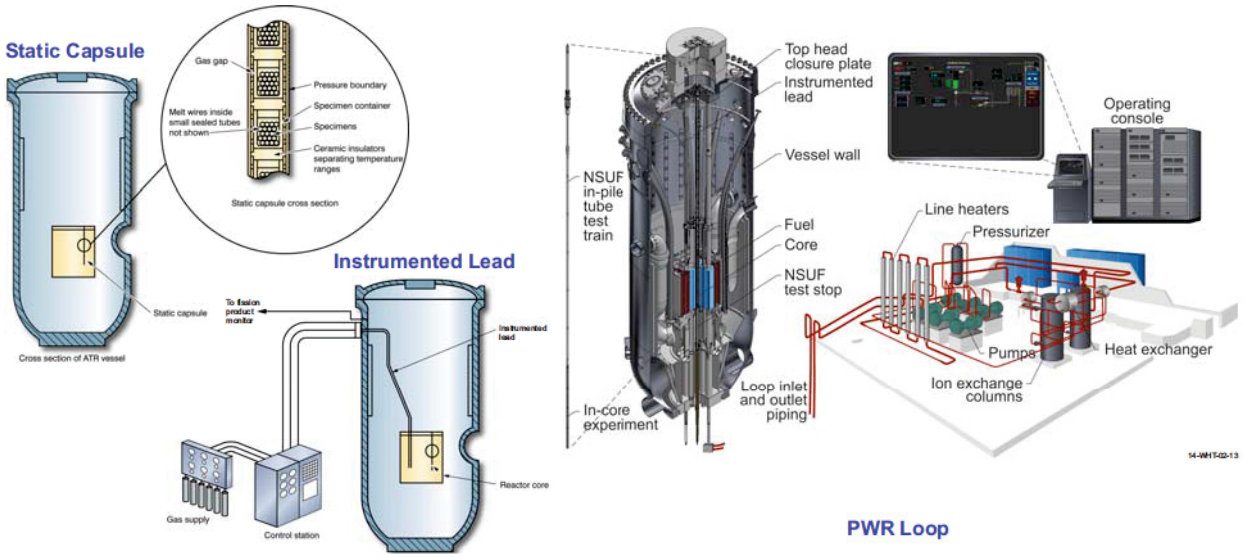

Figure 2-2. Schematic diagrams illustrating primary ATR irradiation locations.

irradiated in any core position, including the flux traps. Irradiation temperature may be selected, within limits, by including a gas gap in the capsule with a known thermal conductance. Peak temperatures may be measured using a series of melt wires or silicon carbide temperature monitors. Accumulated neutron fluences may be verified using flux wires or activation foils.

- ***Instrumented Lead Experiments*** - Active control of experiments and data from test capsules during irradiation is achieved using core positions with instrumentation cables and temperature control gases in ATR instrumented lead experiments. Such experiments can have instrumentation, such as thermocouples, connected to individual capsules or single specimens. This instrumentation can be used to control and monitor conditions within the capsule. For example, temperature control in individual zones is performed by varying the gas mixture (typically helium and neon) in the gas gap that thermally links the capsule to the water-cooled reactor structure. In addition to temperature, instrumented lead experiments can be configured to monitor the gas around the test specimen. In a fueled experiment, the presence of fission gases due to fuel failures or oxidation can be detected via gas chromatography. Instrument leads allow real time display of experimental parameters in the control room.
- ***Pressurized Water Loop Experiments*** - Five of the nine ATR flux traps used for materials and fuels testing are equipped with pressurized water loops (at the NW, N, SE, SW, and W locations). A sixth loop became operational in 2012. Each of the water loops can be operated at different temperatures, pressures, flow rates, or water chemistry requirements. These loops can operate above the standard temperatures and pressure of a commercial Pressurized Water Reactor (PWR) power plant. The great advantage of loop tests is the ease with which a variety of samples can be subjected to conditions specified for any PWR design. Each ATR pressurized loop is instrumented to measure and control coolant flows (both inert gas and water), temperatures, pressures and sample test data.
- ***Rabbit Tests*** - The HSIS, or "rabbit", enables insertion and removal of experiment specimens during ATR operational cycles. The HSIS is installed in the B-7 reflector position, which is one of the higher flux positions in the reactor with typical thermal and fast (>1 MeV) fluxes of approximately 2.5E+14 n/cm^2/sec and 8.0E+13 n/cm^2/sec, respectively. The titanium experiment capsules, or shuttles, are approximately 16 mm in diameter x 57 mm in length with interior usable dimensions of 14 mm in diameter x 50 mm long. Up to 14 capsules can be used for irradiations simultaneously, although one does not need to fill all 14 capsules for a test.

2.2. ATRC

Located at the INL, the ATRC Facility is a full-size nuclear mock-up of the ATR core that allows researchers to characterize in advance the expected changes in ATR core reactivity due to a proposed test. This facility generally operates at a thermal power of less than 5 kW (with associated peak thermal fluxes of around 10^{10} n/cm^2-s and a maximum fast neutron flux of around 10^9 n/cm^2-s).

2.2.1. Reactor Design and Characteristics

The primary difference between the ATRC Facility and ATR is that the ATRC Facility is a pool reactor, while the ATR is a pressurized water reactor contained in a vessel. In addition, a second difference is that the highly-enriched uranium fuel in the ATRC Facility is uniformly loaded with boron while the ATR

fuel is not. A third difference of note is that the ATRC Facility uses five cadmium-plated safety rods while the ATR uses six hafnium-plated safety rods. During operation, these differences are insignificant. ATRC Facility criticality is normally attained at a power greater than 0.25 mW. However, this pool-type reactor (Figure 2-3) usually operates at a power level of about 600 W and provides useful physics data for evaluating:

- worth and calibration of control elements,
- excess reactivities and charge lifetimes,
- thermal and fast neutron distributions,
- gamma heat generation rates,
- fuel loading requirements,
- effects of inserting and removing experiments and experiment void reactivities, and temperature and void reactivity coefficients.

Figure 2-3. ATRC Facility layout.

2.2.2. Test Configurations and Conditions

As part of the ATR NSUF, specialized fixtures and associated positioning software were developed and installed by INL to evaluate and calibrate real-time flux sensors and irradiate fuels and materials. Initial ATRC Facility tests (see Figure 2-4), which began in 2010, compare the response and accuracy of specially-developed real-time flux detectors to integral fluence monitors. This testing effort includes experimental guide tubes (EGTs) that can position the detectors at up to six of the N-16 positions and spe-

cialized fixtures that can position detectors in the Northwest Flux Trap and the Southeast Standard In-Pile Tube. Additional information about this effort is provided in Section 5. However, it should also be noted that the ATRC Facility's pool type design offers users enhanced flexibility for testing in lower flux conditions. Instrumented lead tests are more easily included in ATRC Facility test configurations because no pressure vessel penetrations are required.

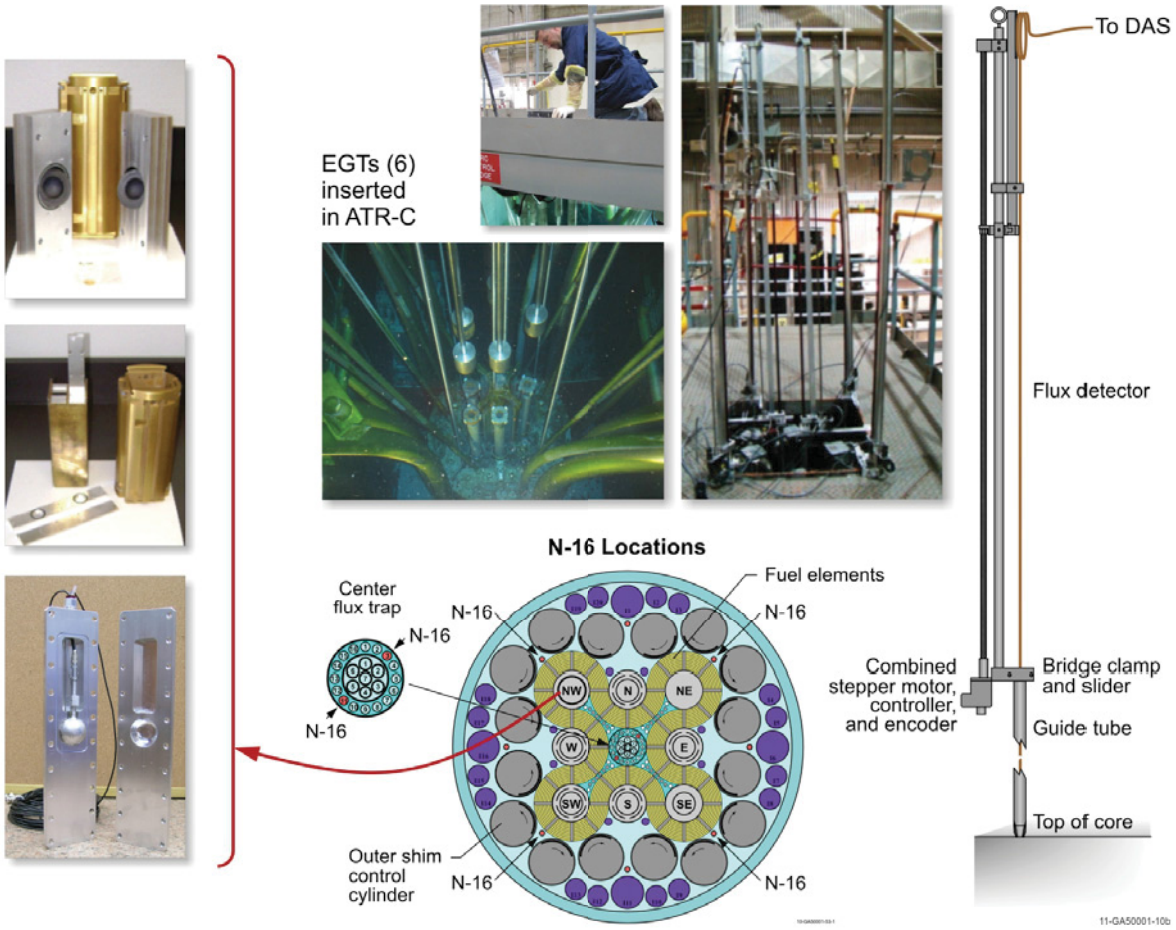

Figure 2-4. Sample /sensor positioning equipment and insertion locations at ATRC Facility.

2.2.3. Other MTRs

Table 2-1 compares operating parameters for selected test and prototype reactors used (or under construction) throughout the world. Information in this table was primarily obtained from the International Atomic Energy Agency (IAEA) Nuclear Research Reactor Database,[10] which contains information from nearly 280 research reactors (operating, shutdown, and proposed). Although these reactors range in power levels from 0 to several hundred MWt, nearly 200 of them have power levels below 5 MWt. Most of the reactors listed in Table 2-1 achieved criticality in the 1960s (or earlier). Among the operating reactors, there are two exceptions: the High Advanced Neutron Application Reactor (HANARO) reactor in South Korea, which went critical in 1995 and the prototype High Temperature Test Reactor (HTTR) in Japan, which went critical in 1998.

Table 2-1. Comparison of design parameters in selected operating test reactors.[10]

Parameter	ATR (USA)	HFIR (USA)	MITR (USA)	HBWR (Norway)	HFR (Netherlands)	OSIRIS[a] (France)	JHR (France)	BR2 (Belgium)	Hanaro (South Korea)	JMTR (Japan)
First criticality	1967	1965	1958	1959	1961	1966	2017	1961	1995	1968
Maximum thermal power, MW_{th}	250	100	5	20	60[b]	70	100	100	30	50
Max. thermal neutron flux, n/cm^2-sec	$1x\ 10^{15}$	$2x\ 10^{15}$	4×10^{13}	$1x\ 10^{14}$	3×10^{14}	3×10^{14}	5×10^{14}	1×10^{15}	5×10^{14}	4×10^{14}
Max. fast flux, n/cm^2-sec[c]	5×10^{14}	$1x\ 10^{15}$	1×10^{14}	1×10^{14}	5×10^{14}	3×10^{14}	1×10^{15}	7×10^{14}	3×10^{14}	4×10^{14}
Fuel material	UAl	U_3O_8-Al	UAl	UO_2	U-Al Alloy	U_3Si_2 Al	UMo-Al[d]	UAl	U_3Si - Al	USi_2Alx
Fuel rod/plate length, m	1.22	0.61	0.56	0.80	0.63	0.95	0.60	0.91	0.70	1.27
Primary coolant	H_2O	H_2O	H_2O	D_2O	H_2O	H_2O	H_2O	H_2O	H_2O	H_2O
Test conditions[e]	PWR, HTGR	PWR, HTGR	PWR, BWR, HTGR	PWR, BWR, PHWR, VVER, HTGR	PWR, BWR, HTGR	PWR	PWR, HTGR	PWR	PWR, PHWR	BWR,

a. Scheduled for shutdown in 2015. France is constructing a new 100 MW_{th} materials test reactor, the Jules Horowitz Reactor (JHR).
b. Uprate possible in 1984 after new reactor vessel installed.
c. E > 0.1 MeV
d. The reactor will be started with U_3Si_2-Al fuel, and transitions when it becomes available.
e. PWR- Pressurized Water Reactor; HTGR - High Temperature Gas Cooled Reactor; BWR-Boiling Water Reactor; PHWR - Pressurized Heavy Water Reactor; and VVER - Vodo-Vodyanoi Energetichesky Reactor (Pressurized Water Reactor)

The Jules Horowitz Reactor (JHR),[11 through 15] which is scheduled to go critical in 2017, is another exception with respect to its initial date for achieving criticality. The JHR is being built to replace materials irradiation capabilities of older reactors in Europe as they are retired from service. This 100 MWt reactor is designed to include static capsules, instrumented capsules, and in-pile loops. To support irradiation programs anticipated for the JHR, Commissariat à l'Énergie Atomique et aux Energies Alternatives (CEA) is developing several standard test train types for experiments in loops at nominal and off-normal Light Water Reactor (LWR) conditions, for capsules at LWR accident conditions, for tests in loops containing sodium potassium with high dpa and low thermal gradients, and for tests in loops at gas reactor conditions (see Figure 2-5).[13] Recent reports[12 through 15] indicate that these devices will be deployed in phases. Efforts are underway to qualify prototypes for the first phase of these devices, such as:

- MADISON (Multirod Adaptable Device for Irradiations of LWR fuel Samples Operating in Normal conditions) -A test train in an in-core loop for fuel testing under normal LWR (PWR or BWR) conditions; will measure temperature, pressure, water flow and cladding elongation using Linear Variable Differential Transformers (LVDTs)
- CALIPSO (In Core Advanced Loop for Irradiation in Potassium SOdium) - A test train for in-core irradiation at controlled temperature, at low pressure, under high flux, and forced Sodium-Potassium (NaK) convection; CALIPSO is an in-core sodium potassium loop for material testing under high (~16) dpa/year, temperatures between 250 and 450 °C, and limited thermal gradients (< 8 °C); seeking to qualify for higher temperatures (up to 650 °C)
- MICA (Material Irradiation CApsule) - A test train for in-core irradiation at controlled temperature, at low pressure, under medium flux (with static NaK), similar to CALIPSO; alternate design allows testing at high temperatures (up to 1000 °C) gas reactor conditions.
- ADELINE (Advanced Device for Experimenting up to Limits Irradiated Nuclear fuel Elements) - A test train in an in-pile loop for fuel testing under LWR (BWR or PWR) off-normal conditions

(e.g. power ramps) with temperature, pressure, water chemistry, elongation, flux (using Self-Powered Neutron Detectors), and fission product measurements.

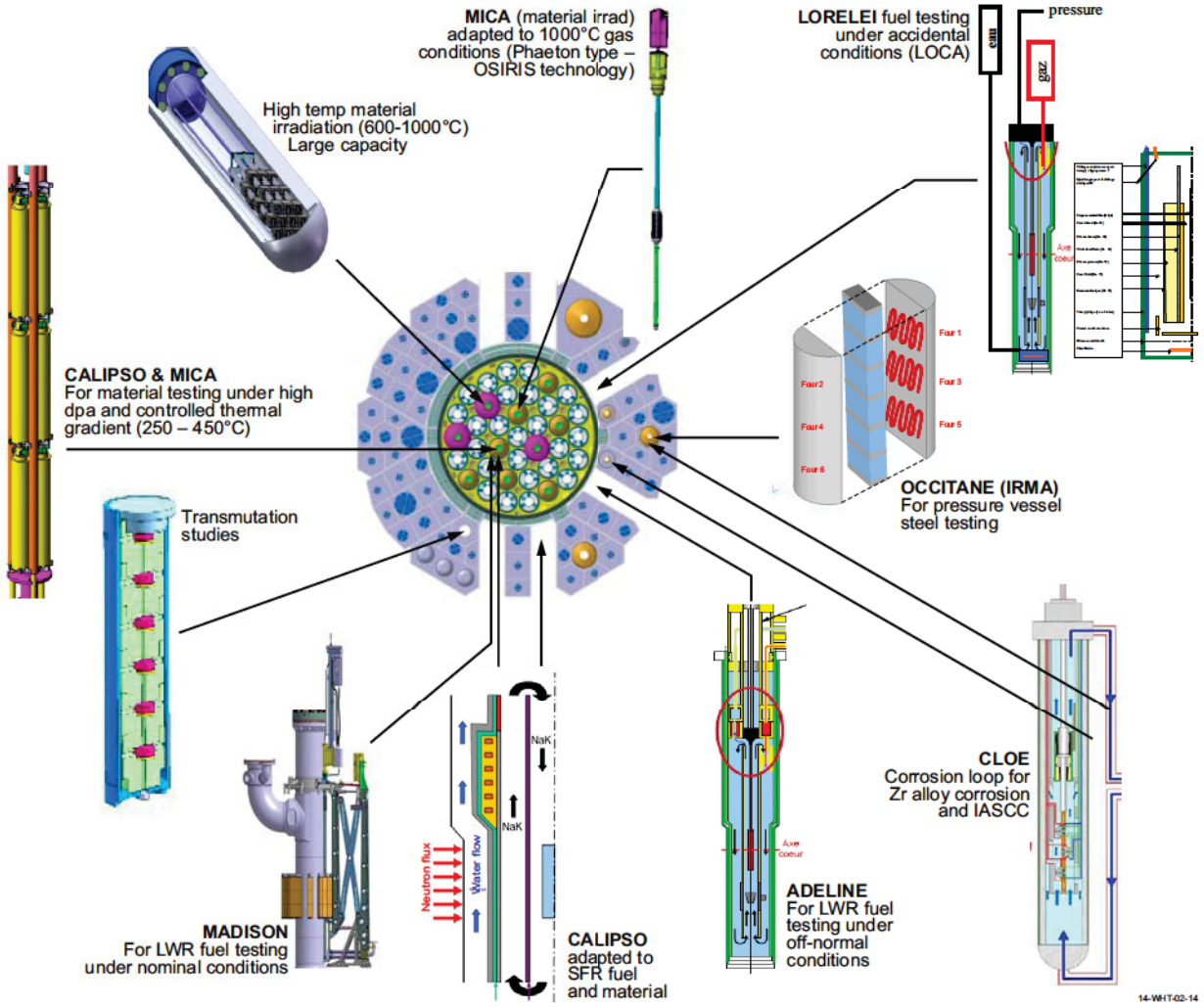

Figure 2-5. Test trains under development for JHR.

Subsequent efforts will focus upon other devices that can be deployed for various tasks, including transient fuel response testing, isotope production, and materials irradiation:

- LORELEI (Light water One-Rod Equipment for Loss of Coolant Accident (LOCA) Experimental Investigations) - A test capsule for fuel testing under LWR (PWR or BWR) LOCA conditions to observe phenomena such as clad ballooning or rupture, corrosion, and quench behavior and investigate fission product release.
- CLOE - Corrosion loop for evaluation of zircaloy alloy corrosion and irradiation assisted stress corrosion cracking.
- MADISON (Multirod Adaptable Device for Irradiations of VVER fuel Samples Operating in Normal conditions) -A second loop for fuel testing under normal VVER conditions; will measure temperature, pressure, water flow and cladding elongation using LVDTs

- IRMA- A static capsule for testing pressure vessel steel
- MOLI - Experimental capsules for radioisotope production

In the longer term, CEA will be developing a large capacity instrumented lead test for high temperature (600-1000 °C) material irradiations, and static capsules for transmutation studies. Irradiation facilities for conducting severe accident evaluations, gas reactor fuel evaluations, and LWR fuel material properties evaluations are also under consideration.

The Halden Boiling Water Reactor (HBWR) also merits further discussion. Although this reactor is older and its maximum power level (20 MWt) is over an order of magnitude smaller than the ATR, its testing flexibility and the expertise of its staff for instrumenting its tests make this facility unique. For decades, organizations within the international community (including the US Nuclear Regulatory Commission, vendors such as General Electric and AREVA, and the US Naval Reactor Program) have utilized this facility for in-pile irradiation needs. Approximately 40% of HBWR testing is devoted to Organization for Economic Cooperation and Development (OECD) programs with the remainder sponsored by bilateral agreements between Norway and customers from other countries.[16,17] Most of these bilateral agreements allow the HBWR to perform tests for utility customers to address issues related to fuel thermal performance, fuel pellet/clad interactions, fuel fission gas release, reactor vessel embrittlement, and structural materials degradation (e.g., corrosion, creep, etc.). As noted in Table 2-1, this reactor has loops for simulating BWR, PWR, Pressurized Heavy Water Reactor (CANDU), and Vodo-Vodyanoi Energetichesky Reactor (VVER) conditions. In addition, as discussed in Section 3.3, their focus on standardized test rigs and sophisticated sensors has made them unique in their ability to investigate a wide range of phenomena of interest to the LWR industry, such as fuel thermal conductivity degradation, irradiation assisted stress corrosion cracking, pellet cladding mechanical interaction, axial offset anomaly, etc.

2.2.4. Summary

Many material and fuel irradiations support research programs for existing LWRs (e.g., PWRs and BWRs) and advanced reactors (e.g., gas-cooled reactors, sodium fast reactors, and fusion reactors). Successful development and deployment of advanced reactors depends to a large extent on demonstration of "enabling" technologies. For example, the high temperature irradiation performance of new fuels and structural materials must be demonstrated with instrumented tests in prototypical environments. In addition, MTRs also support a wide range of non-nuclear programs including medical isotope production research, and semiconductor industry production (neutron transmutation doping of semiconductors). Improved instrumentation for such tests offer the potential to obtain higher fidelity data, reduce irradiation costs, increase isotope production, and improve doping processes. Although other test reactors, such as the HBWR, currently have superior instrumentation capabilities and more flexible test trains, the ATR can be made competitive by adding similar, if not enhanced, capabilities.

3. INTERNATIONAL DEVELOPMENT EFFORTS

As noted in Section 1, new instrumentation is needed to support in-pile irradiation tests MTRs. In recent years, several international organizations have either initiated or enhanced their research instrumentation development programs as outlined in this section.

Table 3-1 summarizes the status of in-pile sensors that are currently-available and under development at various research organizations in Belgium, France, Japan, Korea, Norway, and the Netherlands.[18] Several test reactor programs in Europe, the United States, and Asia, such as the program conducted by the Institute for Energy Technology at the Halden Reactor Project (IFE/HRP), have maintained their instrumentation development capability and offer a selection of sensors for irradiation testing. The Japan Atomic Energy Agency (JAEA) in Japan, Studiecentrum voor Kernenergie Centre d'Étude de l'Énergie Nucléaire (SCK•CEN) in Belgium, and Korea Atomic Energy Research Institute (KAERI) in Korea also offer selected instrumentation to users performing irradiations in their test reactors. The CEA in France, which supports their existing MTR (OSIRIS) and their new MTR (JHR), and INL in the United States, which supports the ATR, not only offer users a suite of instrumentation, but are rapidly trying to increase the types of sensors available to users at their facilities.

Current capabilities and recent advances by several of these foreign organizations are of interest as INL expands ATR NSUF instrumentation capabilities. For example, this section summarizes recent advances by CEA (Section 3.1) to develop calorimetry techniques for measuring localized heating and to develop a test rig capable of biaxial measurements of fuel creep during irradiation and by IFE/HRP (Section 3.3) to enhance their methods for detecting crack initiation and to deploy gamma thermometers to measure localized heating. Because ATR NSUF users have expressed interest in measuring changes in fuel length and diameter, localized heating, crack growth, and diameter changes during irradiation, new efforts (see Section 5) have been initiated at INL to make many of these capabilities available to ATR NSUF users. In addition, INL continues to monitor foreign efforts to deploy advanced technologies, such as the in-pile use of ultrasound-based sensors. Such new INL sensor development efforts are informed by considering applicable foreign experience.

3.1. CEA

The "INSNU" program was initiated by the French CEA with the aim of developing innovative in-pile instrumentation to meet the needs of emerging nuclear programs, such as Generation IV reactor, fusion reactor, and fuel cycle research.[11-15, 19-23] The scope of this program includes:

- radiation measurements (e.g., neutron flux and gamma heating)
- measurements of physical parameters inside the irradiation rigs (e.g., temperature, pressure, sample dimensions, and fission gas release)

The orange boxes in Figure 3-1 identify instrumentation areas studied within the INSNU program.

Originally, CEA instrumentation development was focussed on the INSNU program, which was a combined CEA-Saclay and SCK•CEN effort to improve instrumentation in the OSIRIS reactor in Saclay, France, and the Belgium Reactor 2 (BR2) in Mol, Belgium. However, in preparation for the JHR that will go critical in Cadarache, France in 2016, the CEA instrumentation effort was moved to Cadarache and

Table 3-1. In-pile instrumentation status at SCK•CEN, CEA, JAEA, KAERI, IFE/HRP, and NRG.

Research Organization / Country	Technology		
	Sensor	Parameter Detection	Status
Studiecentrum voor Kernenergie • Centre d'Étude de l'Énergie Nucléaire (SCK•CEN) /Belgium	SPND[a]	Thermal flux	Operational
	Fission chambers	Thermal and fast flux	Operational (fast detectors qualified in 2009; Joint Lab with CEA)
	Fiber optics	Length	Under development (Joint Lab with CEA)
	LVDTs with unstressed bellows and stressed bellows	Length/ creep-induced elongation	Participated in qualification testing with VTT (IFE/HRP LVDTs)
	Flux wires and foils	Fluence (neutron)	Operational
	Melt wires	Peak Temperature	Operational
Commissariat à l'Energie Atomique et aux Energies Alternatives (CEA)/ France	Fission chambers (down to 1.5 mm diameter)	Thermal and fast flux	Operational (Joint Lab with SCK•CEN)
	SPND	Thermal flux	Operational
	SPGD	Gamma flux	Operational
	Flux wires and foils	Fluence (neutron)	Operational
	Gamma calorimeter	Localized heating	Operational
	Melt wires	Peak Temperature	Operational
	Thermocouples (Type K, N, and C thermocouples)	Temperature	Operational; Mo/Nb alloy thermocouples not yet irradiated.
	Noise thermometry	Temperature	Under development
	Fixed point μ-cells	Temperature	Under development
	Counterpressure sensor	Fission gas release (pressure in fuel rod)	Operational (also placed on previously irradiated fuel)
	Acoustics	Fission gas composition and pressure	Operational (placed on previously irradiated fuel rod)
	LVDTs / Diameter Gauge (DG)	Biaxial (length and diameter) measurements of fuel dimensional changes	Operational (To be deployed in OSIRIS in 2014)
	Fiber optics	Length	Operational (Joint Lab with SCK•CEN)
Korea Atomic Energy Research Institute (KAERI)/ Korea	Melt wires	Peak Temperature	Operational
	Thermocouples (Type K and C)	Temperature	Operational
	Flux wires	Fast fluence	Operational
	LVDT	Pressure, UO_2 elongation / creep-induced elongation	Operational for pressure fuel elongation detection /under evaluation for creep testing (IFE/ HRP LVDTs)
	SPNDs (V-, Rh-emitter)	Thermal flux	Operational (commercially- made SPNDs)
Nuclear Research & Consultancy Group (NRG) / Netherlands	Neutron metrology sets: SS tubes containing quartz minitubes with flux wires (Nb, Ti, Fe, Ni, Co)	Fluence	Operational
	SPNDs	Thermal flux, power, fuel heatup rate	Operational (commercially-made SPNDs)
	Thermocouples (Type K and N)	Temperature	Operational
	LVDT	Pressure	Operational (IFE/HRP LVDTs)
	Silicon chip transducer; tube containing silicon chip influenced by pressure.	Pressure	Operational[b]
	Gamma spectrometry system and temperature monitoring and control by gas mixture	Near real-time fission product sampling and gas temperature control by gas mixture control	Operational

Table 3-1. In-pile instrumentation status at SCK•CEN, CEA, JAEA, KAERI, IFE/HRP, and NRG.

Research Organization / Country	Technology		
	Sensor	Parameter Detection	Status
Japan Atomic Energy Agency (JAEA)/Japan	Fission chambers (1.8 mm diameter)	Thermal flux (with ^{235}U deposits)	Operational
	SPNDs	Thermal flux (Rh, Co, and Pt-40%Rh emitters)	Operational
	Flux wires	Fast (Fe) and thermal (Al-Co, V-Co, and Ti-Co) fluence	Operational
	Melt wires	Peak Temperature	Operational
	Thermocouples (Type K, N, and C)	Temperature	Operational[c] (also placed on previously irradiated fuel
	LVDT (stressed with bellows and unstressed)	Pressure, length/ creep-induced elongation	Operational (Japanese LVDTs and bellows)
	DCPD method with CT specimens and bellows loading	Crack growth	Operational
Institute for Energy Technology/Halden Reactor Project (IFE/HRP) / Norway	LVDT (stressed with bellows and unstressed) and DG	Pressure, length/ creep-induced elongation and diameter changes	Operational (enhancements explored with CEA and INL); DG improvements underway
	Eddy-current probe	Oxide thickness deposited on fuel rods; cladding defects; crack growth	Under development
	Melt wires	Peak Temperature	Operational
	Expansion thermometer	Temperature	Operational
	Thermocouples (Type K, N, and C)	Temperature[c] and thermal conductivity[d]	Operational (also place on previously irradiated fuel
	Flux wires	Fast (Fe, Ni) and thermal (Al-Co) fluence	Operational
	SPNDs	Thermal flux, power, fuel heatup rate and burnup; power	Operational (commercially-made and IFE/HRP-made sensors)
	Gamma thermometer	Gamma flux; gamma heating; water level	Operational (IFE/HRP- sensors)
	DCPD method with CT specimens and bellows	Crack growth	Operational
	Turbine Flowmeter	Inlet /outlet flow (single or two phase); with channel power information, outlet void fraction	Operational
	Electrical chemical potential measurements (platinum or palladium electrodes)	Oxygen concentration, hydrogen concentration (e.g., corrosion potential); Water chemistry	Operational

a. Abbreviations: LVDT, linear variable differential transformer; DG, diameter gauge; SPND, self-powered neutron detector; SPGD, self-powered gamma detector; DCPD, direct-current potential drop; CT, compact tension; HTIR-TC, high-temperature irradiation-resistant thermocouple; SiC, silicon carbide; VTT, Technical Research Center of Finland

b. Using Kulite Semiconductor Products, Inc. outside high neutron and gamma radiation location.

c. HBWR-specific corrections required to compensate for transmutation that occurs in Type C high temperature thermocouples during irradiation. However, similar temperatures and fluxes and temperature gradients and flux distributions must exist during irradiation in order to apply such correction factors, and thermocouple lifetimes are generally limited to 1 year. Informal HRP discussions indicate that batch-to-batch variations in Type C thermocouples adversely affect performance.

d. Thermal conductivity estimates require assumptions about fuel densification, and gap conductance.

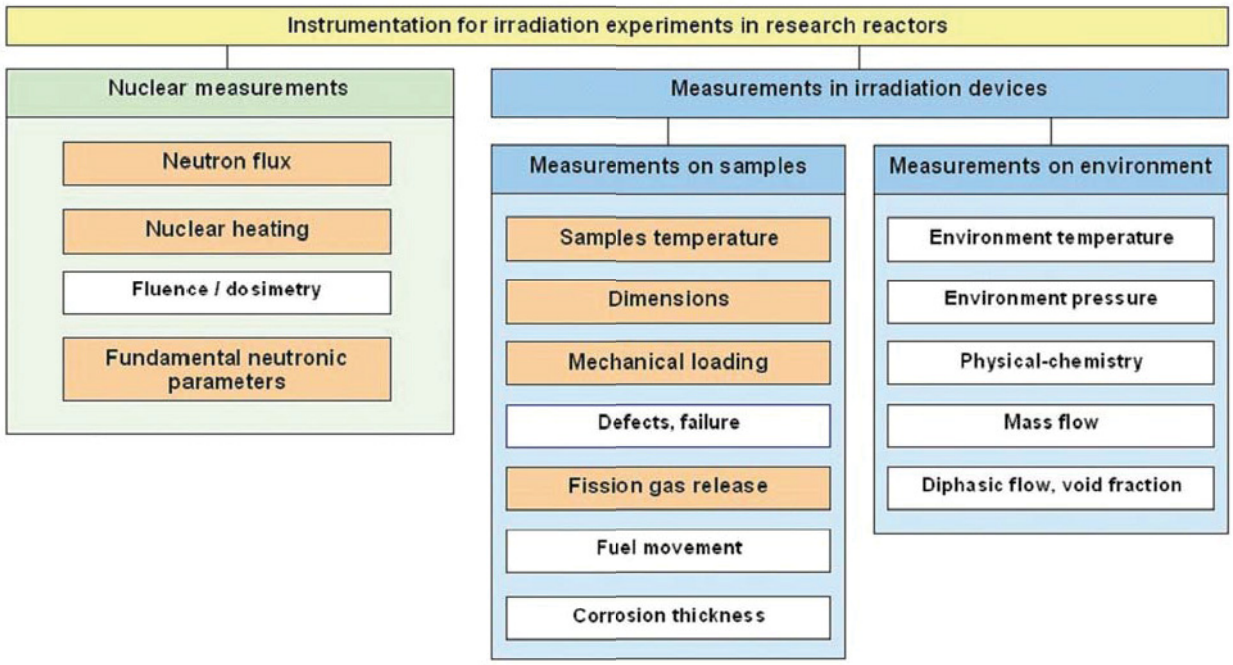

Figure 3-1. In-pile instrumentation needs pursued by INSNU for irradiation experiments.[20]

expanded to include a larger number of organizations and sensor development activities. In addition, as noted in Section 2, efforts include development of standardized test rigs.

As discussed in References 14 and 15, decisions for CEA instrumentation development are based on users-needs, and development efforts include in-pile qualification. Instrumentation development efforts are often a collaborative effort between government research laboratories [CEA, Paul Scherrer Institute (PSI), HRP, etc.] and industry (e.g., Photonis, Thermocoax, etc.). By including industry partners, developers ensure sensor availability from a commercial supplier.

General characteristics of instrumentation developed include:

- Reliable (because it is impossible or difficult to perform maintenance on irradiated objects)
- Accurate (sensors must meet testing requirements; e.g., µm dimensional measurements)
- Miniature (irradiation volumes are limited with narrow dimensions; few mm available)
- High temperature resistant (> 300 °C, up to 1600 °C)
- Corrosion resistant (in pressurized water, high temperature gas, and liquid metals)
- Neutron / γ "resistant" (dose > 1GGy/day and > 10 dpa/year in MTRs)

As noted in References 21 and 23, in-pile instrumentation must be developed that doesn't pose a threat to the safety or economic operation of the test reactor (e.g., "simpler" is smarter). Selected examples of CEA in-pile instrumentation development are discussed below. Because some of their sensor development efforts are collaborations with SCK•CEN, additional examples may be found in Section 3.2.

3.1.1. Subminiature Fission Chambers

For decades, in-pile neutron flux measurements were obtained using Self Powered Neutron Detectors (SPNDs), and signals were generally correlated with post-irradiation analysis of activation foil dosimeters. The development of CEA's sub-miniature fission chambers for in-pile measurements of high thermal neutron fluxes (up to 4×10^{14} n/cm²-s) represents a significant improvement. These sensors, which have external diameters of only 1.5 mm and contain a U^{235} fissile deposit, were qualified in the BR2 in the CALLISTO loop between 2001 and 2004. However, additional studies continue to verify sensor robustness. These sensors are now manufactured by the PHOTONIS Company under the name "CFUZ53" (see Reference 24).

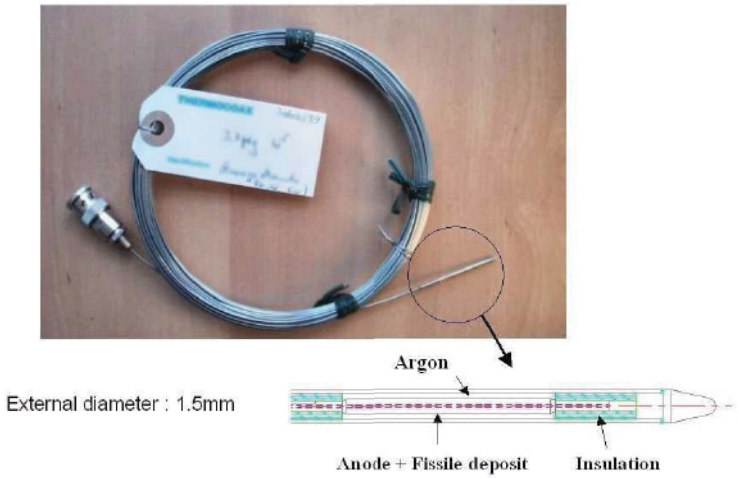

Figure 3-2. CEA-developed sub-miniature fission chamber.

In addition, as part of the Joint Instrumentation Laboratory, CEA-SCK•CEN developed fission chambers for online in-core measurement of the fast component of a high neutron flux (~ 10^{14} n/cm^2-s) with an uncertainty of 10% or less in locations with thermal fluences up to 10^{21} n/cm^2. The fast neutron detection system (FNDS; see Figure 3-3) is based on a patented miniature fission chamber with a special fissile deposit sensitive to fast flux with a low thermal contribution and is operated in Campbelling mode for a high gamma rejection. The choice of the fissile deposit is key in these fission chambers for two main reasons:[25]

- The fission cross-section is usually much larger for thermal neutrons than for fast neutrons. Moreover, even for the few isotopes presenting an energy threshold near 1 MeV, such as ^{238}U or ^{242}Pu, it remains small (e.g., a few barns) for fast neutrons.
- The potential to form other isotopes via radiative capture of (primarily thermal) neutrons. This process, either directly or after some radioactive decay, leads to new isotopes in the deposit that may fission preferentially with thermal neutrons. The sensitivity to thermal neutrons in a chamber based on these isotopes therefore increases gradually. Because of their large size and of the local perturbation induced on the thermal flux, it was decided to not use screen-absorbers that could prevent thermal neutrons from reaching the chamber.

For MTRs, analytical simulations identified ^{242}Pu as the best choice to measure the fast component of a high neutron flux. Its sensitivity to fast neutrons is excellent at the beginning of irradiation and slowly decreases with fluence.

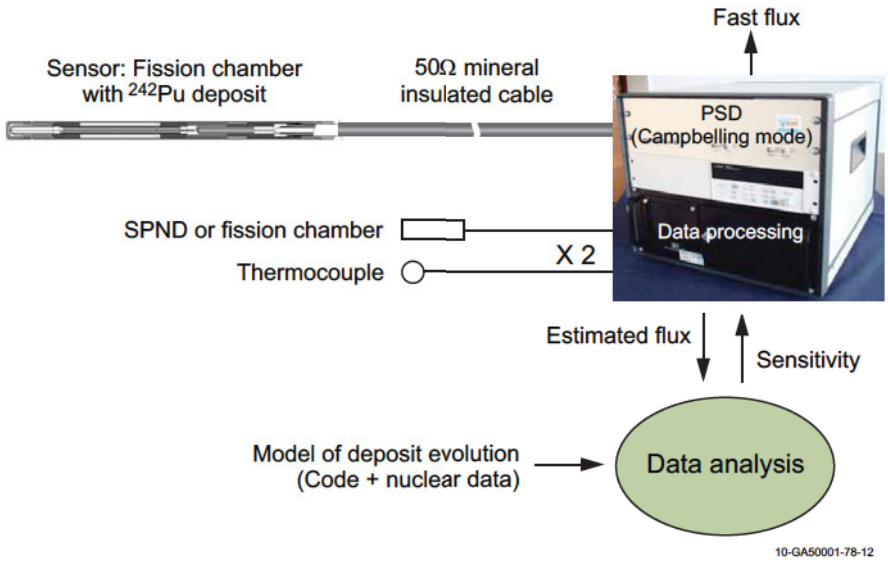

Figure 3-3. Schematic view of the FNDS prototype.

Generally, the signal given by a fission chamber at high counting rates is the sum of a mean constant current, I_o, and a fluctuation around this value. Classically, fission chambers are used in "current mode" under high neutron flux where it is not possible to count individually each event in the detector. However, the FNDS system uses the variance of the signal. This parameter characterizes the random variations of the signal around its mean value and is proportional to the incident neutron flux. This method is called Campbelling mode or Mean Square Voltage (MSV) mode. The advantage of the Campbelling mode is that the gamma contribution to the signal is significantly less than in current mode because it plays a part as the square of the charges, which are notably lower for events generated by gammas than for those induced by fission reactions. Thus, this mode is very useful for a high rejection of the gamma component. Tests performed in the BR2 in 2005 and 2006 demonstrated the viability of the Campbelling mode for measuring the fast neutron flux; the gamma contribution to the signal of a ^{242}Pu fission chamber was reduced from 50% in current mode to 0.6% in Campbelling mode.[26] The developed FNDS system has been qualified in-pile in the BR2 in 2009, and it is now operational at CEA and SCK•CEN.

Prototypes of fission chambers with ^{242}Pu deposit have been manufactured by CEA in Cadarache and tested in 2005 and 2006 in the BR2 of SCK•CEN. As part of an on-going ATR NSUF effort, the use of these fission chambers for ATR applications is being investigated. Initial evaluations began in the ATRC in October 2010 (see Section 5).

CEA continues to perform research to evaluate and improve the performance of these fission chambers. For example, CEA performed[15] the CARMEN-1 experiments which contain two cell probes for characterizing conditions in OSIRIS. As shown in Figure 3-4, one cell contains multiple neutron detectors (fast and thermal fission chambers with SPNDs, and the other cell contains multiple self-powered gamma detector (see Section 3.1.2), a gamma thermometer, and a calorimeter. Comparisons of data to analysis results indicate that these cells can successfully be used to characterize OSIRIS conditions.

A follow-on device, CARMIEN-2, is being designed for use in the JHR.[12] In addition, CEA performed evaluations[27] to assess the impact of fill gas mixture and pressure on fission chamber performance.

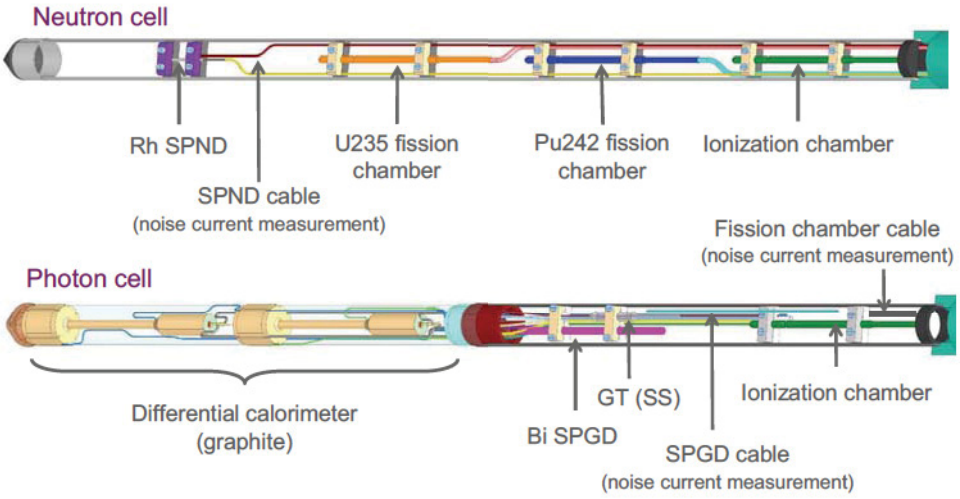

Figure 3-4. Neutron and photon measurement cells in CARMEN-1experiment.

Recently, CEA and SCK•CEN are involved in studies to reduce uncertainties in fission chamber measurements by characterization in various research reactors and by comparing neutron field measurements with those predicted by calculational methods. Results from measurements and calculations for the BR1, the CALIBAN, Jozef Stefan Institute (JSI) Training, Research, Isotopes, General Atomic (TRIGA) Mark II reactor facilities have been found to be within 4% or less.[28, 29]

3.1.2. Self-Powered Gamma Detectors

Nuclear heating measurements in MTRs are commonly based on calorimeter or gamma thermometer technologies. SCK•CEN and CEA have jointly-developed a Self-Powered Gamma Detector (SPGD) for monitoring the gamma field.[30] In order to minimize the neutron response while maximizing the gamma response, bismuth was selected as the emitter material. Based on detailed Monte Carlo Neutron Particle (MCNP) modeling to calculate the gamma/neutron sensitivities and irradiation experiments in pure and mixed gamma spectra (OSIRIS and BR2), a tubular geometry design was selected as the most appropriate for in-core gamma detection because this design allows a larger sensitivity with better response characteristics. These SPGDs, which are produced by THERMOCOAX (see Figure 3-5), are able to measure small power changes (until less than 1%) with a relative accuracy of about 0.2%, which is much better than possible with gamma thermometers. In summary, the bismuth SPGD is a promising small size in-core gamma-selective detector that does not suffer from burn-up effects.[14] Furthermore, this SPGD is easily implemented inside lower temperature experiments (that are well below the bismuth melting temperature of 271 °C).

3.1.3. Mo/Nb Thermocouples

In 2003, CEA initiated a research program in collaboration with the THERMOCOAX Company, to develop high-temperature in-pile thermocouples.[31] This CEA/THERMOCOAX effort initially investigated thermoelements containing molybdenum and niobium because the low neutron absorption cross sections of these elements make them less susceptible to transmutation-induced drift during irradiation. Materials interactions tests conducted by CEA/THERMOCOAX in high temperature furnaces, in the range from 1000 to 1600 °C, indicated that materials less susceptible to interactions with Mo and Nb thermoele-

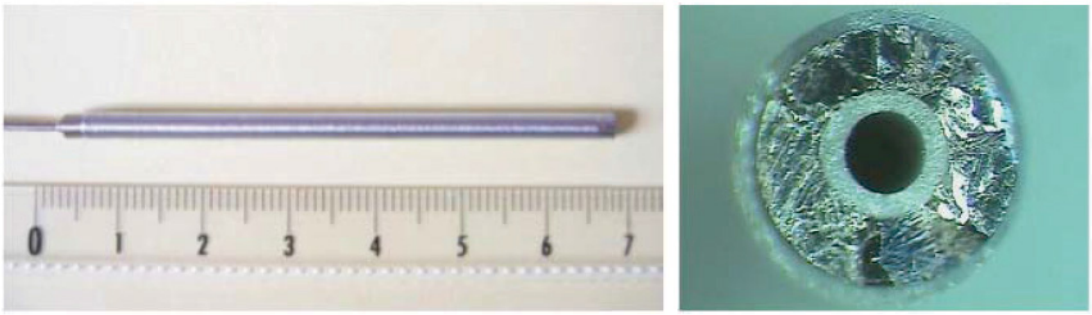

Figure 3-5. Tubular bismuth SPGD developed by SCK•CEN and CEA.

ment wires were HfO_2 insulation and Nb or Ta sheaths. Investigations to quantify the thermoelectric response of a loose-assembly Mo-Nb thermocouple found that its emf in its intended temperature range (1000 to 1600 °C) is of the same order as commercially-available high-temperature Type C or S thermocouples.

Thermal stabilization of these thermocouples was also investigated. Candidate heat treatments to stabilize grain growth to minimize drift during high temperature use were evaluated using long-duration high-temperature out-of-pile tests. Reference 19 reports that these thermocouples were drifting at a rate somewhat lower than 0.02 °C/h at 1100 °C. After 5000 hours, this would result in 100 °C or 10% drift, which is higher than observed in the INL long duration evaluations at 1200 °C of their doped Mo/Nb alloy High Temperature Irradiation Resistant ThermoCouple (HTIR-TCs) discussed in Section 5.

References 31 and 32 reported plans for an in-pile high-temperature qualification irradiation of these thermocouples in the OSIRIS reactor. Some reports[34] suggested that there were plans to irradiate these thermocouples in the High Flux Reactor (HFR) as part of CEA's gas reactor research program and that more recent efforts are exploring the use of doped Mo/Nb-alloy thermoelement materials.[34] However, recent references[12, 14, and 15] indicate that no in-pile qualification of these thermocouples has been performed.

3.1.4. In-Pile Noise Thermometry

The thermal motions of the atoms and charge carriers within an electrical resistor generate a broad-band electrical noise signal across the resistor. The noise power generated, called Johnson noise, is proportional to the absolute temperature of the resistor. Noise thermometers provide a signal proportional to the thermodynamic temperature that is independent of the probe material properties and hence of the environmental conditions that may affect them. In particular, the signal of a noise thermometer should not be affected by nuclear irradiations.[35,36] Although experience indicates that signal processing for this sensor is complicated and more expensive than required for thermocouples,[37] this sensor does not require calibration. Hence, CEA is exploring noise thermometry as a method for calibrating and recalibrating thermocouples in-pile.

Figure 3-6 shows a "hardened" mixed thermocouple noise thermometry (TC-NT) probe developed by CEA.[15] Out-of-pile tests and characterization of the probe (at temperatures up to ~400 °C) and its data acquisition and processing system provided by the Forschungszentrum Jülich (Germany) have been completed. Recent reports do not indicate when irradiation qualification of this probe will occur.

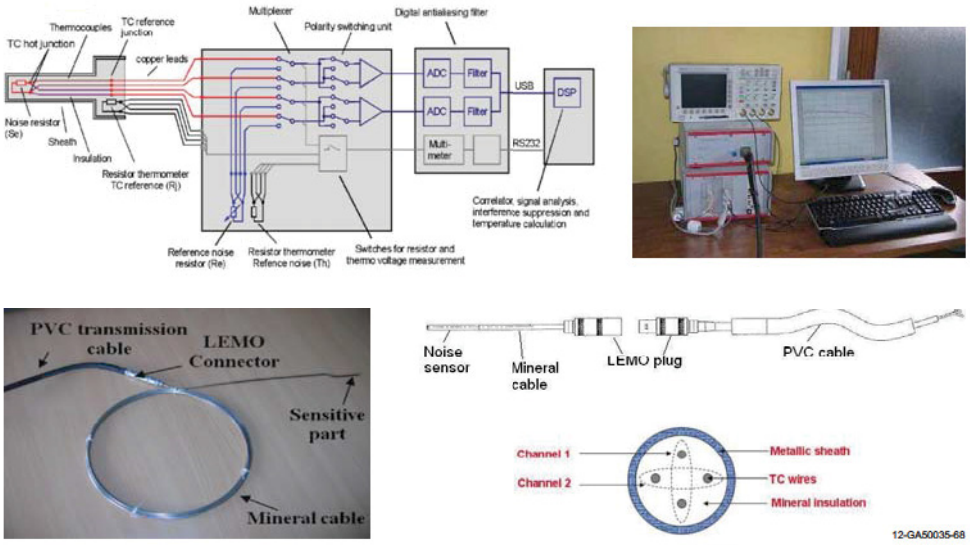

Figure 3-6. Photo and schematic of TC-NT probe developed by CEA.[15]

3.1.5. In-Situ Calibration of Thermocouples

CEA is also participating in a Joint Research Center (JRC) project effort to use fixed point μ-cells for in-situ calibration of thermocouples. As reported in Reference 15, copper and three high temperature metal carbon eutectics with melting temperatures ranging from 1084 to 1492 °C are proposed for use. These μ-cells, which are approximately 1 cm diameter by 1.5 cm long (see Figure 3-7), would be incorporated into irradiation test rigs. High temperature tests have demonstrated the viability of this technique, but references did not indicate when in-pile demonstrations were planned.

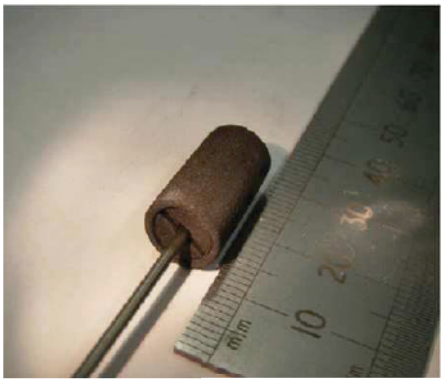

Figure 3-7. Proposed self- calibrating thermocouple design containing a Type C thermocouple with Mo sheath and HfO_2 insulation immersed in a Co-C fixed-point μ-cell.

As proposed in Reference 39, this on-line calibration technique requires some assumptions. The theoretical value of the melting temperature can be affected by the irradiation process. Pure metals and alloys must be carefully enclosed to avoid contact with the corrosive atmosphere and preferentially have low activation characteristics to make them useful for long term irradiation. The mini-cells will need to be located in areas with a homogeneous temperature, neutron flux and gamma radiation field.

3.1.6. Improved LVDTs and DGs

CEA and the IFE/HRP have collaborated on an effort to improve the performance of LVDTs. Since 2005, LVDTs fabricated by IFE-HRP have been used in the OSIRIS reactor with accuracies of ±4 µm and displacements up to ±15 mm (total range) and ± 6 mm (linear range). During 2007, CEA performed a series of out-of-pile tests to characterize and try to improve the performance of these LVDTs and diameter gauges (DGs) based on LVDT sensors. CEA investigations were focussed upon:

- Quantifying usable LVDT temperature range
- Quantifying maximum LVDT measurement range
- Developing the most appropriate LVDT signal correlation versus measurement ranges
- Developing post-test appropriate LVDT adjustments (Gain – Phase)

Tests were conducted at room temperature and at higher temperatures (up to 380 °C) in inert gas, water, and sodium potassium conditions

As part of this effort, CEA proposed several improvements to LVDT designs currently manufactured by IFE/HRP. First, to extend their measurement range, CEA requested that a polynomial equation be used to characterize the signal of LVDTs procured from IFE/HRP. Second, CEA requested that IFE/HRP develop a 'fifth wire' or "self compensating electronics setup." Figure 3-8 illustrates the wiring used for such a setup (compared to the standard 4-wire setup that only uses the wires labeled 1, 2, 3, and 4). In this configuration, wire 3 and 4 are Type K "B" thermocouple wires and Wire 5 is a Type K "A" thermocouple wire. In a 4-wire configuration, only the voltage difference between the two secondary coils is measured. Hence, the voltage output is proportional to the core displacement, or

$$Displacement = G \cdot (V_{C1} - V_{C2}) \tag{9-1}$$

where G is the gain, and V_{C1} and V_{C2}, represent the voltage of coils 1 and 2, respectively. In the 5-wire setup, the additional wire is connected as a zero reference between the two secondary coils. Hence, the ratio between the two secondary coils is used to estimate the displacement, using

$$Displacement = G \cdot \frac{(V_{C1} - V_{C2})}{(V_{C1} + V_{C2})} \tag{9-2}$$

Theoretically, the influence of global changes in the system will have negligible effect on the system because the resulting signal is a ratio. For example, this setup offers several potential improvements:

- improved linearity
- suppression of temperature sensitivity
- suppression of signal aberrations in its central area
- suppression of nickel Curie temperature effects (although experimental confirmation required)
- suppression of signal shift due to irradiation (although experimental confirmation required)

In particular, the ratio of signals from the secondary are used to quantify elongation rather than the combined secondary signal. As long as the LVDT is at a uniform temperature, the signal should be more accurate (because it is no longer susceptible to Curie temperature effects). However, experience indicates that the LVDT is not often at a uniform temperature.

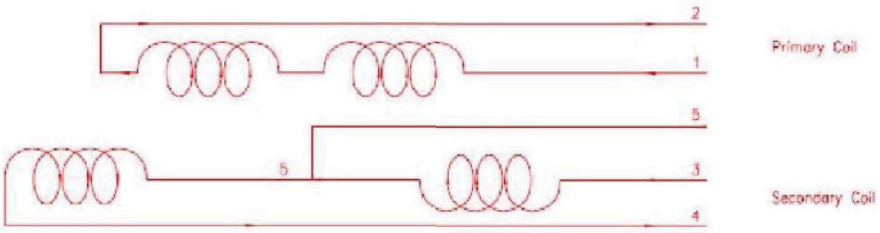

Figure 3-8. Wiring schematic for LVDTs using the five-wire method.

References 15 and 40 report that an in-pile application of the improved LVDT and associated diameter gauges (which relies on LVDT-based technology as discussed in Section 3.3.5) will be evaluated using the Mechanical Loading Device for Irradiation Experiments (MELODIE) test rig. This test rig, which was developed in collaboration with VTT (Finland) and IFE/HRP, is currently undergoing laboratory testing. Irradiations in the OSIRIS reactor are also planned to occur in 2014. Ultimately, this test rig will be deployed in the new JHR.

As shown in Figure 3-9, the MELODIE test is designed to provide real-time elongation and diameter change data from an in-core irradiation of a pre-oxidized PWR fuel cladding tube (90 mm in length) at 350 °C irradiated at peak fast neutron fluxes as high as 4.5×10^{14} n/cm^2-s (E >0.1 MeV) and nuclear heating up to 9.5 W/g.

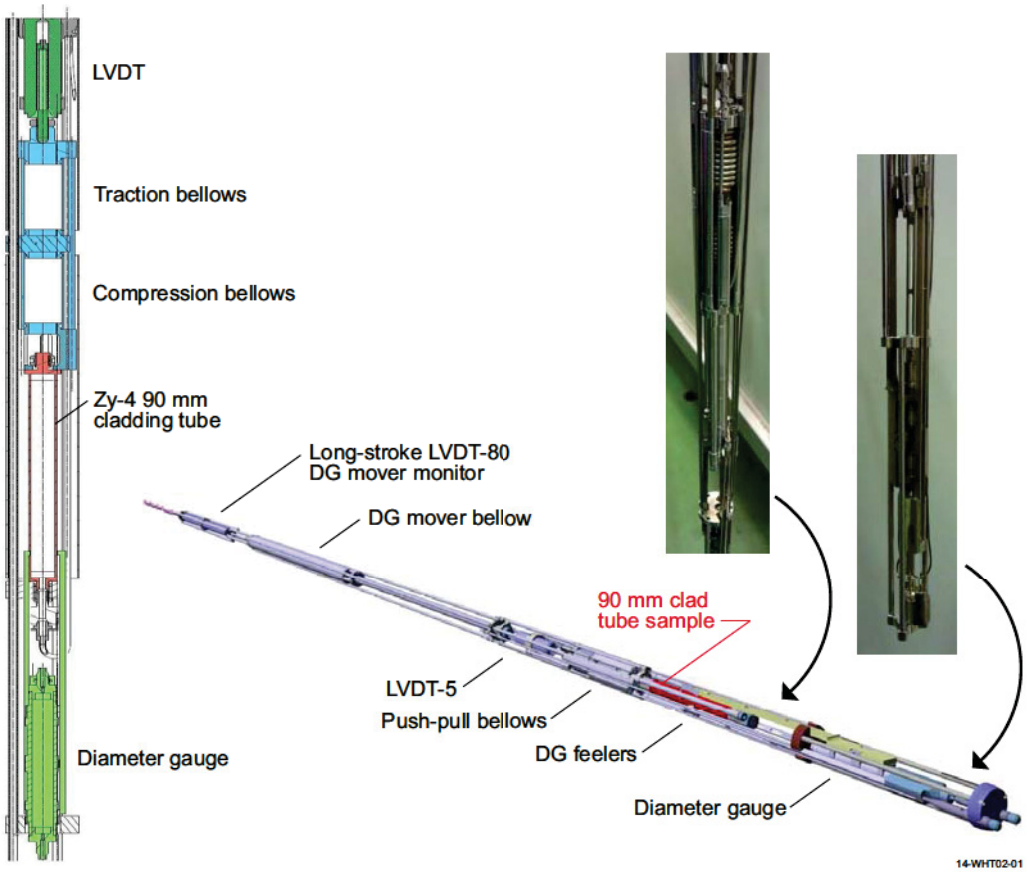

Figure 3-9. MELODIE test rig with individual components.

The MELODIE sample holder is a miniaturized biaxial testing machine. Its length of 1.60 m and diameter of 23.5 mm allows it to be deployed in a CHOUCA hosting device, a sodium-potassium filled double-walled container that is a standard testing device for in-core irradiations of materials in the OSIRIS reactor. Full-control of stress and biaxiality is performed in the MELODIE sample holder, by three independent high pressure helium circuits.

Figure 3-10 shows a schematic of the MELODIE closed helium loop and pressure control circuitry. The objective of the MELODIE closed helium loop is to feed four digitally controlled circuits used to pressurize the specimen, the push-pull bellows, and (at lower pressure) the DG actuator. The 160 bar design pressure of the specimen pressurization system translates to about 117 MPa hoop stress and 55 MPa axial stress for a sample that is the size of standard PWR fuel cladding. The push-pull pressurization systems apply positive or negative axial stress sample.

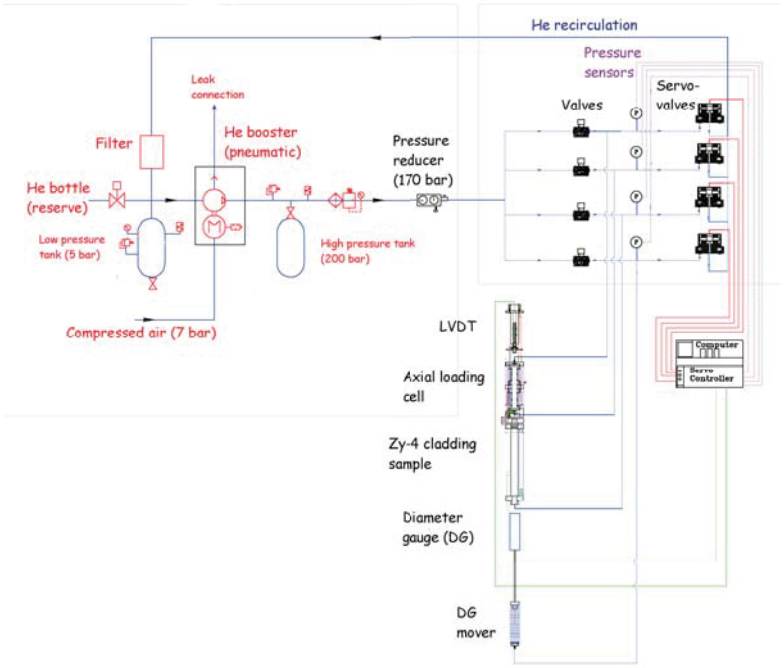

Figure 3-10. Schematic diagram of the MELODIE closed helium loop and pressure control circuitry

Two measurement systems, tailored by the IFE/HRP to MELODIE flux and dimensional requirements, are used in order to obtain the biaxial strain information:

- The elongation of the 90 mm-long clad specimen is measured with an enhanced self-compensating LVDT, that has been slightly modified for operation under OSIRIS high nuclear heating conditions. Laboratory tests in CEA Cadarache showed a 2σ repeatability of 3 µm for this device.
- The diameter of the specimen is acquired along the lower half of the specimen by an electromagnetic Diameter Gauge, modified in collaboration with IFE/HRP to be compatible with the small (24-mm) diameter and higher accuracy measurement requirements for MELODIE.

To avoid unwanted thermal interaction between the feelers (2 reference feelers and one movable) and the specimen, the system is parked at the bottom end of the specimen, where a self-calibrating zone, which is read at the beginning of each scan, allows the system to discard unavoidable drifts due to thermal effects

(expansion or deformation) or ageing.

Both experiments showed that pressure of the feelers has to be carefully chosen to ensure good contact without wearing the surface of the zircaloy. The following measures were taken to improve accuracy of this system:

- Specimen surface is reinforced by a 0.9 µm oxide layer, obtained by heating at 400 °C for 1 week
- Feeler "pressure" was reduced to ~0.2 N,
- Feeler pressure is created by counterweights, making it more stable than if created by springs

In case of a creep experiment like MELODIE, the uncertainties and drifts associated with spring-loaded systems compared to counterweights were amplified by the fact that the measured diameter increases with time significantly, compared to the resting position. Thus, the pressure on the feelers at the end of the experiment could be about twice the initial value, regardless of other reasons of drift.

Several types of laboratory evaluations were completed to evaluate this system. Endurance tests (of at least 1000 scan sequences) to assess accuracy and the reduction in diameter of the specimen associated with wear from the feelers. Results indicate that over 1000 tests are possible but after 1100 scans, the specimen diameter had been reduced by 14 µm. Accuracy and repeatability tests were also completed. Results indicate that diameter gauge signals were accurate to within ± 2µm. As noted in Reference 40, MELODIE test rig performance evaluations are nearly completed. Safety reviews for insertion into the OSIRIS reactor are underway, and it is planned to conduct irradiation testing in 2014.

3.1.7. Fission Gas Release

In-situ measurement of the composition and amount of fission gas release is particularly important in fuel rod irradiations because fission gas release kinetics is an important indicator of nuclear reactions and its measurement is key in fuel performance studies. To address this need, CEA is investigating "counter-pressure" and acoustical measurement techniques.[20]

Figure 3-11 shows the counter-pressure sensor used by CEA to detect the pressure associated with fission gas release from a fuel rod during irradiation. It consists of two gas cavities separated by metallic bellows, as shown in Figure 3-11.[19,41,42] The first cavity communicates with the internal fuel rod pressure. The second cavity is connected to an external helium circuit, which is called the "counter-pressure" circuit. The imbalance between the internal rod pressure and the counter-pressure is detected by two electric contacts, activated by the motion of the bellows. This sensor has been qualified in OSIRIS irradiations. Results indicate that this sensor, which is now operational in OSIRIS, has an accuracy of ±0.32 bar over its pressure range (up to 120 bars). Efforts are underway to design and manufacture an enhanced counter-pressure sensor for high-pressure measurements (up to 250 bar).

A dedicated acoustic sensor containing a piezoelectric PZT (Lead Zirconate Titanate) transducer has been developed to measure online fission gas release pressure and composition in a fuel rod during irradiation experiments. Figure 3-12(a) illustrates some of the details related to the design of this acoustic fission gas release sensor.[20,43-50] This assembly is composed of a small cylindrical cavity containing the gas to be analyzed. The upper part of the cavity is closed by a thin stainless steel plate. The piezoelectric transducer is fixed on this plate, in order to generate and measure acoustic waves, through the plate, in the gas cavity. Wires are directly welded on the piezo-ceramics electrodes. Acoustic waves propagate in the gas inside the cavity (diameter 10 mm and length 12.5 mm) which is connected to the fuel rod plenum. The measurement

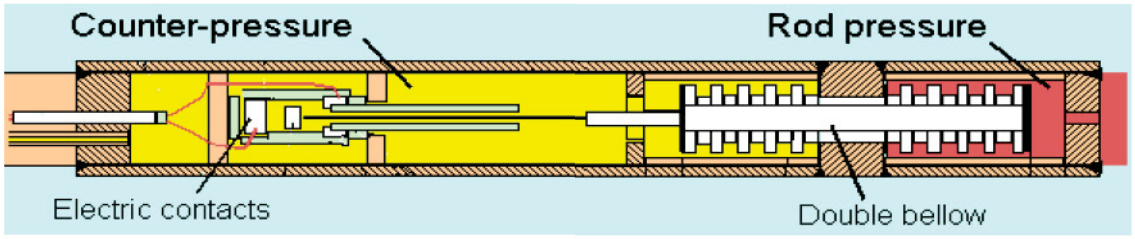

Figure 3-11. CEA counter-pressure sensor for detecting fission gas release amount.

of the reflected waves allows assessment of the acoustic impedance of this system [see Figure 3-12(b)]. The signal and its echoes are recorded, and the time of flight of the signal and its attenuation are measured. From these measurements, it is possible to deduce simultaneously the molar mass of the gas (from the acoustic waves velocity) and the pressure of the gas (from the echoes attenuation). The online assessment of these two parameters is then used to obtain information regarding the fraction of fission gases released in the fuel rod.

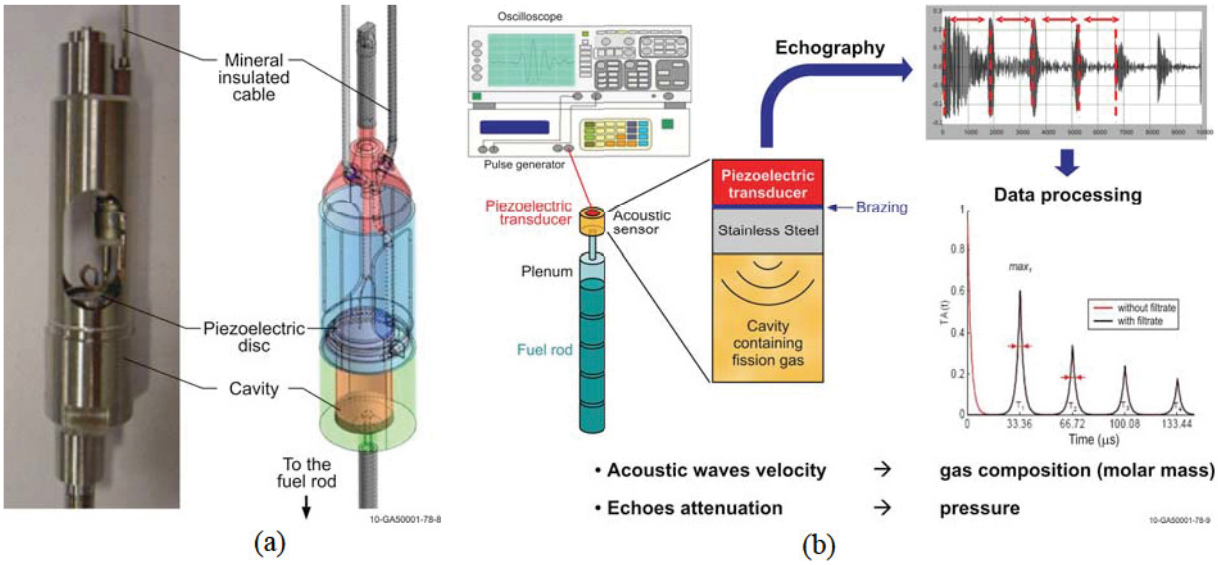

Figure 3-12. CEA fission gas pressure and composition detection (a) sensor and (b) system operation.

After laboratory testing of acoustic sensor prototypes was completed, its performance was evaluated at OSIRIS on a pre-irradiated high burnup mixed oxide PWR fuel rod in the 2010 REMORA-3 irradiation experiment. As shown in Figure 3-13, instrumentation installed on this fuel rod included the acoustic gas sensor, a type C thermocouple, and an acoustic gas sensor. Results indicate that the PZT experienced degradation due to high fluences to which it was exposed [total gamma dose of 0.25 MGy, and thermal fluences of 3.5 $x10^{17}$n/cm²). However, CEA used a differential signal processing method to extract gas composition data (see Figure 3-14). Reference 48 indicates that post-irradiation evaluations would be completed to compare data obtained during the irradiation with gas compositions present in at the end of the irradiation using mass spectrometry. However, results from such evaluations were not found in the literature reviewed.

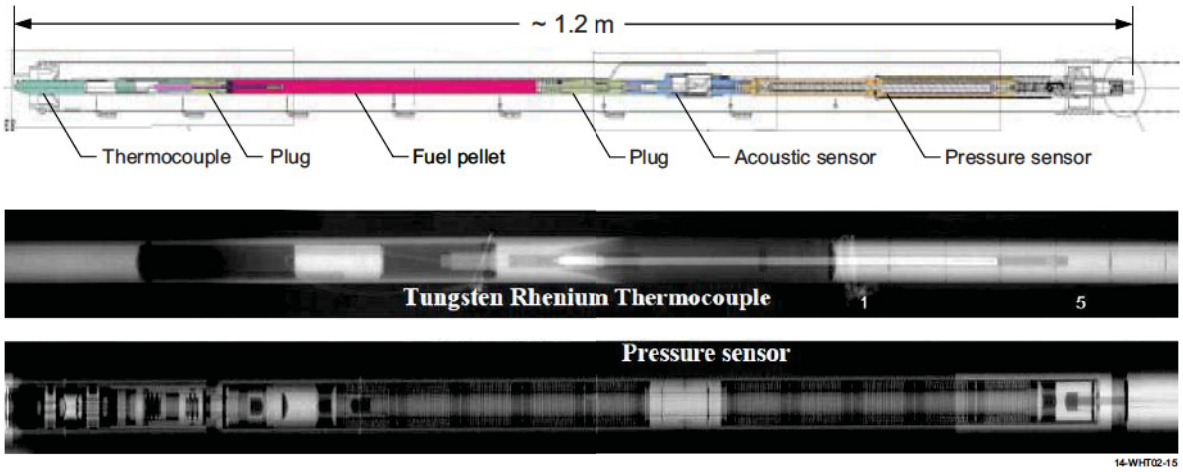

Figure 3-13. Instrumentation installed on fuel rod and neutron radiography of the thermocouple and counter balance pressure sensor for the REMORA 3 irradiation.

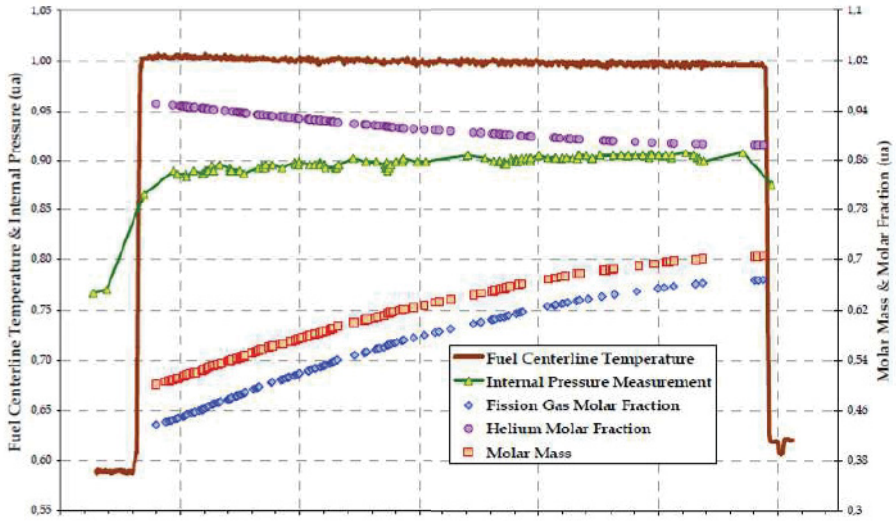

Figure 3-14. REMORA-3 data included fuel centerline temperature, internal pressure, fission gas and helium molar fractions and molar mass histories.

3.1.8. Localized Heating

Nuclear heating inside an MTR has to be known in order to predict the sample temperatures reached during an irradiation experiment and also for safety reasons, to demonstrate that components will not exceed material thermal limits. CEA has also pursued calorimetric techniques for local power measurements.[51]- [55] Accurate measurement of this parameter is important in the OSIRIS reactor, where nuclear heating is approximately 13 W/g. However, it will be more important to quantify this parameter in the JHR MTR, which is anticipated to have a nuclear heating rate of 20 W/g when the reactor is at full power (100 MWt). Calorimeters currently used to measure local power in OSIRIS consist of two pairs of aluminum cells, fixed onto the same aluminum base. The cells of each pair are similar except that one contains a

graphite sample and the other a corresponding volume filled with nitrogen (See Figure 3-15). The two pairs of cells are diametrically opposed on the same aluminum base in order to avoid any gradient effect. The entire structure is enclosed inside a tube in contact with external water flow for heat removal. The pedestal between the upper part of the cell and the base in contact with the external sleeve is a thermal resistance through which the deposited energy inside the cell is transferred. The energy deposit is calculated using a calibration curve obtained from experiments with different electric energy inputs and measured temperature differences between empty and full cells located at the same axial position along the core height. Note that the heating rate unit (W/g) is written as W/g (C) to emphasize the fact that the sample is graphite. Original devices for OSIRIS in-core measurements consist of five different calorimeters (each one made of four cells), positioned along the core height leading to five measurement points, from which the heating profile curve is fitted. Even though these calorimeters are reliable, they have inherent drawbacks, associated with their static nature.

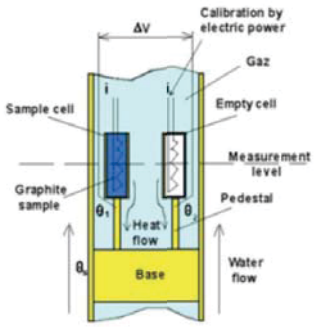

Figure 3-15. Calorimeter design currently used in OSIRIS.

To overcome drawbacks associated with the differential method, a new system, CALMOS, has been developed and tested in OSIRIS. The key point of this new device is to put only two cells (one empty and one equipped with the graphite sample) coaxially inside a same external sleeve and then to move the probe using a displacement system. Hence, this new system is able to measure the heating rate data at any level in the core and determine more accurately the heating profile inside and above the core.

This new CALMOS design includes several new features. Specifically, it:

- allows continuous axial heating rate distribution measurements instead of selected point values,
- extends measurements to locations above the core, where heating levels are sufficiently high that they must be taken into account to design any new experimental device,
- reduces the irradiation aging of the cells. The probe is exposed to the irradiation field only during measurement periods. As a consequence, the aging of heater wires is limited, and calibrations can be performed during the whole calorimeter life for periodic verifications,
- facilitates point measurements because of the small size of the calorimeter (18 mm),
- minimizes radial gradient effect in the probe vicinity (e.g., coaxial configuration and smaller size).

Two identical cells are included in the CALMOS conceptual design shown in Figure 3-16. The upper cell (the sample cell) contains a graphite specimen, whereas the lower cell (the reference cell) is empty. Each cell is surrounded by a gas gap (nitrogen) and located on a base surrounded by a stainless steel external tube in contact with the reactor coolant flow. A thermocouple (Type K) is embedded on the top of each

pedestal (hot temperature), whereas a second one is located on the external surface of the aluminum base (cold temperature). Two heating elements, made of constantan wire embedded in alumina, are inserted inside the cells, thus allowing the calorimeter's calibration. The calorimeter works in a continuous mode, i.e., the energy deposit in each cell is flowing through the pedestal and then through the external sleeve. The temperature difference "ΔT_{sample}" is proportional to the energy deposit in the graphite and cell structure; whereas "$\Delta T_{reference}$" is proportional to the deposit in the empty cell structure. Therefore, in a first approximation, the "$\Delta T_{sample} - \Delta T_{reference}$" quantity ($\Delta\Delta T$) is proportional to the energy deposit inside the only graphite sample. This new nuclear heating measurement method has been patented by CEA.[55]

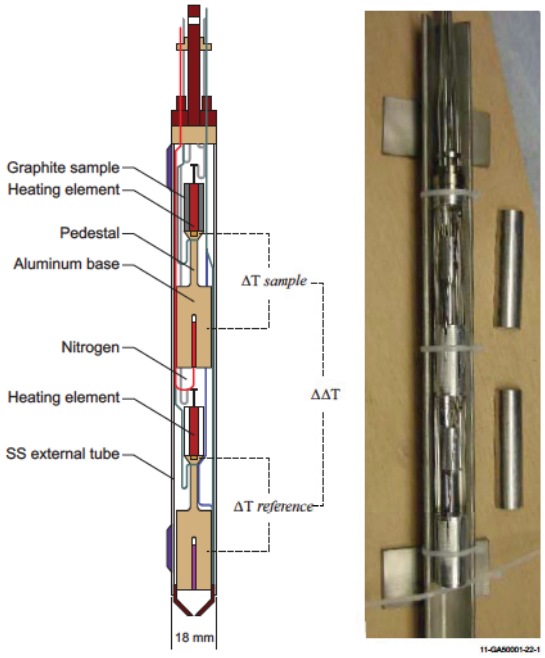

Figure 3-16. CALMOS schematic (a) and prototype (b).

The following functional criteria were defined for CALMOS:

- a large sensitivity range is needed to be able to perform measurements above the core down to 0.1 W/g (C) and inside the core up to 13 W/g (C) [As noted previously, the heating rate unit (W/g) is written as W/g (C) to emphasize the fact that the sample is graphite].
- the cell external diameter is limited to 18 mm in order to be able to insert and move the calorimetric probe inside an external sleeve representative of OSIRIS standard experimental devices.
- the overall probe length should not exceed 220 mm compared to the core fissile height (630 mm).
- good linearity of $\Delta\Delta T$ [$\Delta T_{sample} - \Delta T_{reference}$] versus heating rate in the range of 0.1 to 13 W/g (C) is required. A maximum of 20% from linearity for 13 W/g (C) was set for the design.
- the highest temperature inside the cell structure should not exceed 500 °C in order to have a significant margin with respect to the aluminum melting point.

Key geometric parameters of both cells are the height and diameter of the aluminum base, height and diameter of the pedestal, and height and diameter of the upper part of the cell determining the sample volume. During the design effort, a trade-off had to be found between thermal optimization and technological constraints. Main structural evolutions during the design phase led to the addition of polished stainless

steel screens to limit radiative losses. Furthermore, a highly conductive aluminum alloy (230 W/m-°C) was selected to decrease the peak temperatures of the sensor. As discussed in Reference 53, the calorimeter must be calibrated prior to deployment. A 'calibration coefficient', K, is defined to consider phenomena, such as the remaining radiation heat transfer losses and the temperature dependence of thermal conductivity of the filler gas and the aluminum in the calorimeter cell.

A CALMOS prototype with the displacement system required to move it within the OSIRIS reactor is also shown in Figure 3-17.[15] Additional details about this displacement system are discussed in Reference 53. CALMOS is now operational in OSIRIS and will be adapted for commissioning tests and operation (the CARMEN device discussed in Section 3.1.1) in the JHR.

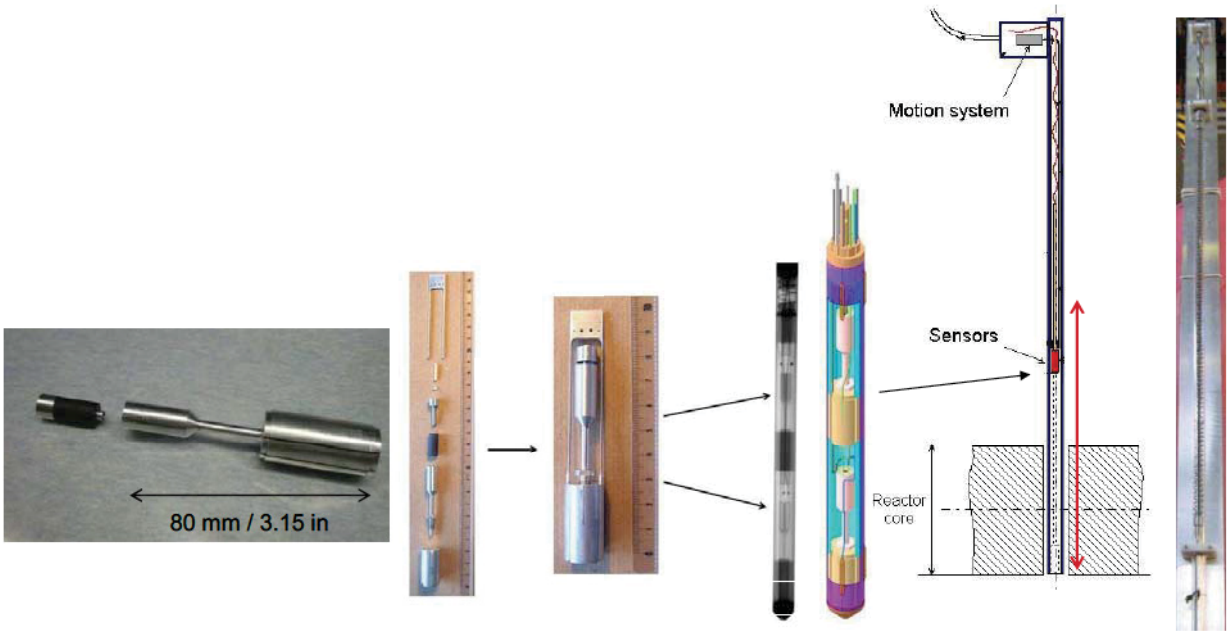

Figure 3-17. CALMOS device deployed in OSIRIS.

3.2. SCK·CEN

In support of their BR1 and BR2 reactors in Belgium and to facilitate irradiations at other nuclear reactors, SCK•CEN continues to perform research in the areas of in-pile instrumentation development, evaluation, and fabrication.[22] Selected projects currently investigated by SCK•CEN are summarized in this section. As noted in Section 3.1, many SCK•CEN instrumentation development efforts are collaborations with CEA and some SCK•CEN efforts may be found in Section 3.1. In particular, it should be noted that SCK•CEN has played a key role in the development and deployment of the fission chambers described in Section 3.1.1 and the development of the SPGD with a bismuth emitter described in Section 3.1.2. In addition, the high neutron fluxes in the BR2 also encourages other international collaborations. For example, Section 3.2.2 describes a collaboration with Technical Research Center of Finland (VTT) that allows in-pile tensile testing with sensors to detect the load applied to the specimen and the elongation of the specimen.[56]

3.2.1. Fiber Optic Testing

MTRs could benefit from advantages offered by fiber-optic communication and sensing systems. However, the deployment of such systems in nuclear environments has been limited up to now, mainly due to reliability constraints. Prior investigations[57,58] have shown that the lifetime of fiber-optic components depends on the fiber composition, the temperature, the total dose, and the operating wavelength. Radiation (gamma and neutron exposure) affects the optical transmission of silica by creating various point defects of different nature that absorb light at specific wavelengths.[59,60] This Radiation-Induced Absorption (RIA) is particularly strong in the ultraviolet (UV) spectrum, which limits the fiber applicability to a very low dose (typically less than 10 -100 Gy) over short fiber lengths. Compared to the UV spectrum, fiber-optic transmission in the visible spectrum is less critical, but transmission can still remain a concern (especially for long fiber paths) due to the formation of an absorption band at 600 nm.

Optical absorption (< 0.5 dB/m at 630 nm) has been demonstrated in aluminum-coated fibers irradiated with γ-rays up to 6 MGy[60] and <5 dB/m under fission reactor irradiation up to ~20 MGy and neutron fluence (E_n > 0.1 MeV) of 5 x 10^{17} n/cm^2.[61,62] At the higher dose regimes encountered in MTRs, optical fiber use is possible for wavelengths above 800 nm. Previous in-core reactor experiments carried out in MTRs in Europe and Japan demonstrated that RIA can remain limited to a few dB/m in the 800 to 1100 nm range even after intense irradiation up to the GGy level and 10^{19} n/cm^2.[63,64,65]

Such RIA in the near infrared spectral region opens perspectives for the development of new types of in-core reactor instrumentation based on optical fiber sensor (OFS) technology.[66-69] OFSs offer attractive and unique sensing capabilities that are of particular benefit for MTR measurements. The major advantages are the capability for passive remote sensing with the potential for high accuracy and operation at high-temperature (500–1000 °C). In addition, OFSs feature capabilities for distributed sensing with extremely limited intrusiveness. Low intrusivity is especially important, not only because of limited space availability but also because small sensors will not disturb the temperature and radiation profile of the material under study.

As part of a collaboration between CEA and SCK•CEN, a program is underway to develop OFS sensors for measuring dimensional changes on nuclear materials irradiated in MTRs.[67,68] As part of this effort, the COSI experiment was completed in which the single mode (SM) and multimode (MM) optical fibers listed in Table 3-2 were irradiated during 2006 in the OSIRIS reactor for 92 days (corresponding to a thermal fluence of 10^{21} n_{th}/cm^2 and a fast fluence of 10^{20} n_{fast}/cm^2, and a calculated gamma dose rate of 7.2 x 10^6 Gy/hr, with an integrated ionizing dose of 16 GGy). This duration, which corresponds to representative conditions during a typical materials irradiation program, is over an order of magnitude increase than other tests reported in the literature.

Table 3-2. Single mode and multimode optical fibers tested in OSIRIS COSI test.

Fibers	Manufacturer	Manufacturer Designator (SM or MM)	Core/Cladding Diameter	Coating
FORC1 FORC2 FORC3	Fiber Optic Research Center (Moscow)	-/SM	~10 µm/150 µm	acrylate
B11 B13	Blaze Photonics (Cristal Fiber)	HC 1060-02/SM	9.7 µm (hole)/125 µm	acrylate
STU1 STU1	Polymicro	FIP100.110.125 STU//MM	~100 µm /110µm	polyimide
FIL1 FIL2	Polymicro	FIP100.110.150 /MM	~100 µm /150µm	aluminum
FVL1 FVL2	Polymicro	FIP100.110.150 /MM	~100 µm /150µm	aluminum

As shown in Figure 3-18, the fibers were mounted onto an aluminum plate and placed in a 2 mm internal diameter stainless steel tube. The fibers made a loop with a bend radius of either 23 or 32 mm. The fluence was measured using an SPND. Although placed in the periphery of the core, the central part of these 40 m fibers was close to the reactor core. Results from this test indicate that there are SM and MM optical fibers with acceptable losses for testing in MTRs. As shown by results in Figure 3-19, the most favorable spectral region (with reduced RIA) lies in the 800-1200 nm range. With measured radiation-induced losses below 10 dB, the COSI experiment confirmed that there are multimode and single-mode fibers of acceptable behavior to develop OFSs to work in the harsh nuclear environments found in MTRs.

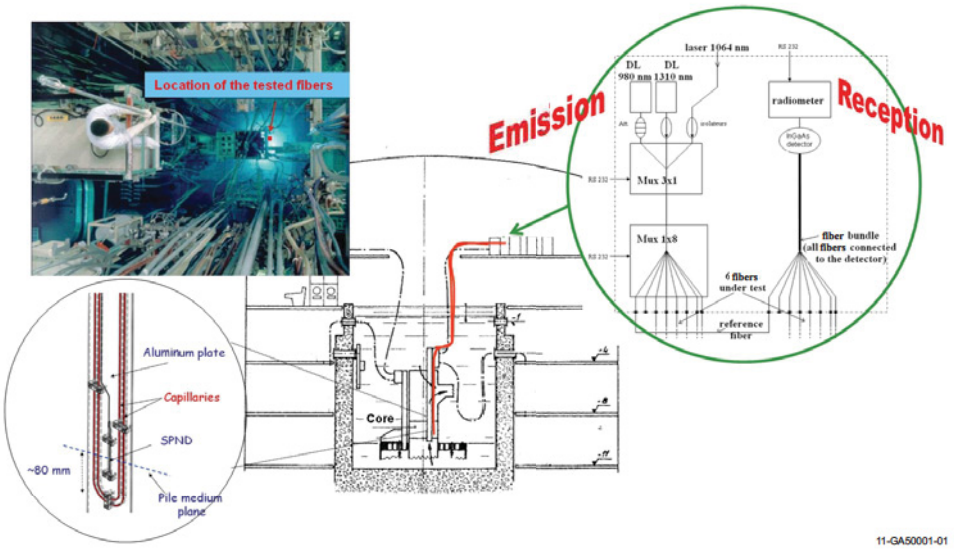

Figure 3-18. COSI test rig setup.

To address concerns about degradation of fiber optic mechanical properties, SCK•CEN also tested four standard telecom acrylate-coated Ge-doped single-mode fibers from three different manufacturers and one acrylate-coated Ge-doped multi-mode fiber. Fiber samples of 50 m were loosely coiled with a diameter of 60 mm and exposed to a dose rate of 27 kGy/h up to a total dose of 15 MGy at an ambient temperature of approximately 55 °C. Several mechanical tests were performed before and after irradiation,

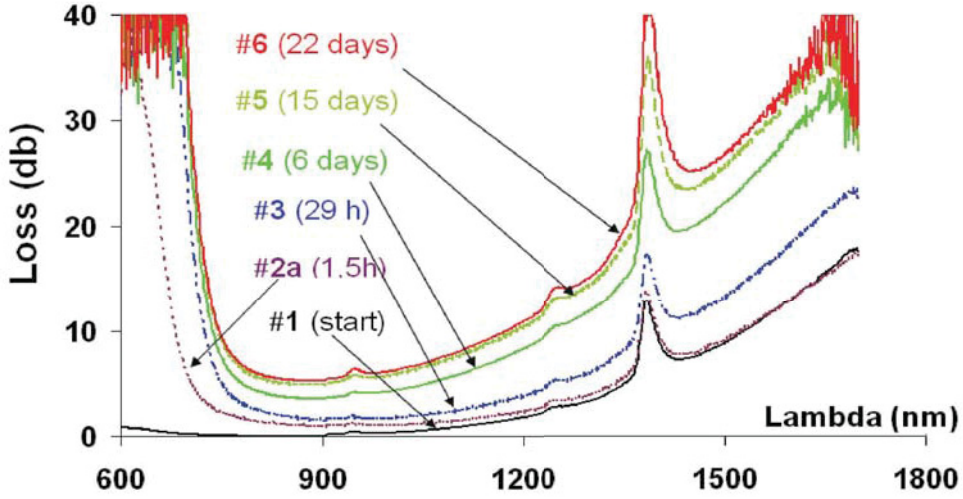

Figure 3-19. Representative results from COSI- Change in loss for the STU2 fiber (22 days corresponds to 3 x 10^{20} n_{th}/cm^2 and 3 x10^{19} n_{fast}/cm^2).

including a two-point bend test. These destructive two-point bend tests allow quantification of the fibers' strength (50% failure stress) and the dynamic fatigue factor. Weibull analysis revealed a strength reduction of about 50% at these MGy dose levels. Scanning Electronic Microscope (SEM) images of fiber samples, which had their coatings removed after irradiation, suggest that 'roughening of the outer glass surface' may cause this degradation. These results indicate that the long-term mechanical strength of optical fibers could be seriously affected when exposed to MGy dose levels.

Figure 3-20 shows a fiber-optic based sensor jointly developed by CEA and SCK•CEN for detecting elongation of material samples during irradiation. This sensor is based on an extrinsic Fabry-Perot (FP) interferometer using a radiation-resistant pure silica core fiber; a cavity is positioned at the end of the fiber and sets an optical path difference (OPD) that can be modulated by the external actions such as sensor elongation. This OPD gives rise to a characteristic optical interference pattern from which the cavity length can be retrieved by signal demodulation. The signal of this miniaturized sensor (outer diameter is about 250 µm) gives the absolute length of the cavity, which is mechanically linked to the sample elongation. This small diameter (less than 2mm) sensor takes advantage of the advantages associated with optic fiber sensors such as high resolution, easy remote sensing and multiplexing, and compact size which is of particular interest for in pile experiments. In addition, the small weight of this sensor reduces thermal effects associated with gamma heating effects. Laboratory tests have demonstrated a good accuracy, less than 1% error over a displacement of 100 µm at room temperature.

Prior to irradiation testing, improvements were made to minimize the consequence of radiation-induced silica compaction and to refine the fixing technique.[57,67,68] Irradiation testing of this sensor was performed in the SMIRNOF-7 experiment in the BR2 during 2012.[15] During this test, temperatures remained below 150 °C. The integrated fast neutron fluence of 2.5 x10^{19} n_{fast}/cm^2. Results indicate drifts that are a factor of 10 smaller than with commercially-available FP sensors.

Current CEA and SCK•CEN efforts in this area[58,68] are focussed on improving the robustness of this FP elongation sensor and on developing and evaluating a prototype of a Michelson type displacement sensor. Recent accomplishments include:

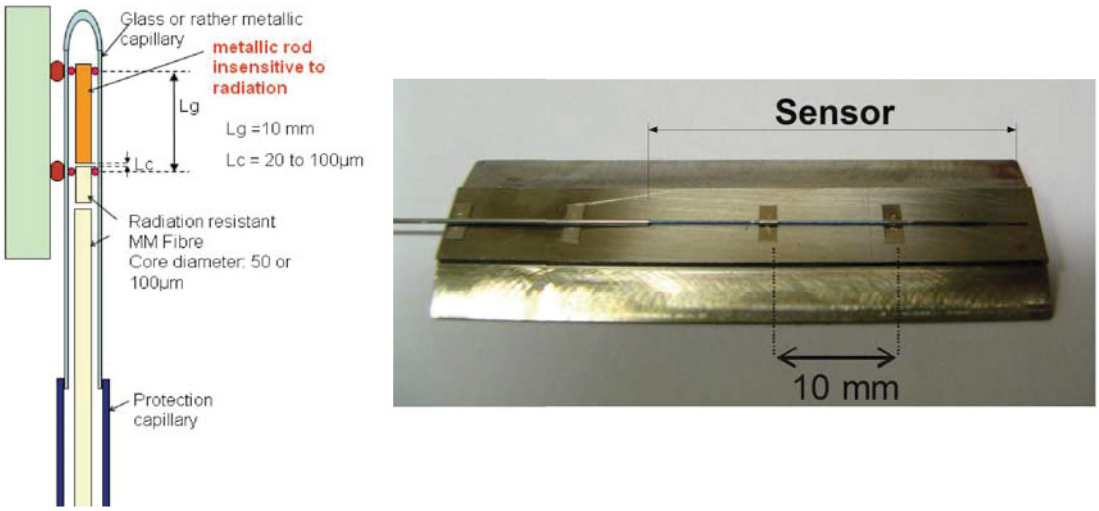

Figure 3-20. Optical fiber based elongation detection sensor developed by CEA and SCK•CEN.

- An enhanced FP design was modified to allow its use at higher temperatures by employing enhanced sealing techniques with a higher temperature optical fiber with an aluminum coating. In addition, the metallic capillary shown in Figure 3-20 was incorporated into the sensor design, and a 1.8 mm diameter sensor (rather than the 0.25 mm diameter used in prior tests) was used to improve robustness. The test rig (see Figure 3-21) featuring this enhanced fiber optics based elongation sensor was subjected to temperatures up to 400 °C in the SMIRNOF-8 test, which was initiated in August 2012 at the BR2.

Figure 3-21. SMIRNOF-8 test rig incorporating fiber optics based elongation sensors.

The six sensors were located in the mid-plane of the reactor core. At that point, for the nominal 59 MWt power, the thermal flux (E<0.5eV) was $1.66 \cdot 10^{14}$ n/cm^2.s and fast flux (E>0.1 MeV) $1.99 \cdot 10^{13}$ n/cm^2.s. The γ dose rate was about 7.2 MGy/h. The total irradiation lasted 27 days, leading to an integrated fluence of about 4.6 10^{19} n_{fast}/cm^2 and 4.5 GGy. A major part of the irradiation was performed at the temperature of 200 °C. At the end of the reactor cycle the temperature was increased up to 395°C for a short period. Results indicate that the sensor survivability was improved. Three of the six sensors exhibited drifts of less than 4 µm for the ~200 µm cavity at the end of the first cycle. However, the drift of Sensor 4 increased more than 50 µm during irradiation

at lower temperatures (see Figure 3-22). Hence, additional work is needed to improve sensor robustness.

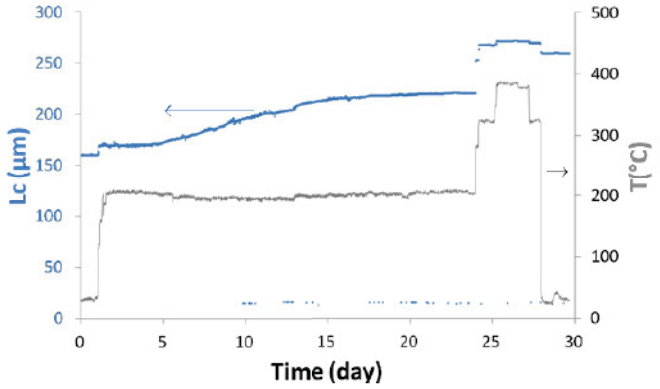

Figure 3-22. Cavity length L_c of Sensor 4 during SMIRNOF-8 irradiation. Drift increased more than 50 µm during the lower temperature portion of this irradiation.

- The potential of a Michelson type interferometer (see Figure 3-23) was evaluated. This probe, which can be used to measure displacements in a direction perpendicular to the fiber, is of interest in smaller regions where the fiber cannot make a 90° turn. It is more flexible, allowing measurement of larger displacements. A mechanical probe design was developed, and the optical module that will be inserted into the mechanical probe was evaluated in laboratory tests up to 400°C. In this initial design, the fiber and signal conditioner are the same as the ones used with the FP extensometer. Results indicate that the probe can measure displacements with an error less than 10 µm over a 0.5 mm range. Future evaluations will evaluate the performance of an optical module integrated into the mechanical probe. These tests will consider the impact of temperature, vibrations, and irradiation.

3.2.2. In-Pile Tensile Testing

As part of a European Fusion Development Agreement (EFDA), the BR2 has been used to demonstrate the performance of an in-pile tensile test module developed by VTT. As discussed in Reference 56, it is recognized that it is unlikely that the primary damage experienced by a specimen will be affected by the applied stress during irradiation. However, it is believed that the subsequent process of dislocation formation, that is responsible for radiation hardening, yield drop, and plastic flow localization, will be substantially altered by the applied stress. It is speculated that the fatigue lifetime during in-situ cyclic loading experiments may be significantly different from the ones obtained during fatigue experiments on specimens in the post-irradiated condition. Hence, an in-situ material testing system was developed by VTT and used to perform fracture mechanic, corrosion fatigue, tensile, and electrochemical measurements in the BR2.

As shown in Figure 3-24, this test system is based on the use of a pneumatic loading unit, which loads a test specimen using gas to pressurize metallic bellows, and a LVDT from IFE/HRP (see Section 3.3.1) to measure the resulting displacement produced in the tensile specimen. The outside diameter of the module is 25 mm, and the total length of the module with the LVDT is 150 mm. Figure 3-25 shows the actual test

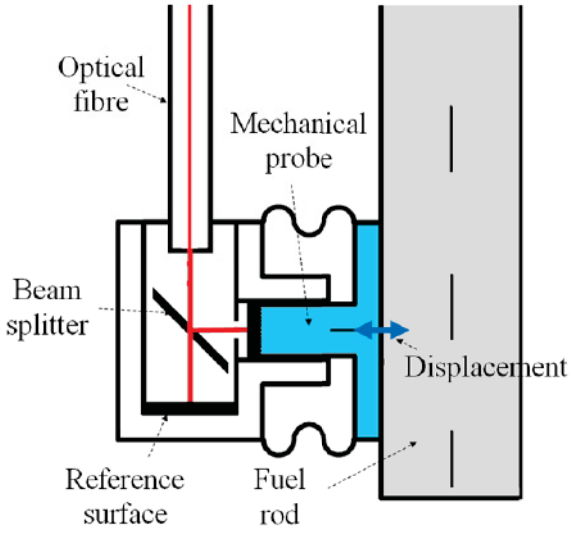

Figure 3-23. Sensor based on a Michelson interferometer for measuring fuel rod swelling.

rig with this module developed by Mol for irradiations in the BR2. During irradiation, the test assembly remained submerged in stagnant demineralized water. For approximately 300 hours, the specimens were exposed to a neutron flux of 3 x 10^{13} n/cm^{2}s (E > 1 MeV) corresponding to a displacement damage rate of ~6 x 10^{-8} dpa/s. The temperature of the test module increased rapidly (up to 90 °C within 15 minutes) due to gamma heating power of 4.4 W/g. Then, the desired strain was applied to the specimen.

The load generated by the pneumatic loading unit with the metallic bellows was calculated from the pressure difference experienced by the bellows. The stiffness and effective cross section of the bellows impacts the load produced by the specimen. However, the 'stiffness' of the pneumatic loading unit differs from the stiffness of the bellows. Hence, VTT developed a calibration unit (see Figure 3-26) to correlate the applied gas pressure in the bellows with the actual load acting on the tensile specimen. A two step calibration procedure was implemented. In the first step, the characteristic stiffness of the bellows together with friction forces of the moving parts of the module were determined. In the second step, the load induced on the tensile specimen by the applied gas was measured by a load cell. Insights from this effort were incorporated into the MELODIE test rig described in Section 3.1.6.

3.3. IFE/HRP

The OECD-sponsored Halden Reactor Project (HRP), which is operated by the Norwegian Institutt for Energiteknikk (Institute for Energy Technology) [IFE], has more than thirty years of experience in performing complicated in-core measurements and experiments in the HBWR using specially-developed sensors.

As listed in Table 3-1, a wide range of in-core instrumentation has been developed, fabricated, and deployed by the IFE/HRP for measuring key fuel and material performance parameters such as fuel temperature, fuel swelling/densification, fission gas release, cladding creep, corrosion/crud buildup, and crack-growth rates.[70-84] Instruments are also available for monitoring the irradiation environment (e.g.,

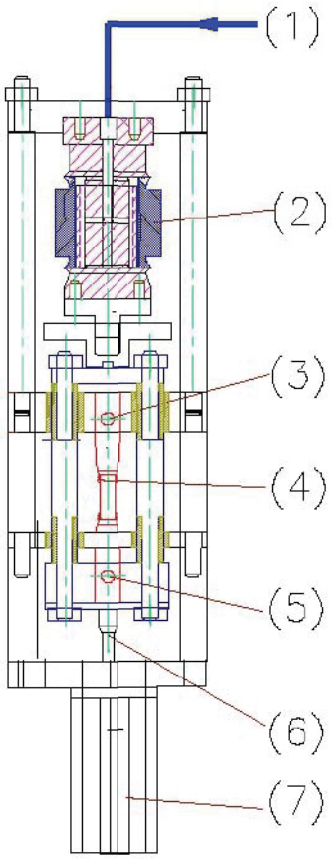

Figure 3-24. Schematic of tensile test module: (1) gas line, (2) pneumatic loading unit, (3) firm specimen fixing point, (4) specimen, (5) movable specimen fixing point, (6) LVDT plunger and (7) LVDT holder.

SPNDs and miniaturized gamma thermometers) and thermal-hydraulic and water chemistry conditions (e.g. flow meters, Electrochemical Corrosion Potential (ECP)-electrodes and conductivity cells). HRP-developed sensors can be attached to non-irradiated fuel rods and material samples or to pre-irradiated fuel rods and material samples by using remote operated manipulators and specially-designed re-instrumentation equipment. Ongoing IFE/HRP instrumentation development focuses on high temperature conditions and on new methods for detection of cracking, corrosion, creep, and crud buildup of materials and improved methods for studying thermo-mechanical behavior and fission gas release from LWR fuel during accident conditions and for characterizing the performance of new fuels and cladding materials proposed for LWRs.[80,81] In recent years, data from tests in the HBWR have provided performance data on significant phenomena that have the potential to affect the performance of US nuclear power plants, such as fuel thermal conductivity degradation as a function of burnup[82] and fuel dispersion and axial relocation during a Loss of Coolant Accident.[83]

The HRP relies heavily on specialized in-core instrumentation and standardized test rigs in order to perform fuel and material irradiation programs in the HBWR. In recent years, IFE/HRP has become a supplier of in-pile instrumentation for other test reactors (e.g., OSIRIS, BR2, and HANARO). In addition, IFE/HRP has been involved in developing test rigs for other test reactors (OSIRIS, JHR, and ATR). This

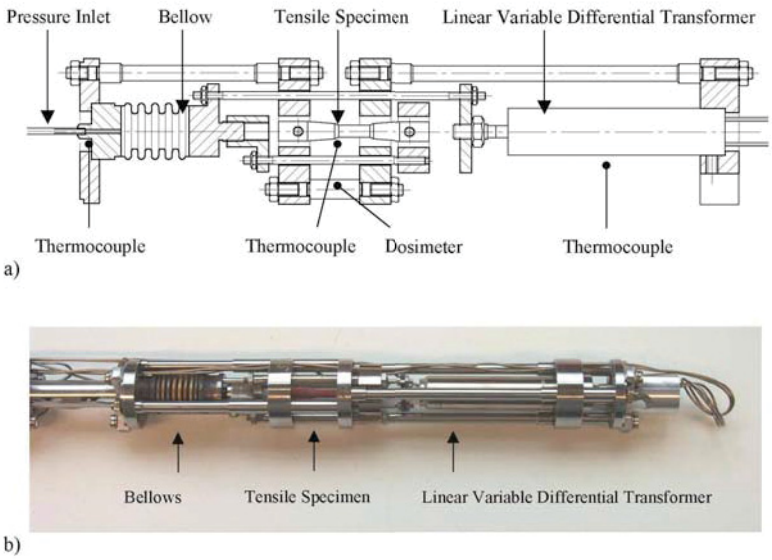

Figure 3-25. Tensile test rig for BR2 irradiations: (a) simplified layout and operational features including necessary instrumentation; and (b) final assembly of test module prior to installation in the test rig.

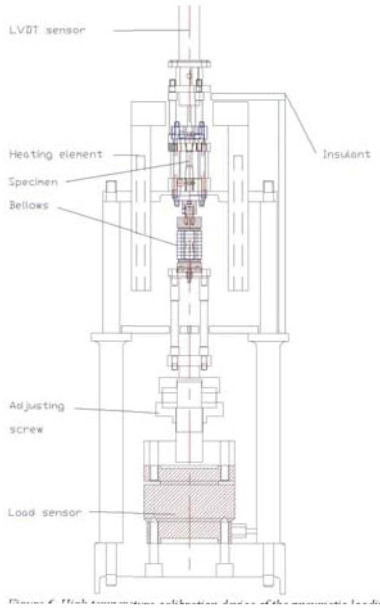

Figure 3-26. High temperature calibration device of the pneumatic loading unit.

section provides additional information about selected IFE/HRP instrumentation development activities. In addition, descriptions are provided for selected standardized test rigs.

3.3.1. LVDTs

Many IFE/HRP-developed sensors rely upon LVDTs as a base instrument. The principle design of an LVDT is shown in Figure 3-27. LVDTs are electrical transformers with three coils placed end-to-end

around a tube (see Figure 3-27a). The center coil is the primary, and the two outer coils are the secondaries. A cylindrical magnetically-permeable core, attached to the object whose position is to be measured, moves along the axis of the tube. An alternating current is driven through the primary, causing a voltage to be induced in each secondary which is proportional to its mutual inductance in the primary. As the core moves, these mutual inductances change, causing the voltages induced in the secondaries to change. The coils are connected in reverse series, so that the output voltage is the difference between the two secondary voltages. When the core is in its central position, equidistant between the two secondaries, equal but opposite voltages are induced in these two coils, so the output voltage is zero (see Figure 3-27b).

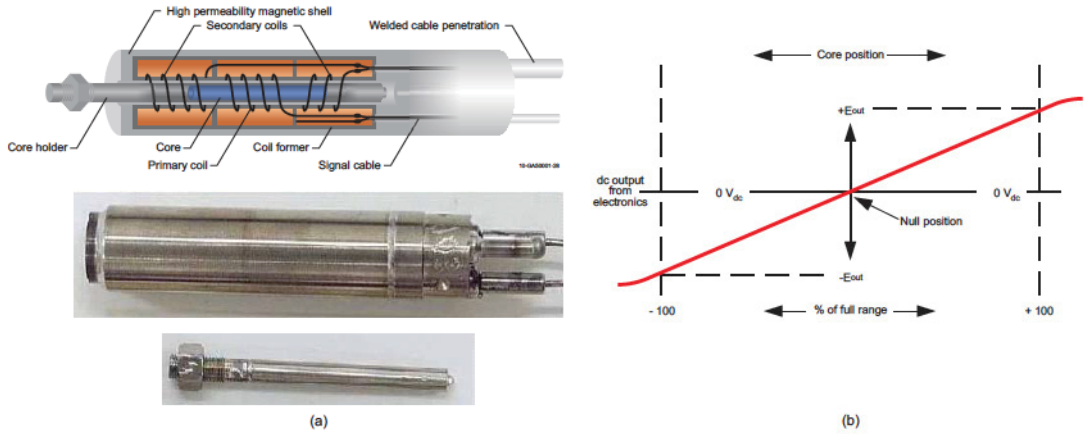

Figure 3-27. Principle design of a LVDT.

In the IFE/HRP LVDTs, the primary coil is activated by a constant current generator (at 400-2500 Hz). The position of the magnetically-permeable core can be measured with an accuracy of ± 1-10 µm (references vary on this value). IFE/HRP fabricates LVDTs in many different sizes. A frequently used size is the "type 5" LVDT, which has a linear range of ±2.5 mm (e.g., the type 5 designation refers to the LVDT's linear range). This LVDT has a diameter of 11.5 mm and a length of 55 mm. The signal cables are two-wire mineral-insulated (Al_2O_3) cables with a 1.0 mm diameter Inconel alloy 600 sheath. Since the IFE/HRP began making in-core measurements, more than 2200 different types of LVDTs have been installed in test rigs in the HBWR and other test reactors around the world. A failure rate of less than 10% after 5 years of operation is typical for IFE/HRP LVDTs operating in BWR, PWR or CANDU conditions. Hence, operating experience has shown that these frictionless sensors are robust instruments for detecting dimensional changes in lower-temperature, irradiation environments. Sections 3.3.2 though 3.3.5 describe some of the LVDT-based sensors developed and deployed by IFE/HRP.

The IFE/HRP 'type 5' LVDTs are designed to operate under PWR conditions (350 °C and 150 bars). The temperature limit is based on the Curie point of nickel. The wire used for the coils of the instruments consists of a copper conductor with nickel cladding. As the temperature passes through the Curie point of nickel (356 °C to 358 °C), there is a noticeable change in the output signal and a change in the instrument sensitivity. However, in collaboration with INL, an LVDT that can operate at temperatures up to 600 °C has been developed using alternative components and fabrication techniques (see Section 5.3). Currently, IFE/HRP is investigating additional options to extend LVDT operating temperatures to 900 °C.[81] By using alternate materials, fabrication, and component drying processes, laboratory evaluations suggest that LVDTs could operate in conditions applicable to gas, supercritical water, sodium, lead, and lead bismuth

cooled reactor conditions. Higher temperature prototype LVDTs have been installed in irradiation test rigs and operated successfully at temperatures up to 700 °C for over a year in the HBWR.

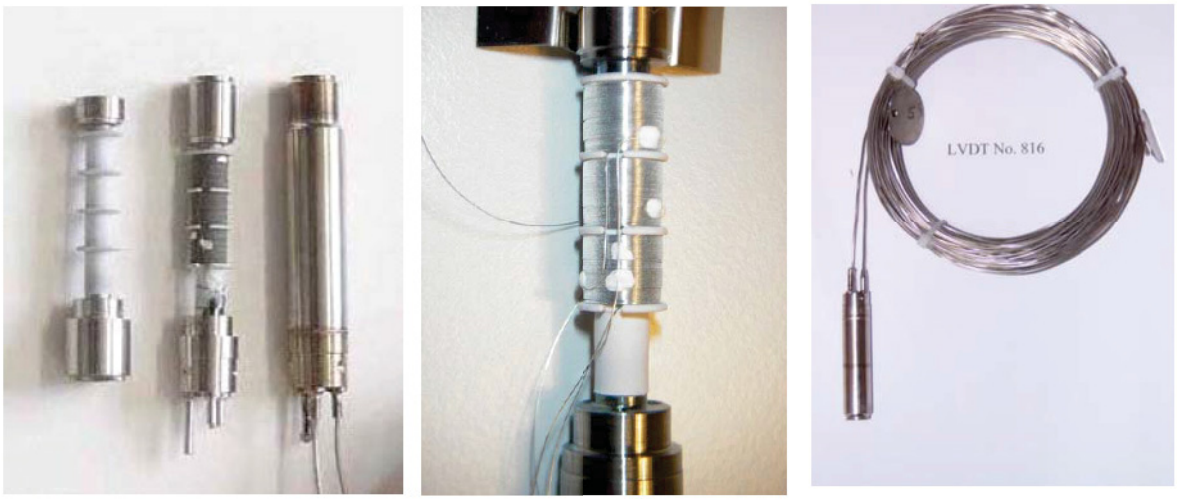

Figure 3-28. IFE/HRP LVDT components and completed sensor prior to shipping.

3.3.2. Fuel centerline temperature measurements

For monitoring fuel centerline temperatures, the IFE/HRP uses thermocouples and/or expansion thermometers. Fuel centerline temperature measurements provide important information on the thermal performance of the fuel and if desired, the fuel thermal conductivity. By monitoring the fuel thermal conductivity over a longer period of time, the fuel thermal conductivity degradation as a function of burn-up is studied. An example of UO_2 thermal conductivity data derived from fuel centerline temperature measurements is illustrated in Figure 3-29. Informal discussions[73] indicate that such tests have been done with specially-designed fuel rods with a small as-fabricated fuel-to-clad gap that minimizes the influence of gap conductance change (densification/swelling, fission gas release) on the fuel center temperature during the irradiation. Smaller diameter fuel rods are often used in such tests to increase the burnup accumulation rate. In addition, in-pile local power measurements are required for such tests.

IFE/HRP fuel centerline thermocouples normally operate for several years in-core without failure, but the lifetime of "Type C" tungsten-rhenium HBWR thermocouples has been found to decrease with increasing fuel centerline temperatures. If the fuel centerline temperature exceeds 1400 to 1500 °C, the expected lifetime of the Type C thermocouples, which must be used with an HBWR-specific correction factor to offset thermocouple decalibration associated with transmutation, is typically less than one year (although no fluence values were cited, HBWR peak thermal flux is 1×10^{14} n/cm^{2}s). Furthermore, informal discussions with HRP staff indicate that 'batch-to-batch' variations have been observed in Type C thermocouples procured from various vendors.[73]

The IFE/HRP expansion thermometer (see Figure 3-30) consists of a tungsten rod (a molybdenum rod may also be used to reduce transmutation concerns) that is inserted through a hole drilled in a fuel stack. The thermal expansion of the tungsten rod is measured using an LVDT. The fuel centerline temperature is then derived from the measured expansion of the tungsten rod. The expected lifetime of an expansion thermometer is longer than for a thermocouple, but the resolution of an expansion thermometer is less than a thermocouple because the expansion thermocouple only provides an estimate of the average temperature

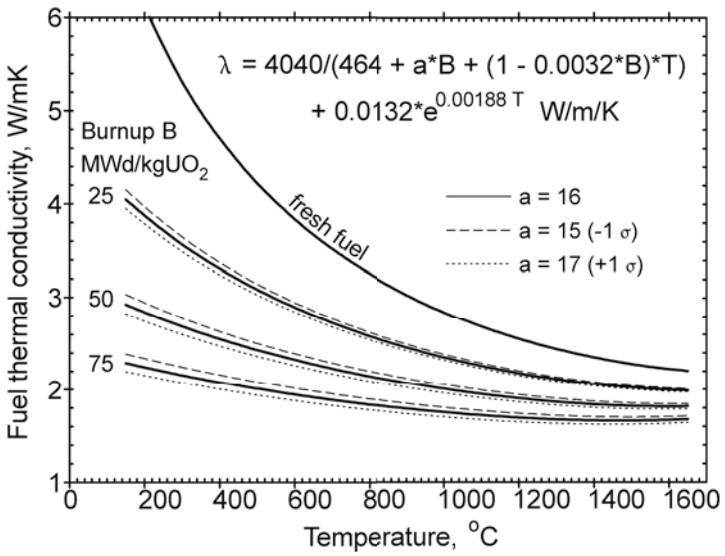

Figure 3-29. Fuel thermal conductivity derived from fuel centerline temperature measurements.

over the length of the rod. There is also the potential for mechanical interactions between the fuel and the tungsten rod that can affect expansion thermometer performance.

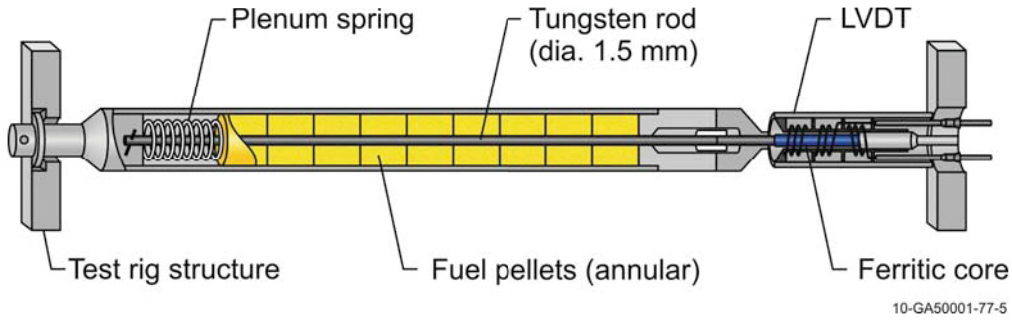

Figure 3-30. Thermal expansion thermometer.

3.3.3. Fuel densification / swelling measurements

The mechanical stability of nuclear fuels is an important performance parameter. For in-pile monitoring fuel stack-length changes, IFE/HRP has developed several instruments based on LVDTs. In order to measure fuel densification and swelling, the LVDT core is attached to a spring-loaded plate in contact with a fuel pellet in one end of the fuel stack (see Figure 3-31). The core then follows the expansion and contraction of the fuel stack and provides data on the fuel's mechanical behavior.

3.3.4. Fuel rod pressure measurements

IFE/HRP monitors fuel rod internal pressure to gain insights about fission gas release during irradiation. The pressure transducer consists of a miniaturized bellows mounted in the fuel rod end plug (see Figure 3-32). A magnetically-permeable core is fixed to the free moving end of the bellows; the other end of the bellows assembly is fixed to the end plug. The bellows is typically pressurized to 2 bar less than the ini-

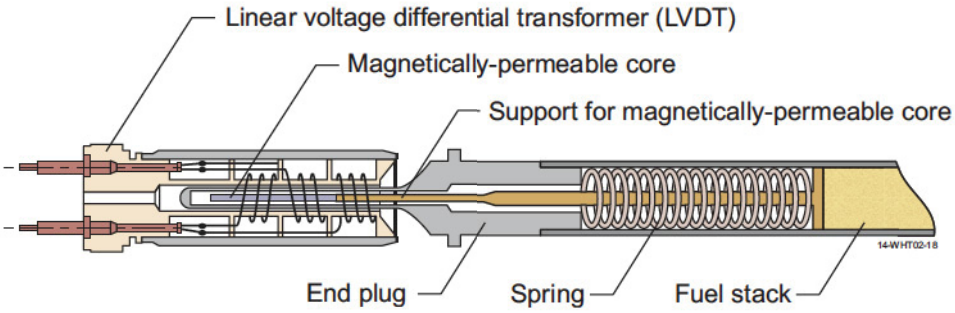

Figure 3-31. Fuel stack elongation detector.

tial rod pressure and seal welded. Bellows/core movements are sensed by an LVDT. The bellows differential pressure will, in addition to release of fission gases, be dependent upon fuel densification/swelling characteristics, changes in gas temperature and fuel/cladding thermal expansion during operation. Densification will lower the fuel rod internal pressure, while swelling and gas temperature effects and fuel differential expansion will increase fuel rod internal pressure.

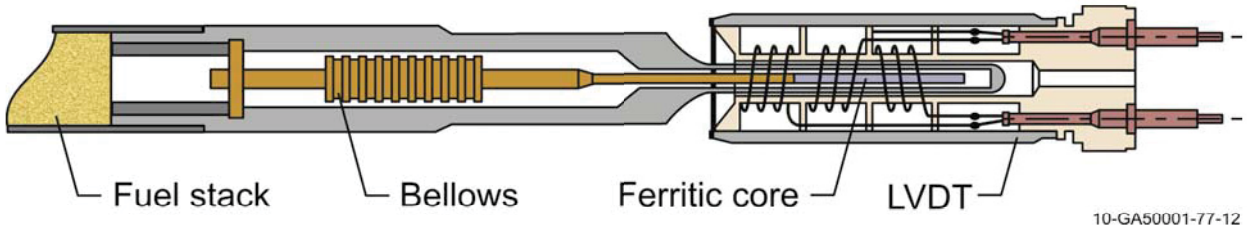

Figure 3-32. Pressure gauge

The pressure transducers are available for different pressure ranges. The most common ranges have a Δp (internal versus external pressure of the bellows) of 15 bar (type I), 30 bar (type II), or 70 bar (type III). The difference between these bellows is related to the stiffness/spring rate. During the initial stages of fission gas production, it is often necessary to use a bellows with high sensitivity (but a limited pressure range). For such conditions, the 15 bar bellows is selected. For high burnup tests in which high rod pressure is expected, the 70 bar bellows is used. The higher pressure range is achieved by sacrificing sensitivity. Under realistic conditions, the uncertainty of the pressure for the 30 bar sensor is ±0.2 bar; for the 70 bar sensor, the uncertainty is ±0.5 bar.

In order to keep the same precision as a type II transducer, while still being able to reach 70 bars, a new type of transducer has been designed. Two different bellows, having different levels of stiffness, are connected in series. In this way, the softer bellows is dominant at lower pressure. When reaching the maximum pressure for the softest bellows of the two, further compression of this bellows is restricted by an internal mechanical stop. The stiffer bellows then becomes the only contributor to the signal output. Measurement ranges up to 150 bar (15 MPa or 2180 psig) are possible. To reduce material creep at high temperature and radiation intensity, the bellows are pre-pressurized (inside) and conditioned for several days at high pressure and temperature. In addition, the pressure transducer can be systematically re-calibrated during reactor outages using procedures developed by IFE/HRP.

3.3.5. Fuel Rod Diameter Measurements

The IFE/HRP DG enables on-line measurement of cladding diameter for assessing cladding creep, pellet-cladding mechanical interaction, fuel creep / relaxation and fuel rod crud deposits. A representative standardized test rig (shown in Figure 3-33a) provides a method for real-time in-pile measurement of fuel rod diameter changes, temperature, neutron exposure and loop coolant temperature, flow, and chemistry (e.g., concentration, pH, etc.). IFE/HRP relies on LVDT-based technology in their DG. However, as shown in Figure 3-33b, the LVDT design has been modified. First, the two primary coils and the two secondary coils are wound on a ferritic bobbin, as opposed to the Inconel alloy bobbin of the LVDT. Second, the DG uses an armature instead of the magnetically permeable core used in the LVDT. As indicated in Figure 3-33b, changes in distance between each of the secondary coil loops and the armature that may occur as the diameter travels along the fuel rod changes the balance between the signals generated in the two secondary loops, leading to a change in the output signal (difference of the two secondary coil signals) from the DG.

The DG travels along the fuel rod using an in-core hydraulic drive and positioning system. In some test rigs (see Figure 3-33a), the fuel rod is moved by the hydraulic drive. The accuracy of the DG is ± 2 μm, and a calibration is performed in conjunction with each diameter trace by having calibration steps on both fuel rod end plugs. The standard DG can operate at up to 165 bar and 325 °C. However, modifications to LVDTs suggested and evaluated by CEA (Section 3.1.6) and INL (Section 5.3.1) in collaboration with IFE/HRP should allow its operation at higher temperatures and IFE/HRP research is underway to produce LVDTs capable of operation up to 900 °C.[81]

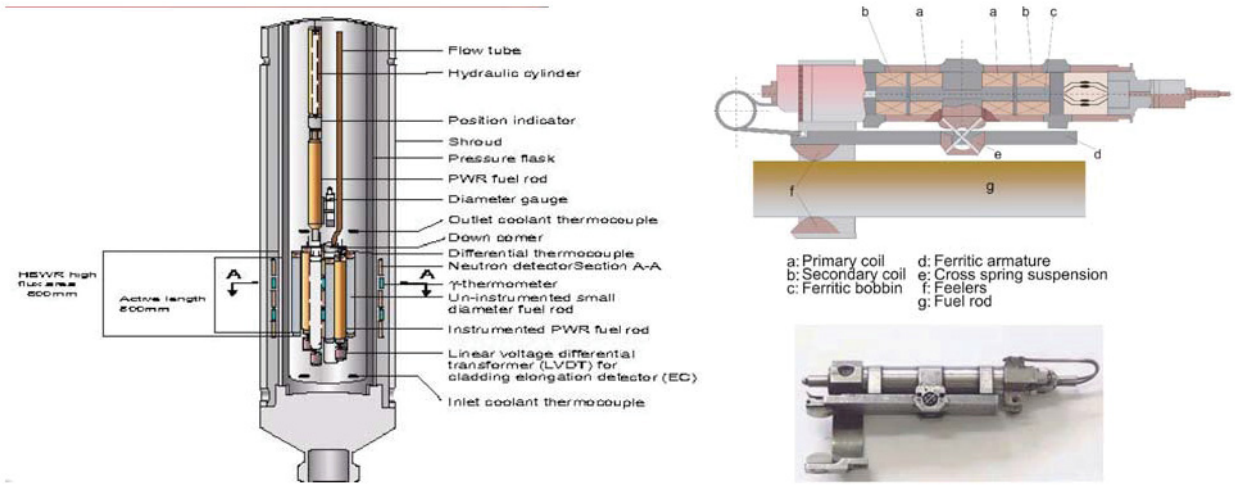

(a) (b)

Figure 3-33. HRP fuel pellet cladding interaction/crud deposition test rig (a) with DG (b).

Figure 3-34 shows results from diameter measurements on a typical PWR fuel rod irradiated in the HBWR as part of a PWR crud evaluation program. The irradiation is performed in a PWR loop system that allows variations in water chemistry parameters during irradiation. DG run no. 7275 was performed immediately after startup of the experiment to provide initial fuel rod diameter data. DG run no. 7739 was performed after approximately 230 days at full power and shows cladding creep-down typical for PWR fuel

rods. Diameter run. no. 7754 was performed after an additional 25 days after changing the water chemistry in the loop system. The water chemistry change included an increase in the iron and nickel content. The diameter trace shows that crud deposits formed on the upper part of the fuel rod. The possibility of observing the formation of crud by monitoring the fuel rod diameter on-line along with changes in neutron flux and fuel temperature provides the IFE/HRP insights into developing a remedy for crud and related phenomena such as "Axial Offset Anomaly".[75]

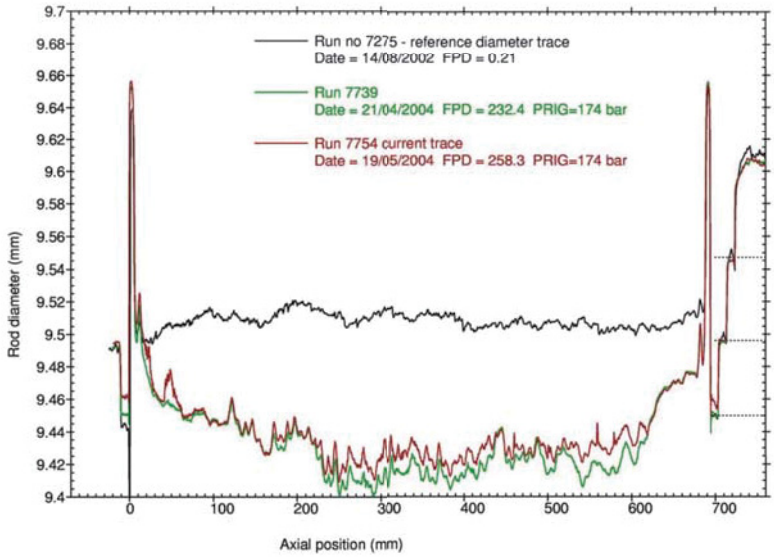

Figure 3-34. Fuel rod diameter traces showing cladding creep down and crud deposition.

As can be seen from Figure 3-33b, the design of the DG is rather complicated, and sections of nonmagnetic material have to be welded to sections of magnetic material. Therefore, a new design is under investigation by IFE/HRP in which the outer wall of the DG consists of a single tube of Inconel alloy 600. The design was optimized using finite element calculations to minimize magnetic flux leakage.

The inner body is now made from one piece, where the coil separators are integral parts of the body. In order to prevent flux linkage between the (magnetic) coil separators and the ferritic armature ("anchor"), the part of the separators facing the anchor is shaved off, making a large air gap between coil separators and the housing (see Figure 3-35). Using an outer body of Inconel increases the distance between the magnetic inner parts and the anchor, leading to a loss of sensitivity. To compensate for this, the distance between the anchor and housing has been slightly reduced. In addition, the inner body will be made out of silicon iron, which should have a significantly higher magnetic permeability than the AISI 403 currently used in the standard DG. Other possible benefits of this material are reduced eddy current losses, leading to reduced temperature sensitivity. Figure 3-35 shows an example of the coiled DG body. Tests show that the new DG, operated in self-compensating mode, has a linear response over the range ±0.9 mm, which is much longer than the 0.2-mm range typically required for in-pile applications. The accuracy of the new type of DG is ~2 μm.

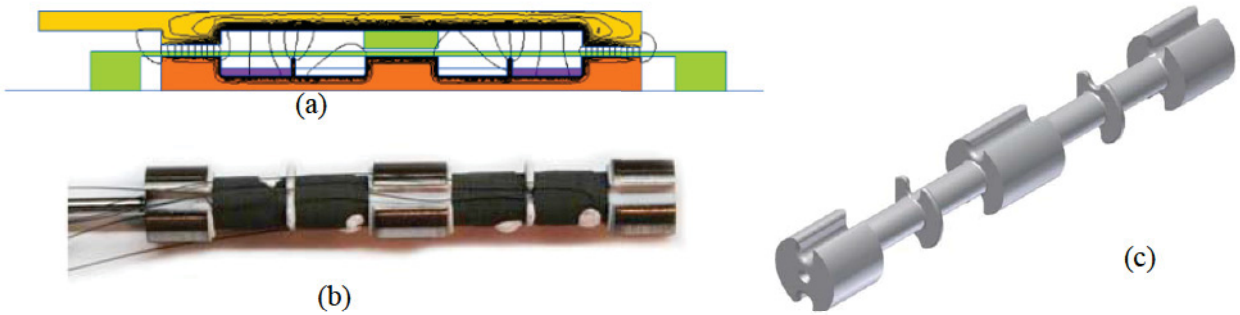

Figure 3-35. Simplified DG; (a) finite element analysis showing magnetic field patterns; (b) inner body with coils; and (c) inner body.[78]

3.3.6. Crack-growth measurements

In order to monitor crack-growth rates in core structural component materials, the IFE/HRP utilizes miniaturized Compact Tension (CT) specimens and the "direct current potential drop method" for measuring crack propagation. The direct current potential drop (DCDP) method (see Figure 3-36) is based on sending an electrical current through the specimen and measuring the potential (voltage) at several locations on the CT-specimen. The measured potentials depend on the propagation of the crack. Thus, the crack-length can be determined from the measured potential drops. Reference 78 reports results in which this approach was successfully applied to detect changes in crack growth rate due to variations in coolant pH for various metals. IFE/HRP has applied this technology to detect the impact of coolant parameters (pH, impurities, boron concentration, etc.) on fuel cladding corrosion. In addition, IFE/HRP can perform such measurements on pre-irradiated fuel components removed from commercial reactors.

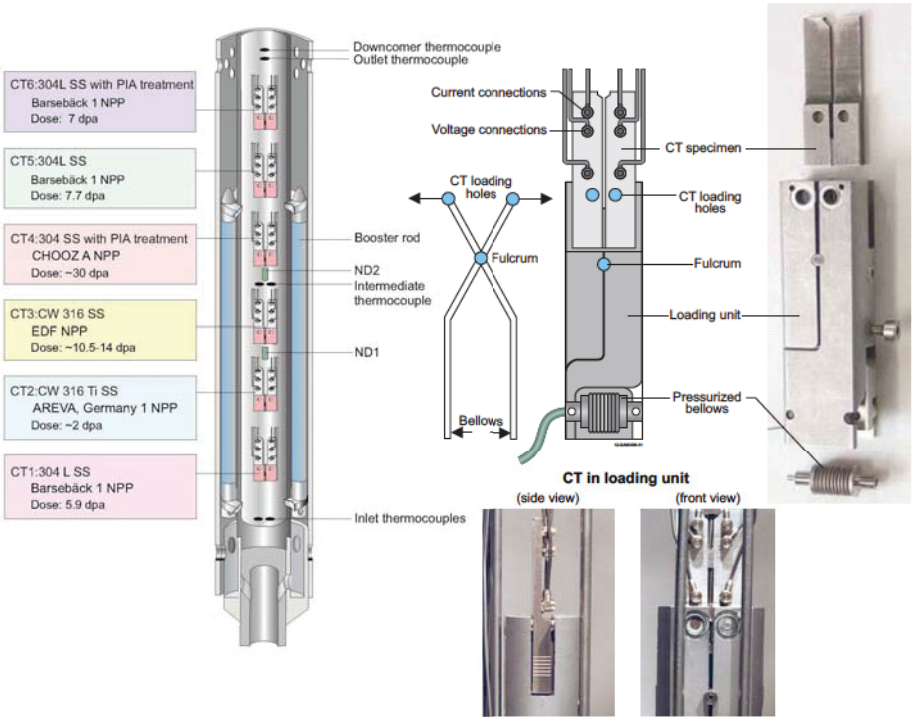

Figure 3-36. Typical crack growth test rig.

Figure 3-36 shows a CT sample for online crack growth rate measurements and a loading unit for CT specimens used in the HBWR. The figure shows a CT specimen with a square geometry. Depending on the availability of materials, the CT specimens can be made entirely from fresh materials, pre-irradiated materials, or different types of pre-irradiated inserts (square or circular). A dynamic load is applied to the CT specimens by means of individually calibrated loading units that are equipped with bellows that are pressurized with helium gas through an external system. The Direct Current Potential Drop (DCPD) method is used to measure the crack growth rate (CGR) under defined water chemistry conditions. Data for periods of stable CGR (typically 100 h) are used to calculate the actual growth rate for a CT at the given temperature, load, and water chemistry. The DCPD method can typically measure changes of ~10 μm.[18]

3.3.7. Electrochemical Corrosion Potential

The ECP is determined by a combination of the surface conditions of the specimen and concentrations of dissolved oxidants. The ECP is a key measurement for assessing the performance of reactor structural materials. For in-core measurements, reference electrodes must be capable of withstanding in-core conditions. Although there are commercial ECP sensors on the market, the IFE/HRP has developed its own ECP reference electrodes for enhanced in-pile robustness.

Different reference electrodes are needed for different environments. A Pt electrode has been developed for use in reducing conditions. The potential sensing element consists of a Pt cylinder and end plate. The large surface area of the Pt serves to reduce the effect of any mixed potentials caused by other metal components. A schematic drawing is shown in Figure 3-37a. A Pd reference electrode is used in oxygenated water. The potential-determining reaction of the Pd hydrogen electrode is similar to that of the Pt hydrogen electrode. Palladium differs from platinum in that it can hold hydrogen within its lattice; in aqueous solutions, hydrogen can be produced by cathodic charging of the Pd. When sufficient hydrogen is produced, some will diffuse to the surface of the Pd, which can then function as a hydrogen electrode. A schematic drawing of a Pd electrode is shown in Figure 3-37b.

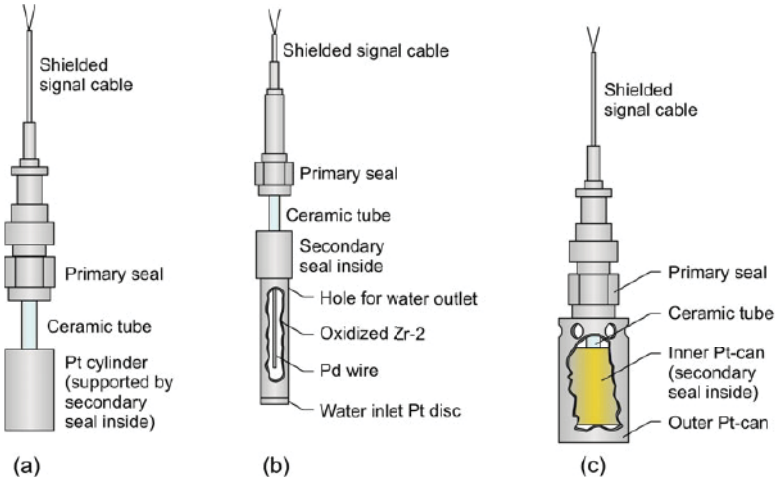

Figure 3-37. ECP sensors and conductivity cell (a) Pt ECP sensor, (b) Pd ECP sensor, and (c) conductivity cell.[77]

A novel conductivity cell, which is a modification of the Pt ECP electrode in which the Pt sensing element is surrounded by a second Pt cylinder, has been developed by IFE/HRP that can be installed in-core

within pressure flasks. This design allows coolant conductivity measurements at operating temperature and pressure. An additional signal cable is included to provide current, and the conductivity of the coolant is determined from the measured voltage difference between the two Pt cylinders. A schematic drawing is shown in 3-37c. In order to characterize the chemical conditions, the IFE/HRP is also developing a miniaturized Pt electrode and a miniaturized Fe/Fe_3O_4 reference electrode (see Figure 3-38). These electrodes, which have been tested in an autoclave at 600 °C and supercritical water conditions,[81] will soon undergo in-pile testing.

(a) (b)

Figure 3-38. ECP-based sensors (a) Brazed Pt electrode and (b) brazed Fe/Fe_3O_4 electrode.

3.3.8. Localized Heating

Local power measurements have been made at the HBWR since 1962 using gamma thermometers that detect heat produced by fission and fission product gamma rays.[79] Heat is transferred to the coolant sink along a closely controlled conduction path while the temperature drop is measured by a differential Type K thermocouple (see Figure 3-39). The hot junction is situated in the center of the lower end of the inner body and is insulated from the coolant by a gas-filled region. The cold junction is situated outside the housing and responds quickly to the conditions in the cooling medium. The generated signal, which is proportional to the fuel power, is strong and constant with fuel burn-up. The current miniaturized gamma thermometer design has a 3.9 mm outer diameter sheath and a 84 mm length. The inner body has a diameter of 2.1 mm and a length of 50 mm. The thermal insulation of the inner body is achieved by the Xe- or Ar-filled gap which is pre-pressurized at room temperature (typically 20 - 30 bar). The internal gas pressure has the purpose of reducing unwanted creep of the outer cladding and minimizing the effect of possible gas contamination. Heat produced by gamma absorption in an inner, thermally insulated, body results in a local rise in temperature. The temperature increase and the time constant of the gamma thermometer are used to calculate the actual gamma irradiation. The gamma thermometer can be re-calibrated in-core by applying a low direct current (DC) voltage to the differential thermocouple. The inner body of the gamma thermometer is heated by the current applied to the thermocouple for a short period of time. The decay of temperature is monitored, and a relationship between temperature and decay time is used to recalibrate the gamma thermometer (see Figure 3-40).

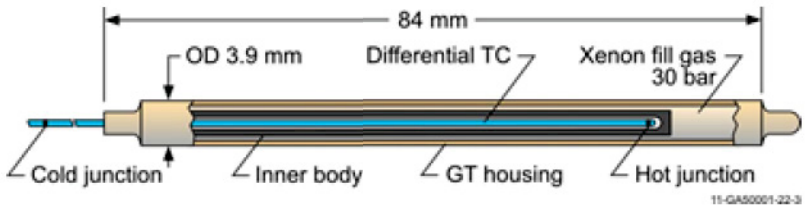

Figure 3-39. Halden miniaturized gamma thermometer.

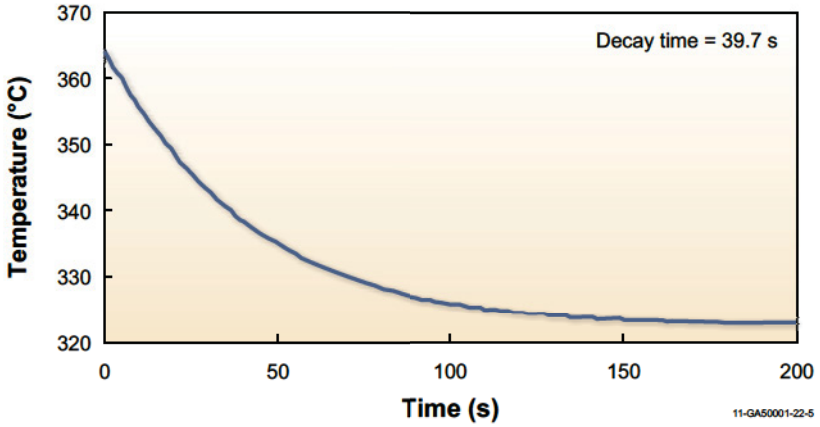

Figure 3-40. Signal decay curve used to recalibrate the Halden gamma thermometer.

3.3.9. Flowrate

The turbine flow meter (Figure 3-41) was the first instrument developed at the IFE/HRP. The need for accurate power calibration of individual fuel assemblies led to the development of in-core turbine flow-meters. The turbine flow meter consists of two parts: one turbine installed in a housing, and the pick up coil mounted in the test rig. If the flow meter fails, it is possible to remove the failed unit and install a new one as there are no cables associated with the turbine unit because the pick-up coil is installed in the test rig itself. Normally, there are two turbines installed in an IFE/HRP test rig; one to measure the inlet flow, and one to measure the outlet flow. The in-core turbine flow-meters use an electro-magnetic coil system for measuring the speed of the turbine. The rotor blades are magnetic; and each time the rotor blades pass over the pickup coil, a pulse is induced in this coil. The pulses are sensed by the electronics system giving online information of the flow in each test rig. Because of the high failure rates of these flowmeters, IFE/HRP is contemplating design improvements.

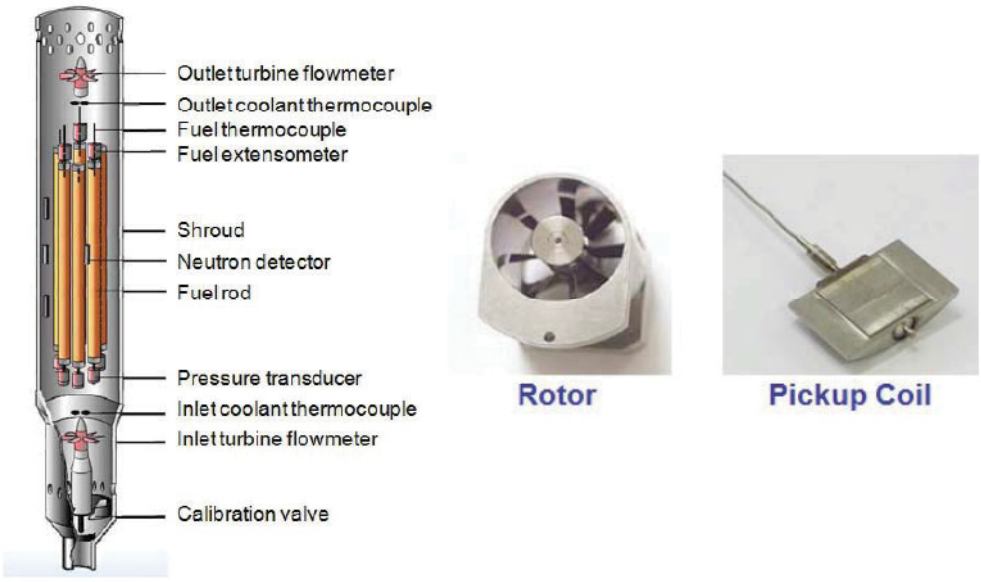

Figure 3-41. Components and position of turbine flowmeter.

3.3.10. Oxide Thickness Measurements on Fuel Cladding

Corrosion of fuel cladding under various chemical and power load conditions remains an active field of research. With the exception of the IFE/HRP DGs, such corrosion studies are nearly always performed by postirradiation examination. As an alternative to the DG, IFE/HRP is developing a probe for online in-pile measurements of oxide thickness. The probe is based on the eddy-current principle (see Figure 3-42). It consists of one sensing coil (slightly extruding) and one reference coil (situated completely inside the housing and shielded by it). The two coils are part of a resistance bridge circuit so that a small difference in coil impedance can be detected. The reason for situating the reference coil inside the probe (rather than outside the reactor) is that it allows compensation for resistance changes in the coil and the signal cables due to temperature variations. The top of the sensing coil has been designed to be sufficiently strong to withstand the external pressure while at the same time being thin enough to transmit enough of the radio frequency field to generate the eddy currents in the fuel cladding. Test results performed at room temperature show a linear response for the 0- to 100-μm region. The test setup is included in Figure 3-42. Calibrations show that the probe has a resolution as low as 1 μm. The performance of this probe has also been verified in an autoclave test (at 350 °C and 165 bar). The probe housing itself is used as the common ground connection for both coils (and in turn is connected to the cable sheath). It is planned to verify the probe in an in-pile experiment at the HBWR.

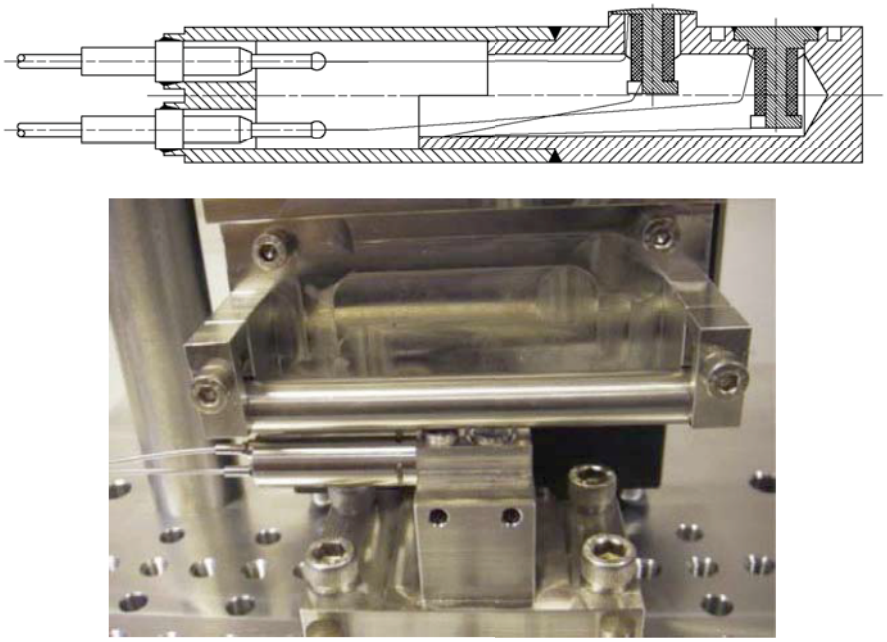

Figure 3-42. Oxide thickness probe: schematic drawing and test setup of probe with zircaloy test tube.[78]

3.3.11. Summary

Although the HBWR has a much lower power rating and is considerably older than the ATR, the instrumentation capabilities developed by IFE/HRP staff have significantly extended its irradiation capabilities. In addition, the IFE/HRP has leveraged this expertise to supply instrumentation and test rigs to commercial reactors, naval reactors, and other MTRs.

The IFE/HRP uses specialized in-core instrumentation in order to perform fuel and material irradiation programs in the HBWR. As discussed in this section, the IFE/HRP also has the ability to attach in-core instrumentation to pre-irradiated fuel rods and material samples from power reactors. Typically, IFE/HRP applies instrumentation to detect fission gas release and thermal conductivity degradation to pre-irradiated fuel rods. Irradiated structural material samples have also been instrumented to detect crack growth. The IFE/HRP continues to refine its existing in-pile instrumentation and develop new instruments. As discussed in this section, ongoing IFE/HRP instrumentation development focuses on high temperature conditions and on new methods for detection of cracking, corrosion, and crud buildup of materials.

3.4. JAEA

The Japan Atomic Energy Agency (JAEA) [formerly the Japan Atomic Energy Research Institute (JAERI)] provides several types of instrumentation to support tests in the JMTR.[85] Commercially-available sensors procured from Japanese vendors allow JMTR customers to detect temperatures using thermocouples and melt wires, length and diameters (using LVDT-based sensors made by Japanese vendors), fission gas release, and neutron flux (using fission chambers, SPNDs, or flux wires), and crack growth (using bellows to load a pre-cracked sample with direct current potential drop techniques). JAEA can also re-instrument previously irradiated fuel rods. JAEA continues to conduct research to enhance specialized instrumentation to support high temperature irradiations. As discussed in References 85 through 90, research is focussing on new technologies for in-pile measurements of temperature, creep, neutron flux, and gamma-ray intensity distributions.

Prior to unplanned difficulties during refueling of the JOYO reactor in 2007, JAEA also conducted instrumented irradiations in this fast reactor using in-core test rigs, such as a Material Testing Rig with Temperature Control (MARICO) test rig and an Instrumented Test Assembly (INTA), and ex-vessel test rigs. In fact, the difficulties that have prevented operation of this MTR since 2007 were associated with movement of the MARICO-2 instrumented test rig. Nevertheless, some of the instrumentation typically used in JOYO tests is of interest in this review.[91]

3.4.1. Temperature

For peak irradiation temperature indication, JAEA customers may select from a range of melt wire materials, including In, Sn, Pb, Ag, and Zn, and a range of alloys. Figure 3-43 illustrates a typical melt wire holder containing seven melt wires with melting temperatures ranging from 1050 to 1150 °C. In addition, Reference 91 reports the use of sodium-filled stainless steel capsules, known as Thermal Expansion Devices (TEDs) in JOYO. As shown in Figure 3-44, calibration curves have been developed for inferring the peak irradiation temperature to the observed volumetric expansion of the stainless steel capsules. JAEA reports accuracies of ± 25 °C, but earlier applications by EBR-I of TEDs report accuracies of ± 5 °C.[92]

JAEA relies on commercially-available thermocouples (e.g., Type N, K, and C thermocouples) to measure temperatures during JMTR irradiations. Reference 90 reports JAEA efforts to develop and deploy multi-point or "multi-paired" Type K and N thermocouples (see Figure 3-45). The design of these multi-paired thermocouples is similar in that they are fabricated with MgO insulation and contained within a 1.8 mm diameter sheath (either stainless steel or Inconel). There are typically three to seven hot junction points spaced between 20 and 30 mm apart. As shown in Figure 3-45, 'dummy' MgO insulators and wires are included to fix the position of thermocouple hot junctions. Type K multi-pair thermocouples have been

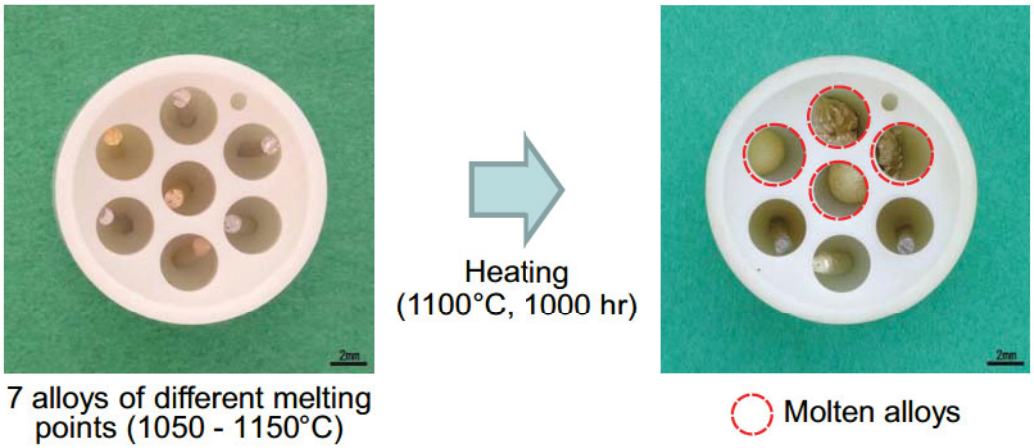

Figure 3-43. JAEA melt wire holder prior and after irradiation.

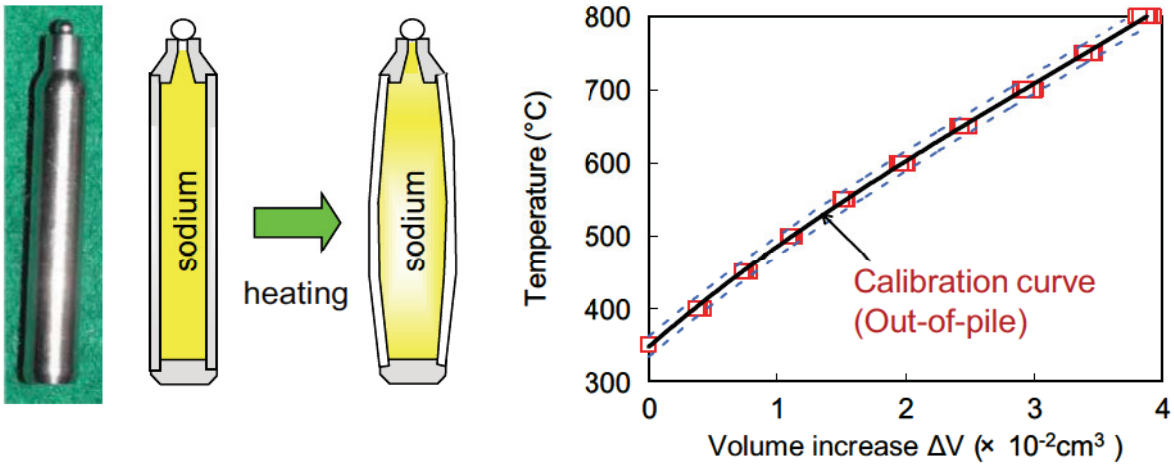

Figure 3-44. TED capsule and calibration curve relating volumetric expansion to temperature.

deployed in a 17,000 hour irradiation with peak temperatures of 700 °C. Furnace tests have demonstrated that type N multi-paired thermocouple response will remain stable after heating at 1000 °C for 3000 hours.

3.4.2. Length and Diameter

In-pile changes in length and diameter are measured by LVDTs that are made by Japanese vendors. Reference 90 reports JAEA efforts to increase the peak operating temperatures of two LVDT designs: one design using ceramic coated coil wire that can operate up to 550 °C and a higher temperature design mineral insulated cable for the coils that can operate up to 650 °C. The performance of these higher temperature LVDTs were recently demonstrated in a lower temperature (300 °C) irradiation test conducted at the WWR-K reactor at the Institute of Nuclear Physics at the National Nuclear Center (INP NNC) in the Republic of Kazakhstan (total fluence of ~1.5x 10^{24} n/m^2, E >1 MeV).

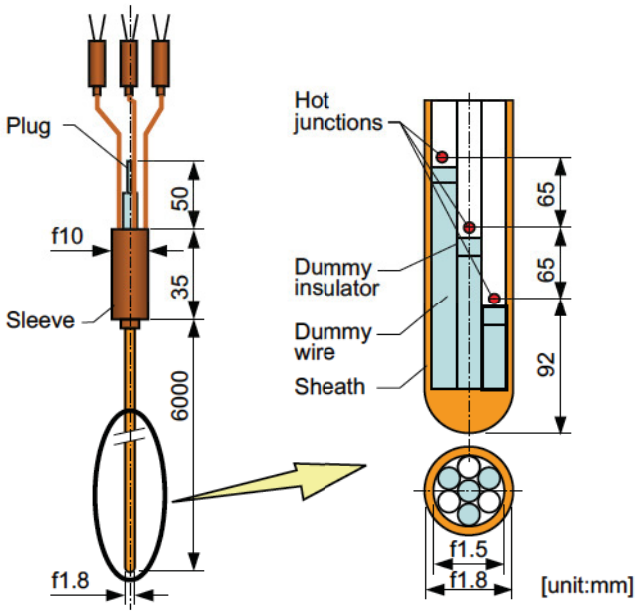

Figure 3-45. Multi-paired thermocouple design.

3.4.3. Creep and Deformation

Reference 87 describes JAEA efforts to develop irradiation equipment for in-pile creep and deformation of specimens subjected to loads of up to 10 kN at temperatures up to 600 °C. The in-vessel parts of this unit (see Figure 3-46) are installed in the reactor pressure vessel through a standpipe. This in-vessel part is 8.9 m long with the lower portion consisting of three tubular parts, two irradiation units and a guide tube, that are each 2.6 m long and 0.113 m in diameter. Although the specimens are primarily heated from reactor core heat, a smaller 300 W electric heater is included for supplementary temperature control. The neutron flux that specimens experience is monitored using SPNDs containing rhodium as the emitter. Small fluence wires are also included for post-irradiation fast and thermal fluence measurements. Temperature is monitored using Type K thermocouples, and specimen elongation is monitored by JAEA-developed LVDTs containing mineral-insulated coil material.

3.4.4. Fission Gas Pressure

Reference 90 also reports JAEA efforts to design and demonstrate the performance of fission gas pressure gauges that can operate at temperatures up to 650 °C and pressures up to 10 MPa. As shown in Figure 3-47, this gauge includes two springs, a bellows, and a high temperature LVDT (see Section 3.4.2). Laboratory tests indicate measurement accuracies of 1.8%. The irradiation performance of this test rig was recently demonstrated in a lower temperature (300 °C) irradiation tests conducted at the WWR-K reactor at the INP NNC in the Republic of Kazakhstan (total fluence of ~1.5x 10^{24} n/m^2, E >1 MeV).

3.4.5. Neutron Flux

For flux and fluence measurements, JMTR irradiations can include 1.8 mm diameter fission chambers, SPNDs, or flux wires--Fe for fast flux and Al-Co, V-Co, or Ti-Co for thermal flux. For real-time measure-

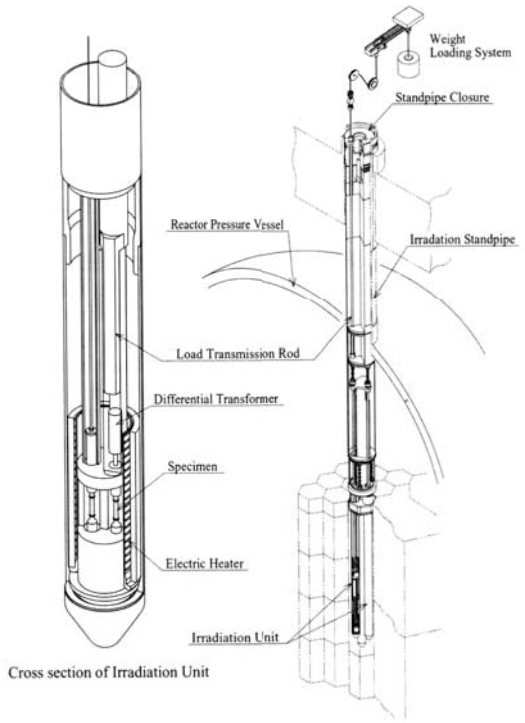

Figure 3-46. I-I type irradiation unit with weight loading equipment.

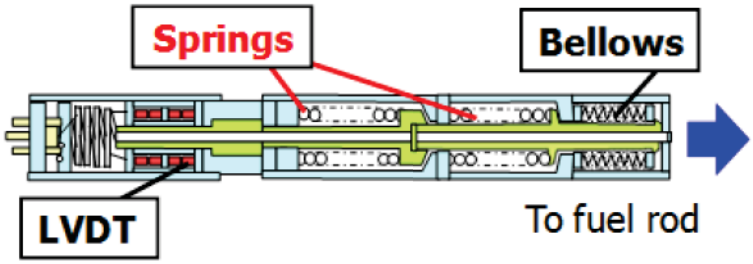

Figure 3-47. JEA fission gas pressure gauge.

ment of thermal neutron flux, JAEA uses Rh, Co, and Pt SPNDs.[90] In addition, JAEA is developing fast response/high output SPNDs containing Co emitters surrounded by Rh and Pt emitters surrounded by Rh. The irradiation performance of this new Pt-Rh type SPNDs was successfully demonstrated at the JMTR in a 17,000 hour test with a peak temperature was 700 °C.

JAEA is also exploring the use of two flux characterization methods: a scintillator optical fiber with a scanning driver and a self-powered detector with a driver. Tests were completed using the driver system to insert each type of detector into the TRIGA II reactor at the Institute for Atomic Energy at Rikkyo University. Results indicate that scanning a one meter long core using an optical fiber with a scintillator (ruby) attached to the tip yields neutron flux distributions similar to that obtained with foil activation methods (see Figure 3-49). However, foil activation methods require 4 to 5 hours whereas the fiber method only requires 10 minutes.

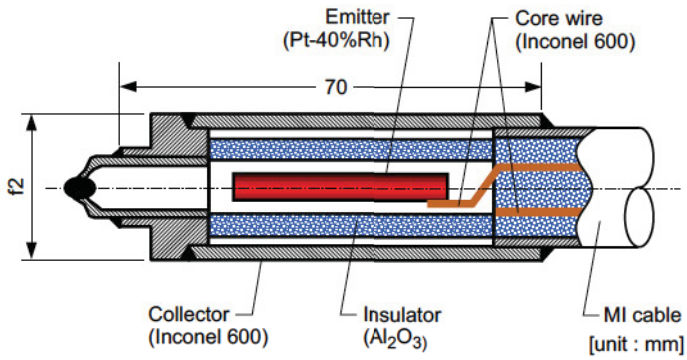

Figure 3-48. JAEA-developed Pt-40% Rh SPND.

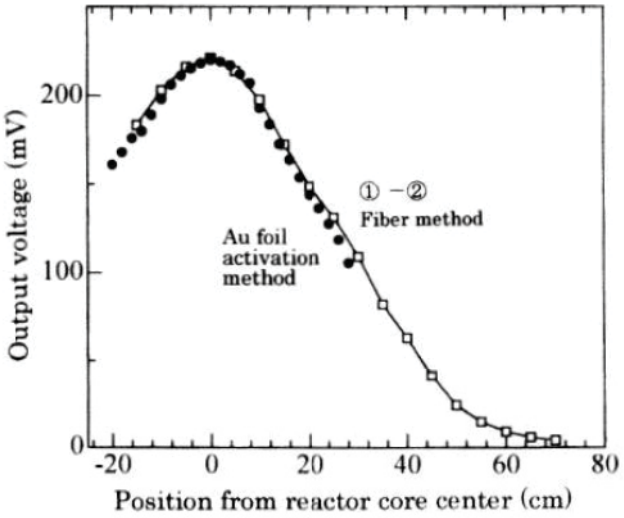

Figure 3-49. Signals obtained with optical fiber detector and Au foil activation methods.

Because light emission of the ruby scintillator decreases at high temperatures, this method is limited to temperatures of around 100 °C. Although JAEA is continuing to explore the potential of other scintillators, Reference 89 also reports results from tests using the driver system with self-powered detectors containing quartz insulators were found to function for temperatures up to 500 °C. Detectors with alumina tubes were only found to function up to 400 °C.

3.4.6. Gamma Flux

Reference 90 reports that JAEA has recently started developing of SPGDs using a lead emitter, alumina insulators, and an Inconel 600 collector (see Figure 3-50). Calibration evaluations of these SPGDs were performed using an alanine dosimeter in a Co-60 gamma-ray irradiation facility at the Takasaki Advanced Radiation Research Institute.

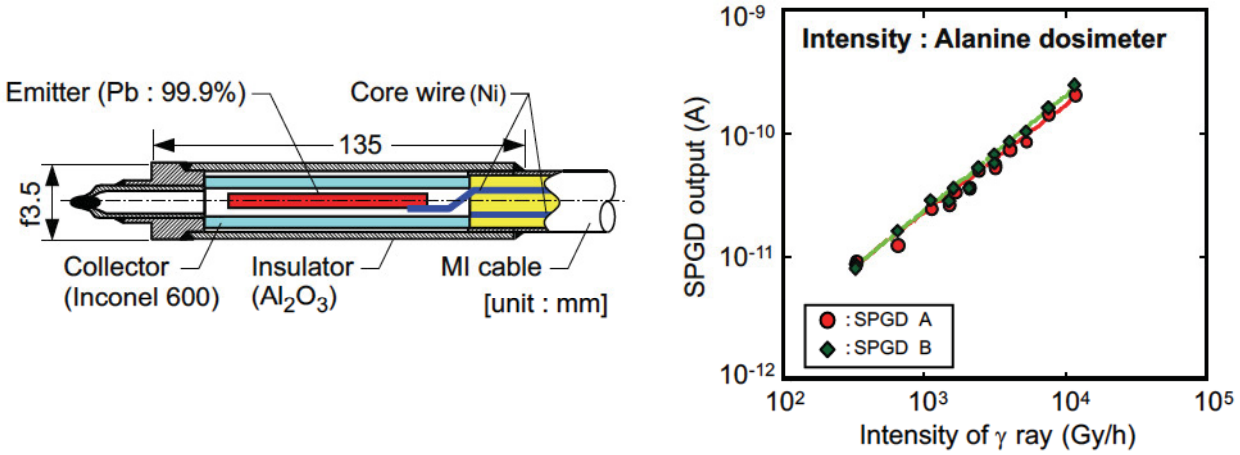

Figure 3-50. JAEA SPGD design and calibration results.

3.4.7. Optical Diagnostic Techniques

JAEA has been active in research to use optical diagnostic techniques to measure temperatures, reactor power, and other operating parameters. Reference 88 reports research results indicating that newly-developed fluorine doped (F-doped) optical fibers can withstand radiation damage better than silicon core fibers. Results for an F-doped optical fiber indicate that the radiation-induced optical absorption at about 600 nm was less than 0.2 dB/m for an electronic excitation exposure dose of 1.9E6 Gy (1.9E13 rads).

3.5. NRG

The HFR at Petten, which is owned by the European Communities and operated by the Netherlands Energy Research Foundation (ECN), has been conducting fuel irradiations using instrumented test rigs for over 40 years. The Nuclear Research and consultancy Group (NRG) was established as a Partnership Firm in 1998 through the merger of ECN's (70% share) and KEMA's (30% share) business activities in the nuclear fields. HFR test capsules have been successfully used to investigate power cycles and ramping behavior on PWR and BWR fuel rods.[93] Although the HFR originally focussed on LWR fuel irradiations, significant testing of HTGR and Sodium Fast Reactor (SFR) fuels have also been conducted in this facility. Typical instrumentation in such capsules allows measurement of fuel stack displacement, fuel rod length, fuel rod internal pressure, neutron flux, gamma flux, and fuel rod central temperatures (up to 1350 °C).

Discussions with Petten staff indicates that instruments are primarily obtained from commercial vendors or IFE/HRP.[94,95] Typical instruments employed in specialized ECN test rigs are listed in Table 3-1. Reference 96 describes a testing facility installed in Petten for continuous in-pile crack testing of samples up to 730 °C. In recent years, NRG has been involved in several internationally-sponsored tests for advanced reactor fuels.[97,98] In particular, this reference discusses recently completed and ongoing campaigns to evaluate gas reactor fuel elements (the HFR-EU1bis and HFR-EU1 tests), gas reactor fuel coating materials (the PYCAASSO I and II tests), liquid metal fast reactor and accelerator driven system fuel tests (CONFIRM, FUJI), transmutation fuel tests (HELIOS irradiations), and advanced fuel cycle (e.g., U-Pu and Th-U cycle tests). As documented in Reference 98, evaluations included a near-real time capability of measuring fission gas release, temperature, and pressure during the irradiation.

3.6. KAERI

The Korea Atomic Energy Research Institute (KAERI) utilizes specialized instrumentation in test capsules supporting materials and fuel irradiations in their HANARO multi-purpose, pool-type research reactor. HANARO was designed to provide a peak thermal and fast flux of $5x10^{14}$ n/cm^2·sec (E < 0.625eV) and $2.1x10^{14}$ n/cm^2·sec (E>1.0MeV) at a 30 MW thermal power, respectively. Since HANARO began operation in 1995, numerous experimental facilities have been developed and installed in its 32 vertical holes and 7 horizontal beam ports to support fuels and material irradiations.[99 through 102]

Test equipment for irradiating nuclear fuels and materials in HANARO are classified into two categories: capsules (non-instrumented and instrumented), and FTL (Fuel Test Loop). Instrumented capsules or test rigs for materials irradiations may include thermocouples, fluence monitors, and heaters. Fuel tests may include thermocouples (Types K and C), pressure transducers and elongation thermometers to measure fuel temperature, internal pressure of the fuel rod, and fuel deformation, respectively, and SPNDs to detect neutron flux. KAERI has also developed specialized capsules for creep and fatigue testing. These capsules include thermocouples, fluence monitors, and heaters. KAERI typically procures commercially-available sensors from Thermocoax (thermocouples and SPNDs), Studsvik (SPNDs) and IFE/HRP (LVDTs). Recently, KAERI has initiated efforts to obtain enhanced instrumentation for testing of LWR and advanced reactor fuels and materials, including the use of instrumentation from other countries.[100]

3.7. ORNL

The High-Flux Isotope Reactor (HFIR), which is located at and operated by Oak Ridge National Laboratory (ORNL), is an 100-MW_{th} isotope production and test reactor that is beryllium-reflected, light-water-cooled and -moderated, with highly enriched uranium-235 as the fuel. HFIR provides one of the highest steady-state neutron fluxes available in any of the world's reactors, and neutron currents from its four horizontal beam tubes are among the highest available.

Originally, HFIR was primarily designed for producing transuranium isotopes. However, many experiment-irradiation facilities were included in its original design; and several others have been added. Experiment-irradiation facilities available include (1) four horizontal beam tubes, which originate in the beryllium reflector; (2) the hydraulic tube facility, located in the very high flux region of the flux trap, which allows for insertion and removal of irradiation samples while the reactor is operating; (3) thirty target positions in the flux trap, which normally contain transuranium production rods but which can be used for the irradiation of other experiments (two are instrumented target positions provided by a recent modification); (4) six peripheral target positions located at the outer edge of the flux trap; (5) numerous vertical irradiation facilities of various sizes located throughout the beryllium reflector; (6) two pneumatic tube facilities in the beryllium reflector, which allow for insertion and removal of irradiation samples while the reactor is operating for activation analysis; and (7) four slant access facilities, called "engineering facilities," located adjacent to the outer edge of the beryllium reflector. In addition, spent fuel assemblies are used for gamma irradiation in the gamma irradiation facility in the reactor pool.

Today, HFIR is principally used to provide a stable neutron source for fundamental scientific experiments associated with neutron scattering. A 5 inch deep flux trap located at the center of the HFIR fuel element provides a thermal neutron flux of 2 $x10^{15}$ n/cm^2-sec for instrumented lead capsules and loop tests; reflector positions are available for exposing samples in static capsules, loop, and isotope production tests

to fluxes of 1 x 10^{15} n/cm^2-sec. Access to some experimental positions is via a pneumatic tube to allow rapid insertion and removal during reactor operation. HFIR irradiations are typically "static capsule" and "rabbit" tests and rely on sensors that can provide integral values, such as fluence wires, or peak values, such as flux wires. However, ORNL has significantly advanced the use of one unique sensor, Silicon Carbide (SiC) temperature monitors for detecting peak temperature in static capsule tests. The capability to deploy and evaluate these sensors, which are discussed in Section 3.7.1, has been replicated at INL to support ATR NSUF irradiations.

3.7.1. Silicon Carbide Temperature Monitors for Peak Temperature Detection

Since the early 1960s, the observation that irradiation-induced swelling of SiC begins to anneal out at temperatures exceeding its irradiation temperature has been used as a post-irradiation temperature monitor.[108 through 110] Various approaches (e.g., changes in length, density, thermal conductivity, and electrical resistivity) have been used to infer irradiation temperature from this observed phenomena. Snead et al.[109] recommends using changes in resistivity because of improved accuracy, ease of measurement, and reduced costs. Work presented by Snead in Reference 108 was conducted on SiC produced by chemical vapor deposition (CVD). This material is fully dense (3.203 g/cc) and stoichiometric. Comparisons between SiC measurements and thermocouples indicate that accuracies of approximately 20 °C are possible for dose ranges of 1 to 8 dpa and temperatures from 200 to at least 800 °C. Absolute limits for this approach are 150 °C (an amorphorous threshold) and 875 °C (due to recrystallization). Note that Reference 109 cites that measurements should be taken in a controlled environment (within 0.4 °C) with annealing periods of approximately 30 minutes to obtain these accuracies.

Figure 3-51 (from Reference 109) shows data obtained from this technique. The curves shown in this figure represent data obtained from a series of samples, all irradiated in the ORNL HFIR core at similar dose rates of ~ 8 x 10^{14} n/cm^2-s (E > 0.1 MeV). The total dose for the curves is not identical. The curve for an irradiation temperature of ~350 °C is at the lowest dose (~0.1 dpa, assuming 1 dpa = 1 x 10^{21} n/cm^2; E>0.1 MeV) while the remainder are from ~1-8 dpa. It is speculated that the apparent saturation in normalized resistivity for the 0.1 dpa sample represents the point at which the simplest of the defects in the irradiated SiC have annealed away and represents conductivity at the new dopant level for the irradiated SiC.

It should be noted that there are several limitations associated with the use of SiC temperature detectors. As discussed in Reference 109, temperatures are inferred by post-irradiation detection of changes in the stable defect population within SiC monitors that were incurred during irradiation. Some examples where errors could be inferred from SiC monitors cited in Reference 109 include:

- *Irradiation temperatures rising during the latter part of irradiation.* For damages greater than 0.1 dpa, the increasing temperature will anneal out defects that occur at the lower irradiation temperature, while creating stable defects at the higher temperature. When isochronal annealing is performed, lower temperature defects (to some or great extent) will have already been removed, and the recovery curve will be smeared to somewhat higher temperatures. If the temperature increase during irradiation is small, or the time at higher temperature is short, then the original departure from linearity will give the earlier irradiation temperature.
- *Irradiation temperatures decreasing during irradiation.* This decrease will lead to defects being created and frozen-in at the higher-temperature, while continuing to create lower temperature defects. The isochronal anneal will then give an indication of the lowest irradiation temperature (in

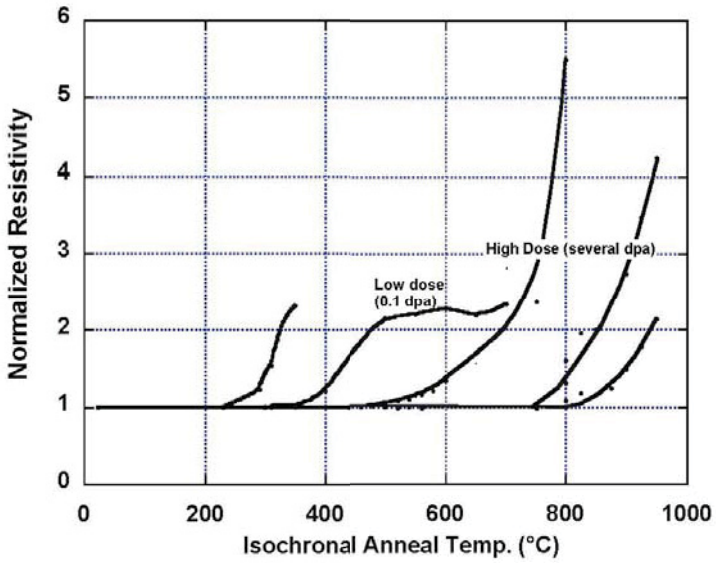

Figure 3-51. Electrical resistivity technique applied over a range of irradiation temperatures.

this case at the end of the irradiation period), and the recovery curve will be smeared due to annealing of higher temperature defects.

- *Upward or downward temperature spikes during irradiation.* This case has the potential to lead to partially created or annealed defects, depending on the change and duration of the temperature increase and the damage to the SiC monitor during irradiation.

However, if irradiation tests are conducted at or near the same temperature when the reactor is at power, none of these situations are of concern.

4. ENHANCED ATR INSTRUMENTATION STRATEGY

INL has a long history of developing highly specialized instrumentation to meet demands of customers conducting unique tests in INL facilities. Such instrumentation was used in INL test reactors and in facilities from the Power Burst Facility (PBF) and Loss of Fluid Test (LOFT) research programs. Unfortunately, INL instrumentation development and research funding declined significantly in the 1980s, when large test facility programs ended. Until this in-pile instrumentation enhancement effort was initiated, ATR irradiation testing relied primarily on commercial vendors for instrumentation.

As documented in Section 3, several test reactor programs in Europe and Asia, such as the HFR (Petten), HBWR (Halden), and JAEA (JMTR and JOYO) have maintained their instrumentation development and evaluation research capability. Others, such as CEA, are rapidly trying to regain this expertise. As part of the ATR NSUF, it was recognized that a focussed effort was needed at INL if the ATR is to become competitive as a world class irradiation facility. Hence, a research and development plan was developed in 2008 so that ATR users would have access to enhanced real-time in-pile instrumentation, comparable to (and, in some cases, superior to) that available at other MTRs, by 2015. This plan identifies and prioritizes instrumentation research considering ATR NSUF customer and reactor staff needs along with technology readiness. INL progress in accomplishing the objectives outlined in the research plan is presented in this section.

When the ATR NSUF instrumentation strategic plan was originally developed, estimates for the funding required to obtain a world-class instrumentation and testing capability for ATR were identified. During the subsequent years, the allocated ATR NSUF funding level has often been less than the estimates to implement this strategy. However, the instrumentation capability developed with ATR NSUF funds has been sufficient for this effort to continue and to attract funding from other sources. For example, during FY13, the DOE-NE FCRD program, the ATR Life Extension Project (LEP), and the NEET programs funded selected instrumentation development and deployment activities. In addition, selected programs are supported by INL's Laboratory Directed Research and Development (LDRD) program. Hence, having a focussed and coordinated effort to provide US MTRs advanced in-pile instrumentation and standardized test rigs incorporating such instrumentation is essential if the US is to benefit from this DOE investment.

4.1. Motivation/Justification for Investment

This research and development program is sorely needed and necessary if the ATR NSUF wishes to attract additional researchers from universities, laboratories, and industry. Key points for the business case to support this effort include:

- ***Vital Component for ATR NSUF Success.*** If the ATR is to become a world-class irradiation facility, adequate instrumentation must be available to its users. As noted in Section 2, the ATR has advantages over many other MTRs with smaller irradiation test locations and lower flux levels. Yet, instrumentation capabilities developed by research staff at other test reactors allow their customers to obtain real-time data from tests that cannot be obtained from tests conducted in the ATR.
- ***Focussed Instrumentation Development to Attract Near-term Customers.*** INL's position as the lead DOE-NE lab uniquely positions this research program so that it can easily focus instrumentation research and development efforts to help meet near-term DOE-NE customer needs and help the ATR attract other customers, such as the US Nuclear Regulatory Commission (US NRC) and

DOE-NE's Advanced Reactor Concepts (ARC), Next Generation Nuclear Plant (NGNP), Advanced Small Modular Reactor (SMR), and LWR Sustainability (LWRS) programs.

- ***Expertise and Facilities for Deploying Unique Instrumentation***. Much of the investment has already been made to obtain the right equipment and trained staff. INL's HTTL possesses unique equipment for evaluating and fabricating required instrumentation. The newly-relocated HTTL a world-class facility for sensor fabrication and evaluation, and the TTAF is a world-class test rig fabrication and assembly facility. INL also has unique test reactors and gamma irradiation facilities for demonstrating and using new instrumentation for in-pile measurements.

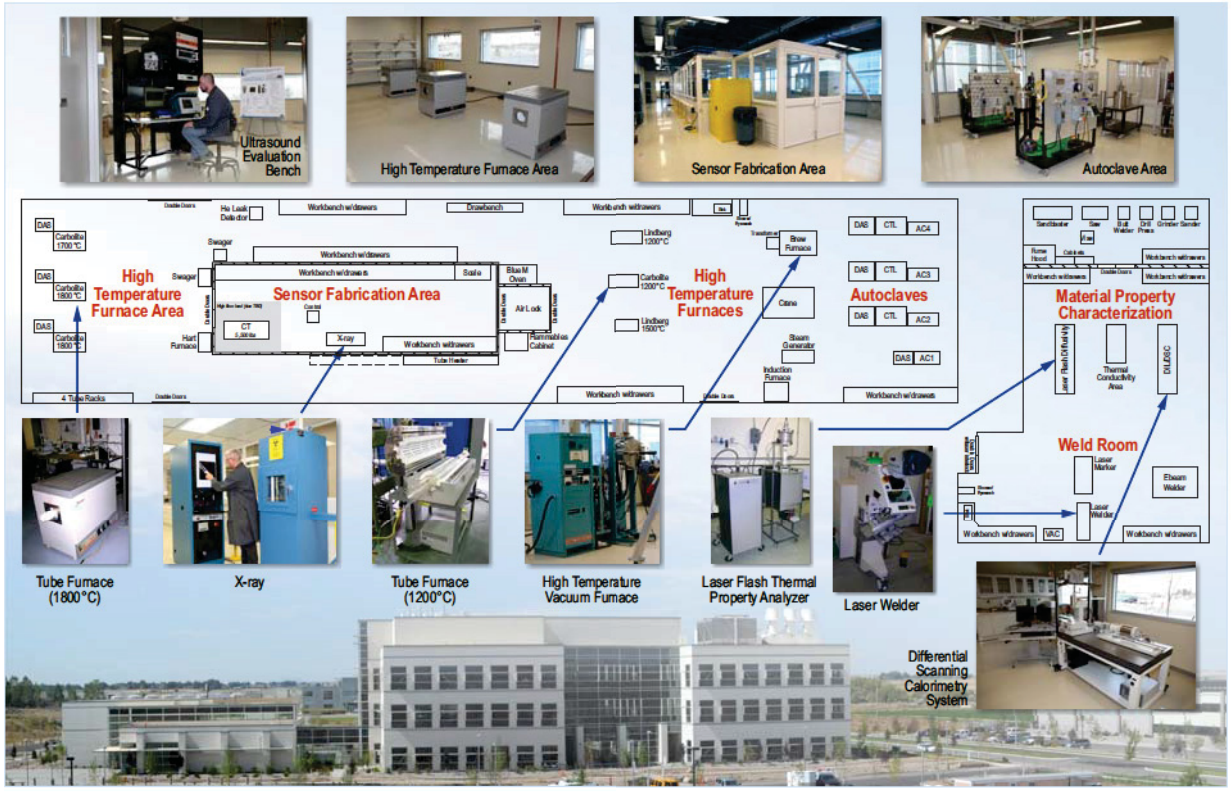

Figure 4-1. HTTL layout and equipment.

- ***Increased usage of US MTRs.*** As documented in Section 3.3, data from irradiation tests at international MTRs have identified issues affecting US commercial nuclear power plants, such as thermal conductivity degradation in fuel as a function of burnup and dispersion and axial relocation of fuel during a Loss of Coolant Accident. As US vendors strive to enhance LWR fuels, it is important to have a domestic capability for evaluating fuel irradiation performance.
- ***Market for research program task collaboration and products.*** Clearly, the primary market for products from this effort is ATR NSUF users. However, INL-developed instrumentation is also attracting customers that operate other MTRs (e.g., HBWR, OSIRIS, and the MITR). In addition, there is the potential for adapted versions of instrumentation developed and deployed from this research to be used in commercial nuclear power plants, in spent fuel dry storage casks, and in applications funded by the National Aeronautics and Space Administration (NASA) or the Department of Defense (DOD).

Potential funding sources for an ATR NSUF instrumentation program and its products are summarized in Table 4-1. This table also lists potential collaborators for various instrumentation program elements.

Table 4-1. Funding sources and potential collaborators for INL instrumentation elements.

Program Elements	Funding Sources	Collaborators
Sensor Development	DOE-NE LWRS; DOE-NE FCRD; DOE-NE NEET (ATR NSUF, Advanced Sensors Initiative). Others, such as the DOE-EM; US NRC; DOD; Naval Reactors, NASA); INL LDRD	IFE/HRP; CEA; SCK•CEN KAERI; JAEA International Funding Agencies [OECD, IAEA, Joint Research Centre (JRC)]
Developed Sensors-Nuclear Customers	Other MTRs (CEA-OSIRIS and JHR, NRG/JRC - HFR, KAERI-HANARO, ORNL-HFIR, IFE/HRP- HBWR, JAEA- JMTR, SNL-Annular Core Research Reactor (ACRR), MIT-MITR) Commercial Nuclear Reactors DOE-NE (NGNP, FCRD, LWRS, ARC, Advanced SMRs) Others, such as the US NRC, Department of Defense (DOD); Naval Reactors, NASA).	Commercial Industry (fiber optic and thermocouple vendors via government sponsored grants or venture capital) to transfer technology.
Developed Sensors-Non-Nuclear Customers	DOD, NASA, Aircraft Industry, Petroleum Industry, Coal Industry	Commercial Industry (fiber optic and thermocouple vendors via government sponsored grants or venture capital) to transfer technology.

4.2. Currently Available ATR NSUF Instrumentation

Table 4-2 identifies instrumentation currently available for ATR NSUF experiments. As discussed in Section 2, ATR irradiation capabilities in static capsule, shuttle, instrumented lead, and PWR loop tests, are unparalleled. However, as indicated in column 5 of Table 4-2, available instrumentation for measuring parameters of interest during an irradiation test is limited at each irradiation location. As indicated by column 6, sensors available at other MTRs could increase measurement capabilities during ATR irradiations. Note that adapting instrumentation from other test reactors often requires laboratory demonstrations because of ATR-specific irradiation conditions and test capsule geometries. For example, devices may be required that can withstand higher temperatures and fluences. Column 7, which is labeled "Developmental" under "Proposed Instrumentation Advancement" lists developmental or non-nuclear technologies that could offer enhanced in-pile measurement capabilities. Typically, technologies listed in this column are considered to be less "ready" for implementation.

Table 4-2. Instrumentation available at ATR and proposed advanced technologies.

Parameter	Location			Available Technology at ATR	Proposed Advanced Technology	
	Static Capsule/ Shuttle	Instr. Lead	PWR Loop		Available at Other MTRs	Developmental
Temperature	✔	✔	✔	-Melt wires (peak)[a,b] -Silicon Carbide (SiC) temperature monitors (range)	-Paint spots (peak) -Thermal Expansion Devices (TEDs)	
		✔	✔	-Thermocouples (Type N, K, C[c], and HTIR-TCs[d])	-Expansion thermometer	- Fiber optics -Noise thermometry -Ultrasonic thermometers (UTs)
Thermal Conductivity		✔	✔	- Transient Hot Wire Method Needle Probe (THWM NP)	-Degradation using signal changes in thermocouples	
Flux/Fluence (neutron)	✔	✔	✔	-Flux wires and foils		
		✔	✔		-Self-Powered Neutron Detectors (SPNDs) -Subminiature / miniature fission chambers	- Moveable SPNDs - Micro-Pocket Fission Detectors (MPFDs)
Gamma Heating / Gamma Flux		✔	✔		-Calorimeters -Gamma thermometers -Self-Powered Gamma Detectors (SPGDs)	
Dimensional		✔	✔	-LVDT-based elongation	-Diameter gauge	-Ultrasonic techniques -Fiber optics
Fission Gas (Amount, Composition)		✔	✔	-On-line Sampling -Pressure gauge	-LVDT-based pressure monitors	-Acoustic measurements with high-frequency echography
Loop Pressure			✔	-Differential pressure transmitters -Pressure gauges with impulse lines		
Loop Flowrate			✔	-Flow venturis -Orifice plates	-Turbine flow meters (for individual fuel assemblies)	
Loop Water Chemistry			✔	-Off-line sampling / analysis	-Electrical chemical potential probes	
Crud Deposition			✔		- Diameter gauge with neutron detectors, and thermocouples	
Crack Growth Rate			✔		-Direct current potential drop (DCPD) technique	

a. Text color in Columns 5 through 7 designates:
Black - Sensors or capabilities existing at the ATR or existing or under development at other MTRs
Blue - New or enhanced sensors being investigated or for which investigations were initiated but deferred due to funding limitations
Magenta - New or enhanced sensors or capabilities for which laboratory investigations have been completed but require irradiation evaluation
Red - New or enhanced sensors or test rigs now deployed at the ATR because of recent instrumentation research
b. Although melt wires have been used at ATR, recent efforts have expanded the types offered to our users, allowing more accurate estimates of peak temperature with enhanced encapsulation methods.
c. Type C thermocouple use requires a "correction factor" to correct for decalibration during irradiation.
d. High Temperature Irradiation Resistant ThermoCouple (HTIR-TC)

As part of the ATR NSUF program (and several other DOE-NE programs), several activities have been initiated to develop and implement new in-pile instrumentation capabilities. Blue text in Table 4-2 indicates current instrumentation research efforts, red text indicates demonstrated new or enhanced sensors

now available to users as a result of recent instrumentation research, and magenta text indicates new sensors and capabilities that are now ready for deployment as a result of recent instrumentation research. Instrumentation development tasks were selected based on anticipated user needs by the ATR NSUF or other DOE-NE programs and 'technology readiness' (providing users needed instrumentation in the near-term). The ultimate goal of this effort is to provide ATR users with sensors for detecting all of the parameters listed in Table 4-2.

Many instrumentation development efforts are in collaboration with other organizations. As indicated in Table 4-2, several new or enhanced sensors are now available to ATR users as a result of this instrumentation development effort. In many cases, it would not have been possible to have such sensors available so quickly to ATR users without the assistance obtained from collaborations with other organizations.

4.3. Current Prioritization for Instrumentation Development

Figure 5 graphically illustrates the process for developing and demonstrating instrumentation needed to advance ATR NSUF testing capabilities. There are several major activities identified, "Near-Term Technologies", and "Developmental", and "Expansion". Representative tasks identified in each area are also shown with qualitative judgments with respect to ATR capabilities compared to other test reactors. As indicated, the ATR NSUF is expected to have comparable instrumentation for many parameters during FY14, and "world class" (e.g., comparable in many cases, and in some cases, superior) irradiation capabilities by FY15. Nevertheless, the ability to meet such goals is dependent upon allocated funding levels and sensor irradiation schedules. Current efforts to meet this national need come from various sources, and the ability to meet this FY15 goal is dependent upon allocated funding levels and sensor irradiation schedules. For example, delays in completing planned tests in the ATRC facility during 2012 and 2013 have delayed progress in providing real-time flux monitors to ATR NSUF users. Likewise, 2014 ATR NSU&F funding allocations have delayed progress on activities related to evaluations of gamma thermometers and SPGDs.

Table 4-3 summarizes the status of the effort to provide enhanced in-pile instrumentation to ATR users. Similar to Table 4-2, blue text indicates current instrumentation research efforts, and red and magenta text indicates new sensors now available to users as a result of recent instrumentation research. More detailed information about on-going instrumentation activities is provided in Section 5. As indicated in Tables 4-2 and 4-3, considerable progress has been made in this program since its inception. Several new sensors are now available to users; and as indicated in Section 5, several additional sensors should soon be available. It is also encouraging to see that some level of research has been initiated on many of the sensor technologies identified in this table. However, funding availability has delayed certain instrumentation deployment activities. For example, the FCRD program has been interested in (and funded development of) ultrasound-based and fiber optic-based instrumentation that can provide higher resolution/higher accuracy data than currently-available instrumentation. Unfortunately, decreases in FCRD funding for in-pile instrumentation has delayed planned deployment of such sensors. Blue italics text indicates instrumentation efforts in which activities have been delayed in FY14 due to such funding limitations.

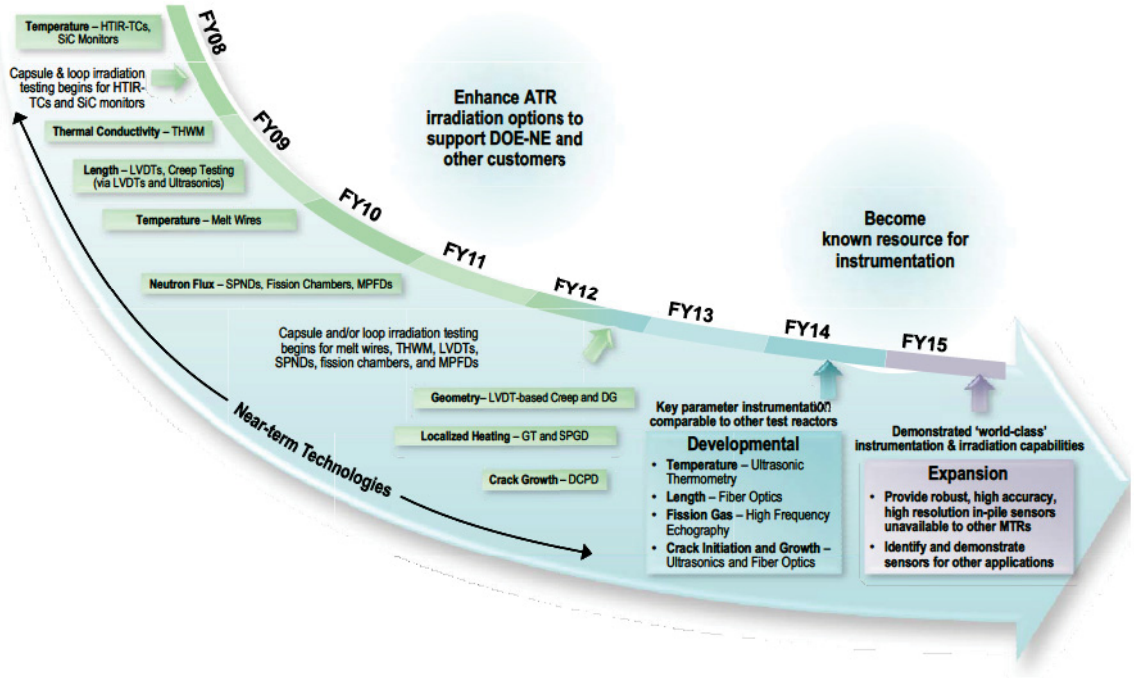

Figure ES-5. ATR NSUF advanced instrumentation research and development (timing is dependent on funding availability).

Table 4-3. Status of ATR NSUF sensor development and enhancement efforts.

Parameter	Sensor	Status
Temperature	Melt Wires[a]	Currently used in several ATR NSUF irradiations. Both quartz and vanadium encapsulation available for wires with melting temperatures between 85 and 1455 °C.
	SiC Temperature Monitors	Currently used in several ATR NSUF irradiations.
	HTIR-TC	Initial out-of-pile testing completed. In-pile testing (in the first Advanced Gas Reactor (AGR-1) NGNP fuel irradiation test) and sensor enhancement evaluations completed; HTIR-TCs provided to MIT and IFE/HRP. Additional HTIR-TCs being fabricated for NGNP program in FY14.
	Ultrasonic Thermometers (UTs)	FCRD program funded first two years of a three year effort to develop and evaluate an enhanced prototype. Additional funding required to complete prototype evaluations and design optimization. Although prototype is focussed on use of magnetostrictive transducers, deployment will benefit from MITR test to compare irradiation-related survivability of piezoelectric and magnetostrictive transducers.
Thermal Conductivity	THWM NP	Prototype design developed and initial laboratory testing completed. Prototype THWM probe prepared and shipped to CEA and being prepared for shipment to IFE/HRP.

Table 4-3. Status of ATR NSUF sensor development and enhancement efforts.

Parameter	Sensor	Status
Elongation, Crud deposition, Corrosion	LVDTs	Out-of-pile testing completed on developmental LVDT that resists high temperature degradation and eliminates Curie temperature effects.
	Diameter gauge	Currently used in the Halden Boiling Water Reactor (HBWR) for detecting swelling, corrosion, and crud buildup. Three year LDRD initiated in FY14.
	Ultrasonic Techniques	Scoping tests completed on elongation prototype. Prior to deployment, additional prototype out-of-pile testing needed and results from NEET-funded MITR piezoelectric and magnetostrictive transducer irradiation test needed.
	Fiber Optic Techniques	FCRD funded first two years of a three year effort to develop and evaluate the accuracy of a candidate probe. Prior to deployment, an instrumented lead test needed to evaluate fiber optic survivability in radiation environments.
In-pile Creep Test Rig	LVDT-based rig with bellows	Design developed and prototype evaluated at PWR conditions in a laboratory autoclave. Enhanced design, with variable load capability, developed and evaluated in a laboratory autoclave. Both designs developed for future use an ATR PWR loop.
Neutron Flux	Flux wires and foils	Various flux wires and foils available. Vanadium encapsulation available.
	SPNDs and fission chambers	Specially-developed fixturing designed, fabricated, and installed at ATRC. In FY13, additional evaluations of detectors completed. Additional ATRC evaluations planned for FY14. In addition, SPND will be included in NEET-funded MITR. Development of MPFDs for ATRC evaluations underway.
Gamma Heating	*SPGDs and Gamma thermometers*	Currently used at HBWR; SPGDs will be included in NEET-funded MITR irradiation in FY14.
Crack propagation	DCPD method with CT specimens	Currently used at HBWR; Investigations initiated in 2012.
	Ultrasonic techniques	Funding source needed for laboratory evaluations. Prior to deployment, results of piezoelectric and magnetostrictive transducer irradiation test at MITR needed.
	Fiber optics techniques	Funding source needed for laboratory evaluations. Prior to deployment, an instrumented lead test needed to evaluate fiber optic survivability in radiation environments.

a. Font in Column 2 designates:
Black - Sensors or capabilities existing at the ATR or existing or under development at other MTRs
Blue - New or enhanced sensors being investigated or if italics, for which investigations were initiated but deferred due to funding limitations
Magenta - New or enhanced sensors or capabilities for which laboratory investigations have been completed but require irradiation evaluation
Red - New or enhanced sensors or test rigs now deployed at the ATR because of recent instrumentation research

In addition to providing ATR customers the instrumentation required for their irradiation tests, this program has clearly added to the prestige and capabilities of the ATR NSUF, INL, and to the DOE. International collaborations have been established with leading in-pile testing organizations, such as IFE/HRP and CEA. Partnerships with universities have not only helped students successfully complete their graduate level research, but have led to new INL employees. Over 29 peer-reviewed conference papers and 22 archival journal papers have been produced, and several patents have been awarded or are pending from this research.

5. DEVELOPMENT - IDAHO NATIONAL LABORATORY

Several INL efforts are underway to enhance in-pile instrumentation for ATR users. As indicated in Section 4, these efforts continue to focus on obtaining and deploying instrumentation for measuring a wide range of parameters and conditions to support irradiation needs for the ATR NSUF and other DOE programs. This section summarizes the status of on-going and planned sensor development and evaluation efforts at INL. Additional details related to sensor development and deployment activities are found in References 103 though 105.

5.1. Temperature Sensors

Temperature is a key parameter of interest during fuel and material irradiations. As indicated in Table 4-2, available temperature detection sensors to ATR NSUF users are comparable, if not superior, to those used at other MTRs. Melt wires and commercially-available thermocouples (e.g., Types K, N, and C) have been available for decades, but were procured from external vendors. To meet recent customer requests for peak temperature indicators in static capsule and hydraulic shuttle locations, an increased selection of melt wires with enhanced encapsulation is now available from in-house sources. In addition, SiC temperature monitors can now be evaluated by HTTL staff. These 'peak temperature' indicators, commercially-produced thermocouples, and doped molybdenum/niobium alloy HTIR-TCs are available for instrumented lead and PWR loop applications. Development of enhanced ultrasonic thermometers for temperature measurement is also underway.

5.1.1. Melt wires

Melt wires are the simplest and least expensive option available for monitoring temperature in ATR tests. Metallic wires of a known composition and well characterized melting temperature are included in a test to determine if a specific peak temperature has been reached or exceeded. As described in American Society for Testing and Materials (ASTM) E 1214-06,[106] melt wire materials should consist of metals with 99.9% purity or be eutectic alloys such that their measured melting temperatures are within ± 3 °C of the recognized melting temperatures. The standard states that transmutation-induced changes of selected wires should not be considered significant up to 1 x 10^{20} n/cm^2 (E > 1 MeV). As noted in Reference 106, melt wires should be selected to measure temperature at 5 to 12 °C intervals, with at least one melt wire that possesses a melting temperature greater than the highest anticipated temperature.

INL has established a library of melt wires and developed in-house capabilities to verify the melting temperature of candidate wire materials (ranging from ~85 to 1455 °C) using a DSC installed at INL's HTTL.[107] When possible, INL selects high purity materials with low thermal neutron capture cross-sections. Table 5-1 lists the melt wire materials currently available for irradiation testing that have undergone verification testing. Note that the current library has been developed according to user requests. It is anticipated that the number of materials in this library will increase as additional user requests are received.

INL has developed several options for encasing melt wires, including encasing multiple melt wires into a single 1.6 mm diameter quartz tube or a single wire in a 1.7 mm diameter metallic capsule. Figure 5-1 shows a quartz tube containing multiple melt wires after progressive heating steps during verification testing in high temperature furnaces installed at INL's HTTL. The wires selected are chosen based

Table 5-1. Melt wire materials and melting temperatures currently available in INL library.

Material (component weight%)	Melt Onset Temperature, °C
56.2Bi 33.8Pb 10Sn	85.0
65Bi35In	110.6
55.2Bi 44.8Pb	126.4
57Bi43Sn	139.4
100Sn	231.8
95Sn5Sb	238.6
90Pb10Sb	252.4
80Au 20Sn	279.5
100 Bi	271.4
97.5Pb5Ag5Sn	302.9
97.5Pb0.75Sn 1.75Ag	309.3
100 Pb	327.5
95Zn5Al	381.2
95Zn5Al	381.2
85Te 15Sn	399.4
100 Zn	419.6
80Sb20Zn	507.8
100 Al	660.5
49Ag16Cu23Zn7.5Mn4.5Ni	681.3
40Ti20Zr20Cu20Ni	850.7
98.2Cu1.8Be	865.1
100Ge	938.3
82Au 18Ni	955.0
100 Ag	961.9
65Cu35Au	995.6
100Au	1064.0
100Cu	1084.6
70Cu30Ni	1191.0
28Mo69Ni2Fe1Co1Cr	1370.0
Ni	1455.0

on expected irradiation test temperatures and required resolution. The melt wires depicted in Figure 5-1a are considered good materials for this purpose because melting may be determined by visual inspection. This is important because this determination must be made during Post Irradiation Examination (PIE) in a hot cell. Figure 5-1b shows melt wires that were determined to be less-ideal choices for use. For these wires, melting (confirmed through DSC testing) could not easily be determined by visual inspection; and microscopic examination was required. Melting in these cases had to be determined by changes to the surface condition of the wires rather than bulk deformation of the wires. As noted above, metallic tubes are also available for encapsulation in ATR tests. However, post-test examination is more complicated, requir-

ing radiography, computer tomography, or destructive examination of the tube to allow inspection of the wire after irradiation.

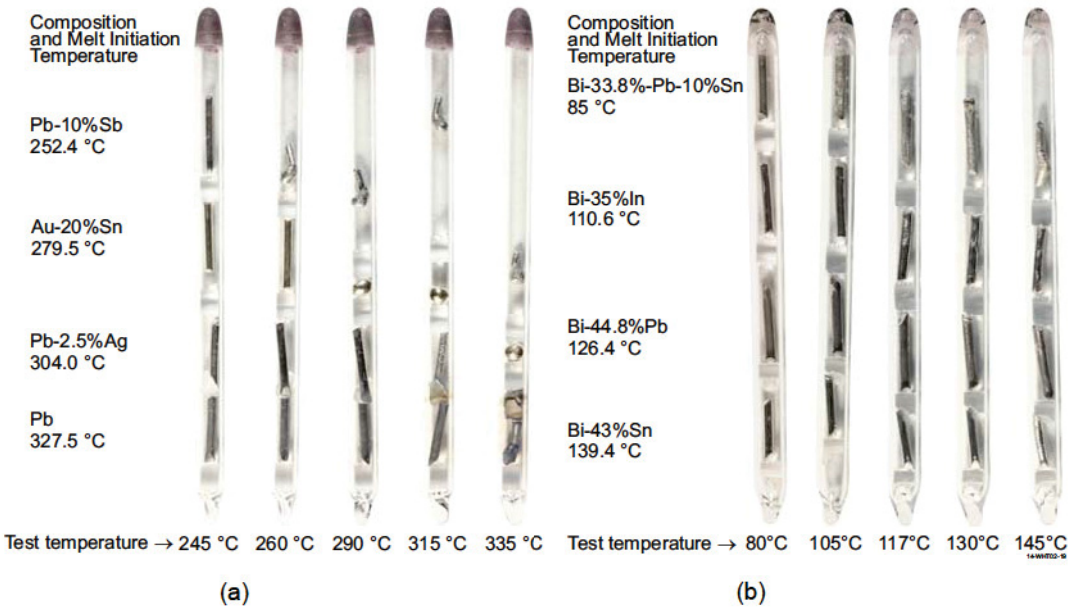

Figure 5-1. Quartz tube containing four melt wires in separated compartments: (a) Example of ideal indicator melt wires; (b) Example of non-ideal indicator melt wires.

5.1.2. Silicon Carbide Temperature Monitors

Another option available to ATR users for peak temperature detection is the use of SiC temperature monitors. The benefit of this option is that a single small monitor (typically 1 mm x 1 mm x 10 mm or 1 mm diameter x 10 mm length) can be used to detect peak irradiation temperatures between 200 and 800 °C (and possibly up to temperatures near 900 °C). SiC incurs damage in its crystalline structure during irradiation. This causes several measurable physical changes to the monitor (i.e. changes in dimensions, thermal conductivity, electrical resistivity, etc.). When the monitor is annealed at a temperature greater than the peak irradiation temperature, the altered properties rapidly change.[108-110]

As discussed in Section 3.7.1, Snead et al. at ORNL successfully used changes in electrical resistivity to detect peak irradiation temperatures with accuracies of approximately 20 °C for dose ranges of 1 to 8 dpa and temperatures between 200 and 800 °C.[109] Experimental data[110] suggest that upper and lower bounds for this range may be extended.

Specialized equipment at INL's HTTL now allows peak temperature detection with irradiated SiC monitors. With this equipment, the SiC sensor electrical resistivity is measured after annealing in a furnace located within a stainless steel enclosure at the HTTL (shown in Figure 5-2). After annealing, cooled samples are placed into a constant temperature environmental test chamber to ensure electrical resistivity measurements are taken within 0.2 °C of a predetermined temperature (typically near 30 °C). A high accuracy (9 digit) multimeter, located outside the stainless steel enclosure, is used to obtain resistance measurements. Specialized fixturing (Figure 5-2) was developed to ensure that measurements are taken with the SiC sensors placed consistently in the same orientation. A four point probe technique is used with the

points connected to the sample through spring-loaded, angled electrodes that hold the SiC temperature monitor in place. Current and voltage are provided to the sample via wires that are threaded through the holes in the electrodes. The accuracy of this new INL capability was verified by completing comparison measurements with ORNL on identical sensors that had been subjected to identical irradiation conditions.[107] Results, as shown in Figure 5-3, indicate that similar peak irradiation temperatures are inferred from ORNL and INL measurements in these evaluations (e.g., significant increases in normalized electrical resistivity at 300 °C and at 670 °C were observed).

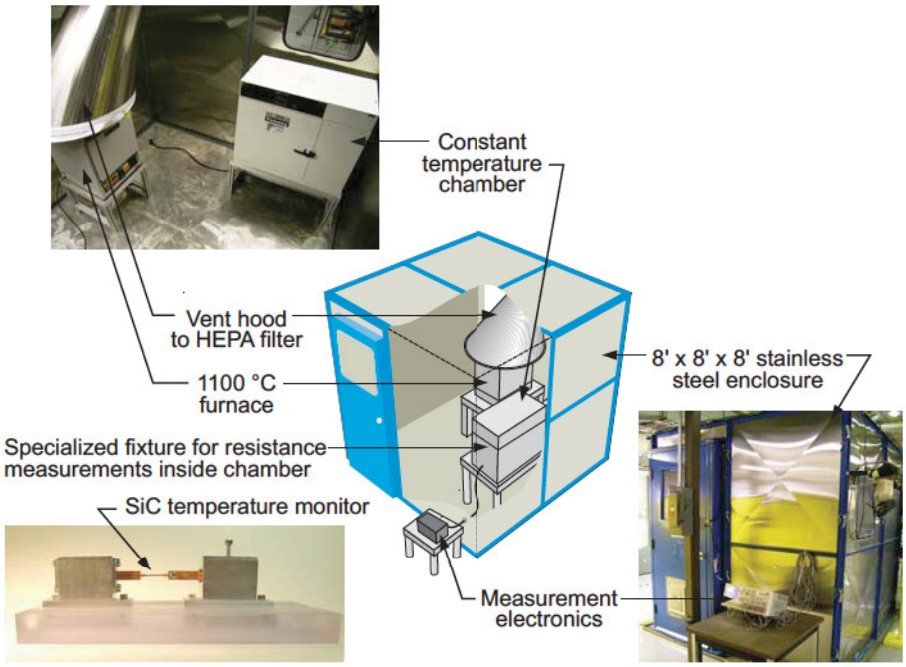

Figure 5-2. Setup to anneal and measure electrical resistivity of SiC temperature monitors.

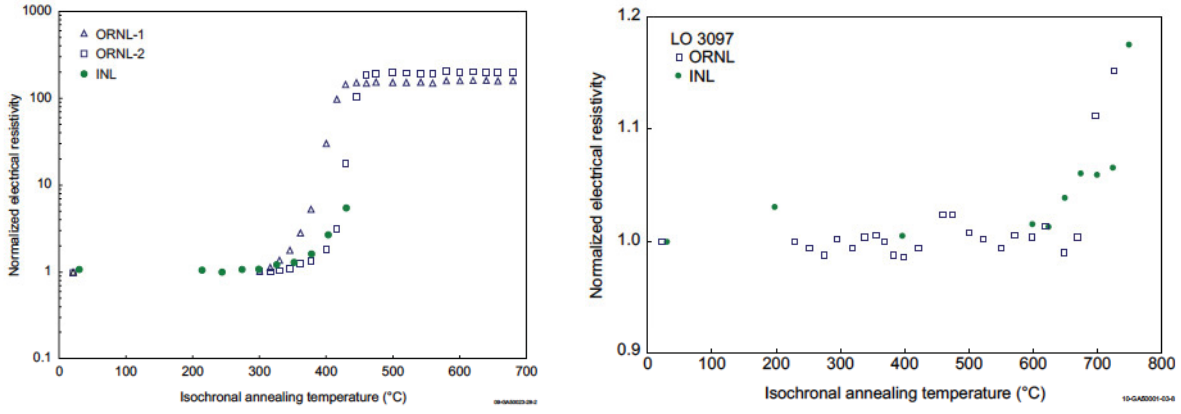

Figure 5-3. Electrical resistivity measurement comparison on SiC monitors irradiated at peak temperatures of (a) 300 °C and (b) 670 °C.

Several irradiation capsules in the ATR now contain SiC temperature monitors. During 2011, two of the SiC monitors included in the ATR NSUF University of Wisconsin test[112] were evaluated using the HTTL procedure[113] developed for such evaluations; and results are documented in Reference 114. It is

anticipated that the use of SiC monitors will continue to increase as additional ATR users include SiC temperature monitors in their tests. In particular, monitors from several ATR NSUF university-led experiments and an EPRI test are scheduled for evaluation in 2014.

5.1.3. High Temperature Irradiation Resistant Thermocouples (HTIR-TCs)

Real-time temperature measurements during irradiation tests are typically made with commercially-available, mineral insulated, metallic sheathed thermocouples. These thermocouples are used to monitor and/or control the temperature achieved during irradiation. For temperatures below 1000 °C, experimental needs are typically met using Type K or Type N thermocouples, which have excellent reliability and signal stability under irradiation, even for very high neutron fluences exceeding 10^{22} n/cm^2 (thermal neutrons). However, these thermocouples decalibrate when exposed to temperatures above 1100 °C. Although other types of commercially-available thermocouples exist for higher temperature applications (up to 1800 °C), the thermoelements used in these thermocouples contain materials such as tungsten and rhenium (in the case of Type C and D thermocouples) or platinum and rhodium (Type R, S, and B) that decalibrate due to transmutation from absorption of neutrons. Hence, thermocouples were needed that could withstand both high temperature and high radiation environments.

To address this need, INL developed a HTIR-TC that contains commercially-available doped molybdenum alloy paired with a niobium alloy. HTIR-TC component materials were selected based on data obtained from materials interaction tests, ductility investigations, and resolution evaluations (see References 115 through 122). HTIR-TC long duration performance has been demonstrated through testing, in which thermocouples were held at elevated temperatures (from 1200 °C to 1800 °C) for up to 6 months. The 1200 °C test included nineteen commercially-available Type N thermocouples, three commercially-available Type K thermocouples, and nine INL-developed swaged HTIR-TCs. As indicated in Figure 5-4, some Type K and N thermocouples drifted by over 100 °C or 8%. Much smaller drifts (typically less than 20 °C or 2%) were observed in the INL-developed HTIR-TCs. As documented in Reference 116, similar drifts (2%) were observed in HTIR-TCs in a long duration (4000 hour) test completed at 1400 °C and smaller drifts (less than 1%) have been observed in HTIR-TCs with enhanced fabrication techniques for higher temperatures (up to 1800 °C).

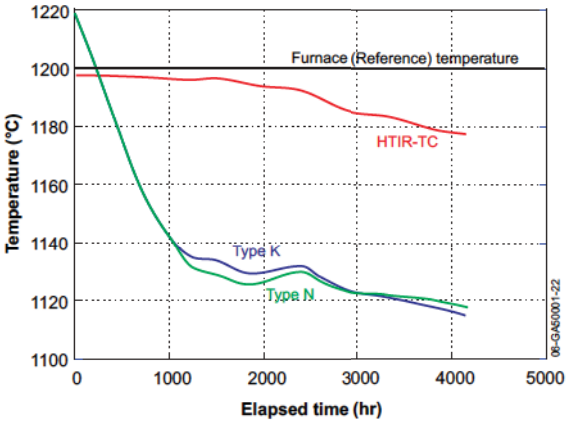

Figure 5-4. Representative thermocouple response in INL 1200 °C tests.

HTIR-TCs were installed in a multi-capsule experiment, in which gas reactor fuel samples were irradiated at temperatures up to 1200 °C in INL's ATR. The test started in February 2007 and ended in October

2009. Figure 5-5 shows signals from two INL-developed HTIR-TCs and one Type N thermocouple located within one of the capsules (Capsule 4). Signal variations are due to ATR power fluctuations and outages (e.g., gray regions correspond to when the ATR was shutdown). As shown in this figure, the HTIR-TC (TC-4-1) located near the Type N thermocouple (TC-4-3) yielded a signal consistent with the signal from this Type N thermocouple at the beginning of this irradiation. In addition, the HTIR-TC located at a higher temperature region within the capsule (TC-4-2) yielded a consistent, but higher temperature, signal. However, in October 2008, the Type N thermocouple failed; and its signal ceased. The successful operation of HTIR-TCs in this test has led to INL supplying them to other test reactors.

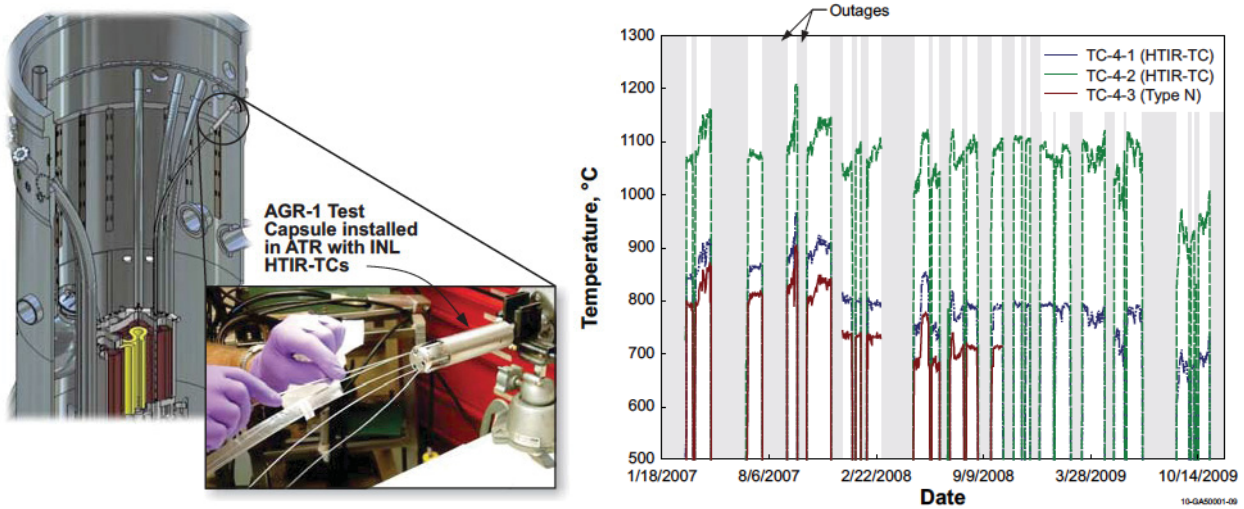

Figure 5-5. HTIR-TCs installed in AGR-1 test capsule and representative HTIR-TC and Type N data during AGR-1 irradiation.

In 2010, three HTIR-TCs were supplied to the Massachusetts Institute of Technology (MIT) for an irradiation test in their research reactor. As discussed in Reference 123, two HTIR-TCs were included in a MIT research reactor (MITR) In-core Sample Assembly (ICSA) test of materials with four capsules (see Figure 5-6). These two HITR-TCs were positioned in the lower two capsules of this test, where peak temperatures were less than 800 °C. The test was conducted in three phases. At the end of the first phase, the upper two capsules were removed (with the lower two capsules and the HTIR-TCs remaining in position). At the start of the third phase, two new upper capsules were inserted. One of the two HTIR-TCs failed during the middle of the second phase of this test, while the second HITR-TCs remained stable throughout the duration of the test. It is suspected that the removal of the upper two capsules after the first phase of the test could have led to mechanical damage to the HTIR-TC that failed.

As part of a Memo of Understanding (MOU) between the IFE/HRP and the INL, the HTTL shipped four HTIR-TCs to IFE/HRP in 2011 for use as fuel centerline thermocouples in upcoming HBWR irradiations. Deployment of HTIR-TCs at the HBWR represents a unique opportunity to observe the performance of HTIR-TCs in a higher temperature (1600 °C) irradiation (although HTIR-TC performance at 1800 °C has been demonstrated in laboratory furnaces, prior irradiations have been limited to peak temperatures of 1200 °C and did not include sensors fabricated with improved processes to enhance HTIR-TC ductility). As indicated in Figure 5-7, prototypes of the enhanced HTIR-TCs exhibited good ductility after stabilization heat treatments.

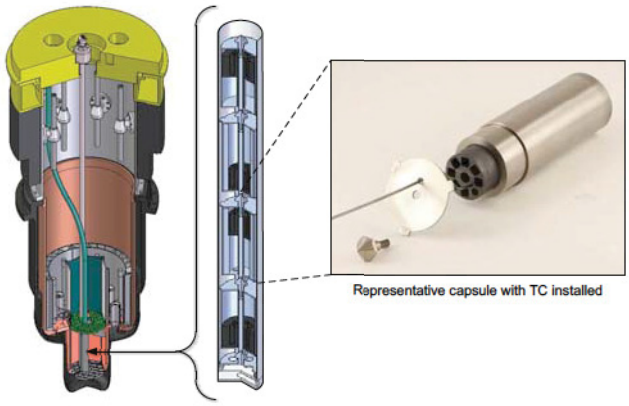

Figure 5-6. Cutaway of MITR core showing position of ICSA assembly with four sample capsules) installed in an in-core position (reactor fuel elements not shown for clarity).

As noted in Section 3.3, the HBWR has relied on Type C thermocouples to support high temperature irradiations. To overcome the decalibration that occurs in Type C thermocouples due to transmutation, the IFE/HRP applies correction factors (based on the fact that the irradiations are always performed at the same flux and temperature distributions in the HBWR). However, in recent years, IFE/HRP staff has expressed interested in deploying HTTL-developed HTIR-TCs. The four HTIR-TCs were shipped to the IFE/HRP in November 2011. IFE/HRP currently plans to include these HTIR-TCs in a fuel irradiation test rig that will be inserted into the HBWR in June 2014. This HBWR irradiation will be the first time that HTTL-developed sensors have been deployed in a foreign MTR. Transmittal of these sensors facilitates on-going HTTL efforts to obtain IFE/HRP assistance in deploying their LVDT-based test rigs for measuring creep elongation and changes in fuel diameter and crack growth rate test rigs at the ATR.

Last, it should be emphasized that the HTIR-TCs are the ONLY thermocouples capable of withstanding temperatures in excess of 1100 °C during an irradiation without decalibration or degradation. In recognition of this fact, the NGNP has commissioned the HTTL to provide them additional HTIR-TCs to support their fuel qualification test program. These HTIR-TCs will be fabricated in FY14.

5.1.4. Ultrasonic Thermometers

Ultrasonic thermometry has the potential to improve upon temperature sensors currently used for in-core temperature measurements.[124] Ultrasonic Thermometers (UTs) can be made with very small diameters while maintaining a high level of durability because the sensor consists of a small diameter rod (typical diameters range from 0.25 mm to 1 mm, although a sheath may be required for some environments).[125] In fact, a small diameter rod is desirable; as ultrasonic wave dispersion is avoided when the rod diameter is sufficiently smaller than the acoustic wavelength.[126] Even though the HTIR-TCs developed by INL have overcome most of the difficulties associated with nuclear-based applications of thermocouples, the resistivity of electrical insulators can degrade if subjected to high temperatures (> 1800 °C), causing shunting errors. However, UT temperature measurements may potentially be made near the melting point of the sensor material, allowing temperatures in excess of 3000 °C to be monitored for certain sensor materials. A clear line of sight is not required with UTs, as is the case for most optical pyrometry applications. With proper selection of materials, UTs may be used in very harsh environments, such as high temperature steam or liquid metals. Furthermore, thermocouples typically only allow measurement at a single location, and examination of melt wires or silicon carbide monitors only allow estimation of the maximum test tem-

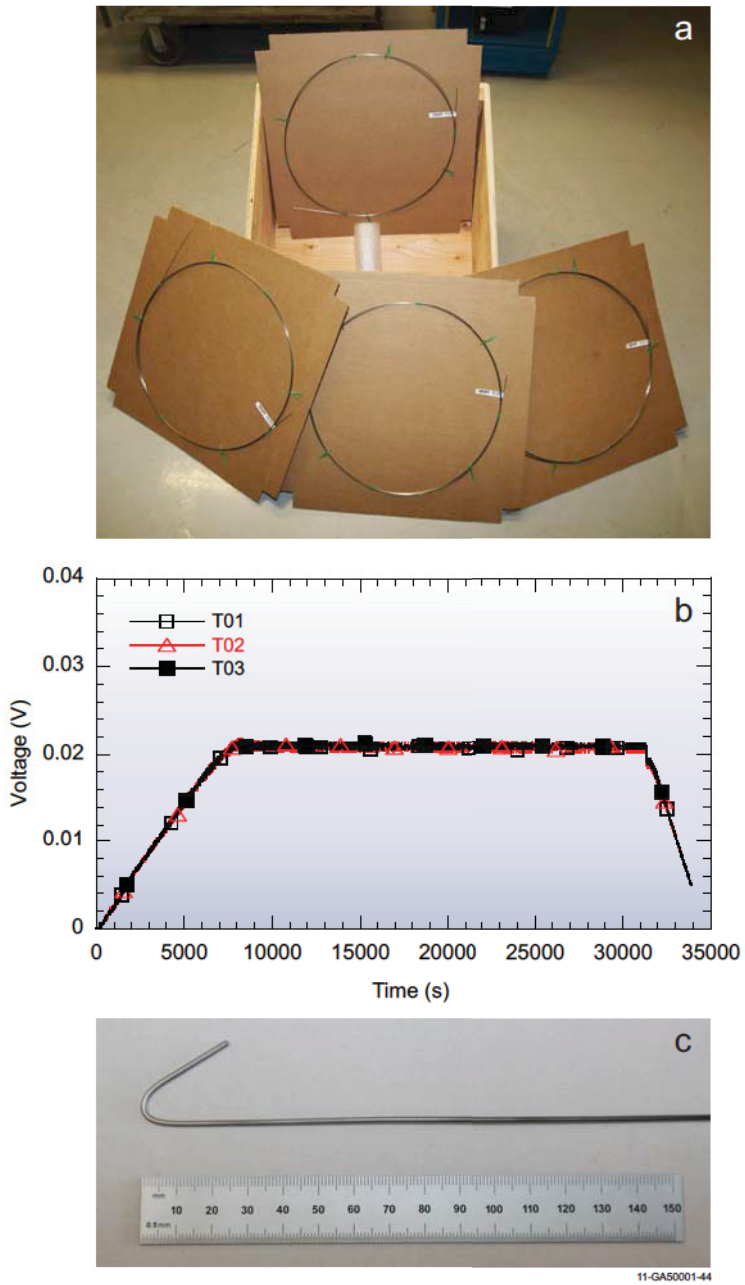

Figure 5-7. HTIR-TCs for IFE/HRP: (a) final HTIR-TCs prior to shipment; Enhanced fabrication techniques demonstrated (b) enhanced stability and (c) ductility after 1700 °C stabilization heat treatment.

peratures at the point of installation. However, UTs offer the potential for real time in-pile measurement of a temperature profile using a single multi-segment sensor. By introducing multiple acoustic discontinuities into the sensor, UTs are able to perform temperature measurements at several points along the sensor length.

UTs work on the principle that the speed at which sound travels through a material (acoustic velocity) is dependant on the temperature of the material. Temperatures may be derived by introducing an acoustic pulse to the sensor and measuring the time delay of echoes. A conceptual design of a 'notched-probe' UT,

with key components identified, is shown in Figure 5-8. If the magnetostrictive transducer shown in this figure is considered, a narrow ultrasonic pulse is generated in the probe by a short duration magnetic field pulse produced by an excitation coil (though previous in-pile research utilized magnetostrictive transducers, piezoelectric transducers may potentially be used in this effort). The ultrasonic pulse propagates to the sensor wire, where a fraction of the pulse energy is reflected at each discontinuity (notches or diameter change). Each reflected pulse is received by the excitation coil, transformed into an electrical signal, amplified and evaluated in a start/stop counter system. The time interval between two adjacent echoes is evaluated and compared to a calibration curve to give the average temperature in the corresponding sensor segment. When a number of notches are available on the wire sensor, the various measurements give access to a temperature profile along the probe.

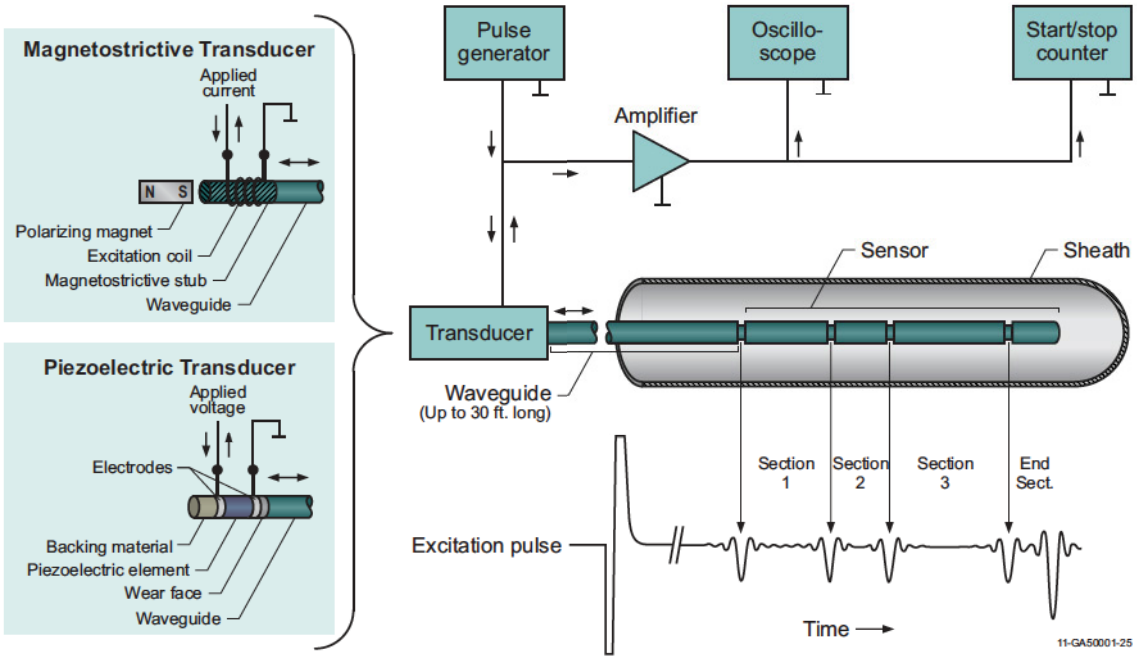

Figure 5-8. Schematic showing typical components of a UT and signal processing equipment.

Prior US UT applications demonstrated the viability of this technology for LWR, HTGR, and SFR test conditions (see Figure 5-9).[127] However, prior in-pile applications were primarily limited to fuel damage tests that ceased several decades ago.[127] Although these tests clearly demonstrated the ability of UTs to withstand high temperatures (up to nearly 2900 °C), test durations were typically limited to less than 100 hours; and data acquisition was cumbersome due to the limitations of signal processing systems available at the time. The availability of new materials and signal processing techniques suggests that this technology could be ideally suited for irradiations that require robust, high accuracy, compact sensors.

The FCRD program funded initial INL efforts to develop an optimized UT design. As discussed in this section, optimization activities[128, 129] focussed on component construction, material selection, stabilization and calibration, and enhanced signal processing development. However, a reduced FY14 FCRD budget led to this effort being prematurely truncated. With a limited amount of additional funding, it is estimated that these development and deployment activities could be completed and a prototype would be ready for deployment in an irradiation test. Proposals have been submitted to allow completion of this UT development and evaluation activity.

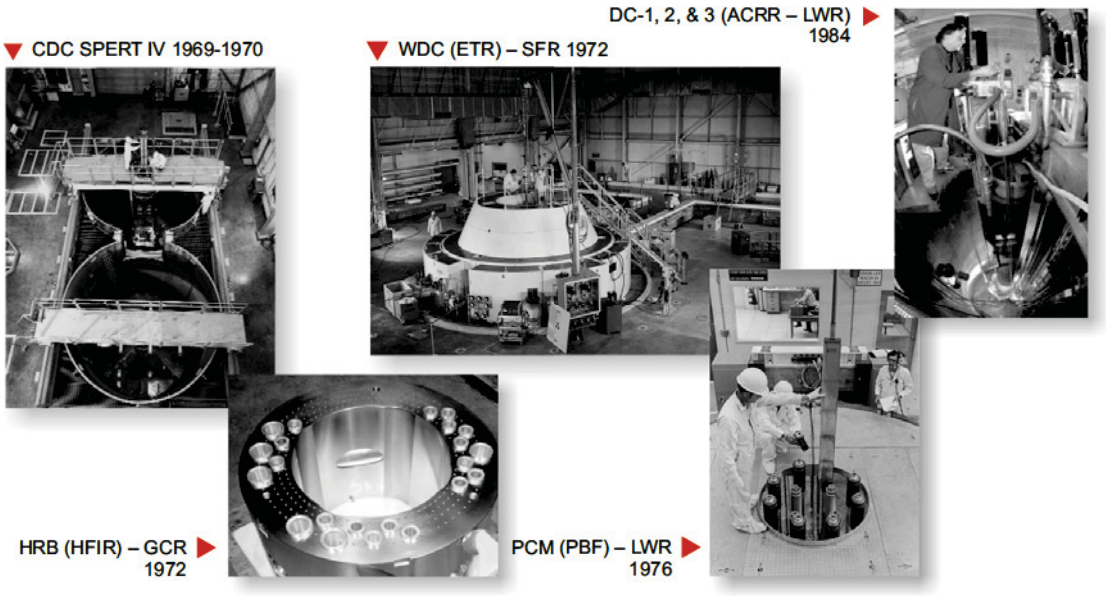

Figure 5-9. Prior UT in-pile applications in the US.

5.1.4.1. Acoustic Velocity Measurement of Candidate Sensor Materials

As an initial step in the UT system development effort, acoustic velocity characterization tests were completed in order to reduce the number of candidate materials by comparing temperature response, ease of fabrication, transmitted signal quality, etc. The tests were also used to evaluate and make appropriate adjustments to a signal processing technique for UT applications. The steps required to perform these tests (candidate material selection, test sample fabrication, test setup, and signal processing adaptation) are summarized in this section.

The materials selected for initial evaluations are listed in Table 5-2 with relevant material properties and envisioned irradiation environments. Candidate sensor materials were selected based on melting temperature, thermal neutron capture cross section, and compatibility with anticipated in-pile test conditions. For higher temperature applications, such as inert gas-filled tests of oxide fuels, refractory metals are an obvious choice due to their high melting temperatures. Tungsten and rhenium were not considered (despite high melting points and previous use in UTs for very short term measurements) due to their high thermal neutron capture cross sections, as both are known to be prone to decalibration due to transmutation. Molybdenum and niobium have high melting points and low thermal neutron capture cross sections. Variations of these materials, KW-molybdenum (e.g., molybdenum doped with small amounts of potassium, silicon, and tungsten) and niobium-1% zirconium were selected for initial testing. Prior experience with these materials indicates that they retain ductility better than pure metals after heating. For lower temperature tests (less than 1000 °C) in liquid metal or liquid sodium bonded metallic fuels, stainless steel and Inconel were selected for cost, corrosion resistance, and ease of fabrication.

Test specimens were isolated from each other in alumina tubes, which were installed in a tube furnace equipped with an argon purge gas system (note that Figure 5-10 shows a single installed sample, but a total of six were included in the test). Signals were generated using a commercial pulser/receiver system, and coils were fabricated in-house. Data were monitored and recorded using a high speed digital oscilloscope.

Table 5-2. Candidate sensor materials.

Material	Melting Temperature, °C	Thermal Neutron Capture Cross Section, Barns	Identified Irradiation Test Application
302 Stainless Steel	1510	3.02	Liquid Metal Bonded Metallic Fuel (T<1000 °C)
304 Stainless Steel	1510	3.03	
Inconel 606	1400	4.35	
Molybdenum	2620	2.51	Inert Gas Filled Ceramic Fuel (T>1000 °C)
KW-Molybdenum	2620	2.51	
Niobium-1%Zirconium	2470	1.14	

Temperatures were monitored using a National Institute of Standards and Technology traceable Type-S thermocouple. Data were collected in 100 °C increments from room temperature to 1300 °C.

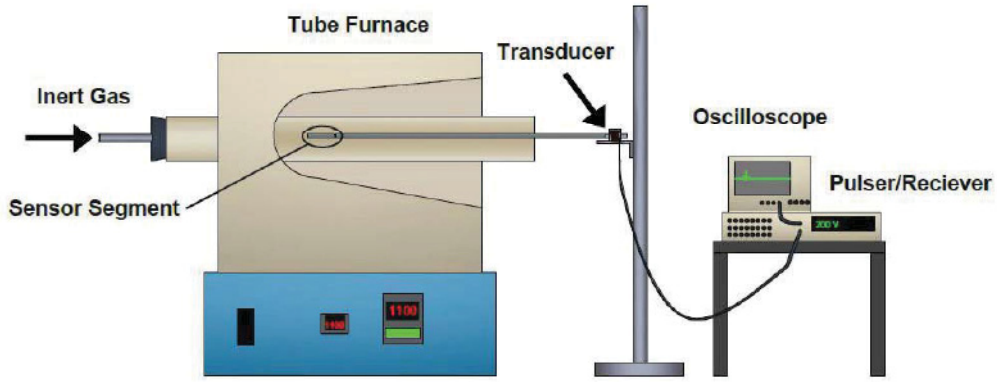

Figure 5-10. Acoustic velocity characterization test setup.

Acoustic velocity was calculated from the delay time between the maxima in the filtered data and the known length of the sensor segment (after correcting for thermal expansion) using the following equation:

$$c = \frac{2(l + \Delta l)}{\Delta t} \tag{5-1}$$

where:

c is the acoustic velocity,

l is the initial sensor length at room temperature,

Δl is the change in length due to thermal expansion, and

Δt is the delay time between maxima.

Results from the acoustic velocity characterization tests, which are documented in References 130, 131, and 132 indicate that stainless steel and molybdenum are ideal candidates for the two temperature ranges considered in the current evaluations.

Figure 5-11 compares measured acoustic velocities of 302 and 304 series stainless steel samples to values calculated from reference data.[133,134] As shown in this figure, calculated velocities based on test data are somewhat higher than reference values found in the literature (about 5% for temperatures below 800 °C). This difference can be attributed to differences in the manufacturing process used in production of the wires. However, the trend is appropriate for UT applications. High temperature attenuation increased signal noise and eventual loss of signal for temperatures above 1100 °C for the 0.254 mm diameter sample and above 1200 °C for the 1.58 mm diameter sample. It was also observed that the increased signal noise remained after cooling the samples.

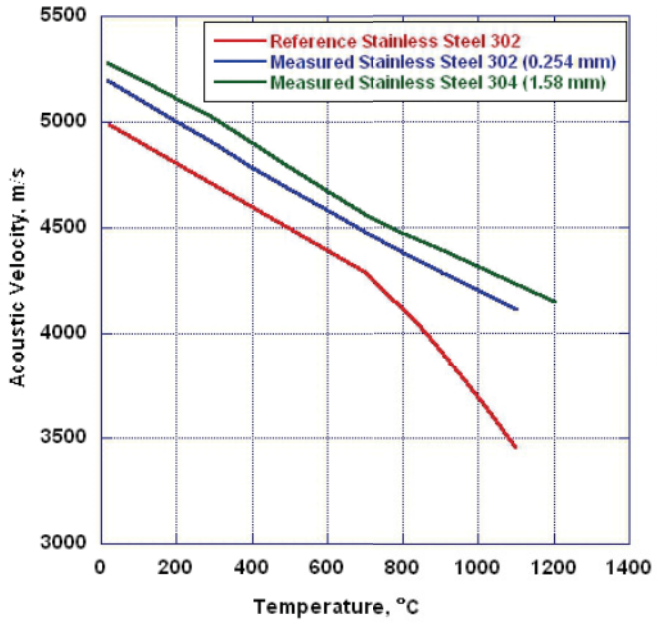

Figure 5-11. Comparison of measured acoustic velocity of stainless steel to calculated reference values.

Figure 5-12 compares measured acoustic velocities for pure molybdenum and KW-molybdenum samples to values calculated from reference data.[133,135] The temperature response of the molybdenum samples is close to values inferred from the literature, except at the highest and lowest test temperatures. Signals for molybdenum samples did not attenuate significantly over the evaluated temperature range.

Inconel 606 was also a good candidate, but test results indicated that it does not offer any significant advantages over stainless steel. In addition, sticking, a form of contact bonding between the sensor and its surroundings that can interfere with and obscure acoustic signals, occurred for Inconel 606 at temperatures above 1000 °C. Due to difficulty in manufacturing the samples as well as poor temperature response, testing indicated that niobium-1% zirconium was not a good candidate.

In summary, temperature-dependent signal response evaluations indicate that stainless steel is the preferred probe for temperature measurements below 1000 °C and doped molybdenum is the preferred probe material for higher temperatures. Inconel 606 is also a good candidate, but does not offer any significant

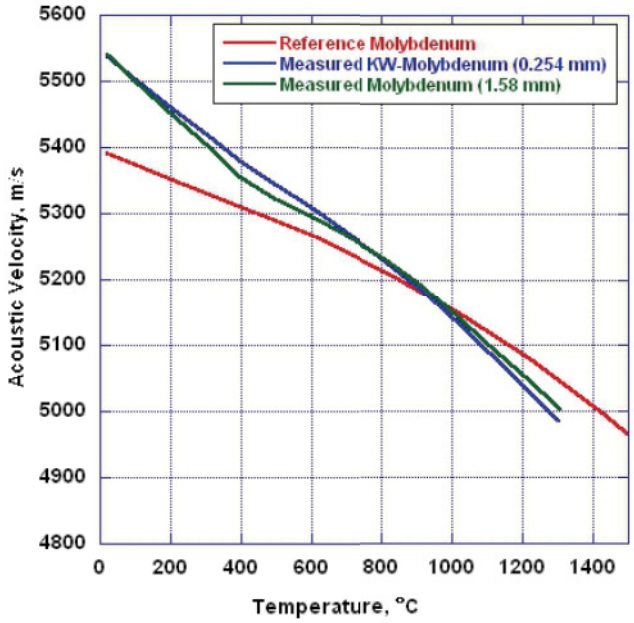

Figure 5-12. Comparison of measured acoustic velocity of molybdenum to calculated reference values.

advantages over stainless steel. Due to difficulty in manufacturing the samples as well as poor temperature response, niobium-1% zirconium is not a good candidate.

5.1.4.2. Damping

Ultrasonic transducers generate acoustic waves in both directions along the wire (both toward and away from the sensor section of the waveguide). The waves propagating away from the sensor strike the free end of the waveguide and are reflected back toward the transducer, where they may interfere with the signals being used for measurement. To eliminate this problem, the free end of an ultrasonic transducer is damped. This is typically accomplished (in the case of piezoelectric transducers) by compressing a highly attenuating material against the free side of the transducer crystal. This is not an option with a small wire waveguide, as the wire end area is too small.

One method used to obscure the undesired free-end echo was to place the end of the magnetostrictive rod at the center of the driving coil. While this does effectively eliminate the free-end echo, it significantly reduces the strength of the ultrasonic pulse. This method also does nothing to reduce the interfering effects of reflections created by the weld between the magnetostrictive rod and the waveguide.

During FY12, a different damping method was developed that allows complete damping of the back end echo when used with a small waveguide (i.e., 0.254 mm/0.01 inch diameter). For a thin wire waveguide, a short section of metallic tubing is filled with an attenuating material and swaged onto the free end of the waveguide, compressing the damping material (see Figure 5-13). However, this method becomes significantly less effective as waveguide diameter increases.

For in-pile testing with a stainless steel or Remendur waveguide, most damping materials (i.e. polymers and greases/gels) are not usable. Therefore, crushable oxides and stainless steel wool were selected as potential damping materials. It was determined that the signal improvement yielded by a swaged damper is

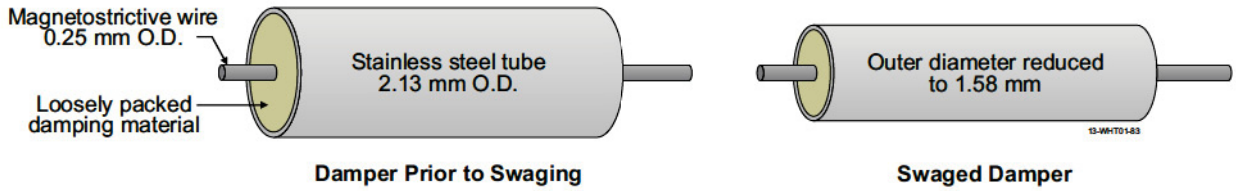

Figure 5-13. Description of swaged damper.

primarily dependent on two properties; the acoustic impedance mismatch between the damping material and the waveguide, and the compression of the damper. For a 26% reduction in damper diameter (7.6 mm/ 3 inch damper length), complete back-end echo attenuation was observed for dampers constructed with stainless steel wool or magnesium oxide powder.

5.1.4.3. Transducer Development and Sensor Resolution Impact

The resolution of an ultrasonic system is partially dependent on the operating frequency of its transducer. Higher frequencies allow detection of smaller physical features (such as reflectors) as well as greater time resolution of signal features (such as zero crossings). The frequency of a magnetostrictive transducer is primarily a function of the transducer (i.e. coil or rod) length, with the transducer length equating to one half of its acoustic wavelength. Increasing frequency necessarily requires decreasing length. However, decreasing transducer length also decreases signal strength. To overcome this, a new coil type, capable of higher frequency operation, was developed in FY13. Some additional development is necessary to produce a high frequency transducer capable of operating at high temperatures (200-900 °C). A patent for the high frequency transducer design is currently being pursued.[136]

Construction of high temperature magnetostrictive transducers is a multi-step process that involves several heat treatment steps. First, the coil is formed by wrapping several layers of silver-palladium wire around an alumina bobbin (Figure 5-14a). The wire is coated in a standoff insulation (a particulate alumina silica mix with a burnable binder). The insulation requires a heat treatment step prior to high temperature use, and becomes brittle after heating (Figure 5-14b). After heat treatment, the coil is coated with alumina cement and heat treated a second time to cure the cement (Figure 5-14c). The coil is then securely placed in a fixture, and the wire leads are laser welded to a high temperature coaxial cable (one lead to the center conductor and one to the sheath as shown in Figure 5-14d). As the welds are fragile, the end of the cable and the coil are coated in another layer of alumina cement and cured. The magnetostrictive wire (previously welded to the waveguide) is next threaded through the coil. The assembly is then placed into a pre-fabricated transducer housing and seal welded (possibly after vacuum purging and backfilling with an inert gas, depending on anticipated service environment; see Figure 5-14e). The transducer housing is composed of stainless steel; but for high temperature (over 1000 °C) thermometry, a molybdenum waveguide housing would be used. The assembled transducer is shown in Figure 5-14e.

This type of magnetostrictive transducer will be tested in an ATR-NSUF ultrasonic transducer irradiation test that will be performed at the MITR in order to assess the survivability of candidate magnetostrictive and piezoelectric transducers under irradiation (see Section 5.7.1). As part of the HTTL's effort to support this irradiation funded by the ATR NSUF, four magnetostrictive transducers were shipped to MIT in August 2013 (see Figure 5-15).

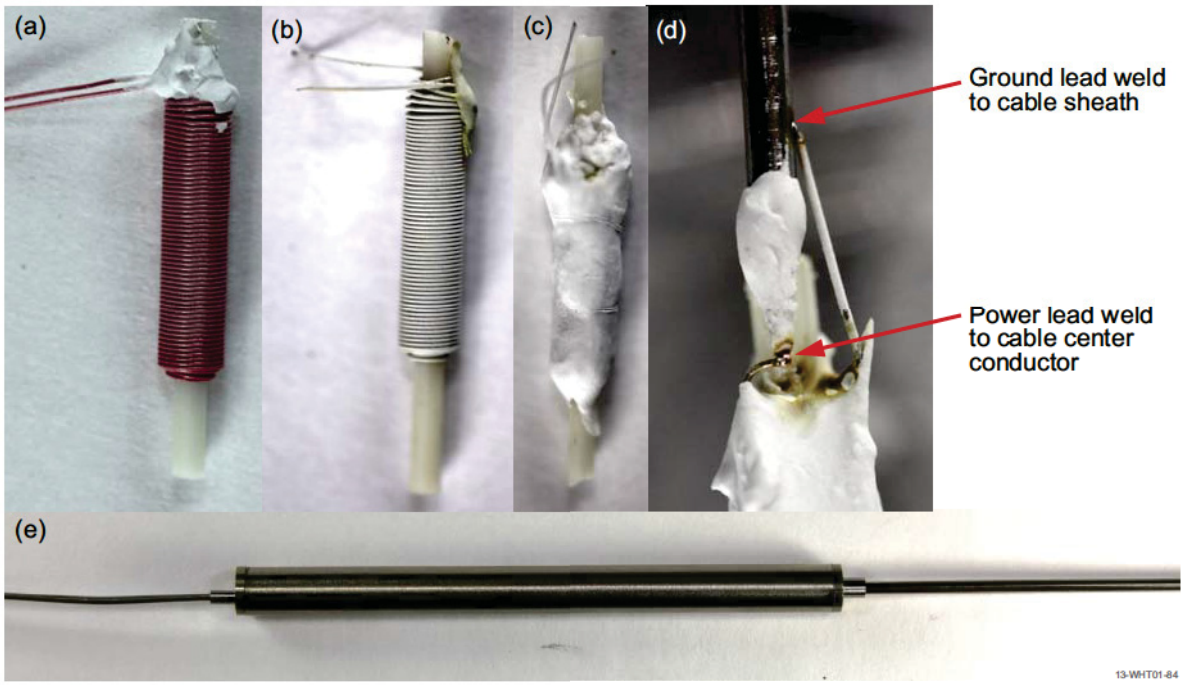

Figure 5-14. Steps involved in making high temperature capable magnetostrictive transducer.

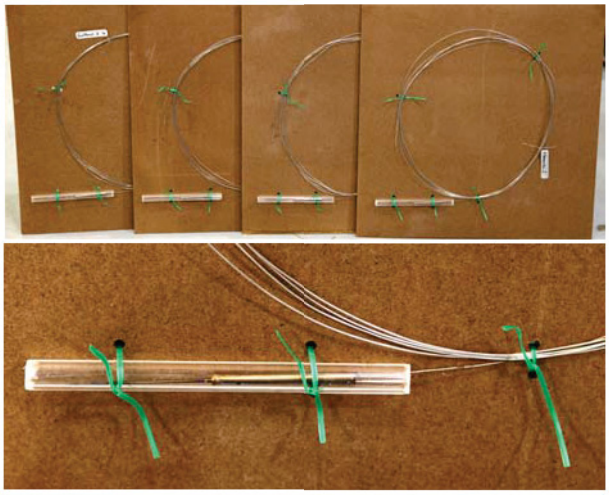

Figure 5-15. HTTL-fabricated magnetostrictive transducers prior to shipment to MIT.

The primary effect of increasing the operating frequency of the transducer is in reducing the required distance between reflectors on the waveguide. This increases the spatial resolution of the system and allows for smaller temperature sensor segments (producing a temperature measurement that is less "blurred" due to averaging over the length of the segment). A goal of this research was to achieve the ability to distinguish reflectors spaced one centimeter apart or smaller. The bench test configuration shown in Figure 5-16 was used to compare the performance of transducers operating at different frequencies, and to evaluate the spatial resolution available with each, with a 0.25 mm waveguide. Copper clips were used to create reflections with easily varied spacing.

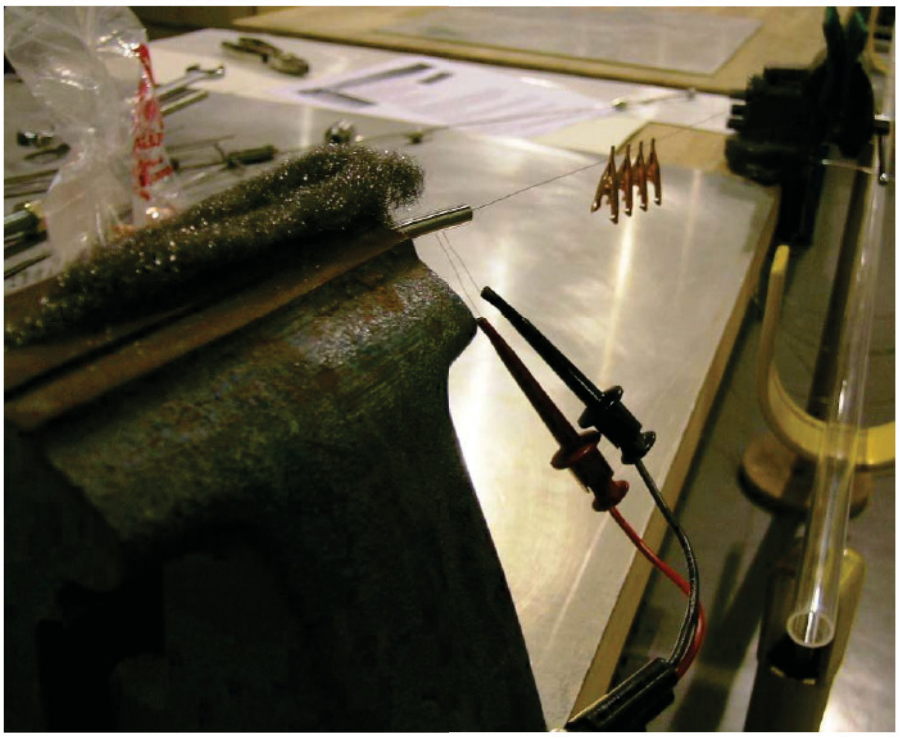

Figure 5-16. Test configuration used to test effect of transducer frequency on spatial resolution.

At the beginning of the current effort, the magnetostrictive transducers that were available were limited to frequencies up to approximately 200 kHz. Figure 5-17a shows a recorded waveform captured using a 200 kHz transducer and a waveguide with reflectors separated by 2.5 cm. The reflector configuration did not allow the use of more than two reflectors at this frequency, as the amplitude became too small to detect.Figure 5-17b shows the signal recorded for a transducer operating at 1.9 MHz with reflectors spaced 0.7 cm apart. The multiple period reflections are due to the need to pulse the tone-burst for several cycles in order to generate a sufficiently strong signal. Even so, the four reflections are clearly separated. It is expected that if sufficient energy could be introduced into the transducer over a single tone-burst cycle, the spacing between reflectors could be reduced even further. The effect of reverberations is less pronounced for the higher frequency transducer, allowing four reflectors to be clearly distinguished. This appears to be because the reflection coefficient (the fraction of acoustic energy reflected at each clip) is a function of frequency. The reflected waveforms are more consistent in amplitude than those observed with lower frequency transducers, and the reverberations appear to attenuate more rapidly.

5.1.4.4. Signal Generation and Processing

A signal processing method described by Roberts, et al.,[137] was used during initial acoustic velocity characterization testing. This method consists of cross-correlating the time series data to a known signal (typically either the input signal or the expected reflection), then squaring and low pass filtering the correlated data. This method greatly increased the signal-to-noise ratio and simplifies identification of reflections, even in the presence of significant noise. The input signal used for these tests was a simple square pulse, and could not be used in the cross-correlation. Two issues were observed with this initial method. First, the short (80 ns) square pulse is best suited for powering high frequency, voltage based transducers (such as piezoelectric crystals). The inductive coils used to drive the magnetostrictive transducers require

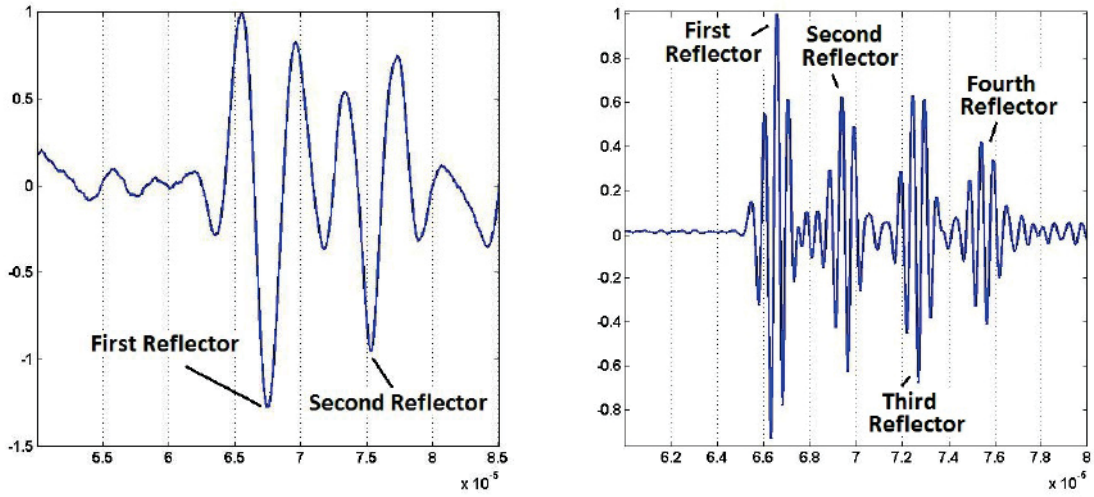

(a) 200 kHz transducer with reflectors spaced 2.5 cm apart.

(b) 1.9 MHz transducer with reflectors spaced 0.7 cm apart.

Figure 5-17. Comparison of detectable reflections with different frequency transducers.

more time to fully charge and develop a strong magnetic field. The use of the short square pulse results in a clean, but weak signal that could be overwhelmed by noise in an extreme environment or by excessive attenuation at high temperatures. The second issue observed is that although the input pulse is very short, the measured signals are quite long and require a large amount of space between reflectors for sufficient echo separation. Use of the signal processing method mentioned above results in broad, flat peaks instead of sharp, easily resolved signals.

The first issue has been resolved by switching the driving signal from a short square pulse to a longer tone-burst. The tone-burst is a sinusoidal signal several periods in length. This input results in a signal many times more powerful than the simple square pulse, without making the received signals significantly more complex (the echo shape is unchanged if the burst length is not overly long). As both the length and the frequency of the tone-burst can be varied, the signal may be optimized for different sensors and testing conditions.

The second issue is also partially solved by use of the tone-burst input signal. Although the input signal has longer duration than the square pulse, the frequency content of the input is narrow. This results in less ringing of the transducer. This means that the received signals are of similar duration to those observed with the square pulse, but with greater amplitude. A new signal processing method based on Weiner filtering and auto-regressive spectral extrapolation[138] has been identified that could make further significant improvements over the previous method adapted from Roberts, et al.[137]

5.1.4.5. Remaining Tasks prior to UT Deployment

Tasks remaining prior to higher temperature UT deployment include furnace testing of a prototype ultrasonic thermometer constructed with a molybdenum sensor at higher temperatures (up to 2600 °C) or a stainless steel sensor for lower temperatures (less than 1000 °C) For higher temperature applications, a method is also needed to eliminate sticking and reduce embrittlement of molybdenum waveguides during welding of the reflectors; possible options under consideration include employing a variant of the

KW-doped molybdenum currently used, such as Oxide Dispersion Strengthened (ODS)-molybdenum, or development of a heat treatment process. Further improvement of a signal processing method will also be required to enhance spatial resolution and reduce necessary spacing between reflectors. Finally, a prototype system will be developed and tested to evaluate the potential accuracy and resolution possible with the UT system. Although the FY14 NEET program (see Section 5.7.1) will fund some of the signal processing method improvements, additional funding will be required to replace the last year of FCRD program funding required to complete evaluations required for UT deployment. Several proposals have been submitted to request this funding.

5.2. Thermal Conductivity Sensors

Thermal conductivity is a key property needed to characterize fuel or material performance during irradiation testing. Thermal conductivity is highly dependent on the physical structure, chemical composition, and the state of the material. Currently, changes in fuel or material thermal conductivity during ATR irradiations are evaluated out-of-pile. However, as discussed in this section, a new real-time method for detecting changes in thermal conductivity during irradiation in instrumented lead and loop tests is now available.

Historically, in-pile thermal conductivity measurements were made using an approach with one (or more) thermocouples embedded near the center of the fuel rod and one exterior to the fuel (in the coolant or a structure outside the fuel element). As part of a collaborative effort with Utah State University (USU) and the IFE/HRP, INL compared the multiple thermocouple steady-state thermal conductivity approach and the transient hot wire thermal conductivity method (with a single probe containing a line heat source and thermocouple embedded in the fuel as shown in Figure 5-18b) as candidate in-pile effective thermal conductivity measurement techniques.[139 through 143] Evaluations compared the accuracy of each approach for various fuel types and test conditions. Results indicate that the Transient Hot Wire Method Needle Probe (THWM NP) offers an enhanced method for in-pile detection for thermal conductivity, and the US DOE has filed a patent on the THWM NP.[144]

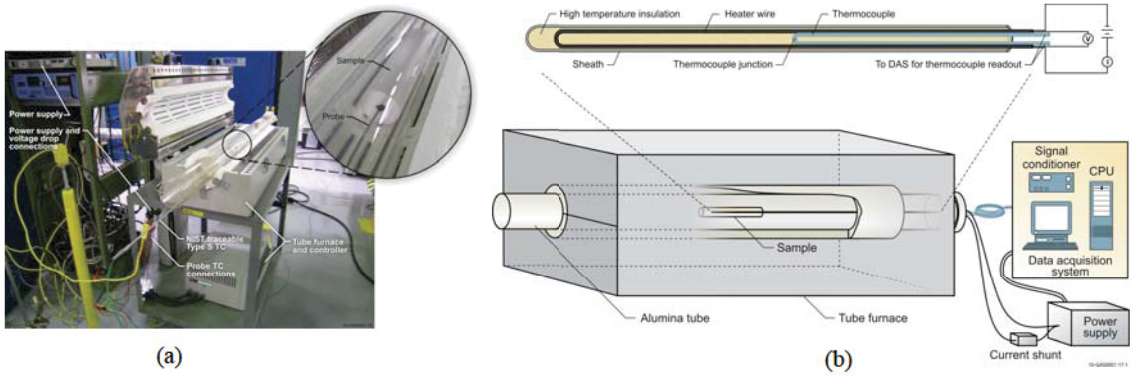

Figure 5-18. Setup for evaluating transient hot wire needle probe.

The THWM or line heat source method was first suggested by Schleirmacher.[145] Numerous references may be found in the literature describing applications of this method to measure the thermal conductivity of solids, fluids, and gases (e.g., see References 146 through 151). In the THWM approach, thermal conductivity is determined from the temperature rise in the sample when the heat source is energized.[146] In a

solid, this method may be applied by embedding the probe in the material whose thermal conductivity is to be measured. From a condition of thermal equilibrium, the probe is energized and heats the sample with constant power. The temperature response of the sample is a function of its thermal properties, and the thermal conductivity is calculated from the temperature rise detected in the sample. Following a brief transient period, a plot of temperature versus the natural logarithm of time becomes linear, as shown in Figure 5-19 (linear region of the time period between times, t_2 and t_1, and temperatures, T_2 and T_1). The slope of the linear region is used to calculate the test material thermal conductivity.

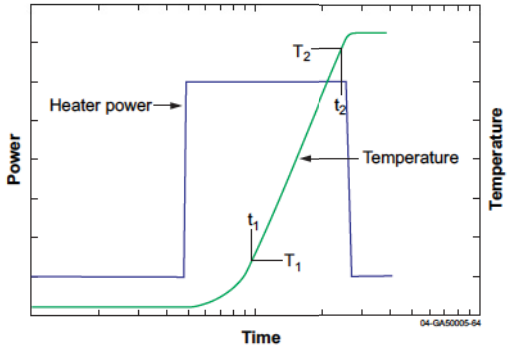

Figure 5-19. Semi-log temperature rise plot for transient hot wire methods.

THWM NPs were designed and fabricated by INL for room temperature proof-of-concept evaluations and high temperature testing. Using the setup shown in Fig. 5-18a, the needle probe was demonstrated to work very well for materials with thermal conductivity ranging from 0.2 to 16 W/m-K with measurement errors of less than 5%, delivering thermal conductivity measurements with a high degree of accuracy and consistency (see Figure 5-20). Test results indicate that special considerations are needed for high thermal conductivity sample materials and for smaller diameter samples. Methods were explored to reduce the challenges associated with such samples, primarily techniques that could reduce signal noise and allow better characterization of the probe response time. In addition, results from long term evaluations indicate that the INL-developed THWM NP for in-pile detection of thermal conductivity is a robust sensor that could survive in the harsh environments associated with in-pile fuel testing.

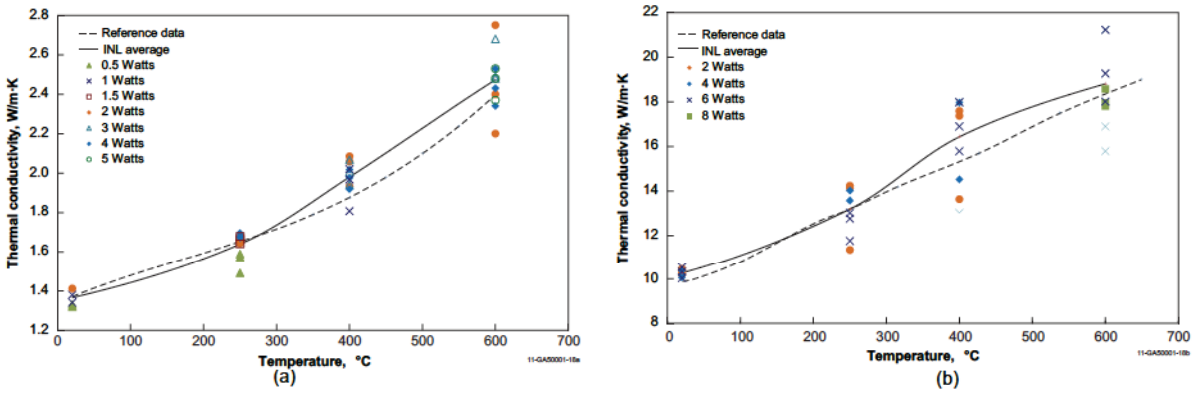

Figure 5-20. THWM NP test results for various power levels for (a) fused silica and (b) Inconel Alloy 625.

Insights gained from these evaluations have been used to develop probes for several organizations. During FY11, a prototype needle probe (see Figure 5-21a) was fabricated and shipped to MIT for a MITR irradiation with high thermal conductivity, hydride fuel, with peak temperatures less than 700 °C. During

FY13, INL fabricated and shipped a THWM NP to CEA for a low temperature fuel thermal conductivity measurements in a hot cell containing a furnace with peak temperatures less than 400 °C (see Figure 5-21b); and in FY14, INL will fabricate and ship a THWM NP to IFE/HRP for measuring thermal conductivity of ceramic fuel during a HBWR irradiation with peak temperatures less than 1300 °C (see Figure 5-21c). Materials and geometries for each THWM NP are optimized for the test materials and conditions.

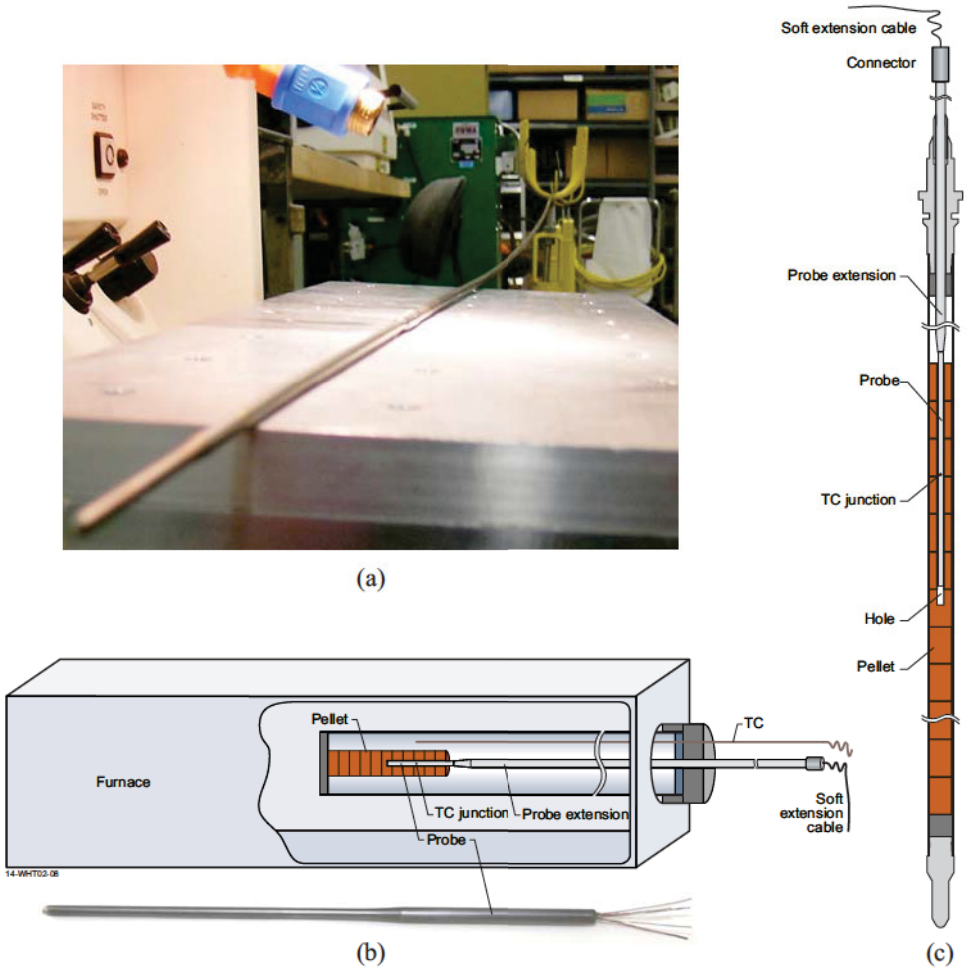

Figure 5-21. THWM NPs completed for (a) MITR and (b) CEA and under development for (b) IFE/HRP.

5.3. Elongation/Deformation/Creep/Swelling

New materials are being considered for fuel, cladding, and structures in next-generation and existing nuclear reactors. Such materials can experience significant dimensional and physical changes during irradiation. Currently, such changes are measured at the ATR by repeatedly irradiating a specimen for a specified period of time and then removing it from the reactor for evaluation. The labor and time to remove, examine, and return irradiated samples for each measurement makes this approach very expensive. In addition, such techniques provide limited data and handling may disturb the phenomena of interest. Commercially-available LVDTs are being evaluated as a near-term option for detecting geometry changes in-pile during ATR irradiations; thereby eliminating the problems associated with the current "cook and look"

approach. In addition, ultrasonics and fiber optic technologies are being explored as options that can measure geometry changes with higher precision in multiple dimensions at higher temperatures.

5.3.1. LVDT-based Elongation

Earlier references[152,153] report using miniature strain gauges encased in zircaloy sheaths welded on the cladding in the circumferential and axial directions to detect dimensional changes. These references indicate that strain gauge measurements were unstable due to high sensitivities of the gauges to temperature and neutron fluence. Today, most MTRs rely on LVDTs (see Section 3.3) to detect dimensional changes during irradiation; and many of the LVDTs in use today are made by the IFE/HRP. As discussed in Section 3.3, operating experience has shown that these sensors are a robust, frictionless, high resolution instrument for detecting dimensional changes in lower-temperature, irradiation environments. However, some IFE/HRP LVDTS suffer from Curie temperature effects near 360 °C, the temperature that corresponds to the Curie point for the nickel used in the LVDT windings. More recent HTTL evaluations of LVDTs using alternate coil materials, completed in collaboration with IFE/HRP, have led to an LVDT without Curie temperature limitations for detecting dimensional changes during irradiation testing.

Initially, nuclear-grade LVDTs from US and foreign sources were evaluated as candidates for in-pile deployment. INL efforts, which included calibration evaluations and long duration, high temperature testing, clearly indicated the superiority of LVDTs supplied by the IFE/HRP (see Figure 5-22a). However, evaluations indicated that Curie temperature effects, due to the nickel contained in the LVDT coil material, have the potential to affect accuracy near 360 °C. Consequently, use of these LVDTs could yield inaccurate data depending on the in-core position of the sensor and the corresponding gamma heating levels. For that reason, INL worked with IFE/HRP to develop and evaluate enhanced LVDTs with an alternate coil material that is not susceptible to the Curie effect. Calibration and long term high temperature testing of these enhanced LVDTs, which was performed by INL, demonstrate that the enhanced LVDTs can operate in a very stable manner for long periods (1000 h) at high temperatures (500 °C). As shown in Figure 5-22b, the degradation of the original LVDTs was not observed in the enhanced LVDTs provided by IFE/HRP. Hence, these enhanced LVDTs are recommended for use in ATR high temperature irradiation tests.

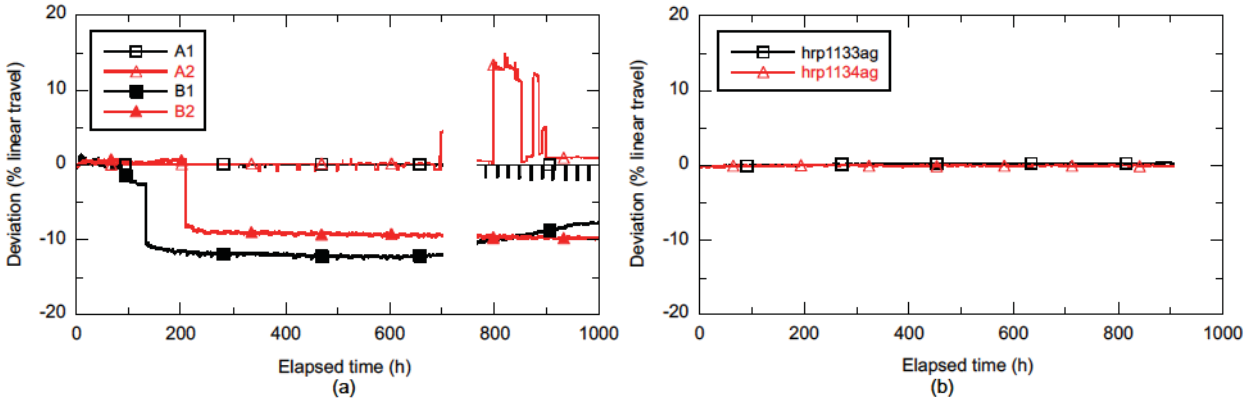

Figure 5-22. Long duration (1000 hour) test at 500 °C results: (a) LVDTs originally provided by nuclear grade vendors (IFE/HRP LVDTs designated with "A"); and (b) enhanced IFE/HRP LVDTs.

5.3.2. Initial LVDT/bellows-based Creep and Tensile Test Rigs

As discussed in Section 3, several organizations (e.g., VTT, INL, KAERI, and CEA) have been involved in developing and deploying in-pile tensile test rigs to detect growth of tensile and creep specimens using a bellows to apply a load to a specimen and LVDTs to detect growth of the specimen. During 2013, the FCRD program funded INL to complete efforts to develop two types of in-pile creep test rigs for deployment in an ATR PWR loop: an enhanced creep test rig and a variable load creep test.

5.3.2.1. Enhanced Creep Test Rig

Design. As discussed in References 154 through 162, the enhanced creep test rig design shown in Figure 5-23 represents a refinement of the original creep test rig shown in Figure 5-24. As indicated in both figures, major components include a tensile specimen, a bellows, an LVDT, and the fixturing needed to connect these components within a supporting frame. (In a pressurized water environment [i.e., an autoclave or a PWR test loop], external water pressures tend to collapse the bellows producing a tensile load on the specimen.) IFE/HRP provided the LVDT and welded the LVDT, bellows, and the associated connecting fixturing in both test rigs using e-beam welding techniques.

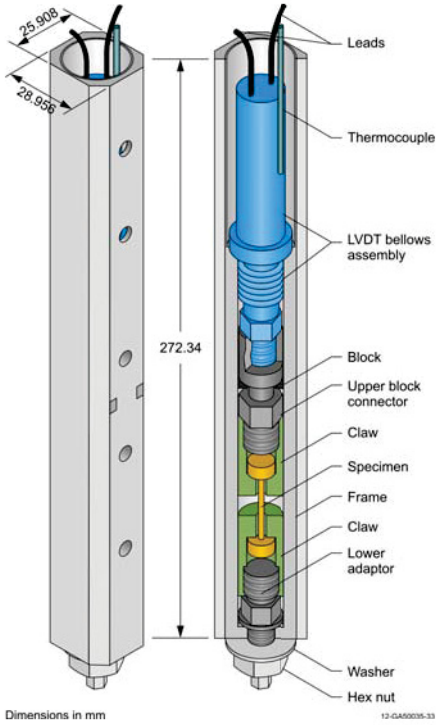

Figure 5-23. Enhanced creep test rig.

The primary refinements embodied in the enhanced creep test rig (relative to the original creep test rig), and the factors motivating those modifications, include changes in the:

- LVDT - Coil wires are made from a silver alloy rather than a copper-nickel alloy to eliminate Curie-point temperature instabilities associated with earlier versions of the IFE/HRP LVDT (see Reference 157).

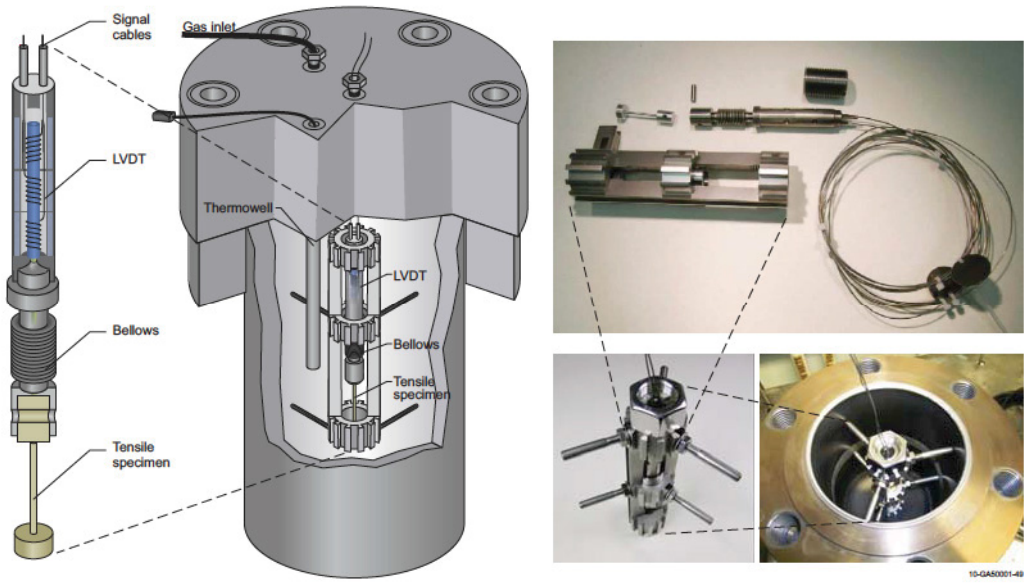

Figure 5-24. Original creep test rig positioned in autoclave for testing.

- Connecting Fixturing - Specimen to fixture interfaces were designed to minimize potential mating mismatch while promoting easier assembly/disassembly. In addition, the lower adaptor was fitted with a hex nut to allow pre-loading sufficient to minimize the effects of compliance issues.
- Frame - The mass of stainless steel was reduced to minimize gamma heating. The frame was also re-designed to ensure compatibility with the ATR test holder for PWR Loop 2A (see Figure 5-25).

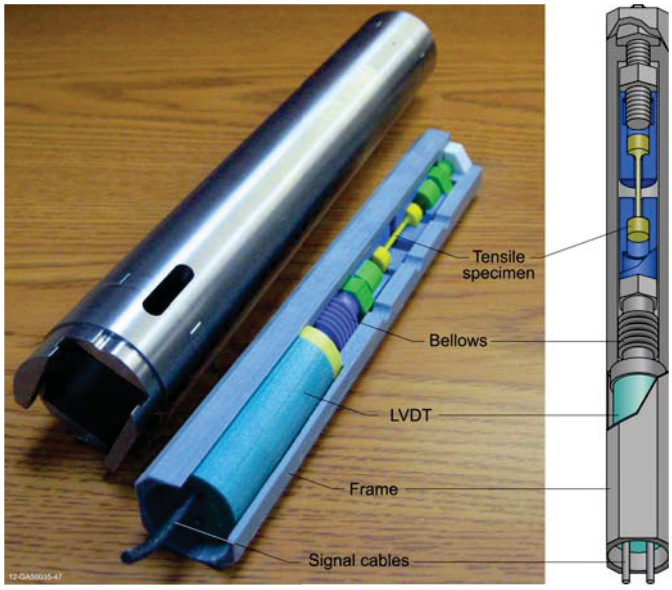

Figure 5-25. Enhanced creep test rig (holder, three-dimensional model and schematic).

Key components in the enhanced test rig design are listed in Table 5-3. Note that an aged Inconel 718 bellows was selected because of its higher strength, although the bellows may be fabricated from other

materials (e.g., Inconel 625, Inconel X-750, or stainless steel). Additional information regarding the enhanced creep test rig can be found in References 158 through 162.

Table 5-3. Summary description of components used in enhanced creep test rig.

Component	Manufacturer	Model Number	Material
Bellows	Mini-Flex	I718-320-110-790, Rev: -- C	Inconel 718, aged
LVDT	IFE/HRP	Type 5	Inconel 600; Core - AISI 403; Coils - Silver Alloy (Alloy 406; Alcal Type E Insulation)
Connecting Fixturing	IFE/HRP	NA	Inconel 600
Tensile Specimen	INL	NA	304 stainless steel and copper

Characterization. Characterization was needed to determine the bellows spring rate and effective area. These bellows characteristics must be known to quantify the load applied to any given specimen. Based on the configuration shown in Figure 5-26a, the specimen load (F_S) is given by

$$F_s = \Delta P A_B - k_B \Delta L \tag{5-2}$$

where

ΔP = differential pressure ($P_{external} - P_{internal}$) acting on the bellows effective area,

A_B = bellows effective area,

k_B = bellows spring rate,

ΔL = displacement of the bellows (and the specimen) as detected by the LVDT.

Because the setup shown in Figure 5-26a has no means for internally pressurizing the bellows, $P_{external} \gg P_{internal}$, and $\Delta P \approx P_{external}$.

If the spring rate and effective area have been characterized, the specimen load can be readily determined as a function of pressure and displacement measurements. Spring rate and effective area characterization required use of a specialized fixture as shown in Figure 5-27.

The bellows spring rate was determined through a series of bench top measurements where the probe assembly was constrained by one end of the fixture so that the bellows could be collapsed by incrementally tightening the Allen bolt into threads in the opposite end of the fixture. (Note that the adaptor mating with the Allen bolt is not threaded so the Allen bolt simply pushed the adaptor toward the bellows with each rotation.) As the Allen bolt was tightened, an ever increasing force was registered by the (calibrated) load cell consistent with the bellows spring rate and displacement. Displacement of the bellows was periodically measured during incremental bolt tightening, using a depth micrometer and/or by converting the revolutions of the Allen bolt into an equivalent linear movement based on the bolt pitch. The depth micrometer was clamped in line with the fixture and the micrometer was simply advanced to touch the head of the hex bolt each time the bolt was tightened as indicated in Figure 5-28. Relative to Equation (5-2), ΔP was effectively zero; and (F_S) was registered through the load cell while ΔL was measured. That allowed direct calculation of the bellows spring rate (k_B) based on the measured values. Results from this effort are provided in Table 5-4. (Note that all bench top measurements were completed at room temperature with the assumption that the spring rate is temperature independent.)

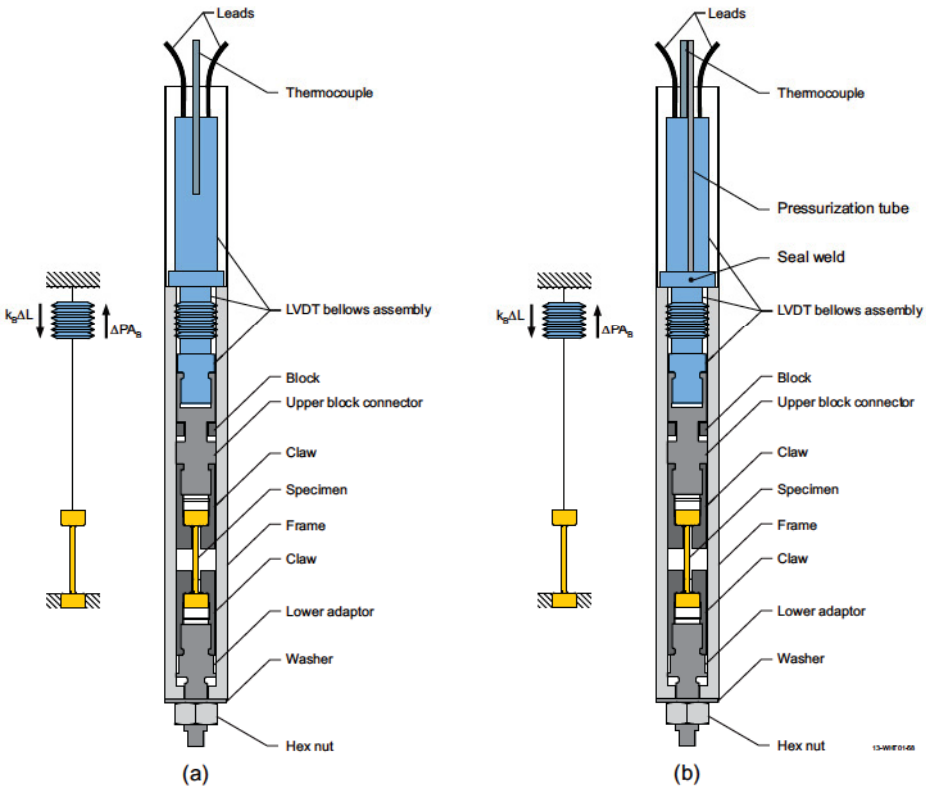

Figure 5-26. Test configuration with an equivalent specimen load diagram for (a) enhanced creep test rig and (b) variable load creep test rig.

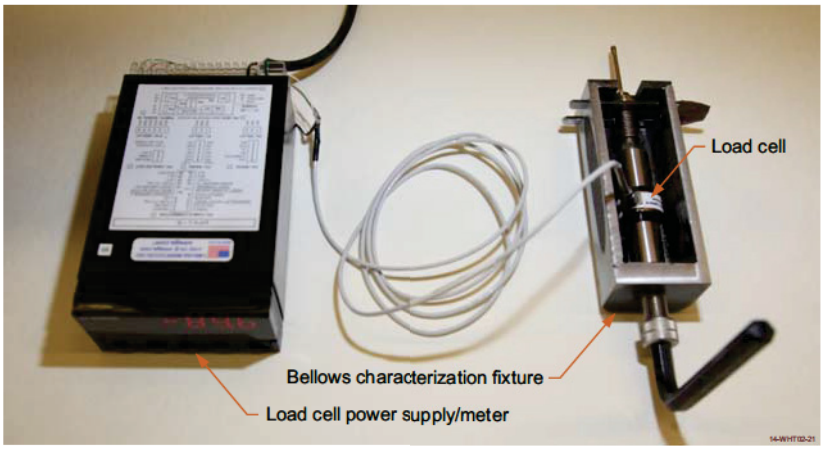

Figure 5-27. Bellows characterization test setup.

Representative data from one test (Test 1) are provided in Figure 5-29. Additional data may be found in Reference 158. From these tests, the average bellows spring rate was found to be 151 N/mm. This result can be compared with the manufacturer's nominal specification of 138 to 175 N/mm. The variation in the manufacturer's specification primarily depends on the nature of the bellows heat treatment. Although the bellows was heat treated, specifics of that heat treatment are unknown so any value within the specified range (i.e., 151 N/mm) is reasonable.

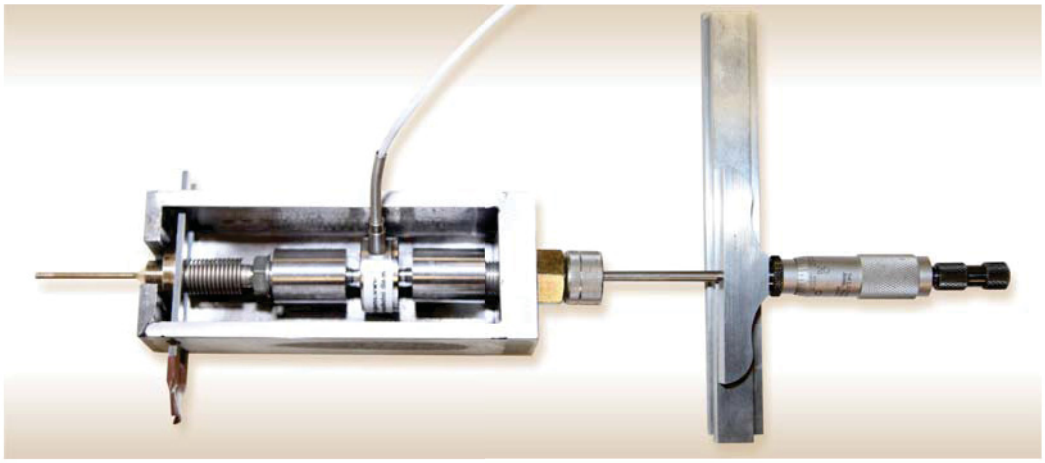

Figure 5-28. Depth micrometer configuration (without clamps) for measuring the bellows spring rate.

Table 5-4. Results from bellows spring rate measurements.

Test	Description (relative to calibration)	Measurement Method	Spring Rate (N/mm)[a]	
			micrometer	bolt rotation
1	before	micrometer / bolt rotation	154	150
2	before	micrometer / bolt rotation	186	168
3	before	micrometer / bolt rotation	149	154
4	after	micrometer	150	

a. From a best-fit linear approximation of the measured data.

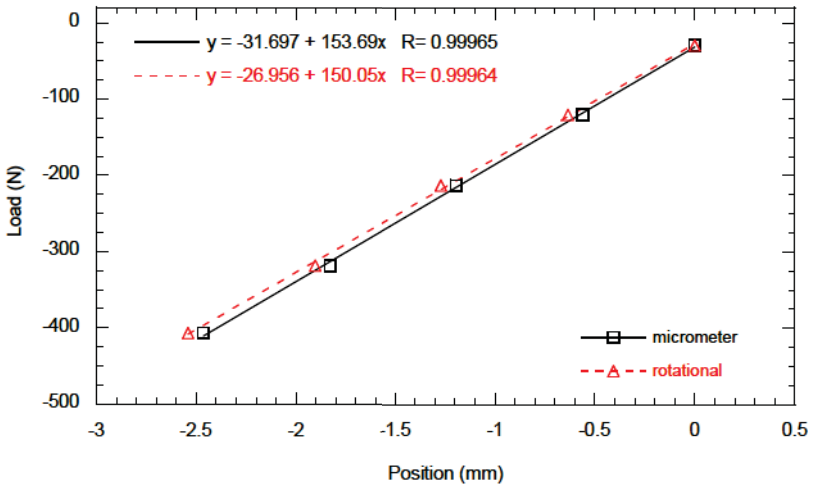

Figure 5-29. Bellows spring rates based on micrometer and rotational measurements in Test 1.

The bellows effective area was determined through a series of measurements in an argon atmosphere in an autoclave using a configuration very similar to that shown in Figure 5-27. In this case, however, the fixture and a threaded bolt adaptor were used to eliminate all movement of the bellows. As autoclave pressures were increased, the (constrained) bellows imparted an ever increasing force in the (calibrated) load cell.

The effective area characterization process consisted of incrementally increasing the autoclave pressure and recording that pressure along with the associated load cell output. Relative to Equation (5-2), it should be clear that ΔL was held at zero while (F_S) was registered through the load cell and ΔP was measured. That allowed direct calculation of the bellows effective area (A_B) based on the measured values. Results from this effort (data are provided in Reference 161) indicate that the bellows average effective area s 76.0 mm^2. Relative to the manufacturer's nominal reported area of 79.4 mm^2, this measured discrepancy (of ~4%) is believed to be within normal manufacturing tolerances.

Calibration. As discussed in Reference 162, the LVDT bellows assembly was calibrated at room temperature and at 150, 250, and 350 °C, which covers the range of temperatures expected during deployment in the ATR Loop 2A. This calibration provides the means to relate any measured LVDT output voltage to a corresponding displacement. Although IFE/HRP provided calibration as part of their LVDT delivery agreement with INL, their calibration could differ from INL data primarily due to potential differences in signal conditioning electronics. INL calibration was therefore required.

Bench top and autoclave calibrations at room temperature were completed. Bench top measurements (at room temperature) provided a way to check results that were subsequently obtained through (room temperature) autoclave testing. That way, a degree of confidence was achieved relative to the validity of all autoclave testing, which was deemed the best method to obtain higher temperature calibration results.

The bench top setup was essentially identical to Figure 5-28. The addition of the LVDT to the end of the probe assembly was the only difference relative to the figure. With the LVDT in place, each advancement of the Allen bolt (which was measured with the depth micrometer) was accompanied by a change in the LVDT output voltage. The bench top calibration process consisted of incrementally tightening the Allen bolt, recording the LVDT output voltage, and measuring the associated displacement.

Autoclave testing was considerably more complex than bench top testing because of difficulties measuring displacement inside the autoclave. Those difficulties were addressed through the design and fabrication of a specialized fixture with positive mechanical stops to accurately define a displacement. Components in that fixture are shown in Figure 5-30, and the (semi-)assembled fixture is shown in Figure 5-31.

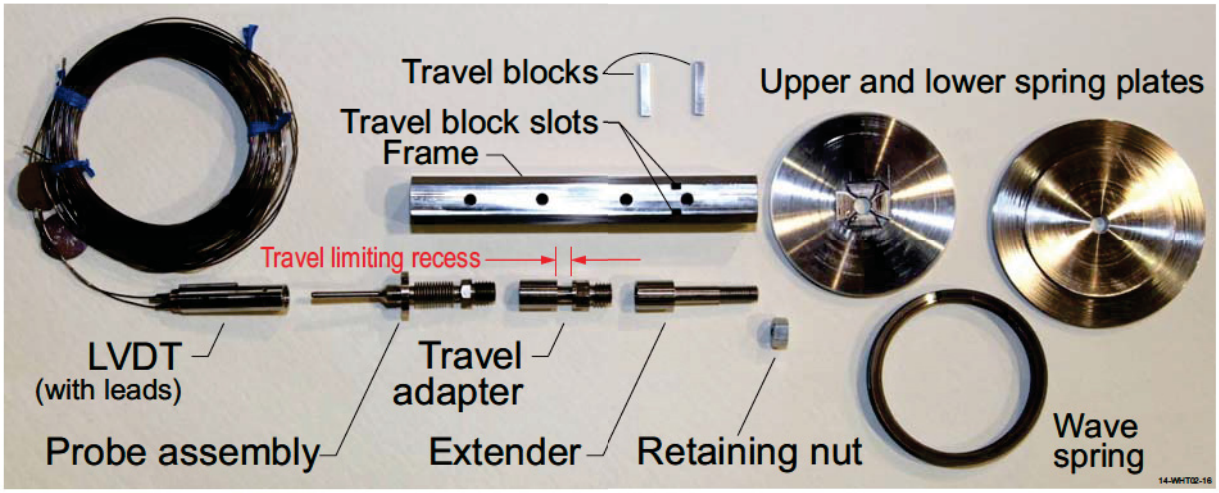

Figure 5-30. Autoclave calibration fixture components.

Figure 5-31. Assembled autoclave calibration fixture.

The specialized autoclave calibration fixture was assembled with the retaining nut tightened just enough to (slightly) stretch the bellows and pull the top of the travel limiting recess (in the travel adapter) into contact with the travel blocks. That provides the initial position of the LVDT for all autoclave testing. As the pressure is increased during each test, the bellows contracts, which collapses the wave spring and allows movement of the travel adapter. At some autoclave pressure, bellows contraction is sufficient for the bottom of the traveling limit recess to contact the travel blocks, which defines the final LVDT position for all autoclave testing. (Note that the travel limit is the difference between the travel limit recess of 7.34 mm and the travel block height of 5.08 mm for a total of 2.26 mm, which is within the bellows maximum travel limit of 3.7 mm.)

All autoclave calibration testing was conducted in a pressurized argon environment where autoclave heaters were used to achieve the desired temperature for each test. This was a practical way to complete the calibration as a function of temperature.

Calibration test results at room temperature and at 150, 250, and 350 °C are listed in Table 5-5. As indicated in the table, room temperature tests were conducted on the bench top and in an autoclave. Results from Test 1 are shown in Figure 5-32, which are typical of the room temperature bench top data. Corresponding room temperature autoclave results are provided in Figure 5-33.

As indicated in Figure 5-32, the LVDT output voltage and the associated displacement were collected as the Allen bolt was incrementally tightened (yielding a total of 9 data points in this case). In contrast, autoclave data shown in Figure 5-33 were limited to just 2 points; one where the travel adapter was pulled downward (with the retaining nut) to contact the top of the travel blocks and one where bellows compression (due to autoclave pressurization) pulled the travel adapter upward to contact the bottom of the travel blocks. Regardless of these differences in the method for data collection, the room temperature results

Table 5-5. Calibration results.

Test	Description	Temperature (°C)	Sensitivity (mV/mm)
1	bench top	room	1687
2	bench top	room	1678
3	autoclave	room	1694
4	autoclave	150	1719
5	autoclave	250	1749
6	autoclave	350	1767

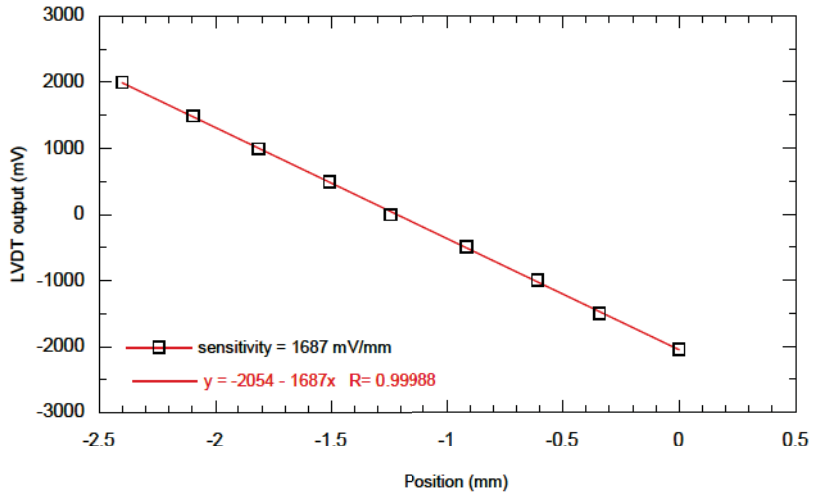

Figure 5-32. Bench top calibration results from Test 1 (at room temperature).

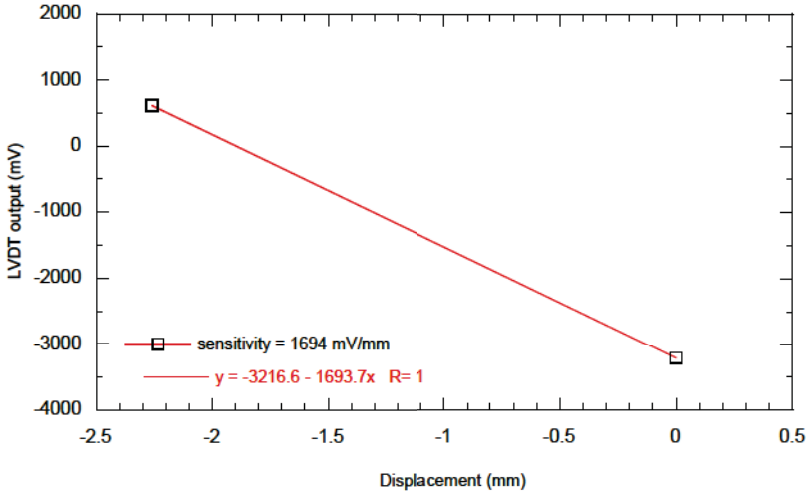

Figure 5-33. Autoclave calibration results from Test 3 (at room temperature).

were found to be consistent. Hence, it was concluded that the specialized autoclave fixture can be used to accurately collect calibration data inside the autoclave.

Averaging all room temperature calibration data yields a value of 1686 mV/mm. It is worth noting that averaging appears to be justified because differences in the measured calibration values do not translate to any appreciable travel discrepancy. Specifically, the maximum discrepancy for bellows travel across all room temperature data is (at most) 0.035 mm.

In addition to room temperature calibration data, measurements were also completed at 150, 250, and 350 °C as indicated in Table 5-5. This provides the means to relate any measured LVDT output voltage to a corresponding displacement over the range of temperatures anticipated in ATR deployment. These measurements can be compared to IFE/HRP calibration data as shown in Figure 5-34. Although the general trends in the data sets are very similar, there is clearly a shift (or an offset bias) between the data sets. All reason(s) behind this shift are unknown; however, differences between INL and IFE/HRP LVDT signal conditioning electronics have been identified as the major contributor.

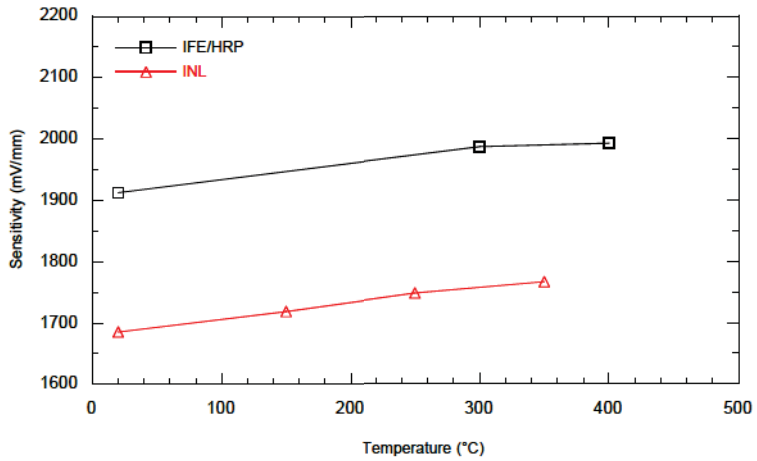

Figure 5-34. Comparison of calibration results from IFE/HRP and INL.

Summary. In summary, an enhanced creep test rig has been designed, characterized, and calibrated. The rig is ready for future use to measure specimen elongation in real time during irradiation testing in ATR Loop 2A. Once it is deployed in the ATR, data from this test rig will be evaluated to assess its performance and refine the design (if appropriate) to develop standard LVDT-based test rig designs for irradiation testing in ATR and other NSUF facilities.

5.3.2.2. Variable Load Creep Test Rig

During FY12, efforts were initiated to develop a conceptual design for a more complex creep test rig for deployment in US MTRs with the ability to apply a variable load to a specimen. Like the enhanced creep test rig (Section 5.3.2.1), this design will allow testing in reactor coolant at PWR conditions. Although the design was influenced by a creep test rig that the VTT developed and tested in the BR2,[163,164] the INL-developed variable load design is less complicated and simpler to operate. Additional details related to the development and evaluation of this INL creep test rig design is documented in References 165.

Design. The variable load creep test rig consists of two major components: the LVDT assembly and the LVDT fixture. The LVDT assembly includes the LVDT (manufactured by IFE/HRP) and the probe assembly (manufactured by INL). The LVDT body is made of Inconel 600 with silver alloy wire used in the con-

struction of the coils. The probe assembly, as shown in Figure 5-36, consists of an LVDT core inside a housing, a bellows, and connecting hardware. Most of the probe assembly was made from Inconel 600 with the exception of the core (Type 5 provided by IFE/HRP) and the bellows (Inconel 718 provided by Miniflex Corporation). The housing with connecting hardware provides the mechanism to connect movement of a specimen to movement of the LVDT core as the bellows contracts (or expands). All components of the variable load creep test rig were designed to be interchangeable with the enhanced creep test rig. Hence, all testing and calibration was conducted using the original hardware designed for the enhanced creep test rig. The variable load creep test rig is shown in Figure 5-36.

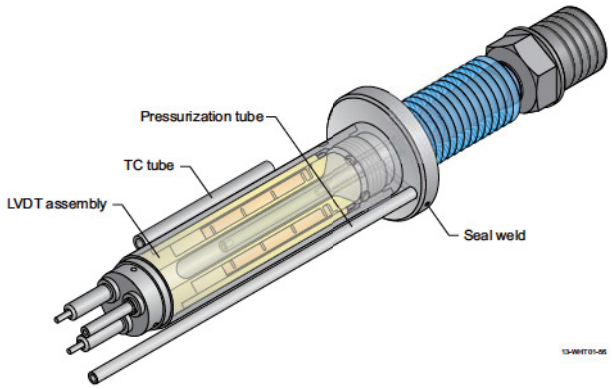

Figure 5-35. LVDT assembly.

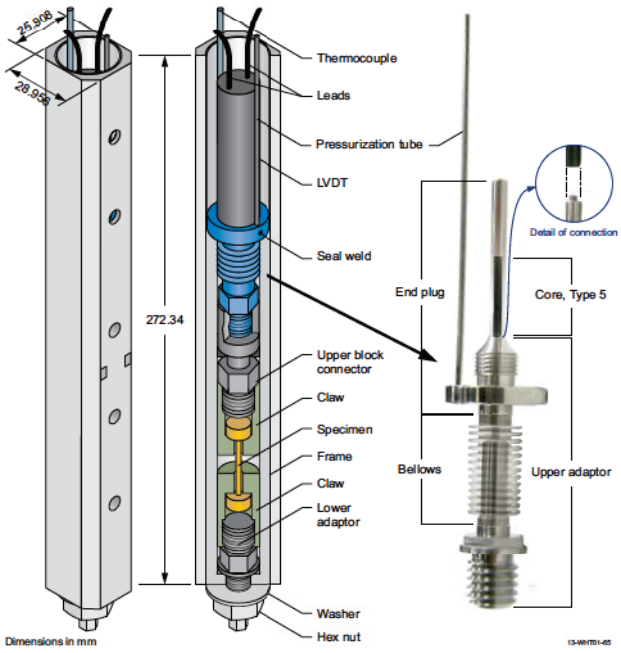

Figure 5-36. Variable lobe creep test rig (laser welding was used to attach the core to the upper adaptor, the bellows to the upper adaptor and end plug and the pressurization tube to the end plug).

The LVDT fixture includes a frame and associated hardware to connect the LVDT assembly to a creep specimen. The fixture is designed to constrain the LVDT assembly and one end of the specimen so that bellows contraction will place the specimen in tension.

Characterization. The bellows spring rate and effective area were characterized so that the load applied to a specimen can be quantified. This subsection describes the characterization process. Based on the configuration shown in Figure 5-26b, the specimen load (F_S) is given by Equation (5-2). However, unlike the enhanced creep test rig case (Section 5.3.2.1), $P_{internal}$ is not assumed to be negligible for variable creep test rig evaluations. Once the spring rate and effective area have been characterized, the specimen load can be readily determined as a function of pressure and displacement measurements using Equation (5-2).

Spring rate and effective area characterization required use of a specialized characterization fixture, which consisted of the components shown in Figure 5-37. The spring rate and the effective area were determined with this fixture, using an appropriate bolt adaptor. Both bolt adaptors have an internal thread on one end to mate with the load cell. However, the opposite ends of the bolt adaptors differ. Specifically, the bolt adaptor used to determine the spring rate has a cup large enough to allow the Allen bolt to freely slide inside, while the adaptor used to determine the effective area has an internal thread to mate with the Allen bolt. Note that the probe assembly is threaded into the LVDT to complete the LVDT assembly shown in Figures 5-35 and 5-36.

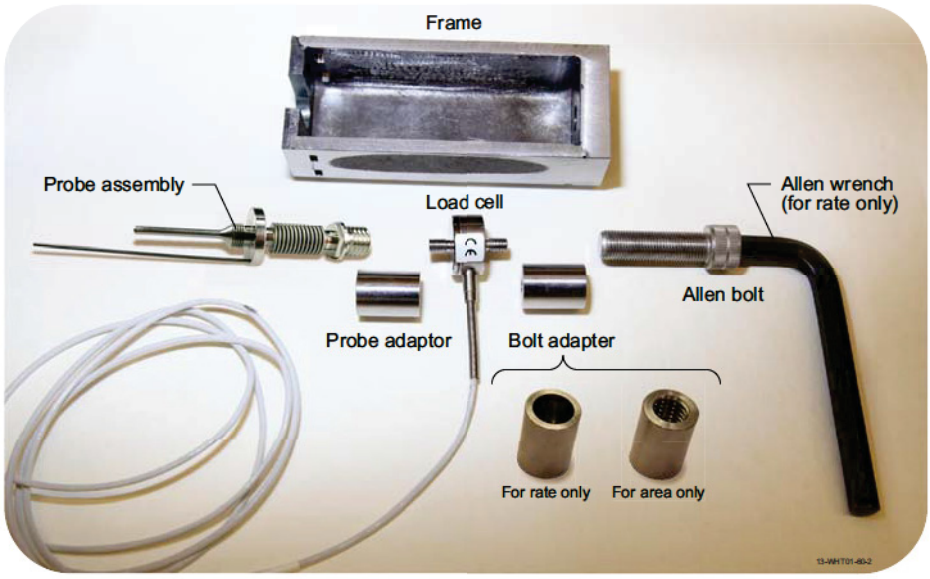

Figure 5-37. Components of the characterization fixture.

The bellows spring rate was determined through a series of bench top measurements using the fixture configuration shown in Figure 5-27 (components of the variable load creep test rig were designed to be interchangeable with the enhanced creep test rig, so test fixturing could be used for both designs). In this case, the probe assembly was constrained by one end of the frame so that the bellows could be collapsed by incrementally tightening the Allen bolt into threads in the opposite end of the frame. Note that the adaptor mating with the Allen bolt is not threaded (as previously explained) so the bolt simply pushed that adaptor toward the bellows with each rotation. As the Allen bolt was tightened, an ever increasing force was registered by the (calibrated) load cell consistent with the bellows spring rate and displacement. Displacement of the bellows was periodically measured during incremental bolt tightening, using a depth micrometer. The depth micrometer was clamped in line with the spring rate fixture and the micrometer was simply advanced to touch the head of the hex bolt each time the bolt was tightened as indicated in Figure 5-28. The spring rate characterization process consisted of incrementally tightening the Allen bolt, recording the load cell output, and measuring the associated displacement. That process was repeated until the total dis-

placement of the bellows reached ~2.5 to ~3 mm. (Displacement of 2.5 to 3 mm was sufficient to exercise the bulk of the bellows allowable travel without pressing the travel limit of 3.7 mm.) Relative to Equation (5-2), ΔP was effectively zero and (F_S) was registered through the load cell while ΔL was measured. That allowed direct calculation of the bellows spring rate (k_B) based on the measured values. All bench top measurements were completed at room temperature with the assumption that the spring rate is temperature independent. Results from these tests[165] indicate that the average bellows spring rate is 137 N/mm. This result compares well with the manufacturer's reported nominal spring rate of 138 N/mm for bellows that have not been age hardened.

The bellows effective area was determined through a series of measurements in an argon atmosphere in an autoclave using a configuration very similar to that shown in Figure 5-28. In this case, however, the frame and the threaded bolt adaptor (see Figure 5-37) were used to eliminate all movement of the bellows. As autoclave pressures were increased, the (constrained) bellows imparted an ever increasing force in the (calibrated) load cell. Internal pressure in the bellows was varied during testing to verify proper design performance. The effective area characterization process consisted of incrementally increasing or decreasing internal and external pressures while recording pressures along with the associated load cell output. The expansion of the bellows could result in plastic deformation, thus the internal pressure was never allowed to exceed the external pressure. A load limit of 1050 N was observed during testing (the load cell has a limit of ~1100 N.) Relative to Equation (5-2), ΔL was held at zero while (F_S) was registered through the load cell, and both external and internal pressures were measured. That allowed direct calculation of the bellows effective area (A_B) based on the measured values. Results from this effort[165] indicate that the bellows average effective area was 78.3 mm^2. Relative to the manufacturer's reported area of 79.4 mm^2, this measured discrepancy (of ~1%) is believed to be well within normal manufacturing tolerances.

Calibration. The LVDT bellows assembly must be calibrated over the range of temperatures that could be expected during deployment in the ATR Loop 2A. This required calibration provides the means to relate any measured LVDT output voltage to a corresponding displacement. Because internal pressure in the bellows assembly was not required, the internal pressure line was capped during calibration. Calibration was completed at room temperature and at 150, 250, and 350 °C. This temperature range is expected to adequately cover operating conditions of interest during ATR deployment. Bench top and autoclave calibrations at room temperature were completed. Bench top measurements (at room temperature) provided a way to check results that were subsequently obtained through (room temperature) autoclave testing. That way, a degree of confidence was achieved relative to the validity of all autoclave testing, which was the only practical method to obtain higher temperature calibration results. Complete details associated with this calibration effort are documented in Reference 165.

Because calibration was completed on the bench top as well as in an autoclave, bench top and autoclave setups were required. The bench top setup was essentially identical to the setup shown in Figure 5-30. The addition of the LVDT to the end of the probe assembly was the only difference. With the LVDT in place, each advancement of the Allen bolt (which was measured with the depth micrometer) was accompanied by a change in the LVDT output voltage. The bench top calibration process consisted of incrementally tightening the Allen bolt, recording the LVDT output voltage, and measuring the associated displacement. That process was repeated until the total displacement approached ~2.5 mm (which is within the bellows travel limit of 3.7 mm).

Autoclave testing was considerably more complex than bench top testing because of difficulties in measuring displacement inside the autoclave. Those difficulties were addressed through the design and fabrication of a specialized fixture with positive mechanical stops to accurately define a displacement.

Components in that fixture are shown in Figure 5-30. The assembled fixture is shown in Figure 5-31. The calibration fixture is assembled by first threading the probe assembly into the LVDT. The travel adapter is then threaded onto the bottom of the probe assembly, and the extender is threaded onto the bottom of the travel adapter. Those assembled components are then lowered inside the frame to a point where the flange on the probe assembly rests on a shoulder internal to the frame. The frame shoulder is positioned so that the top of the travel limiting recess (in the travel adapter) is just slightly above the travel block slots in the frame. After the travel blocks are inserted in the travel block slots, the spring and spring plates are stacked on the bottom of the frame and secured with the retaining and lock nut (see Figure 5-31).

At this point, the retaining nut can be tightened (and secured with a lock nut) just enough to (slightly) stretch the bellows and pull the top of the travel limiting recess (in the travel adapter) into contact with the travel blocks. That provides the initial position of the LVDT for all autoclave testing. As the pressure is increased during each test, the bellows contracts, which collapses the wave spring and allows movement of the travel adapter. At some autoclave pressure, bellows contraction is sufficient for the bottom of the traveling limit recess to contact the travel blocks, which defines the final LVDT position for all autoclave testing. The travel limit is the difference between the travel limit recess of 7.34 mm and the travel block height of 5.08 mm for a total of 2.26 mm, which is within the bellows limit of 3.7 mm.

All autoclave calibration testing was conducted in a pressurized argon or nitrogen environment where autoclave heaters were used to achieve the desired temperature for each test. This was deemed to be the most practical way to complete the calibration as a function of temperature. Calibration tests were completed at room temperature and at 150, 250, and 350 °C. Comparisons between room temperature tests conducted on the bench top and in an autoclave indicate that data were consistent, yielding a value of 1672 mV/mm. Results from measurements completed at 150, 250, and 350 °C allows any measured LVDT output voltage to be correlated to a corresponding displacement over the range of temperatures anticipated.

Summary. The variable load creep test rig characterization and calibration activities have been completed. Specifically, the bellows was characterized, indicating a spring rate of 138 N/mm and an effective area of 78.3 mm. LVDT sensitivity data were obtained that span the range from cold start up conditions to those conditions typical of an operating PWR loop. Hence, the variable load creep test rig is ready for future use in ATR Loop 2A.

5.3.2.3. Diameter Gauge Test Rig

As discussed in Section 3.3.5, the IFE/HRP currently uses a gauge for measurement of diameter during fuel irradiations to assess cladding creep, fuel pellet-cladding mechanical interaction, fuel creep / relaxation, and the accumulation of fuel rod crud deposits. In FY14, the HTTL received a three year LDRD to evaluate an IFE/HRP diameter gauge (and develop, as needed, any enhancements required for deployment in the ATR. HTTL staff are currently working with IFE/HRP staff to procure a diameter gauge and associated testing equipment (e.g., electronics, test rig, etc.) for evaluation at the HTTL.

5.3.3. Ultrasonics

Although LVDTs have been successfully deployed at other test reactors and are being investigated for ATR applications, ultrasonics offer the potential for a more compact, higher temperature, more accurate, and multi-dimensional real-time sensor for detecting geometry changes during irradiation. However, the use of ultrasonic techniques as an in-pile sensor is challenging because most ultrasound sensors rely on

piezoelectric transducer materials. First, typical in-pile operating conditions (350°C) are well above the Curie temperature of piezoelectric transducer materials that are often used for out-of-pile ultrasonic inspections,[166] and the transducer will stop functioning. Second, piezoelectric transducers are typically not suitable for radiation exposure. Although new piezoelectric materials are under investigation, radiation has been shown to damage and degrade the performance of currently proposed piezoelectric transducer materials.[167-168] Finally, conventional piezoelectric transducers often contain elements, such as lead, lithium, and gold, that transmute into toxic substances. Magnetostrictive transducers have been successfully deployed for short duration, lower frequency in-pile applications, such as ultrasonic thermometry (see Section 5.1.4). The use of magnetostrictive transducers in combination with guided wave options has the potential overcome the limitations of the piezoelectric transducers for in-pile measurement of geometry changes. However, irradiation data from a test, such as the test that will be conducted at the MITR (see Section 5.7.1) are needed to demonstrate the viability of using a magnetostrictive transducer or some new materials proposed for piezoelectric transducers.

As part of recently completed three-year INL LDRD, a feasibility study was completed to evaluate the potential to use ultrasound-based methods for in-pile measurement of geometry changes in creep specimens during irradiation testing. In this project, laboratory evaluations were completed at INL and at the Pennsylvania State University (PSU) to optimize components required for using ultrasonic techniques for in-pile elongation measurement. Key components of an in-pile setup initially investigated (see Figure 5-38a) include a magnetostrictive transducer (e.g., a driver coil with magnetostrictive core), a Remendur guide, a coupling between the Remendur guide and a long stainless steel wave guide that allowed the transducer to be located outside of the reactor, and a creep specimen with an acoustic horn to optimize the signal. Laboratory evaluations identified several options that would eliminate unwanted reflections in this initial setup, such as (1) significant reductions in the length of the stainless steel waveguide, (2) elimination of brass coupling between Remendur and stainless steel waveguides, (3) replacement of the acoustic horn on the creep specimen with an acoustically-clean "button," (4) optimization of the magnetostrictive transducers, and (5) elimination of acoustic reflections from the end of the Remendur waveguide. The "buttons" that were found to be superior to acoustic horns were similar to conventional butt-end shoulders used in tensile testing, except the buttons were designed to slide onto the specimen. Attachment methods were developed to ensure that the buttons could impart the desired tensile load and be easily attached without concerns about perfect specimen-to-button alignment. As illustrated in Figure 5-38(b), these buttons were found to be very effective at eliminating unwanted reflections, especially when implemented in conjunction with other enhancements identified in this effort.

Although it was demonstrated that acoustic signals can be transmitted through the very long (~9 m) stainless steel waveguide under carefully controlled laboratory conditions, a number of potential issues were identified that raised concerns about use of this waveguide in any MTR irradiation test. Specifically, unwanted acoustic reflections can occur due to inadvertent contact with surrounding structures along the waveguide length, attenuation of the signal as a function of waveguide length is unavoidable, and the task of routing the waveguide from the core to a point outside the vessel without interference with other reactor components and test train structures would be difficult. Laboratory testing confirmed that unwanted acoustic reflections can completely mask the reflections that are needed to determine specimen elongation. In addition to acoustic reflections associated with inadvertent contact, generation of unwanted reflections by small bends, nicks, and other minor imperfections in the waveguide was also observed. For those reasons, efforts focussed on developing a design that could minimize the stainless steel waveguide length used for irradiation testing in MTRs.

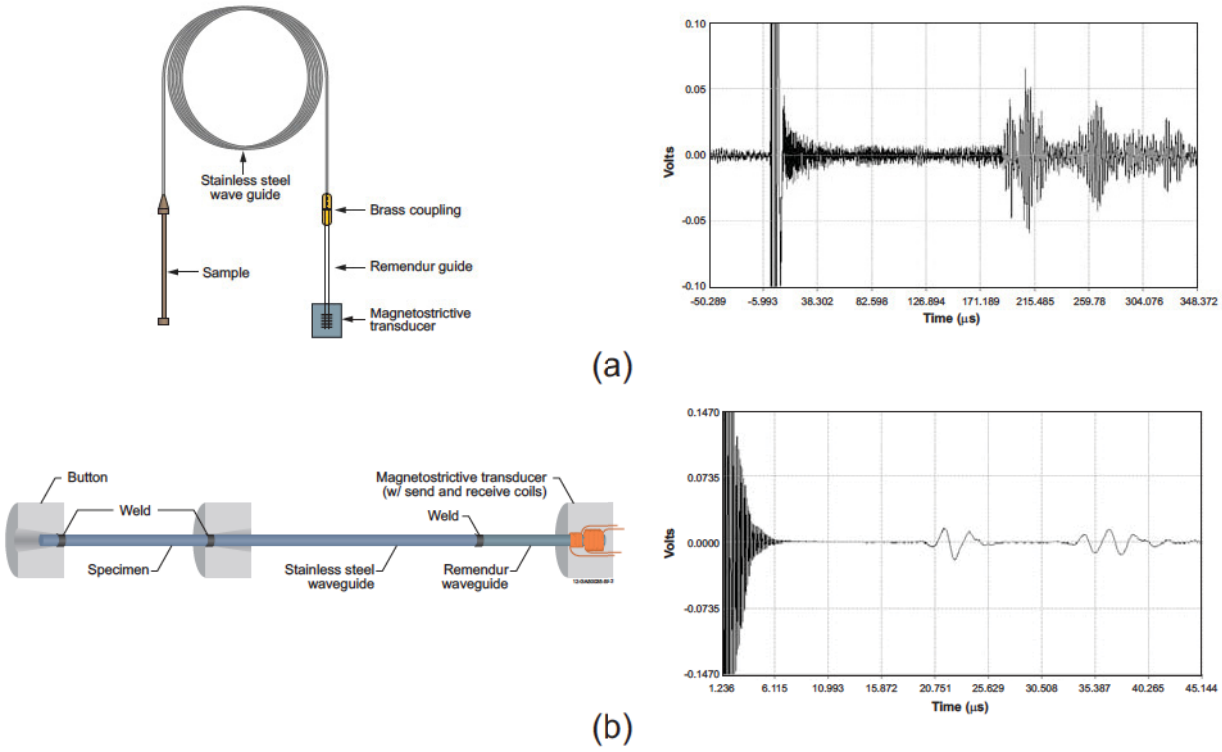

Figure 5-38. Representative system components and typical pulse/echo results using (a) initial concept with an acoustic horn and (b) enhanced concept with buttons.

Hence, laboratory testing was conducted with stainless steel waveguides ~1 m long, or less. This length was deemed sufficient to allow positioning of the creep specimen inside the ATR core and positioning of the magnetostrictive transducer above the core. In addition, an ex-core position of the transducer (where the radiation dose is substantially lower than in-core positions) may be needed given the current uncertainty with respect to the irradiation resistance of magnetostrictive transducers. Further reductions in the stainless steel waveguide length may be possible depending on results from an upcoming ATR NSUF irradiation test of magnetostrictive and piezoelectric transducers (see Section 5.7.1). However, bench top laboratory testing was completed using stainless steel waveguides limited to 1 m in length in the fixture shown in Figure 5-39. (Note that a 0.062 in OD stainless steel rod was used as both the specimen and the waveguide in this figure.)

As previously indicated, this effort focussed on optimizing the test rig design by eliminating unwanted acoustic reflections that adversely affect the accuracy of this method, such as reflections from the brass coupling proposed in the design shown in Figure 5-38a. A number of direct stainless steel to Remendur joining techniques were therefore investigated in an effort to eliminate the coupling. Success was achieved using a tungsten inert gas butt welding process. The resulting joint was found to be durable and very close to ultrasonically transparent, which eliminated the need for the brass coupling.

Laboratory evaluations also indicated that multiple reflections were generated in the acoustic horn. As shown in Figure 5-38a, those reflections make it difficult to accurately determine Time-Of-Flight (TOF) in the gauge length and any elongation. This difficulty arises from the fact that there is no accurate way to identify any characteristic point within reflected waves (i.e., characteristic points such as peak values, zero crossings, or even the onset of refections cannot be identified without considerable uncertainty).

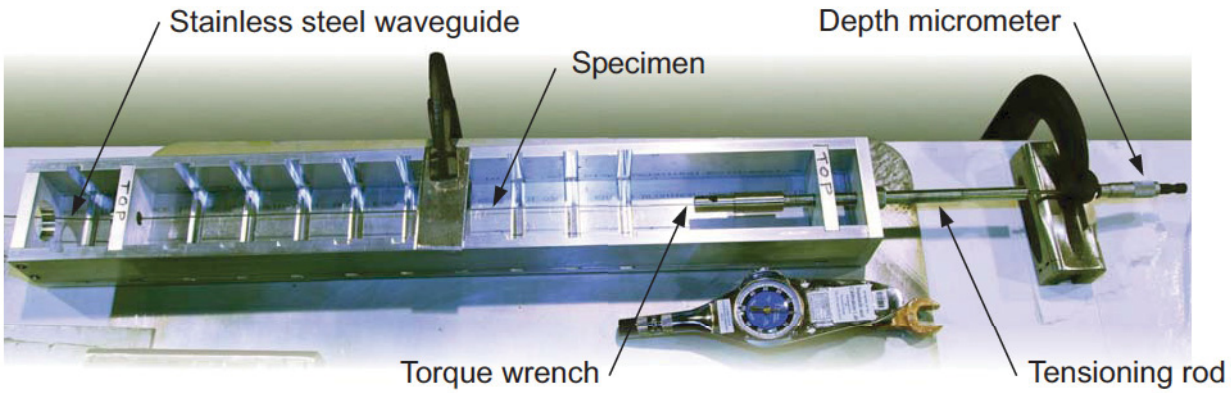

Figure 5-39. Benchtop fixture for laboratory testing of elongation detection using ultrasonic techniques.

Buttons were found to be an improvement over the acoustic horn. The buttons were similar to conventional butt-end shoulders used in tensile testing, except the buttons were designed to slide onto the specimen instead of being a machined part of the specimen. Laboratory testing revealed that a button design with conical recess machined into the button was a superior replacement for the horn because it did not promote unwanted acoustic reflections (see Figure 5-38b). In addition, this button design proved to have sufficient strength to impart the desired tensile load and be attached without rigorous measures to ensure perfect specimen-to-button alignment.

Efforts also were made to improve and optimize the design of the magnetostrictive transducer. Although the initial concept relied on a single transducer for sending and receiving ultrasonic pulses, the use of separate transducers for sending and receiving was evaluated. The motivation for these efforts stem from the fact that sending and receiving ultrasonic pulses tends to have conflicting requirements. Specifically, a low impedance transducer is desirable when sending an ultrasonic pulse while a high impedance transducer is desirable when receiving an ultrasonic pulse. A low impedance transducer, typically constructed using a relatively large diameter wire to form a coil with a relatively small number of turns, allows relatively high current flow (for a given voltage). High current flow is needed to generate a large magnetic field, which, in turn, produces a large magnetostrictive effect in the Remendur resulting in transmission of a strong acoustic pulse into the waveguide. On the other hand, a high impedance transducer, typically constructed using a relatively small diameter wire to form a coil with a relatively large number of turns, is best for transforming a magnetic field (associated with reflection of an acoustic pulse) into a relatively high voltage output signal.

Laboratory testing also indicated that significant reductions in unwanted reflections (i.e., noise) may be achieved using a pitch/catch mode (which requires separate send/receive transducers) as opposed to a pulse/echo mode (which relies on a single transducer for sending/receiving ultrasonic pulses). However, in a conventional pitch/catch configuration, the sending transducer and the receiving transducer are normally separated by the specimen being evaluated. In the case of ATR irradiation testing, that would mean that one of the transducers would normally be positioned in-core near the end of the specimen gauge length. However, as previously discussed, the irradiation resistance of magnetostrictive transducers remains unknown until completion of the ATR NSUF test program described in Section 5.7. This prompted a further refinement of the test concept, which places send and receive transducers next to each other in an ex-core position. The receiving transducer thereby detects acoustic reflections (from the buttons used to impart the specimen tensile load) instead of detecting acoustic transmission (through those buttons). The

fact that reflections are detected improves resolution and accuracy (compared to conventional pitch/catch arrangements) because TOF is effectively doubled.

Laboratory evaluations also indicated that coil length can negatively extend the pulse width. Wider pulses (and corresponding increases in the reflected pulses) tends to reduce the accuracy of TOF measurements from point to point. For that reason, efforts were made to produce transducers with the shortest length physically possible. Send and receive coils consistent with that objective are shown in Figure 5-40.

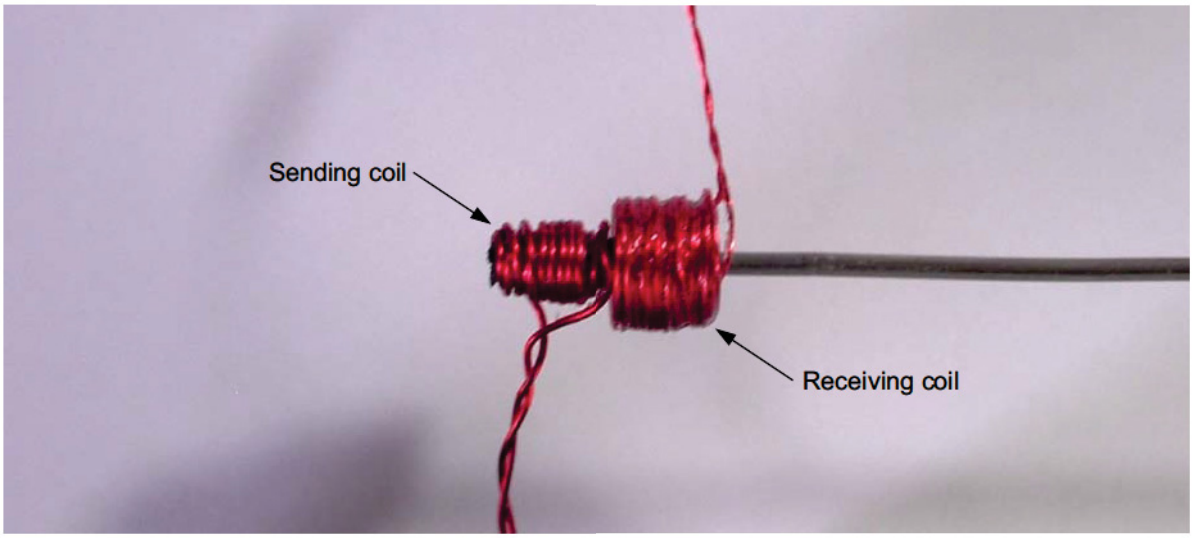

Figure 5-40. Coils developed and evaluated for use in sending and receiving transducers.

Finally, efforts were made to minimize acoustic reflections from the end of the Remendur. This was necessary because these reflections interfere with the waveforms needed to correctly interpret specimen response (like all other unwanted reflections). Although a wide variety of different damping mechanisms may conceivably work, a very simple approach was adopted for use during laboratory evaluations. Specifically, a long length of Remendur wire was welded to the stainless steel waveguide. The Remendur length was sufficient to ensure that acoustic reflections from the end of the Remendur will not arrive at the transducers until a time well past arrival of specimen acoustic reflections. In other words, TOF associated with the long Remendur wire eliminates interference by separating the Remendur reflections from the specimen reflections of interest. While this approach was perfectly acceptable for laboratory evaluations, a more compact solution may be preferable for irradiation testing in MTRs.

Significant progress was made with LDRD funding to examine the viability of using ultrasonic techniques for the in-pile measurement of elongation due to creep. Laboratory evaluations resulted in enhanced designs for components that could be used for these in-pile measurements. However, several activities are still required to enable in-pile deployment of ultrasonic techniques for elongation measurement. Those activities include development of a pressure and water resistant case for magnetostrictive transducers, laboratory temperature/pressure testing of magnetostrictive transducers, monitoring results from the ATR NSUF irradiation testing of magnetostrictive and piezoelectric transducers, further elimination of acoustic reflections (including development of a more compact solution for handling Remendur reflections), and finalization of a creep test rig design. It is currently planned to defer further exploration of this method until irradiation tests described in Section 5.7.1 are completed.

5.3.4. Fiber Optic Elongation Measurements

The FCRD funded the first three years of a four year effort to develop and deploy an optical fiber sensor for the measurement of fuel rod elongation. The sensing method for this sensor is based on the Extrinsic Fabry-Perot Interferometer (EFPI) using a low coherence white light source. In order for any fiber optic technique to be deployed in-pile, the following parameters of the sensing technique and probe must be determined or developed:

- The accuracy of the proposed approach must meet objectives (e.g., selecting appropriate system components to obtain measurement with desired accuracy),
- A probe design that can be deployed in a MTR instrumented lead capsule must be developed, and
- The life expectancy requirements under irradiations at proposed test conditions.

During the first two years of this effort, efforts were initiated to gain insights about the first two parameters. The technique was demonstrated in the lab, and the accuracy and limitations of the sensing methodology were evaluated. Laboratory evaluations were also completed to develop and test an optimized sealed probe and to conduct initial high temperature testing in a furnace. Reductions in DOE's allocation to the FCRD program in FY14 led to this effort being prematurely truncated. However, proposals have been submitted to allow this effort to be completed.

5.3.4.1. Laboratory Evaluations to Assess Accuracy

Initial laboratory investigations extended the concept presented by the CEA/SCK•CEN Joint Laboratory (see Section 3.2.1).[58] In this technique, the distance between the end of an optical fiber and a reflecting surface is determined using the interference of the light reflected from the end of the fiber, "R1," and that reflected from surface on the opposite side of the cavity space, "R2," as shown in Figure 5-41.

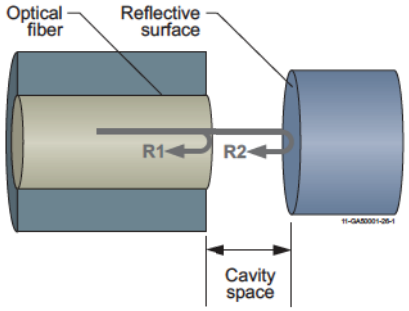

Figure 5-41. Cavity space measurement using EFPI.

The interference of these two beams produces a fringe pattern when viewed using a spectrometer, which displays the returning light intensity versus wavelength. The length of the cavity space can then be determined from the wavelength of two adjacent fringe peaks by using the following equation[170]

$$d = \frac{\lambda_1 \lambda_2}{2(\lambda_1 - \lambda_2)} \tag{5-3}$$

where:

d is the cavity length, and

λ_1 and λ_2 are the wavelengths of adjacent fringe peaks.

Laboratory testing was completed to gain experience using this technique. The technique was implemented by introducing broadband light into an optical fiber. The light in the fiber passed through a 50/50 fiber splitter in which 50% of the light continued to the probe at the end of the fiber. The probe contained a variable cavity space as previously outlined. Reflected probe light returned through the fiber to the beam splitter which delivers 50% of this returning light to the spectrometer as shown in Figure 5-42. A grating in the spectrometer separates the returning light into a spectrum of the wavelengths of light present. The interference creates a modulation of the spectrum intensity as described above.

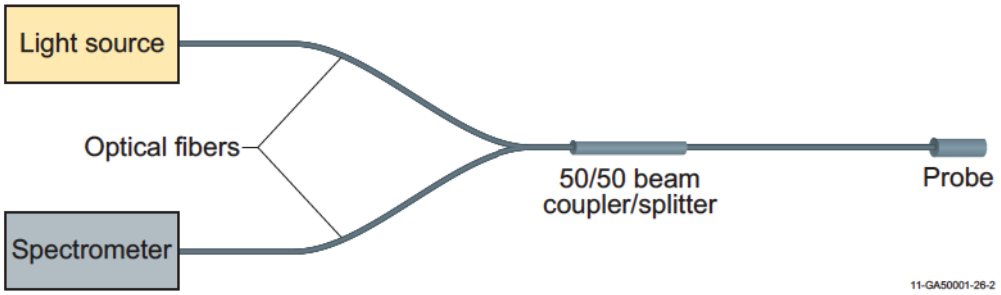

Figure 5-42. Experiment configuration for EFPI technique evaluation.

These evaluations included testing multiple light sources and fiber core sizes. It was determined that a broadband halogen light source was both cost effective and provided a wide usable light spectrum. Multimode fibers with small core sizes (50 µm) produced better results than larger core (200 µm) fibers. It was also determined that for maximum fringe modulation, the light intensity reflected from the fiber tip should be equal to the light intensity from the reflector (R1 and R2 in Figure 5-41). This was accomplished by either using a polished fiber for the reflector or by applying a partial reflective coating to the fiber tip and using polished metal for the reflector. The equipment used for the final technique evaluations and testing included: an Ocean Optics halogen light source (HL-2000-FHSA), an Ocean Optics model QE65000 spectrometer, and a Thor Labs model FCMM50-50A-FC 50/50 fiber optic splitter. The ability to measure elongation was evaluated using a Newport VP-25X stage with a Newport ESP301 driver for control and position readout. This setup is shown in Figure 5-43.

Initial technique evaluations used an optical fiber for delivery and a quartz window for the reflector. The resulting fringe modulation using the halogen light source is shown in Figure 5-44, and the cavity spacing versus the stage readout is shown in Table 5-6.

Minor differences in the absolute cavity length calculated from the fringes versus the readout from the stage controller were attributed to the inability to zero the stage exactly where the cavity length was zero. However, the change in cavity space versus the change in stage position from point to point were in very good agreement (typically less than 0.3 µm). It should be noted that a simple routine of graphically picking fringe peak wavelengths and calculating an average cavity space using Equation (5-3) was used. In future evaluations, a more sophisticated analysis for determining the fringe spacing will be employed to enhance accuracies.

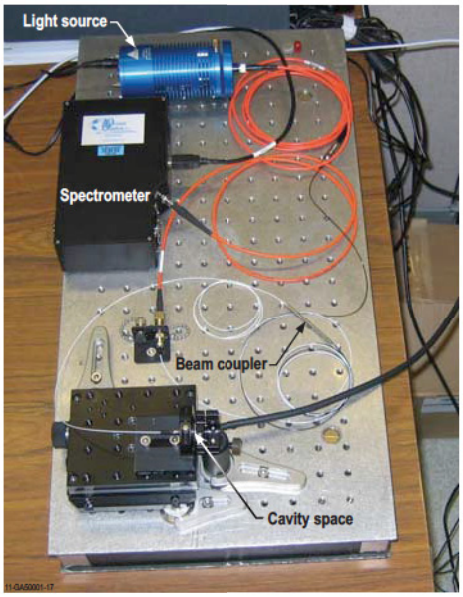

Figure 5-43. Laboratory setup for initial evaluation of fiber optic in-pile elongation detection.

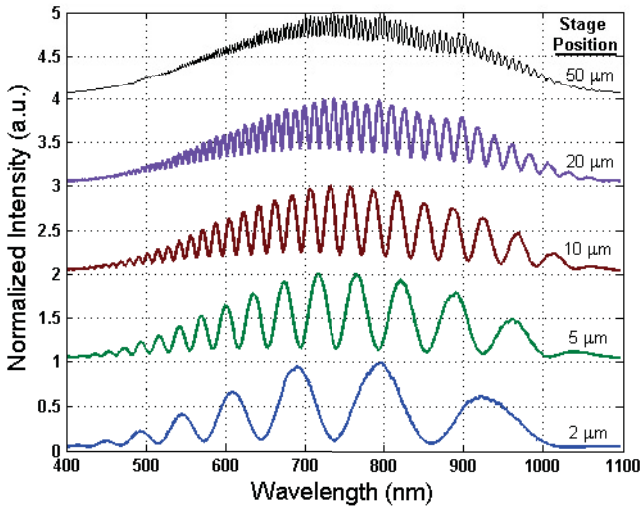

Figure 5-44. Spectra showing EFPI fringe modulation at several cavity lengths.

5.3.4.2. Probe Design and Fabrication

Once the technique was successfully demonstrated, work on conceptual probe designs was begun. An initial probe was fabricated using stainless steel hypodermic tubing. In this design, the optical fiber was bonded inside of a short length of stainless steel tube, and the reflecting side of the cavity was fabricated by bonding a short length of larger core optical fiber into a small piece of the same stainless steel tubing. The fiber ends were polished and inserted into a larger diameter sleeve such that the space between the tips created the measurement cavity. The sleeve served to maintain axial alignment between the fibers as the cavity space was changed. A schematic of the probe design is shown in Figure 5-45.

Table 5-6. Comparison of measured cavity length versus length inferred from fringe spacing.

VP-25X Stage Position (µm)	Cavity Based on Measured Fringe Spacing	Change in Measured Cavity (µm)	Difference Between Change in Stage Position and Measured Cavity (µm)
0	0.73	-	-
1	1.63	0.901	0.10
2	2.64	1.010	-0.01
3	3.55	0.911	0.09
4	4.55	0.995	0.00
5	5.54	0.991	0.01
7	7.45	1.917	0.08
10	10.46	3.009	-0.01
15	15.45	4.988	0.01
20	20.59	5.141	-0.14
25	25.61	5.023	-0.02
30	30.55	4.934	0.07
35	35.48	4.933	0.07
40	40.70	5.219	-0.22
45	45.57	4.871	0.13
50	50.77	5.196	-0.20
60	60.82	10.057	-0.06
70	70.73	9.904	0.10
80	80.75	10.017	-0.02
90	90.78	10.035	-0.03
100	101.06	10.277	-0.28
125	126.06	25.002	0.00

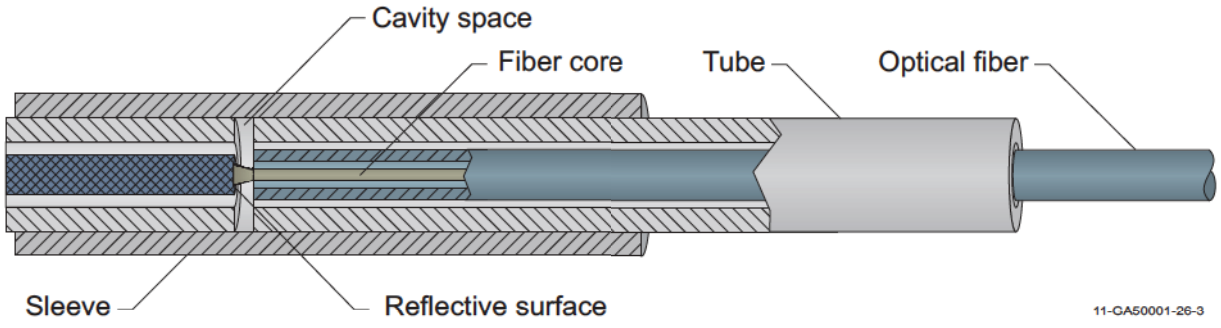

Figure 5-45. Elongation probe concept using hypodermic tubing.

Evaluations of this concept probe yielded promising results. In FY12, efforts were focused on developing a sealed probe that could be deployed in an irradiation test. A probe design was developed that was functionally similar to the concept probe, but incorporated a bellows, which would provide isolation from the environment and allow expansion of the probe. A cross-section of the probe design is shown in Figure 5-46.

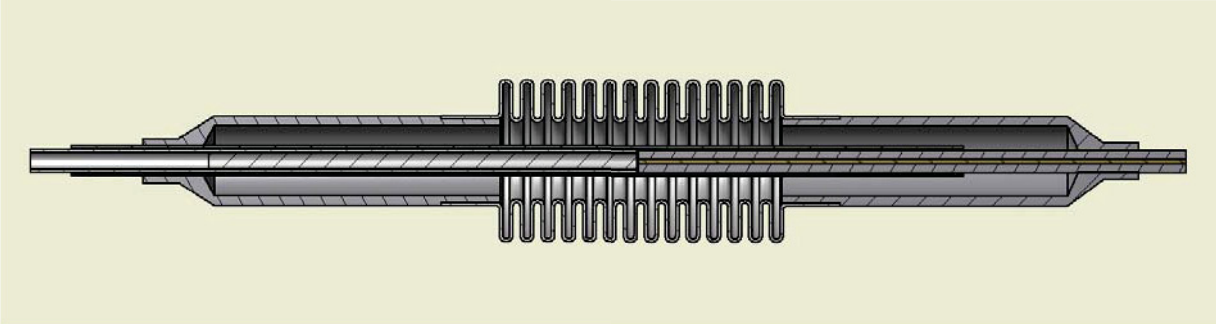

Figure 5-46. Elongation probe cross section.

A number of obstacles were resolved in fabricating this probe. Bonding of the optical fiber in the stainless steel hypodermic tubing presented problems as initial attempts at stripping the fiber coating and bonding in the tube resulted in fracture of the fiber at moderate temperatures. It was found that gold coated fiber, which can withstand temperatures of 700 °C, could be bonded inside the hypodermic tube using Cotronics Resbond 907TS Green threadlocker without fiber fracture at elevated temperatures. Another issue was developing the ability to assemble and weld the small probe components. The smallest readily available stainless steel bellows was a MiniFlex Corporation Model SS-125-46-168. An adapter was developed which could be welded to the bellows on one end and the hypodermic tubing on the other end. Welding of these components was accomplished using a laser welding system. A photo of the completed sensor is shown in Figure 5-47.

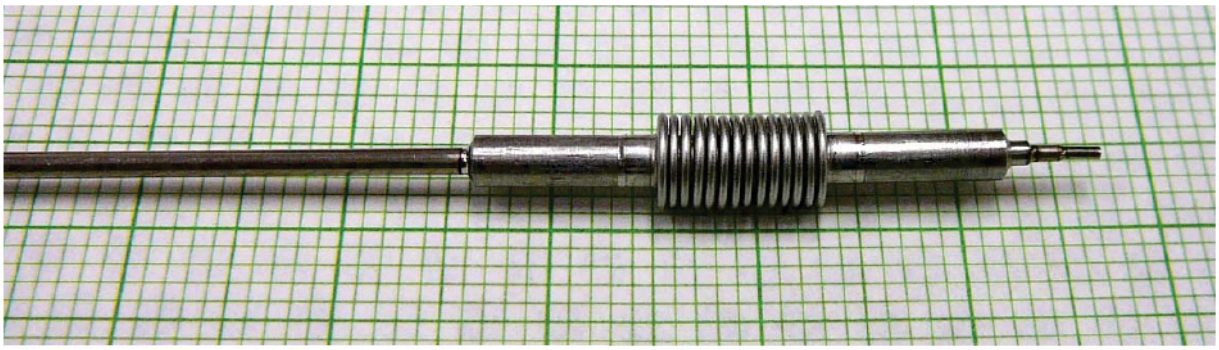

Figure 5-47. Welded elongation probe.

Initial testing of the probe revealed an increasing discrepancy between the readings from the stage and the probe. However, it was determined the discrepancy was due to flexing of the support posts. A more substantial test fixture was fabricated, and the probe was retested. For the first test, the probe was clamped in position, and the stage was first zeroed and then moved from 0 μm to 150 μm in increments from 1 to 10 μm. This test yielded very good results with the discrepancy between the stage position reading and the probe being generally less than 0.3 μm up to a 90 μm displacement. The increased error observed with displacements greater than 100 μm was primarily due to difficulty reading the fringe pattern. Repeatability was then evaluated by randomly moving the stage between 3 and 92 μm. Position readings from both the stage and probe were plotted, and a linear fit performed. The data and linear fit are shown in Figure 5-48a. The linear fit slope was 1.0037, which is close to a perfect match of 1.00; and the intercept was 0.50 μm. The intercept is simply a measure of how close the stage zero was to the probe zero. The average differ-

ence between probe measurements and the stage readings (adjusted for the zero offset) was less than 0.2 µm.

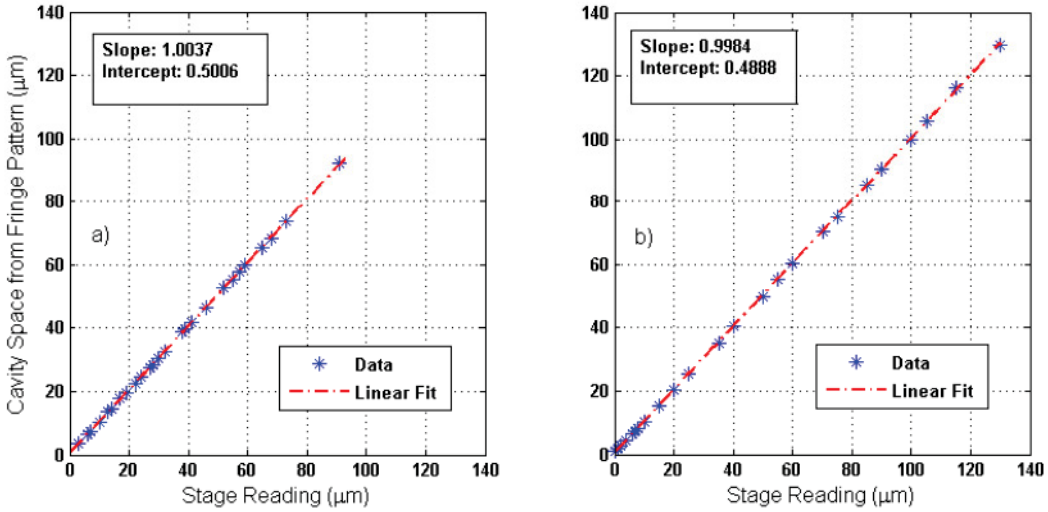

Figure 5-48. Elongation probe data: a) Standard probe, b) Probe with partial reflective coating.

Probe design and testing continued in FY13. A probe incorporating a partial reflective coating on the fiber tip and a polished metal reflector was fabricated. The partial reflective coating was applied by Cascade Optical Corporation and was designed to reflect 25% of incident light compared to a 4% reflection from the bare fiber tip. This design is substantially more light efficient with approximately 14% of the total input light returning to the spectrometer compared to less than 2% for the uncoated design. The improved light efficiency was born out in testing as the source light had to be attenuated to prevent saturation of the spectrometer. Results from the testing revealed improved signal to noise allowing accurate displacement measurements out to 130 µm as shown in Figure 5-48b. This design also results in a simplified sensor as the bonding of a silica reflector in a metal tube is eliminated as are possible reflections from the back of the reflector. However, the survivability of the partial reflective coating for use in elevated temperature and radiation conditions must be verified.

High temperature testing of the probe design using a tube furnace (see Figure 5-49a) was initiated in FY13. For these initial tests, clamps were used to attach the probe to an aluminum rod as shown in Figure 5-49b. The sensor incorporating a partial reflective coating was first tested. This sensor performed well to over 150 °C, at which point the fringe modulation decreased to below the noise level. It was later determined that the partial reflective coating was the limiting factor. Future evaluations should explore commercially-available higher temperature coatings. A sensor without the coating was also tested in the tube furnace. This sensor survived temperatures of over 350 °C, but low signal to noise ratios decreased the accuracy of readings above 200 °C.

Hence, initial high temperature furnace testing and other investigations revealed improvements necessary for a more reliable sensor. Alignment of the fiber and reflector are paramount for improved signal to noise.The fiber tip face must also be flat and perpendicular to the axis of the fiber. A revised sensor design was developed which allows the use of commercially-available Lucent Connector (LC) type ferrules and sleeves to improve alignment. High temperature fibers bonded in the LC ferrules can be procured through vendors with the equipment required to produce these components to industry standards. The improved

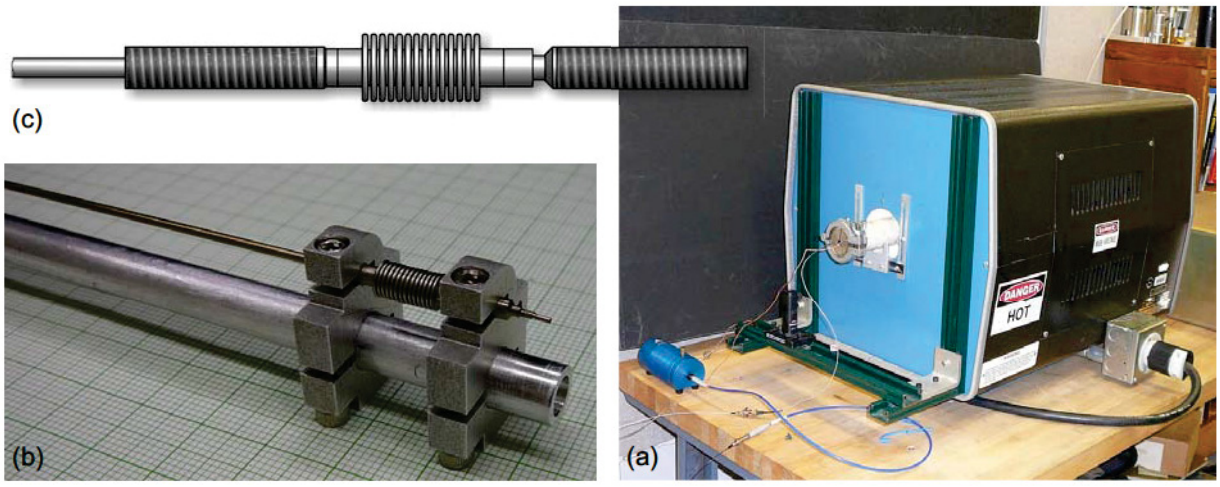

Figure 5-49. FY13 Fiber optic elongation probe design and evaluations efforts - a) High temperature tube furnace testing, b) probe clamped to aluminum rod, c) revised probe design.

design also incorporates threaded ends to simplify sensor attachment. A schematic of the improved sensor design is shown in Figure 5-49c.

5.3.4.3. Elongation Sensor Technique Sensitivity

Evaluation of the EFPI technique and testing of an elongation probe based on this method have led to a better understanding of the sensitivity and cavity length range of this technique. On a closer inspection of Equation (5-3) and observation of the recorded spectrum, it can be seen that the fringe spacing is wide for a small cavity length and narrow for a longer cavity length. Consequently, as the cavity length increases the sensitivity decreases. It has been shown that the radiation induced attenuation of optical fibers is the lowest in the near IR wavelength, particularly in the range from about 800 to 1300 nm.[58] If the probe were designed to operate in this window and two fringe peaks were required within this range to determine fringe spacing, the minimum detectable cavity space would be approximately 1.5 μm. The maximum detectable cavity space is based on the resolution of the spectrometer. As the cavity space increases and the fringe peaks get closer together, the ability to resolve individual peaks becomes the limiting factor. The Ocean Optics QE65000 used in these tests had a resolution of about 0.8 nm which resulted in a maximum measurable cavity space of about 125 μm. Testing of the initial probe revealed high precision for measurements between approximately 3 and 100 μm and the sensor incorporating a partial reflective coated tip and metal reflector extended this range out to around 130 μm. Measurement errors increased above this range. Some improvements for longer displacements may be possible by using a spectrometer which is sensitive to longer wavelengths than the QE65000.

5.3.4.4. Summary and Future Work

Work on the elongation probe has lead to a number of observations about the technique which are summarized below:

- The technique is viable and has demonstrated an accuracy on the order of 0.3 μm.
- Small core, low numerical aperture fibers tend to work better.

- Return light from the reflections at the end of the fiber and the mirrored surface should be approximately the same intensity for good fringe modulation depth. If a polished stainless steel surface is used opposite the fiber end face, the fiber end face should be coated with a roughly 25% reflective coating for best results.
- The fiber face should be polished flat and alignment of the fiber axis perpendicular to the reflective surface must be maintained.
- The sensitivity of the probe is a function of the spectrometer resolution and the fringe modulation depth.
- The minimum detectable cavity space is based on the bandwidth of the light source and "transmission window" of the irradiated optical fiber. The best transmission range for irradiated optical fibers extends from approximately 800 nm to 1300 nm.
- The approximate measurement range of a probe based on this technique is 1.5 to 125 μm (based on the fiber transmission window and a spectrometer resolution of 0.8 nm).

Evaluations have demonstrated the viability of a fiber optic elongation sensor based on the EFPI technique. A probe has been fabricated and tested and an invention disclosure record (IDR) was filed related to its design.[171] However, continued development will be required to produce an in-pile service ready sensor.

The following list outlines the status of activities required to bring the desired sensor to fruition:

- Optimization of probe design parameters - During FY12, an elongation probe was fabricated and tested. Many improvements were made over the initial concept probe. Optimization continued during FY13 with testing of fibers with lower numerical apertures and fibers with partial reflective coatings used in conjunction with stainless steel reflectors. Methods of improving alignment were also implemented. Optimization will continue throughout the development process.
- Fabrication Capabilities - INL capabilities were sufficient for fabrication of the initial elongation probes. Commercial vendors have now been engaged for improved sensor tip fabrication. Additional commercial processes may be used for the final sensors.
- Radiation Resistance - Work to date has been conducted using standard commercially available fibers and components. Radiation resistant fibers and fiber to tube bonding materials/methods need to be incorporated into the design. A broadband light source operating in the 800 to 1300 nm range also needs to be identified or developed. As discussed in Section 5.7.2, results from an irradiation test are required before this probe can be deployed.
- Signal Analysis Software - During the current evaluation phase of sensor development, the signal from the probe is displayed as a modulated wavelength spectrum on the screen of a personal computer (PC). This is not convenient for an operator. Automated signal analysis software will be developed so that cavity length or elongation can be provided directly to the user.
- Final Design & Testing - Once the probe has been optimized, it will still need to be attached to the sample and incorporated into a test capsule. This final design configuration will then be tested in a simulated reactor environment prior to deployment.

Although development efforts were planned to enable deployment of this probe by FY14, development has been indefinitely delayed due to FCRD funding limitations. In addition, deployment will be delayed until completion of the irradiation test discussed in Section 5.7.2.

5.4. Direct Current Potential Drop (DCPD)

A key component in evaluating the ability of LWRs to operate beyond 60 years is characterizing the degradation of materials exposed to radiation and various water chemistries. Of particular concern is the response of reactor materials to Irradiation Assisted Stress Corrosion Cracking (IASCC). Crack initiation and growth of samples irradiated in instrumented lead and PWR loop tests in the ATR are evaluated out-of-pile. However, crack-growth rates in core structural component materials irradiated in MTRs outside the US, such as the HBWR in Norway, are monitored in-pile using miniaturized CT specimens and the DCPD method. As discussed in Section 3.3.6, the DCPD method is based on sending a precisely controlled electrical current through the specimen and measuring the drop in voltage at several locations on the CT-specimen. The measured voltage changes as a function of crack growth. Thus, the crack-length can be determined from the measured voltages. IFE/HRP has applied this technology to detect the impact of coolant parameters (pH, impurities, boron concentration, etc.) on fuel cladding corrosion. In addition, IFE/HRP can also perform such measurements on pre-irradiated fuel removed from commercial reactors.

The major aspects of choosing a crack growth measurement technique are: specimen geometry, loading mode (active or passive) and crack length measurement technique. Crack length measurement by the DCPD technique is very well established and has become a de facto standard for in-core measurements. It is applicable to most specimen geometries, although specimen extensions are often used to provide adequate space to connect current leads and voltage probes. As discussed in Section 3.3.6, this method has been applied in several research and test reactors. In addition, this technique has been applied in-core and in recirculation piping autoclaves of commercial BWRs. Some out-of-core measurements have used AC potential drop, but there do not appear to be significant advantages for this technique. Another method frequently applied in out-of-core tests is to measure "crack tip opening displacement" (COD) using a strain gauge. However, this is a very delicate procedure requiring elements that are not readily adaptable to in-core environments.

Figure 5-50 shows the essential features of the in-pile hardware used at HBWR. A loading mechanism is used to stress the crack in a CT specimen. The mechanism utilizes a miniature high pressure bellows, which expands to apply the force required to propagate the crack. The CT specimens are fabricated with "ears" above the loading holes to provide locations for current and voltage connections. During 2012, an INL-funded LDRD was initiated to adapt the DCDP method used at the HBWR so that it can be deployed in high flux MTRs in the US, such as INL's ATR.

As part of a three year LDRD, INL has teamed with MIT-Nuclear Reactor Laboratory (MIT-NRL) experiment designers to develop the hardware and techniques required to monitor crack growth in a specimen during irradiation. During the first year (FY13) of this three year project, a loading mechanism was designed, fabricated, and tested. Techniques for attaching leads to the specimens were developed, and initial steps for implementing standard DCPD method to the unique specimen geometry and testing environment were completed. Various aspects about each of these tasks are summarized below. Additional details are documented in Reference 172.

5.4.1. Loading Mechanism Design and Testing

During FY13, two specimen loading mechanisms were constructed. INL first constructed an initial prototype from stainless steel. Techniques were developed for making laser welds between the miniature bellows and the end fittings used to transfer the loads. Then, using the INL design as a starting point, the

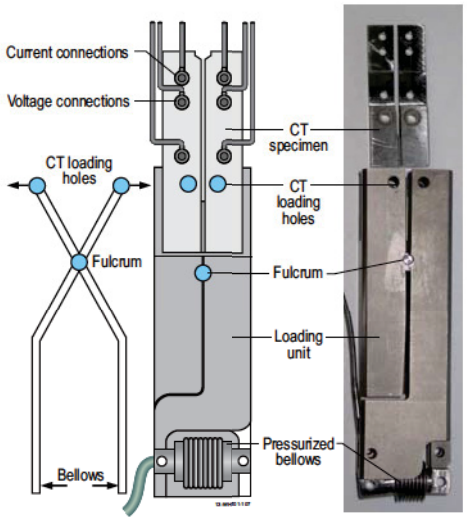

Figure 5-50. DCDP loading mechanisms and connections.

Massachusetts Institute of Technology (MIT) experiment design group completed a full three dimensional finite elements analysis to identify requirements for an enhanced mechanism. Based on the results of their analysis, the MIT mechanism was made from aircraft grade titanium. Use of titanium material had three advantages: 1) lower induced radioactivity after irradiation, 2) higher strength, and 3) essentially immune to corrosion. The operating force for both mechanisms is generated by pressurizing a miniature bellows as shown in Figure 5-50.

Bench top testing was completed on the INL stainless steel and MIT titanium versions to verify that the load applied to the specimen could be accurately predicted for various pressures supplied to the bellows. In these tests, each mechanism was attached to a pre-calibrated force gage, which took the place of the specimen, as shown in Figure 5-51.

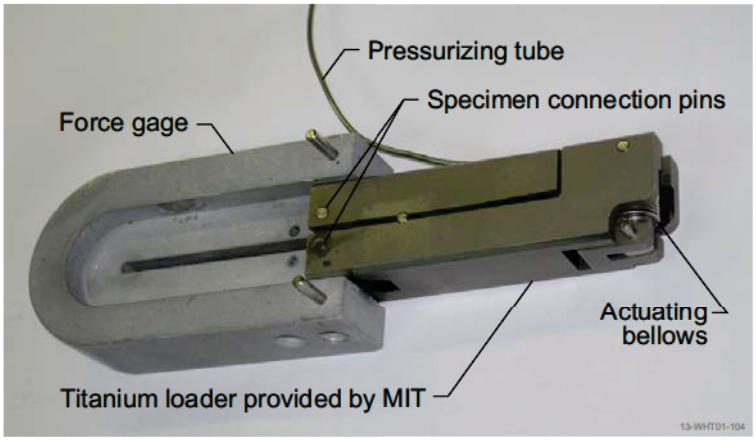

Figure 5-51. Titanium loader connected to force gage for bench top testing.

Although the two loaders had different mechanical advantages (fulcrum positions) and different elastic moduli, the test results (shown in Figure 5-52) demonstrate that the force applied to the specimen pins for

a given pressure was very predictable and repeatable, while the pressure was ramped up or held constant. As the pressure increased, the deviation between calculated and measured force was less than 4%. However, considerable hysteresis was evident as pressure decreased (maximum deviations of ~25% were observed).

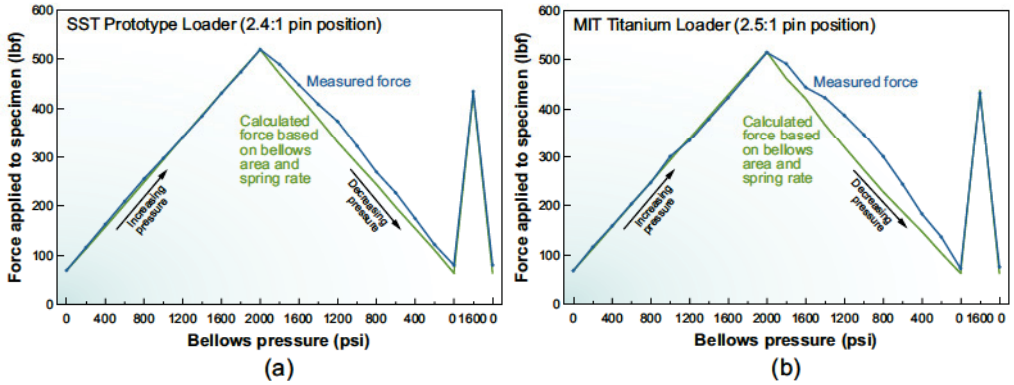

Figure 5-52. Force applied to specimen versus pressure (a) stainless steel loader, and (b) titanium loader.

Shown on the right side of Figures 5-52a and 5-52b are data points taken at 11 MPa after each mechanism was exposed to one pressure cycle. For both the stainless steel and titanium loaders, resulting forces at these points matched the calculated force within 2% and were virtually identical to the forces obtained during the increasing pressure portion of the cycle. This is important because the bellows pressure will be cycled periodically; and it is expected that the peak force achieved at the end of each pressure rise will be relatively hysteresis free.

5.4.2. Specimen Design and Fabrication

Figure 5-53 shows the overall dimensions for the specimen designed to work with the loading mechanism. The lower part of the specimen is essentially a one-quarter scale CT designed in accordance with ASTM E399, Fig. A4.1.[173] The upper part of the specimen consists of integral "ears" extending some distance above the holes for the loading pins. These ears provide locations to connect voltage and current leads. INL has also developed techniques for attaching leads to the specimens that will survive in a radiation environment with high water velocities flowing over the specimens. IFE/HRP experience indicates that the electrical connections needed in such an environment must be extremely robust. During FY13, INL developed and fabricated CT specimens as shown in Figure 5-53. Electrical leads attached to the specimen ears consist of co-axial, single conductor mineral insulated cable. This mineral insulated cable is laser welded to an intermediate boss, and the boss is resistance welded to the specimen ears. This method was developed under the assumption that future experimenters may want to perform in pile crack growth tests on previously irradiated material, and a method adaptable to remote hot cell work was needed. For such an application, the laser welds to the voltage and current leads; and the bosses would be made outside the hot cell, and then the resistance welds of the bosses to the specimen ears would be made inside a hot cell.

The leads for both the current and voltage connections, which consist of co-axial mineral insulated cable, were fabricated with the conductor welded to the tip of the sheath. This was done because of the difficulty of bringing the conductor out of the sheath, keeping it insulated from the sheath, and keeping water under high pressure from entering and soaking the mineral insulation within the insulation. This sealing

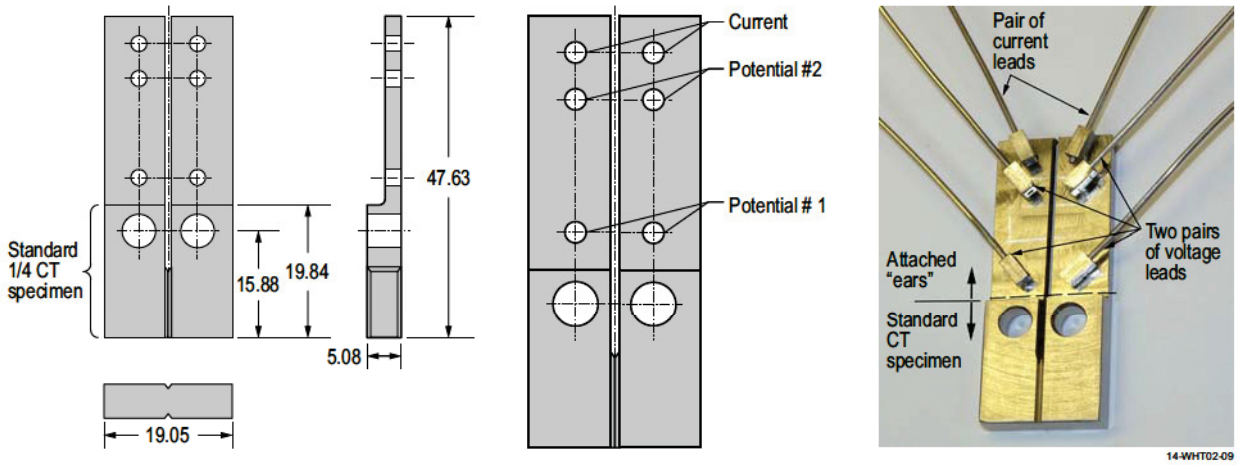

Figure 5-53. Specimen geometry and with leads dry fit attachments.

problem is even more critical because of the extremely high radiation environment of a high power test reactor. However, with the conductors welded to their respective sheaths, provisions must be made to ensure that useful signals can be obtained from the voltage leads. This is done by grounding the sheaths of both the current and voltage leads to a grounding plate about 20 cm away. The leads must not be allowed to touch each other, or other metal until the connection to the grounding plate is made.

The resistance of the Inconel 600 sheaths over this 20 cm distance is about 0.5 Ω. This resistance is about 300 - 500 times the resistance of the specimen itself, and this large difference ensures the success of this approach. As shown in Figure 5-54, because of the connections to the grounding plate, stray currents leak off through both the sheaths of the current and voltage leads; but these stray currents represent less than <0.5% of the total current passing through the specimen, and thus alter the potential read across the specimen by a similar fraction.

5.4.3. In-Pile Implementation of DCPD Method

The key aspect of this project is the ability to measure crack growth in situ using the reversed DCPD technique, which has been shown to provide accurate and reliable measurements in LWR environments. For this technique, a DC source supplies a stable current to the specimen, which is reversed periodically through solid state relays to correct for thermoelectric effects. The potential drop resulting from crack extension in the specimen is measured by a nanovolt meter that averages hundreds or thousands of individual readings. Data acquisition, data averaging, current reversal and the relationship between the measured potential and crack length are controlled by dedicated software. Due to the requirement related to the loading jig design and insertion in a loop of a reactor, the usual CT specimen geometry, the traditional location of the current and potential leads for the DCPD technique, and the nature of such leads, were not appropriate for this project. As discussed in Section 5.4.2, a modified specimen design that can accommodate the required probes and lead fabrication techniques have been developed (see Figure 5-53). However, typical software packages developed for the DCPD method cannot be used, and new mathematical relationships must be developed for these specimens.

To assure the quality of the potential drop readings it is necessary to control current path. This is partially achieved by electrically isolating the specimen from the loading mechanism with zirconia sleeves.

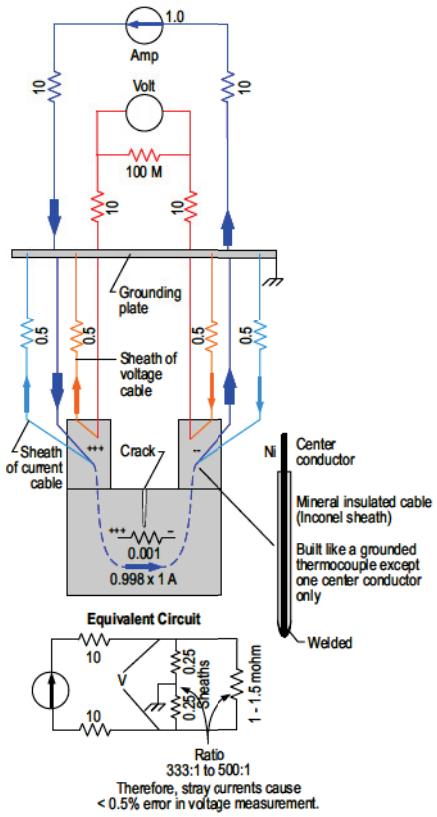

Figure 5-54. Electrical circuit illustrating the effect of grounding current and voltage leads

Assuring the electrical insulation of the current and potential leads, which connect the specimen to the data acquisition system located outside of the core of the reactor, is more challenging than in a normal DCPD set up. As discussed above, grounded mineral insulated cables were used, and bench top testing confirmed that grounding the outer sheath of the cables to a plate near the specimen has little effect on the measurement of potential drop. This has the advantage of allowing the use of such cables through the length of the reactor without worrying about uncontrolled temporary grounding that would affect the measurements.

Last, the relationship between the measured potential and crack length was established for this particular set up. This relationship was obtained by growing a fatigue crack in the specimen while the DCPD system was measuring potential changes as a crack propagated. Four fatigue steps were applied, with changes in loading ratio to create distinctive marks on the fracture surface that allowed measuring the actual crack length and matching it with the potential drop measured. Finally the specimen was fractured by fatigue. Results have been implemented into specialized software that is being 'calibrated' for this setup.

5.5. Flux and Fluence

Typically, ATR tests use flux wires and post-irradiation evaluations to detect the total fluence to which the fuel or sample was exposed. However, as noted in Section 3, MTRs in Norway, France, the Netherlands, Japan, Belgian, and the Republic of Korea routinely incorporate SPNDs during irradiation tests to gain real-time knowledge of the fission reaction rate. In recent years, French and Belgium test reactors have also incorporated specialized fission chambers to provide users real-time data related to neutron flux

(see Section 3).

Several efforts are underway to enhance ATR flux and fluence measurements. As discussed in this section, new in-house capabilities have been developed for encapsulating wires for post-irradiation fluence measurements. In addition, an ATR NSUF project, led by the Idaho State University (ISU) with INL and CEA as collaborators, evaluated new real-time state-of-the-art in-pile flux detection sensors at the ATRC. Finally, efforts are underway to design and deploy a new small compact sensor that can simultaneously measure fast and thermal flux and temperature. More detailed descriptions of each type of sensor and associated test rigs developed for these evaluations at ATRC are provided in this section.

5.5.1. Activation Wires and Foils for ATRC Evaluation

Test hardware with typical activation wires and foils used for activation spectrometry and flux profiling in the ATRC is shown in Figure 5-55. Various materials with different neutron sensitivities as functions of neutron energy were used. During initial evaluations, six different sets of activation foil measurements were performed in the ATRC NW and SE Flux Traps at the axial core mid-plane to determine detailed neutron spectral information at these locations for reactor physics code benchmarking purposes. Detailed measurements of the core flux distribution were also performed, using standard ATRC flux 'wands' in selected fuel elements.

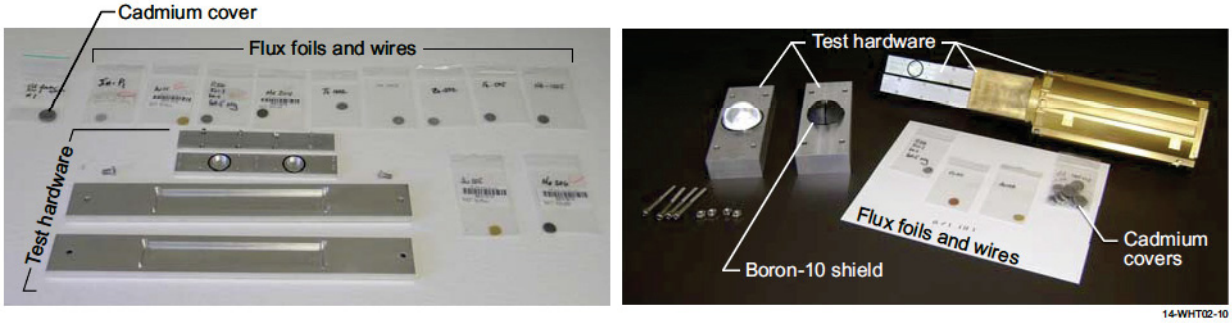

Figure 5-55. ATRC test hardware and activation foils.

Activation wires and foils for these evaluations are listed in Table 5-7, grouped by the range of neutron energies to which each set of foils is sensitive. Some foils were placed inside standard cadmium-foil covers or boron-10 spectral modification shields to enhance their response in the epithermal and fast-neutron ranges. Further experimental setup details related to these activation foils are found in References 178 and 179.

Table 5-7. Flux wires and foils evaluated in ISU/INL/CEA ATRC evaluations.

Detector	Characteristics of Interest	
Flux Wires	Material	
	U235-Aluminum Copper-1.55 Gold	
Flux Foils	Material	Encapsulation Method
Thermal-neutron Detection	Gold (100%) Manganese- Copper (80% / 20% wt)	None
Epithermal-neutron Detection	Indium (> 99%) Gold (> 99%) Tungsten (>99%) Cobalt (>99%) Manganese-Copper (80%/20%) Copper (>99%) Scandium (>99%)	Cadmium (>99%) Covers
Fast-neutron Detection	Niobium (>99%) Rhodium (>99%) Indium (>99%) Titanium (>99%) Zinc (>99%) Nickel (>99%) Iron (>99%) Copper (>99%)	Boron Sphere (>99%)

The foils were activated in the ATRC northwest Large In-Pile Tube (NW LIPT) flux trap, the largest irradiation facility in the ATRC. In addition, the southeast Standard In-Pile Tube (SE SIPT) was used for activation measurements using hardware shown in Figure 5-56. Standardization of flux data from separate reactor runs was accomplished using measured activation of standard copper/gold (1.55 wt% gold) flux wires at specific locations in and around the NW flux trap.

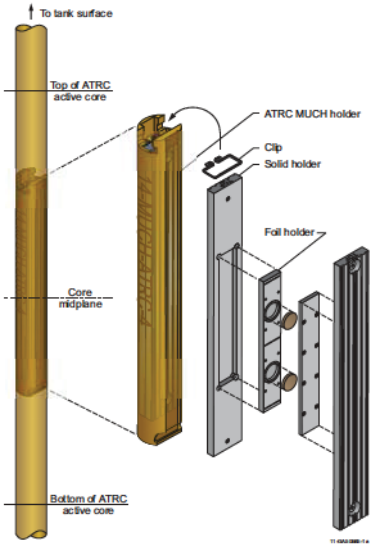

Figure 5-56. Activation detector apparatus for the ATRC SE SIPT.

ATRC flux wire evaluations were completed for balanced critical shim positions at 600 watts. Twenty minute ATRC reactor runs, each at a power in the range of 120 watts average power per lobe (600 watts total core power), were required to complete a set of activation measurements. After irradiation, all foils and wires were transferred to the collocated at the INL Radiation Measurements Laboratory for detailed radiation counting to obtain the data required for final analysis. Results from this effort are documented in Reference 178.

5.5.2. Vanadium Capsules for Encapsulation of Flux Wires for ATR Applications

In response to ATR NSUF experimenter needs, the HTTL developed in-house encapsulation processes using vanadium capsules for iron flux wire monitors. Although a range of geometries are possible, the flux monitor capsules were constructed to fit within a 7.6 mm length and 1.7 mm diameter envelope. Specialized equipment available at the HTTL is used to fabricate and inspect these vanadium capsules. Capsules are constructed from vanadium tubing and rod material. Using a laser welder, the iron wires are encapsulated in the vanadium tubes in an inert atmosphere, typically helium or argon, to avoid oxidation or corrosion issues while under irradiation in ATR experiments. In addition, the capsules are appropriately identified and numbered using a laser marker (see Figure 5-57). A radiograph of a vanadium capsule with iron wire is shown in Figure 5-57. X-ray inspection is used during development to optimize the laser welding parameters and to measure critical dimensions such as wall thickness, iron wire placement, and laser weld penetration. These vanadium encapsulation processes are also used to encapsulate melt wires (Section 5.1.1) or other components as ATR experimental needs arise.

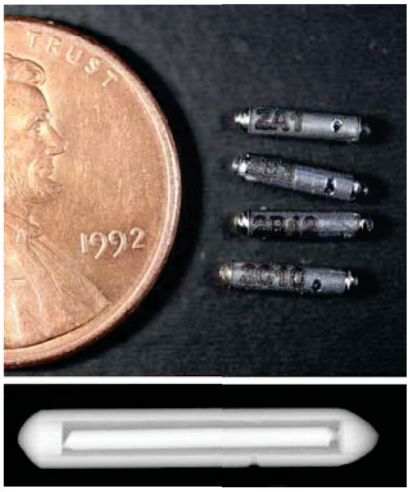

Figure 5-57. INL-encapsulated iron flux wires with radiograph for EPRI irradiation.

5.5.3. Real-time Flux Detectors for ATRC Evaluations

As indicated in Table 5-8, several types of real-time detectors were identified for the ISU/INL/CEA ATR NSUF effort and follow-on ATR NSUF ATRC evaluations. During FY13, this project compared the accuracy, response time, and long duration performance of several real-time flux sensors (see Figure 5-58), including CEA-developed miniature fission chambers, specialized SPNDs developed by the Argentinean National Energy Commission (CNEA), and specially-developed commercial SPNDs.[175 through 177] In addition, FY14 ATR NSUF funding will be used to evaluate real-time flux detector response and accuracy

using back-to-back (BTB) fission chambers[1] developed by ANL for the Zero Power Physics Reactor (ZPPR) programs.

Table 5-8. Real time flux detectors evaluated in ISU/INL/CEA ATRC evaluations.

Detector	Characteristics of Interest			
SPNDs	Emitter	Lead Wires	Insulation	Sheath (Collector)
Hafnium (commercial) Response: Fast Sensitivity: 4.7e-21 A/nv	Hafnium (minimum 97.5% with up to 2.5% Zirconium)	Inconel 600	Al_2O_3 (99.65%)	Inconel 600
Gadolinium: Response: Fast Sensitivity: 5.0e-22A/nv	Gadolinium (99.7%)	Inconel 600	Al_2O_3 (99.65%)	Inconel 600
Rhodium (CNEA) Response: Delayed Sensitivity: ~1e-21 A/nv	Rhodium	Copper	Acrylic	SS-304
CEA Miniature Fission Chambers	Fissile Deposit	Anode/Fill Gas	Cathode/Fill Gas	Extension Cable
Miniature Thermal-fission Chamber	Deposit on anode: U-235: 98.500% U-234: 0.063% U-236: 0.038% U-238: 1.409%	SS304L (impurities of Cobalt 0.02%) Fill Gas: Argon+ 4% Nitrogen	SS347(impurities of Cobalt 0.2%) Fill Gas: Argon+ 4% Nitrogen	Sheath: SS304L Insulation: SiO_2 (>99.5%) Wires: Copper (impurities of Zirconium 0.19%) Shield: Copper
Miniature Fast-fission Chamber	Deposit on cathode: U-238: 99.9640% U-235: 0.0354% U-234: 0.0003%	SS316L Fill Gas: Argon	Material: SS316L ID: 6.3 mm OD: 8 mm Length: 33.5 mm Fill Gas: Argon	Sheath: PVC Insulation: polyethylene (PE) Wires: copper clad steel (CCS)

5.5.3.1. SPNDs

SPNDs have been used effectively as in-core flux monitors for decades in commercial nuclear power reactors and MTRs world-wide. SPNDs rely on interactions of neutrons and atomic nuclei to produce a measurable current which is proportional to the neutron flux. Compared to other in-core detectors, they feature several advantages:

- Power supply not required
- Simple and robust structure
- Relatively small physical size
- Good stability at elevated temperature and pressure
- Generate reproducible linear signals
- Low burn-up rate (dependent on emitter material).

However, there are also some disadvantages associated with SPNDs:

- Limited operating range due to relatively low neutron sensitivity.
- Limited to thermal flux detection.

1. BTB fission chambers are often called 2π fission chambers because they are designed to count almost all fission fragments emitting from a thin deposit in a 2π solid angle.

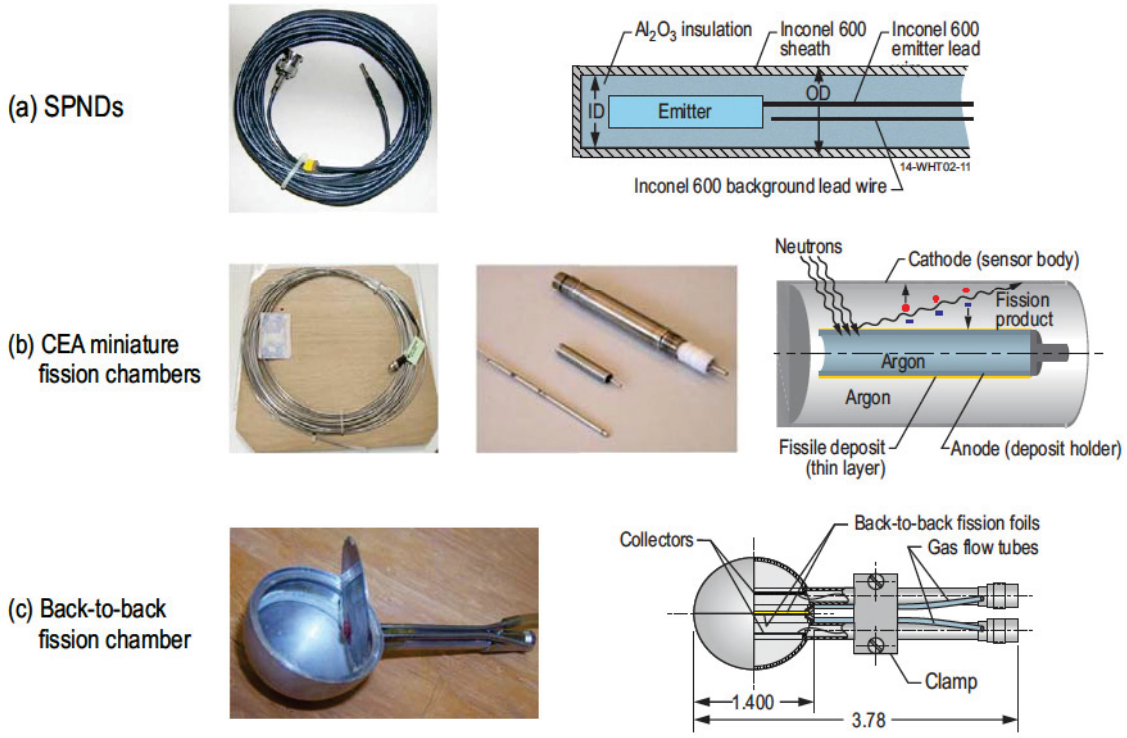

Figure 5-58. Representative real-time flux sensors evaluated at ATRC facility.

- Require background noise compensation (for some emitters).
- Delayed signal response (for some emitters).

A typical SPND consists of a coaxial cable containing an inner electrode (the emitter) surrounded by insulation and an outer electrode (the collector). In an "integral SPND," the lead cable and detector are mated directly to each other; the insulation of both sections are identical; and the collector of the detector section is also the outer sheath of the lead cable section, as shown in Figure 5-58a. Modular SPND assemblies are made from separate detector and lead cable sections. Typically, SPND characteristics of interest include size, material compatibility at high temperatures, sensitivity, response time, and burn-up rate. Characteristics of SPNDs evaluated in the ISU/INL/CEA ATR NSUF project are listed in Table 5-8.

5.5.3.2. Miniature Fission Chambers

Fission chambers (see Figure 5-58b), which are ion chambers with a fissionable material deposit on the inner wall, offer another method for real-time flux measurement. The fission fragments provide a very large pulse from the neutron-induced reaction and can be used in either pulse or direct-current mode. Normally highly-enriched ^{235}U is used for the coating, which makes the chamber sensitive to thermal neutrons. However, other deposits, such as ^{238}U, ^{242}Pu, or ^{232}Th, can be used to make the chamber sensitive to fast neutrons.

Characteristics of the miniature fission chambers included in these ATRC evaluations are listed in Table 5-8. Miniature fission chambers are used in pulse mode. Uranium coating masses were chosen in order to provide a high fission rate in ATRC flux (from 10^3 to 10^5 cps).

5.5.3.3. Real Time Flux Detector Testing at ATRC

Specialized fixturing was designed, fabricated, and installed for evaluating real-time flux detectors in the ATRC. As shown in Figure 5-59, real-time flux detectors (e.g., SPNDs and fission chambers) were inserted into the six ATRC N-16 positions using specially-designed Experiment Guide Tubes (EGTs) that attached to the reactor bridge. The six EGTs mechanically position detectors at a specified vertical location in the four N-16 exterior positions and two Center Flux Trap N-16 positions. Position control and detector response are controlled and measured via specially-developed software to allow all detectors to either individually or simultaneously move and measure the local neutron flux and provide a three-dimensional measurement of the overall neutron flux.

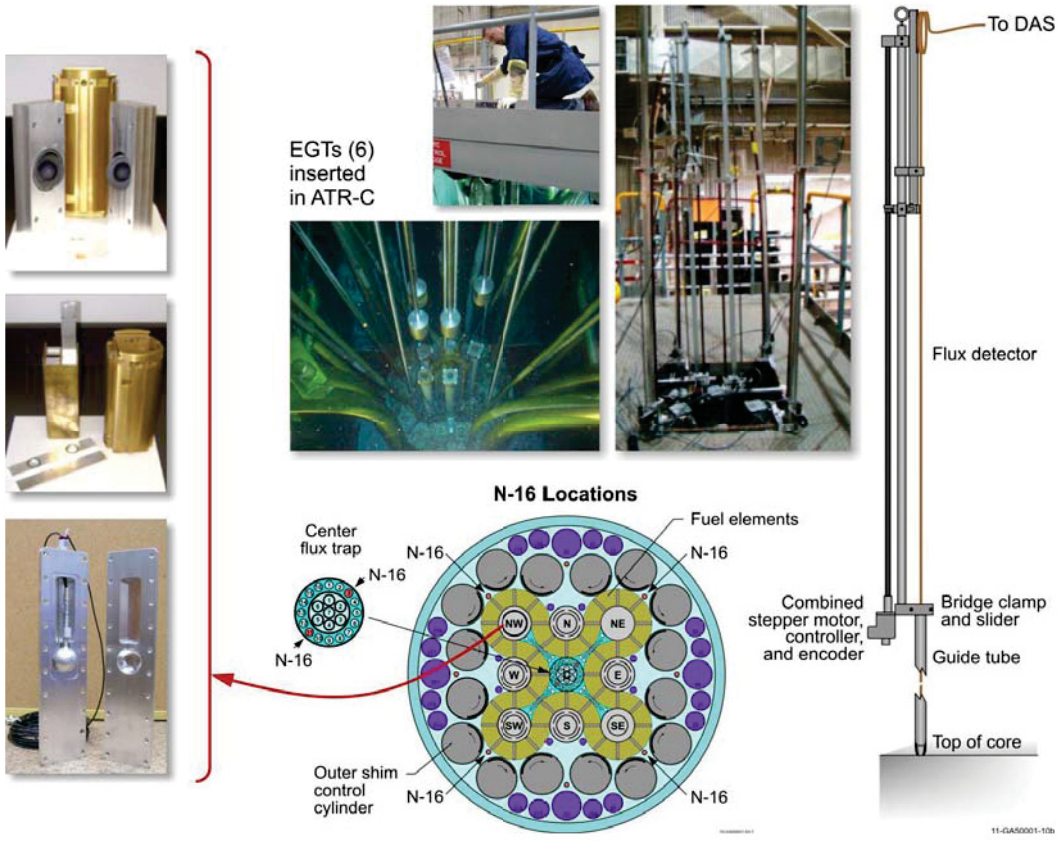

Figure 5-59. Various experimental hardware for testing real-time flux sensors in ATRC

In these evaluations, detectors were encased in tinted Lucite tubes to prevent any unwanted leakage of component materials (if they are not leak-tight) and to reduce unwanted noise produced when the SPND cables come in contact with metal surfaces. SPNDs were inserted into the ATRC N-16 positions using specially-designed experimental guide tubes (EGTs). The EGTs are primarily fabricated from aluminum to minimize their weight. However, selected components, such as the guide tube shown in Figure 5-59 are made from stainless steel 304 for additional robustness.

SPND and fission chamber evaluations were completed by inserting the detectors into various six N-16 positions and comparing the sensor response with each other and results from neutron activation

measurements. Tests were completed for three different critical configurations of the outer shim cylinders—balanced, unbalanced toward the NW flux trap, and unbalanced away from the NW flux trap. For each configuration, measurements were obtained for at least four intermediate power levels between 1 mW and 600 W. At 600 W, axial flux measurements were obtained by varying detector positions using the EGTs. These evaluations allowed the response and accuracy of each type of flux detector to be compared. The SPNDs displayed a current from 0.04 to 6 pico-amps. The fission chambers displayed electrical pulses that corresponded to count rates from 0 to $4x10^6$ counts per second. Unlike the delayed response from the SPNDs, the response from the fission chambers did not have delays built into their signals. In addition, the fission chambers responded instantaneously to reactor power changes; and the repeatability in the measurements was more consistent due to the faster signal response.

Representative results from one of the configurations evaluated are shown in Figure 5-60. Figure 5-60a compares detector data as a function of reactor power, and Figure 5-60b compares axial profile data obtained by moving the detectors with the EGTs. As shown in Figure 5-60a, the detectors demonstrated a linear response to reactor power changes; but each detector exhibited a different sensitivity and depending on core location, the slopes differed between the detectors in the north, south and center locations. This phenomenon was observed in all detectors. Hence, it is suspected that power in various core locations varies linearly with reactor power, but not equally with reactor power. Results from the evaluations are being assessed to determine the optimum sensor to measure regional core power in the ATRC and provide insights into a suitable system for the ATR.

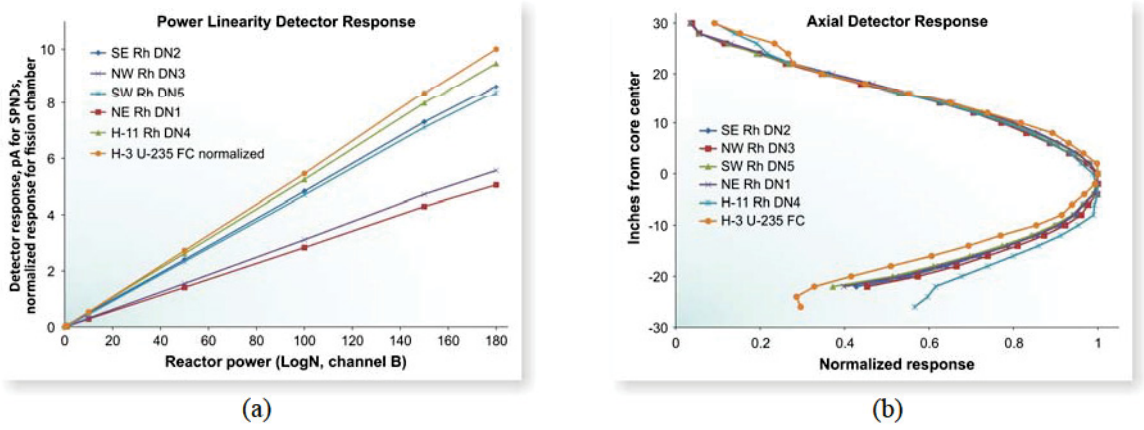

(a) (b)

Figure 5-60. Representative power linearity (a) and axial flux profile measurements (b) from rhodium SPNDs and a U-235 miniature fission chamber.

As shown in Figure 5-59, fixturing was also developed that allow simultaneous evaluations of two or more sensors in the NW LIPT. The specialized fixturing allows a BTB fission chamber to be inserted into the ATRC NW LIPT alongside other real-time flux detectors, such as SPNDs or the CEA fission chambers, to compare responses in nearly identical flux conditions. Another detector holder was also fabricated that positions three miniature in-core sensors across the NW LIPT for assessment of the flux gradient across the flux trap. It is planned that FY14 ATR NSUF funding will be used to perform detector evaluations with this new fixturing.

5.5.4. Real-time Flux Detectors in ATR NSUF Irradiations

Typically, ATR tests use flux wires and post-irradiation evaluations to detect the total fluence to which the fuel or sample was exposed. However, results from recent data to code evaluations suggest that there is uncertainty in current code evaluation predictions.[180] To reduce these uncertainties, ATR NSUF projects are emphasizing the use of real-time flux sensors, and a PSU-led ATR NSUF irradiation at the MITR will be deploying SPNDs. Details related to this irradiation are described in Section 5.7.1.

5.5.5. Micro-Pocket Fission Detector (MPFD) Development

The NEET program is funding a joint INL, Kansas State University (KSU), and CEA project to develop a MPFD. As noted in Section 3, miniature fission chambers and thermocouples have been used in-pile at research and test reactors throughout the world; however, none have been deployed in a single compact package to survive the harsh conditions that exist in high performance MTRs. The MPFD being developed in this effort is unlike typical fission chambers in that it has a very small detection area (~1 mm diameter), incorporates fast and thermal neutron detectors and a thermocouple within a single sensor (Figure 5-61). In addition, MPFDs are constructed from materials that are resistant to radiation damage. These qualities make the MPFD an attractive sensor for ATR users requiring real-time data from experiments.

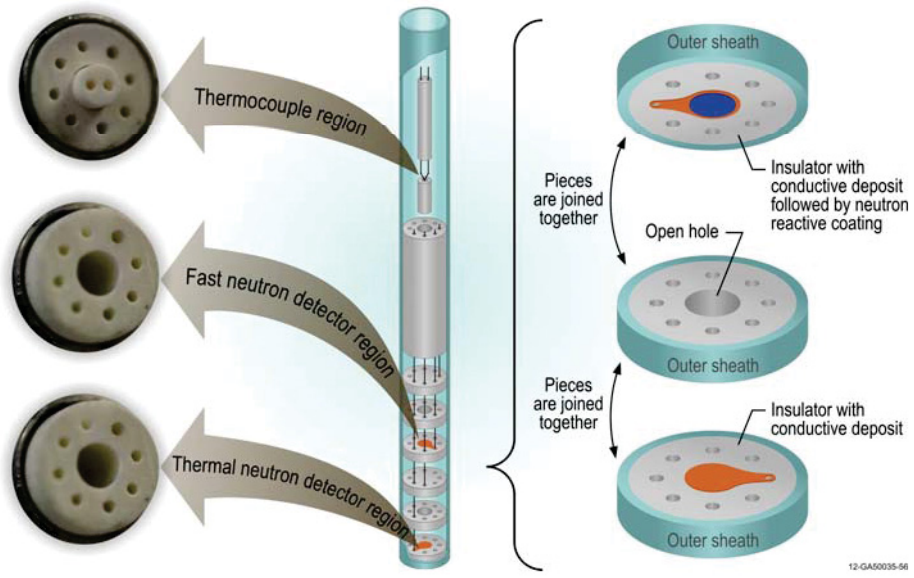

Figure 5-61. MPFD parts and exploded view.

Within the last decade, efforts were initiated by KSU to develop MPFDs. Initial evaluations to demonstrate the MPFD concept were performed at the KSU TRIGA reactor.[181-186] However, prior to deployment of MPFDs in a high pressure, high temperature, and high flux environment of a test reactor, such as the ATR, it was recognized that a more robust sensor design was required. The current effort is focussing on development, evaluation and deployment of a more robust MPFD design using fabrication techniques perfected by INL's HTTL staff during development of high temperature irradiation sensors (as described in this section) and expertise in miniature fission chamber design possessed by CEA.[187,188]

MPFDs are uniquely suited to address several challenges:

- Current fission chamber technologies do not offer the ability to measure fast flux, thermal flux and temperature within a single compact probe; MPFDs offer this option. The real-time, high accuracy data from a MPFD will significantly enhance various development and qualification efforts and new multi-physics code validation efforts.
- MPFD construction is very different then current fission chamber construction; the use of high temperature materials allow MPFDs to be specifically tailored to survive harsh conditions encountered in the core of high performance MTRs.
- New high-fidelity reactor physics codes will need a small, accurate, multipurpose in-pile sensor to validate the codes without perturbing the validation experiment; MPFDs fill this requirement.
- MPFDs can be tailored with variable sensitivities, allowing them to survive the lifetime of various experiment or fuel assemblies in a range of MTRs.
- The small size of the MPFDs allows multiple sensors to be deployed to accurately visualize the flux and temperature profiles in the reactor.

The MPFD project consists of two research tasks. The objective for the first task is to develop an enhanced MPFD design and prototype and test its performance in a laboratory setting, while the objective for the second task is to construct an enhanced MPFD prototype with fissile deposits and evaluate it in reactor facilities. It is currently anticipated that MFPD development and evaluation tasks will be completed in FY14. Work during the first two years of this three year effort was devoted to enhancing the MPFD design to accommodate TCs and improve robustness for high temperature, high pressure, high flux, long-duration ATR applications. Readout electronics have been built at KSU, and prototype fabrication is underway.

5.5.5.1. Design

Fission chambers (see Figure 5-58b) are typically constructed with two coaxial cylindrical electrodes, one of which has a fissile material deposit that is sensitive to neutron interactions. The gap between the electrodes is filled with a gas, typically argon; and a voltage potential is applied between the electrodes. After a neutron interacts with the fissile material, a fission product is ejected into the gas, and a large number of charge pairs are created in the device. These charges are separated and collected at their respective electrode which leads to a current pulse being generated.[189]

MPFDs utilize the same concept, but with a different geometry (see Figure 5-62) that uses parallel plate electrodes instead of coaxial cylinders. This design is known as a parallel plate fission chamber. However, the MPFD design is set apart from other fission chamber designs because their signal is obtained by capturing only part of the available fission product energy deposition whereas all of the energy deposition must be captured in a classical fission chamber. This departure from conventional fission chamber design and operating characteristics allows the MPFDs to have a much smaller chamber size with a much lower fill gas pressure. The design has excellent discrimination characteristics because the energy deposited by the fission products is much greater then that of other types of background radiation interactions in the detector. As another added benefit, the small size allows them to have a faster response time, and thus have the potential to achieve higher count rates then conventional fission chamber designs. As such, MPFDs offer the potential for in-pile applications and for instrumenting the fuel itself.

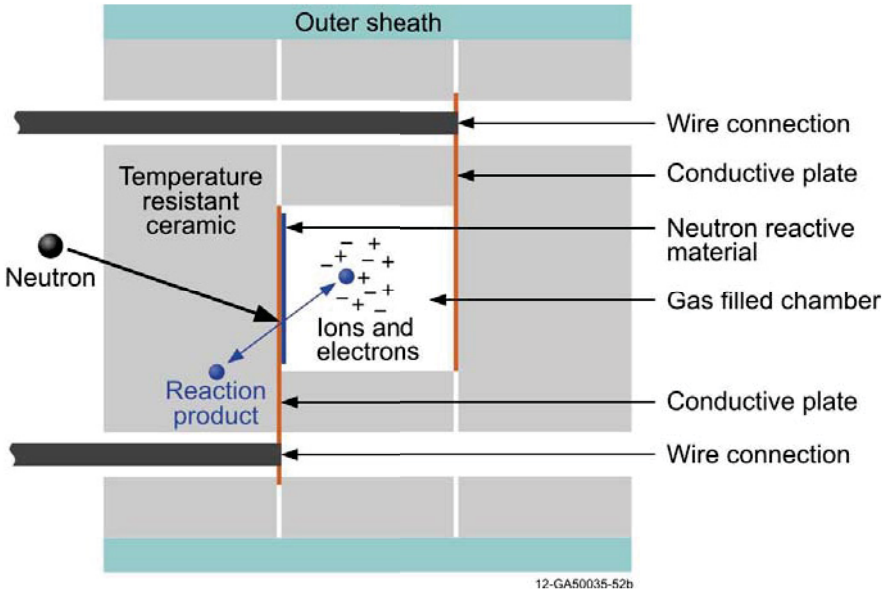

Figure 5-62. Schematic diagram of MPFD fission chamber operation.

5.5.5.2. KSU Activities

KSU experience in fabricating and evaluating the initial MPFD prototypes is beneficial for producing an updated version of MPFDs. The KSU effort for supporting the current NEET MPFD enhancement project includes two tasks: Task 1 - building, testing, and optimizing detector amplifier boards for the new design; and Task 2 - upgrading the fissile deposition system, and purchasing the required raw materials for detector substrate fabrication.

The first task includes activities to develop electronics for the new MPFD design (Figure 5-63). Electronics used in initial MPFD tests suffered from high-frequency noise being passed between channels through a shared high voltage line between several detectors. To avoid this problem with the enhanced MPFD design, the high voltage lines on the amplifier board were separated using low-pass filters. The new amplifier board is powered by ±12V and +5V and incorporates 5V logic signals outputting two channels of analog pulse, analog current and digital timing, that can each output, with 50 Ohm impedance. A prototype amplifier has been assembled at the KSU Electronics Design Laboratory (EDL).[190] After initial testing at EDL was complete, the amplifiers were connected to an older fission chamber installed in the KSU TRIGA Mark II nuclear reactor[191] and demonstrated to verify the amplifier would capture neutron induced pulses. The amplifier captures the expected pulses as shown in Figure 5-63. However, it is recognized that some component values on the amplifier board may require a minor adjustment to match the capacitance of the new MPFD design. These changes will be made when the new MPFDs are assembled and tested for capacitance.

KSU's second task focused on developing an enhanced plating system for deposition of the electrical contacts and fissile material on the MPFDs. The KSU Semiconductor Materials and Radiological Technologies (SMART) Laboratory[192] is responsible for plating all coatings required for MPFD construction. Two plating steps are required; the first step is to plate the electrical contacts or electrodes on the alumina substrates. The second plating step is to deposit the fissile material on one of the electrical contacts.

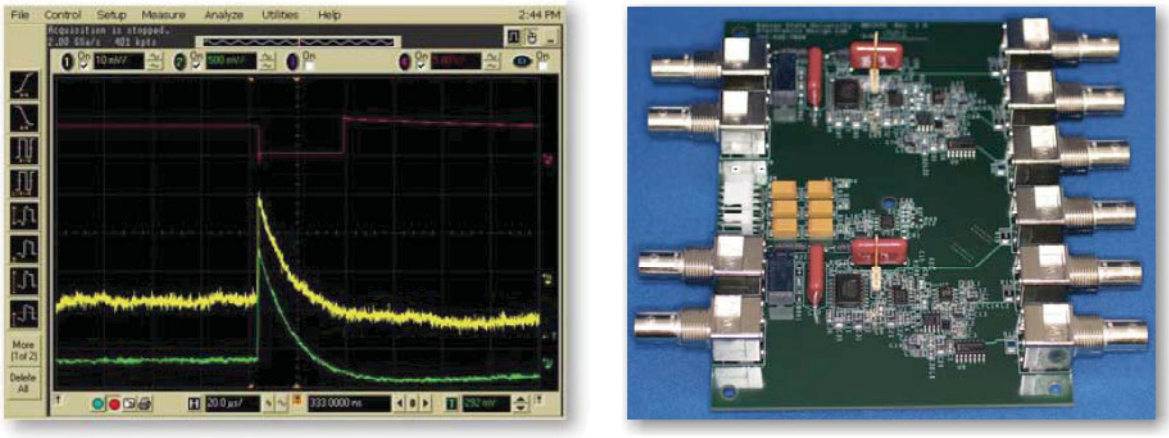

(a) (b)

Figure 5-63. KSU-designed electronics: (a) Neutron induced pulses from MPFD electronics and (b) amplifier board.

The initial plating to deposit the electrical contacts is performed using an electron-beam evaporator (Figure 5-64). The plating requires custom shadow masks for the new design of MPFDs to be machined using a micro-milling machine at KSU. The purpose of the shadow masks is to selectively deposit the contact material that defines the electrical contacts and wire-bonding pad. Titanium and platinum were explored as possible contact materials; and platinum provided the best contact.

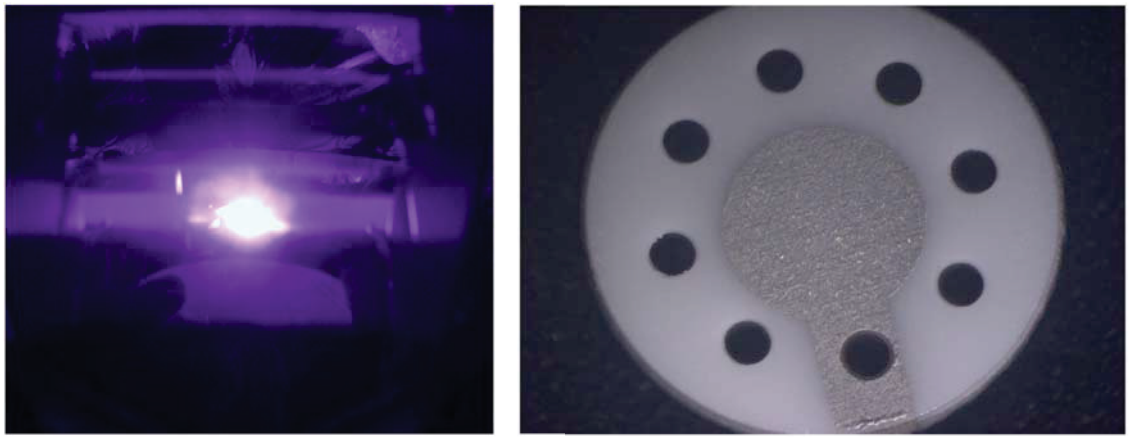

Figure 5-64. Evaporator and sample at the KSU SMART Laboratory.

Initial electrical contact deposition efforts were successful. However, initial evaluations found that many of the alumina substrates were cracked between the outer wiring holes and would lead to poor detector electrodes. These cracks were attributed to the manufacturing process required to harden the alumina, and a different vendor was located to provide alumina substrates that had smoother surfaces without any cracks. In addition, contact deposition quality has greatly improved due to characterization activities using an optical profilometer, x-ray fluorescence analyzer, and electrochemical analyzer.

Once the electrical contacts are in place, a second plating step is needed to deposit the material (uranium-235 for thermal neutron detection and thorium-232 for fast neutron detection). Two methods for fissile material deposition were investigated. The first method was standard electroplating, which was used with previous designs of MPFDs. The small substrates and thin depositions utilize a specialized nA-current micro-electroplating system at KSU. The second method utilized electroless plating that does not require an electric current to be applied to the plating solution. Both methods require a dissolvable resin to be applied to select locations of the electrical contact to avoid fissile material from plating on the wire-bond pad and path of the detector. Evaluations completed in FY13 using the electroless plating method worked but did not deposit the required amount of material on the detector. Hence, the standard micro-electroplating method was chosen for future depositions. Investigations to develop and characterize a robust electrical contact with a fissile material deposition will be completed in FY14.

5.5.5.3. INL Activities

During FY12 and FY13, INL developed a new MPFD design (see Figure 5-61) and procured the materials needed for construction of MPFD prototypes. Initial evaluations are focused on building a robust prototype using less expensive, commercially-available materials that are expected to survive temperatures up to 600 °C. Once fabrication and testing of this MPFD is completed, it will be possible to modify this design for higher temperature applications by substituting more expensive, higher temperature materials.

The main components of the initial MPFD detector and extension cable are specially manufactured hard-fired alumina substrates and crushable alumina insulators (Figure 5-65), respectively, all housed within leak-tight stainless steel tubing. A "loose assembly construction" is used, with a rigid stainless steel tube containing hard-fired alumina substrates for fission chamber electrodes and fissile depositions, a thermocouple, and wire contacts. The crushable alumina insulators serve as an insulator for the 6 wire extension cable with a stainless steel outer sheath. The extension assembly is drawn to the desired length and diameter to provide flexibility for installation.

MPFD construction is underway using equipment and techniques perfected by INL's HTTL staff. The unique design of the MPFD requires several construction steps that aren't required for conventional in-pile sensor fabrication. Specifically, specialized techniques have been developed that emphasize robustness (e.g., minimizing the number of wire splices and component embrittlement associated with welding). Figure 5-66 shows some of the specialized HTTL equipment used in MPFD fabrication. After the parts are assembled, they are inserted into the outer sheath, and welded together (Figure 5-65). The final step to insert the fill gas, typically argon, is performed by sealing a portion of the loose assembly in specialized fixturing at the HTTL prior to performing the final weld.

Testing of the new MPFD design is underway to evaluate the robustness of the epoxy wire connections, thermocouple performance, and the weld integrity. Sensor performance is assessed in the HTTL by considering materials interactions and thermocouple response in HTTL furnaces, x-ray observations, helium leak checks, and resistance and continuity measurements. Weld integrity is evaluated by using the HTTL helium leak testing equipment to verify that the assembly meets requirements for the ASTM leak rate of sheathed thermocouples. Further evaluations are scheduled that will test the integrity of the electrode (non-fissile) deposition under high temperatures once materials are received from KSU. In addition, efforts have been initiated to develop an evaluation plan to test the MPFD performance in radiation fields. Depending on funding and facility availability, the evaluation plan may include the INL Health Physics Instrument Laboratory (HPIL) neutron and gamma panoramic irradiators (see Figure 5-67b), the KSU 1

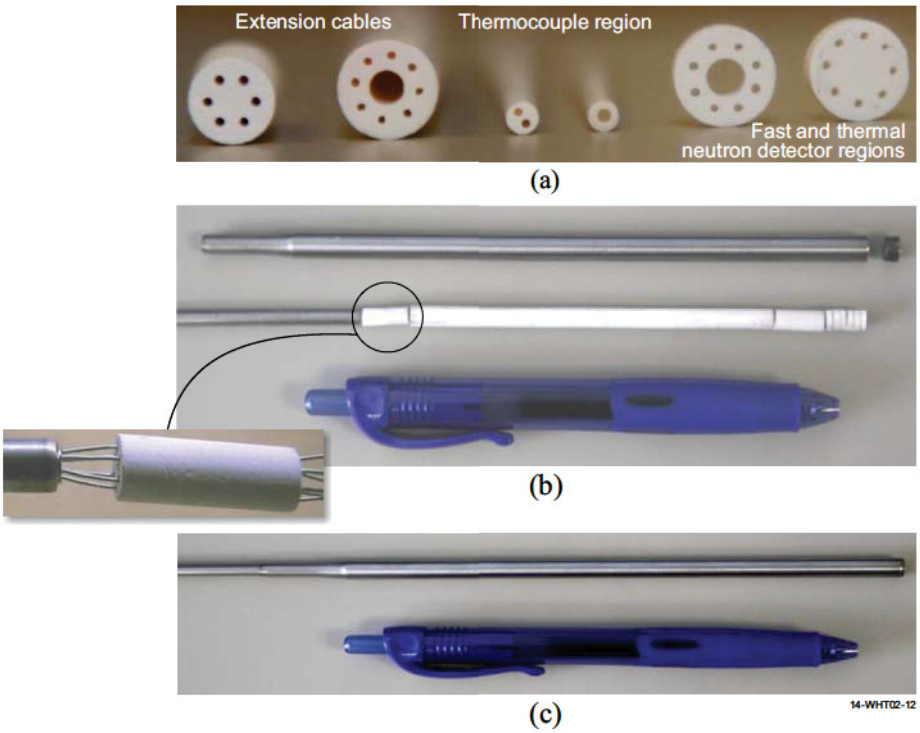

Figure 5-65. MPFD components and fabrication.

Figure 5-66. Various HTTL equipment for MPFD fabrication.

MW TRIGA Mark II research reactor, and INL's ATRC using specialized fixturing installed at the ATRC shown in Figure 5-67a. As discussed in Section 5.5.3, the ATRC fixturing is used to characterize and cross-calibrate a wide range of flux detectors, including SPNDs, CEA-developed fission chambers, and specially-developed back to back fission chambers. In addition, CEA has agreed to model MPFD response and compare to actual results. Although it is not part of the currently-funded NEET program, it is anticipated that the ATR NSUF or another DOE-NE program will ultimately deploy a MPFD in a higher flux reactor irradiation test in a US high flux MTR.

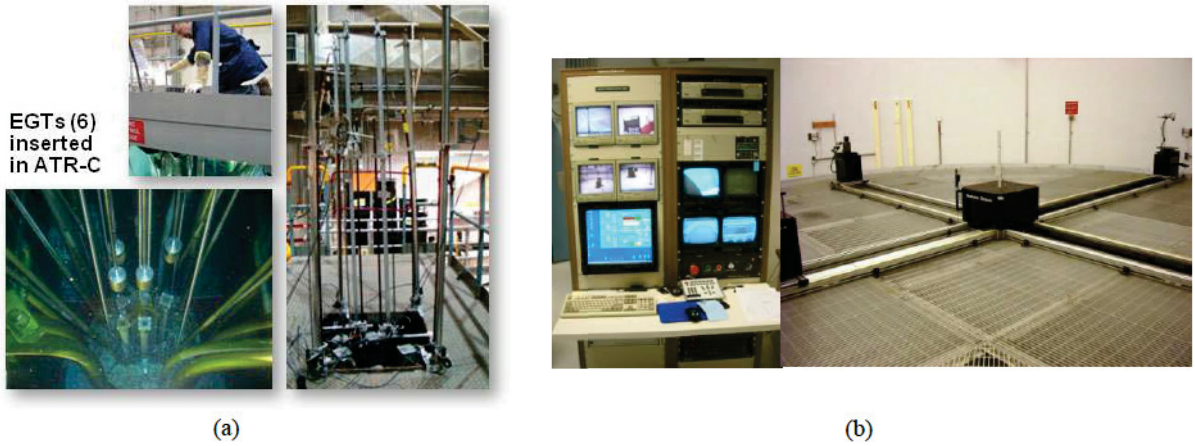

(a) (b)

Figure 5-67. INL irradiation facilities for MPFD evaluation: (a) ATRC and (b) HPIL panoramic irradiator.

5.6. Localized Heating

ATR NSUF experimenters have expressed a need for sensors to measure local power in fuels and materials irradiations. Development of instrumentation that provides real-time localized power measurements with high precision and accuracy is needed to address uncertainties related to gamma heating in ATR NSUF MTR experiments. Large uncertainties in gamma heating are suspected to have caused significant errors in the estimated temperature of test specimens in ATR.[193] Calculated temperatures versus measured temperatures for the University of California at Santa Barbara Number 2 experiment differed by up to ±30°C, as shown in Figure 5-68. Development of improved local power instrumentation will provide enhanced capabilities to customers that want to irradiate fuels or materials in the ATR or other ATR NSUF MTRs. Hence, investigations of local power instruments directly addresses the need to supply ATR NSUF programs with advanced sensors that provide real-time data, with high precision and accuracy, for materials and fuels testing.

Initial HTTL studies of commercially-available local power sensors have identified several improvements that could be incorporated into the design of localized power sensors. Two sensors have been selected as viable options for further evaluation and development. These two devices are gamma thermometers and Self-Powered Gamma Detectors (SPGDs). These sensors measure local power via interactions with gamma rays that are generated from nuclear reactions within the reactor. Progress and plans for future evaluations are provided in this section. However, it should be noted that funding sources for all of these sorely needed evaluations have NOT been identified.

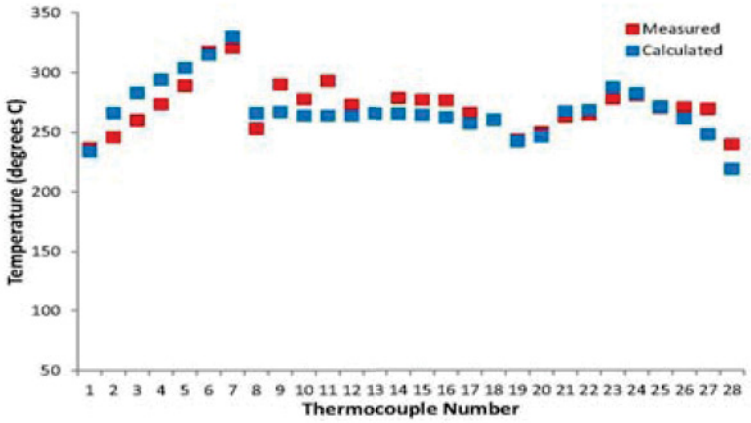

Figure 5-68. Measured versus calculated temperatures for the UCSB-2 experiment1

5.6.1. Gamma Thermometer Design and Evaluations

As discussed in Section 3.3.8, current state-of-the-art gamma thermometers use low temperature (e.g., less than 1100 °C) Type-K thermocouples to measure the differential temperature along an inner body or pin.[193] The technology from the HTTL-developed HTIR-TC could be used to develop a high temperature gamma thermometer. This technology will broaden the range of local power measurements to include high temperature applications. If feasible, this improvement to the current technology could provide fuels and materials test programs with a versatile and reliable sensor for measuring local power over an expanded range of temperatures.

Figure 5-69 shows an IFE/HRP miniaturized gamma thermometer delivered to the HTTL with a schematic that illustrates the internal components compared to an x-ray of the detector. Time constant measurements of the IFE/HRP gamma thermometer (see Figure 5-70) were completed in FY12.

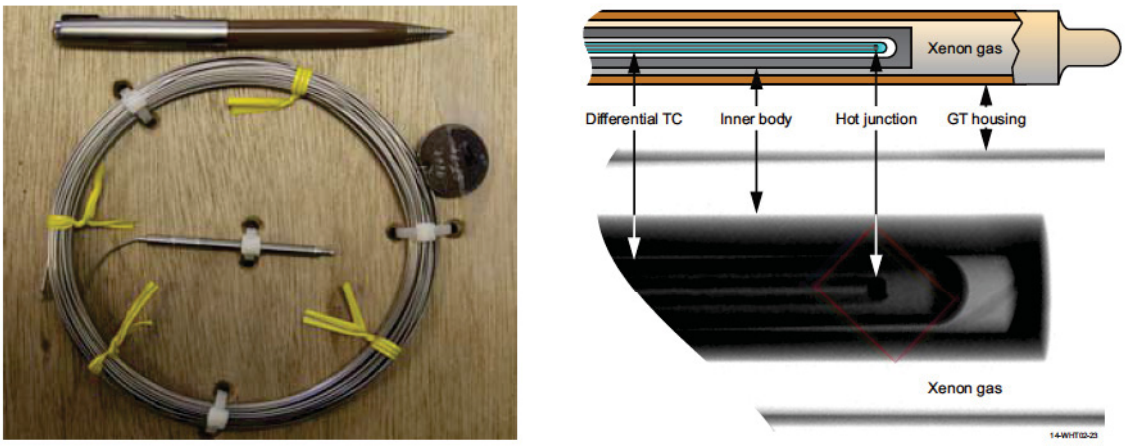

Figure 5-69. IFE/HRP gamma thermometer and associated x-ray of the device.

The data shown in Figure 5-70 were gathered by moving the gamma thermometer between an ice bath and boiling water. After the signal stabilizes in one medium, it is transferred to the other. The change in the

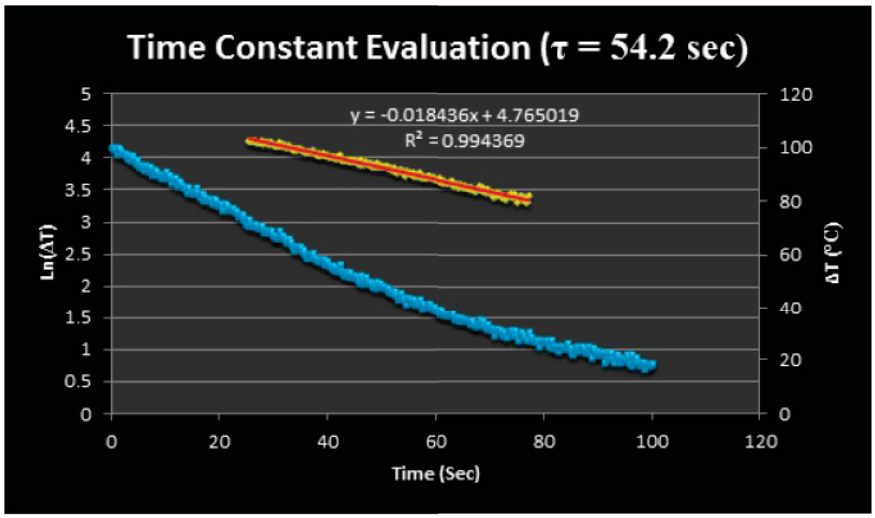

Figure 5-70. Time constant measurement of the IFE/HRP gamma thermometer.

signal is logged until a new equilibrium is reached. The data are then analyzed, and the time constant can be determined from the following relationship (e.g., time constant is calculated from the inverse of the slope when the data is on a logarithmic scale):

$$T = T_0 e^{-\frac{t}{\tau}} \tag{5-4}$$

where

T = temperature,
T_0 = initial temperature,
t = time, and
τ = time constant.

Testing at the gamma irradiation facility at the Health Physics Instrumentation Laboratory (HPIL) was performed to acquire data on the sensitivity of the IFE/HRP gamma thermometer in a known gamma flux. If additional funding becomes available, additional testing of this IFE/HRP gamma thermometer will be completed. The signal response and sensitivity will be evaluated in a series of tests at various facilities. The first phase of testing includes testing the gamma thermometer in a higher flux environment, such as the ATR Canal Irradiation Facility. Next the new fixtures used to evaluate flux detectors in the ATRC (see Section 5.5.3.3) will be used to test the IFE/HRP gamma thermometer. The next step will be to irradiate the gamma thermometer at a university TRIGA reactor. Results from these evaluations will provide insights related to IFE/HRP gamma thermometer operation and design, and the applicability of proposed enhancements for developing an optimized design.

5.6.2. SPGD Design and Evaluation

As discussed in Section 5.5.3, SPNDs measure neutron flux based on the activation and subsequent beta-decay of the emitter material. SPGDs measure gamma flux based on gamma-ray interactions with

matter, specifically, the photoelectric effect, Compton scattering, and pair production. As shown in Figure 5-71, an emitter material is surrounded by an insulator and encased in a conductive housing. Gammas interact with the emitter, and to some extent the insulator, generating free electrons. Those electrons will accumulate on the housing and an electric potential will develop between the housing and the emitter resulting in a measurable current.

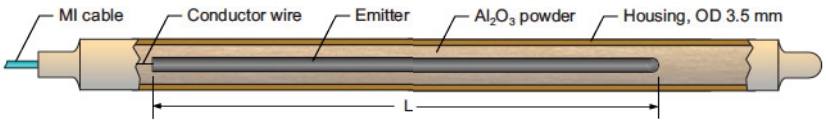

Figure 5-71. General design of a Self Powered Gamma Detector (SPGD)

A plethora of materials have been tested to determine their applicability for self powered detectors.[194] It is known that a portion of the total response associated with an SPND is due to gamma interactions rather than neutron reactions. Some materials will have a higher response from gamma interactions than others based on the relative magnitudes of the neutron cross-section and the gamma attenuation coefficient of the material. Approximately 93% of the response of platinum SPNDs is actually due to gamma interactions.[194] Typically, materials with a high atomic number have high attenuation coefficients and are considered favorable for emitters in SPGDs. Lead and bismuth are common emitter materials in modern SPGDs. Similar to gamma thermometer operation, SPGDs measure local power based on gamma interactions. Therefore, the signal SPGDs produce is constant with fuel burnup as well. This is one of the main advantages to using local power sensors that respond to gamma interactions rather than neutron interactions. If funding is available, enhancements to the current state of SPGD technology will be investigated. In particular, candidate SPGD enhancements include: size reduction, material selection, optimal geometry, and gamma response versus neutron response of select materials.

As part of these evaluations, it is planned to compare and contrast the advantages and disadvantages of SPGDs in relation to gamma thermometers. An ATR NSUF experiment testing HTTL-developed sensors in the MITR will be using a SPGD (Platinum emitter) supplied by Thermocoax to monitor gamma flux (see Section 3.1.2). As part of this proposed effort, a similar SPGD will be evaluated to determine standard operating characteristics of SPGDs. Testing of the SPGD will follow a similar regiment used for the gamma thermometer. Specifically, the sensitivity of the SPGD will be evaluated in the HPIL Gamma Irradiation Facility and the ATR Canal Irradiation Facility. Next, testing in a reactor environment will be pursued in the ATRC and a university TRIGA reactor. Results of these tests will be used for further evaluation of the SPGD, including investigation of emitter materials to determine optimal characteristics for typical applications in ATR. Specifically, the gamma response versus the neutron response will be characterized along with evaluation of the operating temperature of the sensor. Since lead and bismuth have relatively low melting temperatures, other materials may be beneficial as emitters for higher temperature applications; and evaluation and testing of those materials will be pursued.

5.7. Cross-Cutting

Some research activities benefit multiple in-pile instrumentation development and deployment activities. Three such cross-cutting activities are documented in this section: a recently initiated effort to compare the irradiation performance of ultrasonic transducer materials, a proposed effort to compare the irradiation performance of fiber optics, and a much needed joint industry and laboratory effort to develop

an instrumented standardized test rig for fuels evaluations. As discussed below, results from the two irradiation tests have the potential to enable the use of a host of new sensors to support irradiation testing. The instrumented standardized fuel test rig development effort is required if the ATR is to meet US industry needs for fuel irradiations.

5.7.1. Ultrasonic Transducer Irradiation

The long and successful history of out-of-pile ultrasonic measurements suggest that ultrasonics-based sensors could be used in-pile for materials and fuels characterization, including detection and characterization of degradation and damage.[198] Limited PIEs have successfully shown that fuel microstructural parameters, such as porosity and grain size, can be correlated to ultrasonic velocity.[199] According to Villard,[200] frequency requirements for such measurements are restricted to greater than 10 MHz. However, lower frequencies can be used for some applications, such as ultrasonic thermometry, where frequency requirements may be 100 – 150 kHz or lower.[201]

The development of ultrasonic tools to perform a variety of in-pile measurements requires a fundamental understanding of the behavior of ultrasonic transducer materials in high-radiation environments. While a number of irradiation studies of ultrasonic transducers have been described in the literature, a one-to-one comparison of these studies is difficult, as the materials and irradiation test conditions often differ. In addition, the tests to date are generally at lower flux/fluences than what might be seen in US MTRs. As a result, a series of experiments is needed to baseline the performance of ultrasonic transducer materials (in terms of change in sensitivity as a function of temperature and irradiation) to support the irradiation test. Results of such tests will enable development of ultrasonic sensors for in-pile measurements, including fuel and material morphology changes, fission gas composition and pressure measurements, fuel and material geometry changes, and temperature. Hence, such tests will provide a method for selecting optimum ultrasonic transducer materials for different in-pile measurements and guide the development of signal processing tools to enhance the measurement to demonstrate the intended in-pile measurements.

During 2012, the ATR NSUF announced that funding will be provided to support a PSU-led collaboration with INL, MIT, Argonne National Laboratory, Pacific Northwest National Laboratory, CEA, and Bechtel Bettis to perform an ultrasonics transducer irradiation at the MITR[202] to evaluate the most promising candidate piezoelectric and magnetostrictive transducer materials and designs. From the onset of this effort, an instrumented lead test was proposed, such that real time signals are received from the transducers being tested. Collecting real time signals will enable an accurate measure of the performance and possible degradation of candidate transducer and sensor materials under irradiation. In addition, laboratory testing will be completed to verify that transducer materials will survive anticipated thermal conditions and to characterize their pre-irradiation performance. It should also be noted that DOE-NE's NEET program leverages results from this irradiation as part of its effort to enable deployment of ultrasound-based sensors.

5.7.1.1. Selected Ultrasonic Materials and Transducer Designs

To generate and receive ultrasonic pulses and signals, the two most commonly used methods rely on piezoelectric or magnetostrictive materials. Ultrasonic measurements using piezoelectric transducers have been demonstrated over a wide frequency range from kHz and up to GHz; however, most non-destructive examination (NDE), materials characterization, and process monitoring are performed in the range from

1-20 MHz, making piezoelectric transduction ideal. The current capabilities of magnetostrictive transducers are typically limited to operation at frequencies up to the order of 100 kHz, though recent research suggests that higher frequencies may be possible for small transducers. However, mechanical coupling as well as enhanced guided wave mode generation makes magnetostrictive transduction ideal for low frequency measurement, such as ultrasonic thermometry.[203]

Prior studies have shown that typical piezoelectric and magnetostrictive materials used in transducers degrade when subjected to high temperature and radiation.[204-209] Candidate magnetostrictive and piezoelectric materials must, therefore, be carefully selected; and transducer assemblies must be carefully designed. However, only limited radiation effects data are available to guide this process. FY-2013 efforts for this effort focused on developing and fabricating transducer designs developed and fabricated for the MITR irradiation. As summarized below, piezoelectric and magnetostrictive transducer designs were developed, successfully fabricated, and shipped to MIT.

Selected Piezoelectric Materials and Transducer Design. A literature review was completed at the beginning of this effort to identify candidate piezoelectric transducer materials. The piezoelectric materials selected for inclusion in the irradiation test are summarized in Table 5-9. Additional details related to candidate piezoelectric transducer materials may be found in References 210 and 211.

Table 5-9. Candidate piezoelectric materials.

Material	Composition	Transition Temperature, °C	Transition Type	Comments
Bismuth Titanate	Bi_3TiO_9, etc.	909	Curie Temperature	Thought to be radiation tolerant. Most promising previously tested candidate. Good baseline comparator.
Aluminum Nitride	AlN	2200	Melt	Thought to be highly radiation tolerant. Very high temperature capability.
Zinc Oxide	ZnO	>1500	Melt	Thought to be highly radiation tolerant. High temperature capability.

The piezoelectric transducers developed for this irradiation are based on the design used in a prior TRIGA test of AlN.[212] The piezoelectric transducers use pressure for coupling the piezoelectric element to the stainless steel waveguide. Electrical contact with the piezoelectric element is also achieved through application of pressure. A backing layer behind the piezoelectric sensor provides damping (preventing excessive "ringing" of the transducer) and acts as an electrode. The electrical connection from the lead-in cable to the graphite backing is made through a stainless steel plunger, which is isolated from the housing by alumina insulation. The connection to ground is made through the housing, with the waveguide acting as the second electrode. During the irradiation, transducer performance will be measured using pulse/echo measurements through the stainless steel waveguide. A schematic of the design is shown in Figure 5-72a.

Selected Magnetostrictive Materials and Transducer Design. A literature review was also completed at the beginning of this effort to identify candidate magnetostrictive transducer materials. The magnetostrictive materials selected for inclusion in the irradiation test are summarized in Table 5-10. Additional details related to candidate magnetostrictive transducer materials may be found in References 210 and 211.

The magnetostrictive design developed for this effort was influenced by prior research to develop an appropriate transducer for use in ultrasonic thermometry applications.[213-216] As discussed in Section 5.1.4.3, magnetostrictive transducer fabrication efforts were leveraged from FCRD-funded efforts to develop an ultrasonic thermometer. A schematic of the magnetostrictive transducer design is shown in Fig-

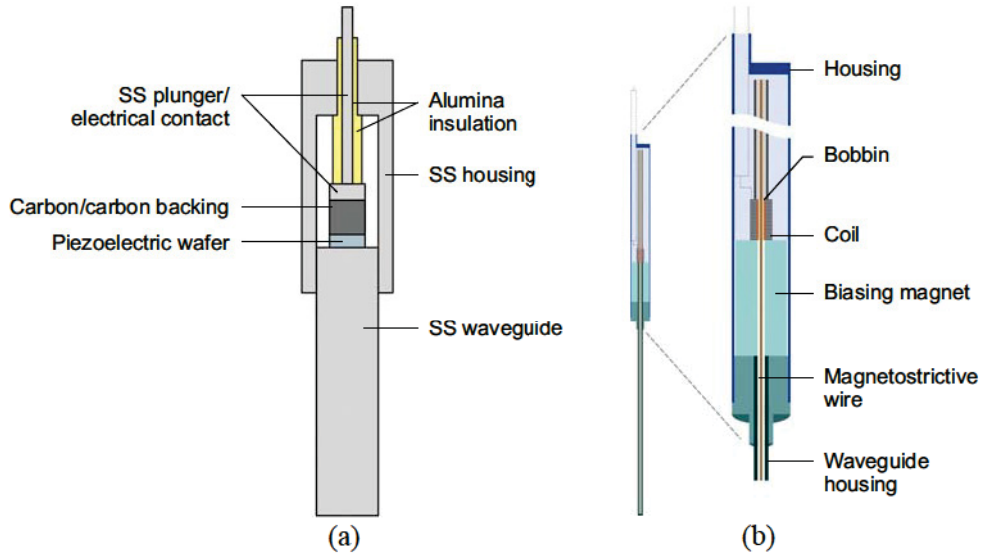

Figure 5-72. Schematic of (a) piezoelectric and (b) magnetostrictive transducer designs.

Table 5-10. Candidate magnetostrictive materials.

Material	Composition	Key Properties	Comments
Remendur	49Fe-49Co-2Va	70-100 μ-strain maximum magnetostriction, curie temperature 950 °C	No longer manufactured, identical/similar alloys available, possible activation of cobalt
Galfenol	Fe-14Ga-NbC	100-400 μ-strain maximum magnetostriction, curie temperature 700 °C	Relatively new, small amounts of data, difficult to acquire
Arnakrome 4	95Fe-5Cr	10-40 μ-strain maximum magnetostriction, curie temperature 770 °C	Low magnetostriction
Arnakrome 5	92Fe-8Mn	10-40 μ-strain maximum magnetostriction, curie temperature 770 °C	Low magnetostriction

ure 5-72b. Additional details related to the fabrication of the magnetostrictive transducer are provided in Section 5.1.4.3 and Reference 211.

Laboratory Evaluations of Candidate Transducer Materials. Several tests are being conducted in conjunction with the irradiation test (prior to the test being preferable, to allow identification of any systematic problems before the full test is installed in the reactor). These tests are needed to help separate the effects of the neutron radiation from effects of the elevated temperature the test will likely reach while in the reactor. A list of planned out-of-pile tests is given in Table 5-11.

5.7.1.2. ATR NSUF Ultrasonic Transducer Irradiation Test

Figure 5-73 shows the position of the test capsule within the MITR core. Based on thermal analysis performed at MIT, the expected operating temperature for the test at steady state will be between 350 and 450 °C. After startup, the target temperature will be controlled by variation of the composition of a gas gap between the test capsule and the in-pile experiment tube. The gas will be a mixture of helium and neon. Is is planned that the reactor will perform a slow startup ramp. This will enable data collection at low fluence levels, where early failures were observed in prior piezoelectric transducer irradiations. Once the reactor

Table 5-11. Proposed out-of-pile tests.

Test	Materials	Description
Endurance test (ET)	All candidate materials	The ET includes operation of candidate transducers at 300 °C. This test is to be used as reference for the data collected during the irradiation test. Two types of endurance tests can be performed, one at an elevated temperature relative to the nuclear reactor environmental conditions to accelerate the degradation process. The other is to be at the anticipated irradiation temperature of 300 °C. The time necessary for each of these tests is at least several weeks, if not for a month. The samples are to be inserted in the reactor for about a year, so a several month long test is proposed. This test will allow separation of temperature induced changes from radiation induced changes, as well as identification of design flaws.
Maximum operating temperature (MOT)	All candidate materials	The MOT is determined by placing the transducer in the tube furnace and increasing the temperature linearly at a slow rate so that at each measurement could be considered isothermal. In the past rates such as 1 degree per minute have been used. As such, the time necessary for each experiment will depend on the Curie temperature; on the order of 500-1000 minutes or 8-16 hours. This test will allow identification of possible temperature induced changes at temperatures near irradiation temperature, effects of temperature transients, and maximum operating temperature.
Saturation magnetostriction	All magnetostrictive candidate materials	This test involves measurement of magnetostriction of candidate materials as a function of applied DC magnetic field using a DC current supply and a pushrod dilatometer. These data are needed to characterize the performance of candidate magnetostrictive materials.
Hysteresis measurement	All candidate materials	The HM characterizes remnant polarization and indicates changes in material structure. This test can be performed with the transducer in situ and will be completed alongside the MOT and ET.

reaches a power level sufficient to maintain the target temperature, the experiment will be placed on automatic temperature control (helium/neon mix) for the remainder of reactor startup. The anticipated steady state fast flux (>1 MeV) will be 4 x 10^{13} n/cm^2-s with reactor at full power. This level of fast flux will require approximately 310 full power days, or 18 calender months, to reach the desired fluence level.

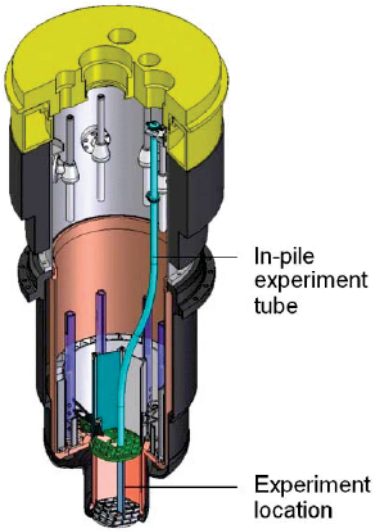

Figure 5-73. Position of irradiation capsule within MITR core.

Capsule Design. The final test capsule design is shown in Figure 5-74. The test capsule design was refined based on thermal analyses performed by MIT to ensure that irradiation temperatures remained between 350 and 450 °C. The final design accommodates four piezoelectric transducers and two magnetostrictive transducers. All of the originally selected transducer materials will still be included as loose samples, but only the ZnO transducer will have two transducers. All of the originally proposed instrumentation will also be included.

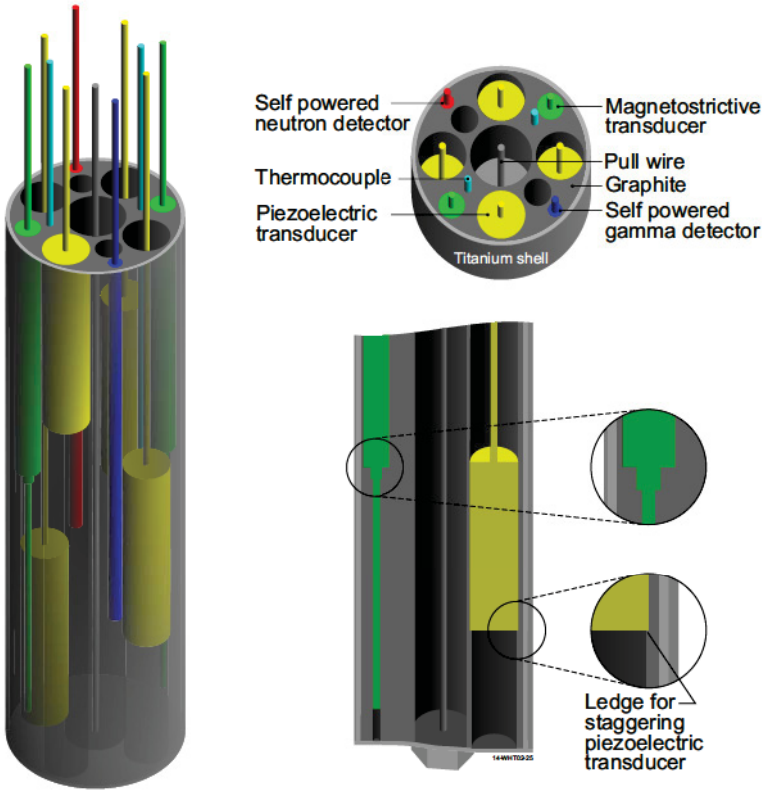

Figure 5-74. Final test capsule graphite sample holder design with sample and instrumentation positions detailed.

Sensors. In order to meet program objectives, it is essential that the irradiation environment be well-characterized. Irradiation test temperatures will be monitored by two Type-K thermocouples. Thermal neutron flux will be monitored by a vanadium emitter SPND. Gamma flux will be monitored by a platinum emitter SPGD. A schematic diagram of the SPND and SPGD is shown in Figure 5-75 (both sensors have identical dimensions).

In addition to the Type K thermocouples, the maximum temperature that the irradiation reaches will be verified using melt wires encapsulated in a quartz tube. Five wire compositions will be included, with melting temperature ranging between approximately 327 and 514 °C. Melting temperatures of the wires will be verified using a DSC. Melt wire compositions and melting temperatures are listed in Table 5-12,

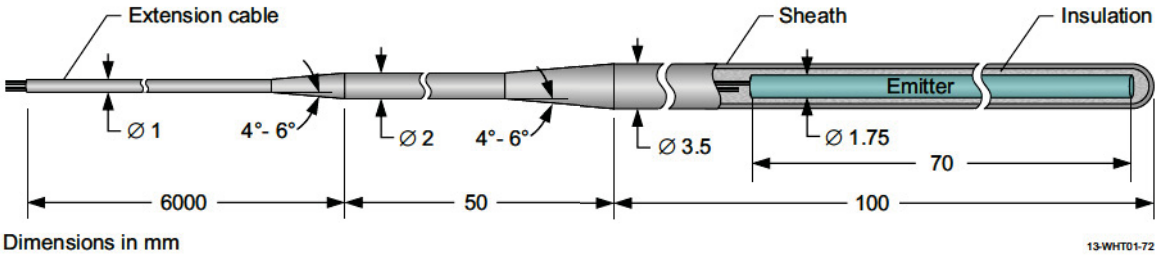

Figure 5-75. Schematic diagram of SPND and SPGD (dimensions are the same for each).

and a picture of a melt wire capsule is shown in Figure 5-76. Integrated thermal and fast neutron fluence will be evaluated through post irradiation analysis of Fe-Ni-Cr flux wires.

Table 5-12. Compositions and melting temperatures of melt wires.

Material Composition, %	Melting Temperature, °C
100 Pb	327.5
94 Zn-6 Al	381.0
85 Te-15 Sn	401.0
100 Zn	419.6
80 Sb-20 Zn	507.8-514.3

Figure 5-76. Example melt wire capsule with four wire types.

Post Irradiation Examinations. The irradiation effects on the candidate materials will be quantified through PIE, and results will be compared with pre-irradiation values. Planned PIEs include:

- *Simple pulse echo measurements.* These tests, which have the potential to reveal information about the quality of the transducer, will first be completed. These measurements can be performed without disassembling the transducer. They can be made in-pile (after reactor shut down) and after removal from the reactor. The pulse-echo measurement is used to measure signal to noise ratio (indicating sensitivity of the transducer), resonance frequency, bandwidth, and the quality factor (a measure of the intrinsic damping of the crystal). These are used as a go/no go test for sensor performance and are most important in ascertaining transducer performance.
- *Impedance measurements*. These measurements can be used to calculate the loss tangent,[1] which is related to the dielectric property changes, as well as the resonance frequency, stiffness, and dielectric constant. This is important in determining loss mechanisms. This measurement can also be made without disassembling the transducer.
- *Hysteresis measurements.* These measurements can indicate remnant polarization, which is necessary for transduction in ferroelectrics as well as the degradation mechanism, such as metamictization[2] versus antiferroelectric tendencies.[3] This measurement can be made without disassembling the transducer.

1. A measure of electrical energy dissipation of the crystal.

- *Density measurements.* Density data are needed to determine material properties from the pulse-echo and impedance measurements. During temperature testing, it is common to see variations in densities of many piezoelectric materials; and it is important to characterize these changes. The sensor material must be removed from the transducer assembly for this measurement.
- *d33 measurements*. The d33 parameter is a material constant and important to piezoelectric transducer signal amplitude. This parameter is most significantly affected during neutron testing in most materials, and it is also important to characterize observed d33 changes. It will be necessary to remove the sensor material from the transducer in order to measure this material property.
- *Color changes.* Some materials change color during irradiation, which can indicate absorption of oxygen and other contaminants. Optical examination would require the sensor material to be removed from the assembly and photographed with a high resolution camera.
- *Grain structure changes.* Scanning Electron Microscopy (SEM) is important to characterizing the grain structure of the sensor and changes that occur during irradiation. SEM examinations may provide insights about the damage mechanisms and how polar domains change during irradiation. SEM examples also require that samples be removed from the transducer assembly.

5.7.1.3. Summary

Currently, it is anticipated that the test capsule will be inserted into the MITR in late February 2014. After insertion, collaborators will continue to support the irradiation test by interpreting data from the irradiation test and completing the out of pile tests used to separate the effects of temperature from irradiation effects on the sensors. In addition, the NEET program, which is leveraging data from this ATR NSUF irradiation, will focus on developing an enhanced signal processing capability for ultrasonic thermometry (selected as an ultrasound based sensor which could be deployed in the near term).

5.7.2. Fiber Optic Irradiation

Radiation effects on optical fibers and the probe components are an important issue for the long term survivability of fiber based in-pile sensors. A summary of the fiber issues and related research has been reported previously.[58] Irradiation testing of the optical fiber and components is paramount to quantitatively determining the effects on the sensor accuracy and lifetime. A collaboration with Ohio State University (OSU) led to the development of a proposal for fiber optic radiation testing. The objective of the proposal was the measurement of radiation induced attenuation in several optical fibers in an ATR instrumented lead experiment. A schematic of the proposed experiment is shown in Figure 5-77 and described below.

The test methodology would involve both through transmission testing using a spectrometer and single ended fiber testing using either OTDR or OBR. In the through transmission test, the fiber would be routed down to the reactor core and back essentially forming a long "U". Light from a broadband source would be coupled into one end of the fiber and the opposite end would be connected to a spectrometer. This would allow attenuation across a broad wavelength range to be continuously monitored. As the tight bend radius necessitated by the small test positions could be detrimental to the fibers, OTDR or OBR instruments would also be employed. These instruments allow attenuation measurements to be made from one end of a

2. The process through which a crystal becomes amorphous through damage processes; in this case neutron radiation, causing a loss of piezoelectricity.
3. A loss of piezoelectricity through depolarization.

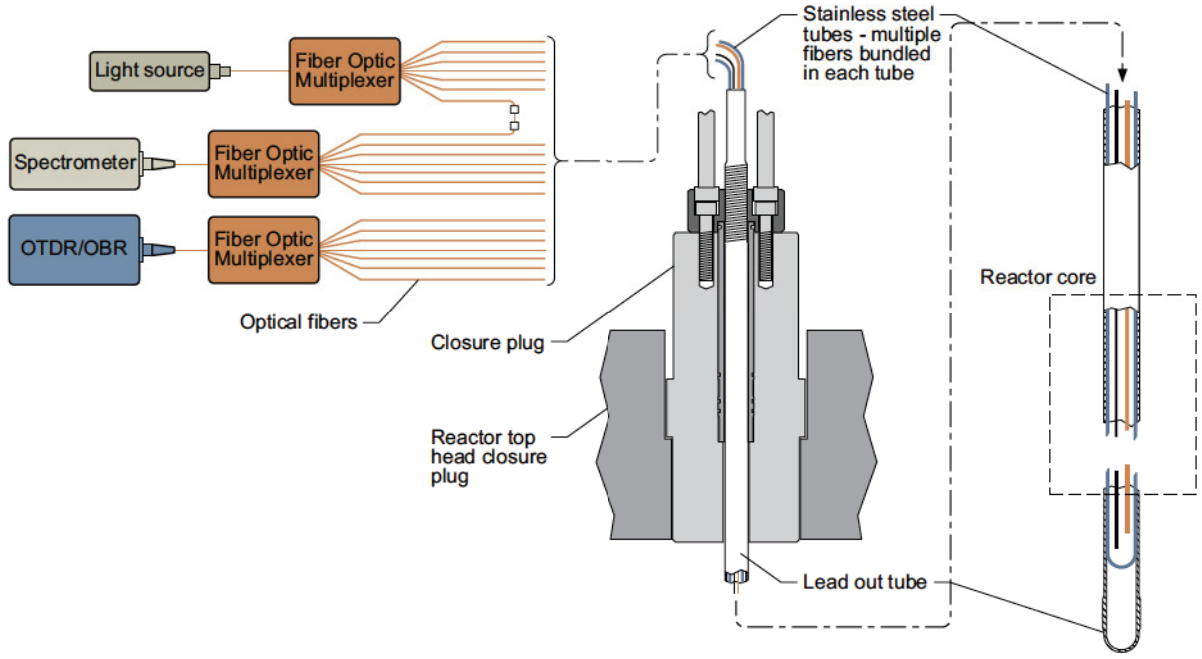

Figure 5-77. ATR fiber optic attenuation test schematic.

fiber but are limited to discrete wavelengths. Fiber optic multiplexers would be implemented in both test methods to allow multiple fibers to be tested using the same instrument.

The design concept uses a lead out tube which would be inserted through the reactor top head closure plate and down into the test position. The lead out tube would serve as the primary pressure boundary. Individual optical fibers would be bundled inside separate small diameter stainless steel tubes. These smaller tubes could be hard mounted in the lead out tube to maintain proper positioning and added protection for the fibers. If funded, the proposal would help answer long standing questions on the longevity of optical fiber based sensors in the ATR and other high flux US MTRs.

5.7.3. Standardized Instrumented Fuel Irradiation Rig

Standardized test rigs, which are regularly used at facilities such as the HBWR in Norway and are under development for the JHR in France, are essential components of world class irradiation facilities. Standardized test rigs with state-of-the-art instrumentation, that are tailored to meet US industry needs for fuel irradiation testing and US regulatory requirements for data acceptance, are essential in order for the ATR and other US MTRs are to be competitive with international MTRs. Evaluations suggest that standardized test rigs have the potential to offer ATR users a one-third reduction in costs and long lead times associated with one-of-a-kind experiment designs. Participation from US vendors, US regulators and experienced ATR analysts and researchers are essential to ensure that the test rig is tailored to economically meet US industry needs and regulatory requirements for fuels and materials testing at ATR. Specially-developed instrumented standardized test rigs will allow DOE-NE programs (ATR NSUF, FCRD, ARC, etc.) to obtain much-needed, high fidelity data for evaluating the performance of new fuels and materials at US MTRs.

To meet this national need, it is proposed that a collaborative project be initiated that includes researchers from INL, other laboratories, and US fuel vendors. The INL team would include HTTL in-pile instrumentation experts and ATR experts in experiment engineering and management, engineering design, reactor physics analysis, and thermal and structural analysis. ATR experiment managers and analysts will ensure that the test rig is appropriately designed and meets ATR acceptance criteria using detailed design drawings and established thermal, structural, and neutronics analysis methods, such as MCNP, ORIGEN, and RELAP, and other processes accepted by ATR engineering. A prototype test rig will be fabricated using an existing INL three dimensional printer followed by instrumented mockups that will be used for verification testing. To the extent possible, approved Computational Fluid Dynamic (CFD) methods will be used to verify the performance of this test rig; but funding has been requested to allow, if needed, evaluation of the test rig (or component testing) in a large-scale loop facility. In addition, selected instrumentation performance will be verified using existing testing capabilities at the HTTL (e.g. furnace testing and autoclave evaluations) to ensure operability for test conditions specified by industry collaborators. These analyses will support the preparation of an Experiment Safety Assurance Package (ESAP) that will approve the test rig for use in the ATR. The analysis and ESAP will be written using worst case assumptions and bounding masses for the fuel content to allow the largest variety of tests possible. As part of the proposed effort, a standard test rig will be fabricated following the INL process for experiment design and fabrication. The standard test rig will also meet the ATR QA and Safety Analysis Report (SAR) requirements so it will be ready for use at the completion of this project. Funding has also been requested for a trial irradiation as a proof-of-concept demonstration that will attract future customers.

Standardized test rigs will differ for specific irradiation facilities and locations. Figure 5-78 illustrates a preliminary conceptual design for a standardized test rig for use in ATR Loop 2A. Based on user specifications, the test rig could be instrumented with sensors capable of withstanding anticipated pressures, temperatures, and radiation levels in Loop 2A fuel tests and providing real-time data to address user needs. In addition to providing sensors within each test rig, supplemental sensors, such as flux wires, melt wires, and silicon carbide temperature monitors, will be included exterior to the test rig to increase confidence in the accuracy of obtained data.

A standardized test rig represents a much needed, final step in efforts to provide the US world class instrumentation and irradiation capabilities. In addition to increasing usage of the recently reactivated ATR Loop 2A, a standardized test rig will also provide a basis for testing at other ATR NSUF facilities, such as the HFIR and MITR, and the Transient Reactor Test (TREAT) facility that DOE-NE is planning to restart. Without such standardized test rigs with advanced instrumentation becoming the norm in US MTR irradiations, US MTRs will be unable to provide economical irradiation facilities for US industry and regulators.

5.8. Summary

As outlined in this section, INL has initiated efforts to develop and obtain new sensors for measuring key parameters (e.g., temperature, length, diameter, etc.) during irradiation testing at the ATR. As discussed in Section 4, initial ATR NSUF efforts are primarily focussing on sensors that can provide data needed for ATR NSUF users with on 'lower risk" technologies that are already deployed at other MTRs. These initial efforts have led to several new or enhanced sensors becoming available to ATR users: the doped Mo/Nb HTIR-TCs (Section 5.1.3), silicon carbide temperature monitors (Section 5.1.2), enhanced melt wire selection and encapsulation options (Section 5.1.1), THWM needle probes for thermal conductivity measurements (Section 5.2) and creep elongation test rigs (Section 5.3.2). In addition, it is antici-

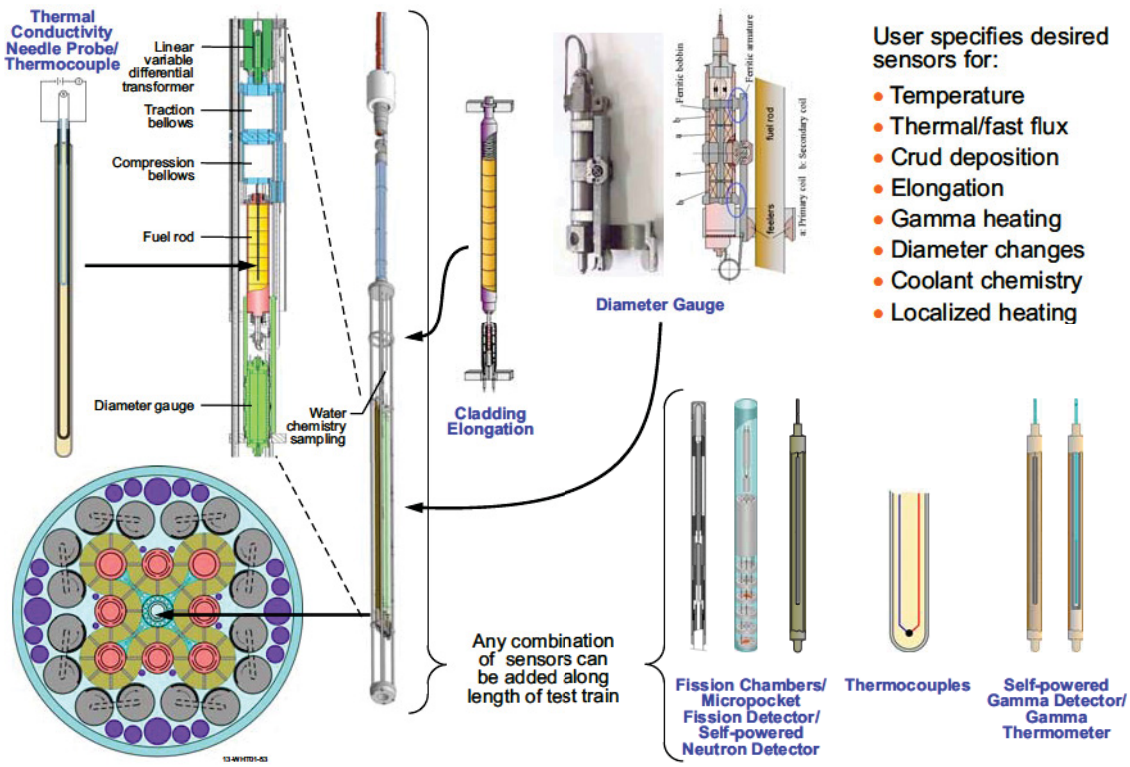

Figure 5-78. Candidate standardized test rig for evaluating fuel rod diameter changes, thermal conductivity, and fission gas release in a PWR loop.

pated that during 2014, HTTL-fabricated HTIR-TCs and THWM NPs will be deployed by IFE/HRP; and an HTTL-fabricated THWM NP will be deployed by CEA. During 2014, it is planned to continue testing of miniature fission chambers developed by CEA and other flux detection systems (e.g., SPNDs) at the ATRC. In addition, efforts will to develop MPFDs will be completed, and efforts to develop a crack growth test rig and evaluated ultrasonic transducers will be continued. Finally, a new effort to evaluate the potential to deploy an LVDT-based diameter gauge has been started in FY14.

As noted within this section, DOE funding reductions have limited planned development and evaluations of some sensors, such as ultrasonic thermometers and gamma thermometers. In addition, funding limitations have restricted the start of a much needed effort to develop and deploy a standardized fuel test rig with advanced instrumentation. As noted within this section, standardized test rigs are essential if US MTRs are to be competitive with international MTRs. With standardized test rigs with advanced instrumentation, US MTRs will be able to more readily meet US industry and regulator needs for sustainment of nuclear energy.

6. REFERENCES

1. J. L. Rempe, et al., *Instrumentation to Enhance Advanced Test Reactor Irradiations*, INL/EXT-08 -13985, September 2009.

2. J. L. Rempe, D. L. Knudson, and J. E. Daw, *Status Report on Efforts to Enhance Instrumentation to Support Advanced Test Reactor Irradiations*, INL/EXT-11-21231, Idaho National Laboratory, March 2011.

3. J. L. Rempe, D. Knudson, J. Daw, T. Unruh, B. Chase, K. Davis, R. Schley, S. Taylor, D. Nigg, and K. Condie, *2011 Status Report on Efforts to Enhance Instrumentation to Support Advanced Test Reactor Irradiations*, INL/EXT-11-24233, December 2011.

4. "FY2009 Advanced Test Reactor National Scientific User Facility User's Guide," INL/ EXT-07-13577, Idaho National Laboratory, 2008.

5. S. B. Grover, "Irradiation Facilities at the Advanced Test Reactor," *Transactions of the 11th International Topical meeting on Research Reactor Fuel Management and Meeting of the International Group on Reactor Research,* March 2007, Lyon, France.

6. R. V. Furstenau and S. Blaine Grover, "The Advanced Test Reactor Irradiation Facilities and Capabilities," *Proceedings of the Americas Nuclear Energy Symposium 2002 (ANES 2002),* October 2002.

7. F. M. Marshall, "Advanced Test Reactor Capabilities and Future Operating Plans," *presented at Test Research and Training Reactors (TRTR) Annual Meeting*, September 2005, Gaithersburg, MD.

8. C. J. Stanley and F. M. Marshall, "Advanced Test Reactor - A National Scientific User Facility," proceedings ICONE2008-48426, May 11-15, 2008, Orlando, Florida, USA.

9. A. J. Palmer, G. L. McCormick, S. J. Corrigan, "Hydraulic Shuttle Irradiation System (HSIS) Recently Installed in the Advanced Test Reactor (ATR)," *Proceedings of ICAPP '10, Paper 10354,* San Diego, CA, USA, June 13-17, 2010

10. International Atomic Energy Agency, "Nuclear Research Reactors in the World," www.iaea.or.at/ worldatom/rrdb/, accessed December 9, 2011.

11. G. Bignan, "The Jules Horowitz Reactor: a new High Performance European MTR open to International Community," *presentation at the Idaho National Laboratory*, Idaho Falls, ID, September 2010.

12. G. Bignan, A. Lyoussi, G. Gonnier, JF Villard, and C. Destouches, "Innovative and Advanced Instrumentation and Measurement Methodologies dedicated to the JHR future European MTR (Material Testing Reactor)," *Proceedings of the 2013 International Conference on Advancements in Nuclear Instrumentation, Measurement Methods and their Applications (ANIMMA2013),* Marseille, France, June 2013.

13. G. Bignan, J.-F. Villard, C. Destouches, P. Baeten, L. Vermeeren, and S. Michiels, "The Key Role of Instrumentation for the New Generation of Research Reactors," *Proceedings of the Second International Conference on Advancements in Nuclear Instrumentation, Measurement Methods and their Applications (ANIMMA2011),* Ghent, Belgium, June 2011.

14. C. Destouches and J.-F. Villard, "Improved In-Pile Measurements for MTR Experiments," *IAEA Technical Meeting on In-Pile Testing and Instrumentation for Development of Generation-IV Fuels and Materials,* 21-24 August 2012, Halden, Norway.

15. J.-F. Villard, "Progress in Instrumentation Development for the Future Jules Horowitz Reactor," *presentation at joint Idaho ANS-IEEE-ICIS Seminar,* September 12, 2012, Idaho Falls, ID.

16. H. Thoresen and S. Solstad, An overview of nuclear fuels and materials research at the OECD Halden Reactor Project, seminar presented at the Idaho National Laboratory, Idaho Falls, ID, July 15, 2008.

17. W. Wisenack, "Institutt for Energiteknikk OECD Halden Reactor Project - Organisation, Facilities, and Research," *IAEA Technical Meeting on In-pile Testing and Instrumentation for Development of Generation IV Fuels and Materials,* August 2012, Halden, Norway

18. B. G. Kim, J. L. Rempe, J-F Villard, and S. Solstad, "Review of Instrumentation for Irradiation Testing of Fuels and Materials," *invited review paper, Nuclear Technology,* **176**, November 2011, p 155-187.

19. J.F. Villard, "Innovative in-pile instrumentation developments for irradiation experiments in MTRs," *IGORR 10,* Gaithersburg, Sept. 2005.

20. J. F. Villard, "INSNU Project - Instrumentation for Irradiation Experiments in Research Reactors," *presentation at the Idaho National Laboratory*, Idaho Falls, ID, June 2008.

21. J. F. Villard, "INSNU Project - Instrumentation for Irradiation Experiments in Research Reactors," *presentation at CEA-Cadarache*, Cadarche, France, October 2008.

22. J-F Villard and M. Schyns, "Advanced In-Pile Measurements of Fast Flux, Dimensions, and Fission Gas Release," *Proceedings of the ANS NPIC HMIT 2009 Topical Meeting on Nuclear Plant Instrumentation, Controls, and Human Machine Interface Technology,* Knoxville, TN, April 2009.

23. D. Iracane, G. Bignan, Ph. Guimbal, and J-F. Villard, "Advanced Instrumentation for Irradiation Experiments in Material Testing Reactors (MTRs)," *Proceedings of the First International Conference on Advancements in Nuclear Instrumentation, Measurement Methods and their Applications (ANIMMA)*, Marseille, France, June 2009.

24. C. Blandin, S. Breaud, JM. Laurens, L. Oriol, L. Vermeeren, M. Weber "In-pile CFUZ53 sub-miniature fission chambers qualification in BR2 under PWR conditions – *10th International Group on Research Reactors (IGORR) meeting,* Gaithersburg (USA), September 2005.

25. P. Philliatre, et al., "Reasons Why Plutonium 242 is the Best Fission Chamber Deposit to Monitor the Fast Component of a High Neutron Flux," *Nucl. Instrum. Meth. Phys. Res. A*, **593**, 510, 2008.

26. L. Vermeeren, M. Wéber, L. Oriol, S. Breaud, P. Filliatre, B. Geslot, C. Jammes, S. Normand, and B. Lescop, "Experimental Verification of the Fission Chamber Gamma Signal Suppression by the Campbelling Mode," *Proceedings of the First International Conference on Advancements in Nuclear Instrumentation, Measurement Methods and their Applications (ANIMMA),* Marseille, France, June 2009.

27. B. Geslot, P. Loiseau, N. Blanc de Lanaute, P. Filliatre, C. Jammes, S. Breaud, J-F. Villard, and P. Blaise, "Impact of Gas Pressure on Fission Chamber Sensitivity in Campbelling Mode," *2013 Conference on Advancements in Nuclear Instrumentation, Measurements Methods* (ANIMMA 2013), Paper #1179, June 23-27, 2013, Marseilles, France.

28. Loic Barbot, Christophe Domergue, Stephane Breaud, Christophe Destouches, Jean-Francois Villard, Luka Snoj, Ziga Stancar, Vladimir Radulovic, and Andrej Trkov, "Neutron Field Characterization of Irradiation Locations Applied to the Slovenian TRIGA Reactor," Paper 1136, *proceedings of the 2013 Conference on Advancements in Nuclear Instrumentation, Measurements Methods* (ANIMMA 2013), Paper #1179, June 23-27, 2013, Marseilles, France.

29. V. Lamirand, B. Geslot, J. Wagemans, L. Borms, E. Malambu, P. Casoli, X. Jacquet, G. Rousseau, G. Grégoire, P. Sauvecane, D. Garnier, S. Bréaud, F. Mellier, J. Di Salvo, C. Destouches and P. Blaise, "Miniature fission chambers calibration in pulse mode: inter laboratory comparison at the SCK•CEN BR1 and CEA CALIBAN reactors," Paper 1190, *proceedings of the 2013 Conference on Advancements in Nuclear Instrumentation, Measurements Methods* (ANIMMA 2013), Paper #1179, June 23-27, 2013, Marseilles, France.

30. L. Vermeeren, H. Carcreff, L. Barbot and al. "Irradiation Tests of Prototype Self-Powered Gamma and Neutron Detectors," *Proceedings of the Second International Conference on Advancements in Nuclear Instrumentation, Measurement Methods and their Applications (ANIMMA2011)*, Ghent, Belgium, June 2011.

31. S. Fourrez, G. Bailleul, M. Kollen, J.-F. Villard, "Characterisation of a thermocouple for high temperature measurement under irradiation - Definition and properties of the Molybdenum Niobium thermocouple, *12th International Metrology Congress*, Lyon (France), June 2005.

32. J. F. Villard, S. Fourrez, "High temperature measurement needs for irradiation experiments in Material Testing Reactors - Development of a new type of thermocouple and interest of high temperature fixed points for its characterisation and in-pile qualification," *Physikalisch-Technische Bundesanstalt Seminar on High-temperature fixed-points for industrial and scientific applications*, Berlin (Germany), April 2005.

33. J. F. Villard, S. Fourrez, D. Fourmentel, and A. Legrand, "Improving IIigh-Temperature Measurements in Nuclear Reactors with Mo/Nb Thermocouples," *Int. J. Thermophys.*, **29**, 1848, 2008.

34. M. Laurie, M. Futterer, J. Lapetite, S. Fourrez, and R. Morice, "New Temperature Monitoring Devices for High-temperature Irradiation Experiments in the High Flux Reactor Petten," P*roceedings of the First International Conference on Advancements in Nuclear Instrumentation, Measurement Methods and their Applications (ANIMMA)*, Marseille, France, June 2009.

35. H. Brixy, H. Hecker, K. F. Rittinghaus, and H. Howener, "Application of Noise Thermometry in Industry Under Plant Conditions," *Temperature, Its Measurement and Control in Science and Industry,* Vol. 5, pp. 1225–1237, American Institute of Physics, New York (1982).

36. M. Decreton, L. Binard, and C. Delrez, "High Temperature Measurements by Noise Thermometry," *High Temp.–High Press.,* **12**, 395, 1980.

37. J. L. Rempe, D. L. Knudson, K. G. Condie, and S. C. Wilkins, "Thermocouples for High-Temperature In-Pile Testing," *Nuclear Technology*, **156**, No. 3, December 2006, pp 320-331.

38. S. Lopez Legrand and J. F. Villard, "Noise Thermometry for Nuclear Applications," *presented at ANIMMA Int. Conf.*, Marseille, France, June 7–10, 2009.

39. M. Laurie, M. A. Fütterer, J.M. Lapetite, S. Fourrez, R. Morice, "New temperature monitoring devices for high-temperature irradiation experiments in the High Flux Reactor Petten," *presented at ANIMMA Int. Conf.*, Marseille, France, June 7–10, 2009.

40. P. Guimbal, S. Huotilainen, S. Tähtinen, G. Thellier, M. Auclaim, M. Patalainen, and J.-F. Villard, "Status of the MeLoDIE Experiment, an Advanced Device for Online Biaxial Study of the Irradiation Creep of LWR Cladding," *Proceedings of the 2013 International Conference on Advancements in Nuclear Instrumentation, Measurement Methods and their Applications (ANIMMA2013),* Paper, #1356, Marseille, France, June 2013.

41. J. F. Villard, "State-of-the-Art and Improvement of Online Measurements in Present and Future French Research Reactors," presented at INL, Idaho Falls, Idaho, September 15, 2009.

42. J. F. Villard, G. Lemaitre, J. M. Chaussy, and F. Lefevre, "High Accuracy Sensor for Online Measurement of the Fuel Rod Internal Pressure During Irradiation Experiments," *7th Int. Topl. Mtg. Research Reactor Fuel Management (RRFM 2003)*, Aix-en-Provence, France, March 9–12, 2003.

43. M. F. Narbey, D. Baron, G Despaux, JM Saurel, "Determination of the composition of a gas mixture in a nuclear fuel rod by an acoustic method," *Journal of the British Institute of Non-Destructive Testing (INSIGHT)*, **42**, 603-605 (2000).

44. J.Y. Ferrandis, G. Leveque, F. Augereau, E. Rosenkrantz, D. Baron, J-F. Villard, "An ultrasonic sensor for pressure and fission-gas release measurements in fuel rods for pressurised water reactors, *9th International conference on CANDU fuel*, Belleville (Canada), September 2005.

45. F. Augereau, J.-Y. Ferrandis, J.-F. Villard, D. Fourmentel, M. Dierckx, and J. Wagemans, "Effect of intense neutron dose irradiation on piezoceramics," *Transactions from Acoustics '08,* June 29-July 4, 2008, Paris, France.

46. D. Fourmentel, J. F. Villard, J. Y. Ferrandis, F. Augereau, E. Rosenkrantz, and M. Dierckx, "Acoustic Sensor for In-Pile Fuel Rod Fission Gas Release Measurement," *presented at ANIMMA Int. Conf.,* Marseille, June 7–10, 2009.

47. F. Algaber, JY. Ferrandis, F. Augereau, J-F. Villard, "PZT Materials under Gamma irradiation," *4th European Workshop on Piezoelectric Materials,* Montpellier (France), July 2004.

48. E. Rosenkrantz, J. Y. Ferrandis, F. Augereau, T. Lambert, D. Fourmentel, and X. Tiratay, "An Innovative Acoustic Sensor for First In-pile Fission Gas Release Determination - REMORA3 Experiment," *Proceedings of the Second International Conference on Advancements in Nuclear Instrumentation, Measurement Methods and their Applications (ANIMMA2011),* Ghent, Belgium, June 2011.

49. T. Lambert, E. Muller1, E. Federici1, E. Rosenkrantz, J.Y. Ferrandis, X. Tiratay, V. Silva, D. Machard, and G. Trillon, "REMORA 3: the fIrst Instrumented Fuel Experiment with On-line Gas Composition Measurement By Acoustic Sensor," *Proceedings of the Second International Conference on Advancements in Nuclear Instrumentation, Measurement Methods and their Applications (ANIMMA2011),* Ghent, Belgium, June 2011.

50. T. Lambert, E. Rosenkrantz, J.Y. Ferrandis, I. Zacharie-Aubrun, K. Hanifi, Ch. Valot, S. Reboul, and X. Tiratay, "Irradiation Behavior and Post-Irradiation Examinations of an Acoustic Sensor Using a Piezoelectric Transducer," *proceedings of the 2013 Conference on Advancements in Nuclear Instrumentation, Measurements Methods (ANIMMA 2013),* June 23-27, 2013, Marseilles, France.

51. A. Péron, F. Malouch, and C. M. Diop, "Simulation and Comparison of the Calorimeters Measuring the Nuclear Heating in the OSIRIS Reactor, with the TRIPOLI-4® Monte-Carlo Code," Paper 1178, *proceedings of the 2013 Conference on Advancements in Nuclear Instrumentation, Measurements Methods (ANIMMA 2013),* June 23-27, 2013 Marseilles, France.

52. J. Brun, C. Reynard-Carette, A. Lyoussi, C. De Vita, M. Carette, M. Muraglia, D. Fourmentel, P. Guimbal, and J-F. Villard, "Comparison of the Thermal Response of Two Calorimetric Cells Dedicated to Nuclear Heating Measurements during Calibration," Paper 1200, *proceedings of the 2013 Conference on Advancements in Nuclear Instrumentation, Measurements Methods (ANIMMA 2013),* June 23-27, 2013 Marseilles, France.

53. H. Carcreff, L. Salmon, and C. Courtaux, "First In-Core Measurement Results Obtained with the Innovative Mobile Calorimeter CALMOS inside the OSIRIS Material Testing Reactor," Paper 1138, *proceedings of the 2013 Conference on Advancements in Nuclear Instrumentation, Measurements Methods (ANIMMA 2013),* June 23-27, 2013 Marseilles, France.

54. H. Carcreff, V. Clouté-Cazalaa, L. Salmon, "Development, calibration and experimental results obtained with an innovative calorimeter (CALMOS) for nuclear heating measurements," *Proceedings of the Second International Conference on Advancements in Nuclear Instrumentation, Measurement Methods and their Applications (ANIMMA2011)*, Ghent, Belgium, June 2011.

55. H. Carcreff, Patent N° FR 1060068, December 3, 2010.

56. P. Moilanen, S. Tahtinen, B.N. Singh, and P. Jacquet, "In-Situ Investigation of the Mechanical Performance and Life Time of Copper - Final report on design, construction, and calibration of test module for in-reactor tensile tests in BR-2 reactor," VTT Report BTUO 76-031127, October 27, 2004.

57. G. Cheymol, B. Brichard, J.F. Villard, "Fiber optics for metrology in nuclear research reactors applications to dimensional measurements," *ANIMMA International Conference,* Marseille, 7-10 June 2009.

58. G. Cheymol, H. Long, J-F. Villard, and B. Brichard, "High Level Gamma and Neutron Irradiation of Silica Optical Fibers in CEA OSIRIS Nuclear Reactor," *IEEE Transactions on Nuclear Science,* Vol. **55**, No. 4, August 2008, pp 2252-2258.

59. L. Skuja, M. Hirano, H. Hosono, and K. Kajihara, "Defects in Oxide Glasses," *Physica Status Solidi C*, Conf., **2**, 15, 2005.

60. D. Griscom, "The Nature of Point Defects in Silicon Dioxide," *Defects in SiO_2 and Related Dielectrics: Science and Technology*, pp. 117–161, Kluwer Academic Publishers, 2000.

61. B. Brichard, A. L. Tomashuk, H. Ooms, V. A. Bogatyrjov, S. N. Klyamkin, A. F. Fernandez, F. Berghmans, and M. Decréton, "Radiation Assessment of Hydrogen-Loaded Aluminium-Coated Pure Silica Core Fibres for ITER Plasma Diagnostic Applications," *Fusion Eng. Des*., **82**, 2451, 2007.

62. B. Brichard, A. F. Fernandez, H. Ooms, F. Berghmans, M. Decréton, A. Tomashuk, S. Klyamkin, M. Zabezhailov, I. V. Nikolin, V. Bogatyrjov, E. Hodgson, T. Kakuta, T. Shikama, T. Nishitani, A. Costley, and G. Vayakis, "Radiation-Hardening Techniques of Dedicated Optical Fibers Used in Plasma Diagnostics Systems in ITER," *J. Nucl. Mater.*, **329**–**333**, 1456, 2004.

63. T. Shikama, T. Kakuta, M. Narui, T. Sagawa, and H. Kayano, "Optical Properties in Fibers During Irradiation in a Fission Reactor," *J. Nucl. Mater.*, **225**, 324, 1995.

64. T. Kakuta, T. Shikama, T. Nishitani, B. Brichard, A. Krassilinikov, A. Tomashuk, S. Yamamoto, and S. Kasai, "Round-Robin Irradiation Test of Radiation Resistant Optical Fibers for ITER Diagnostic Application," *J. Nucl. Mater.*, **307**–**311**, 1277, 2002.

65. B. Brichard, A. F. Fernandez, F. Berghmans, and M. Decréton, "Origin of the Radiation-Induced OH Vibration Band in Polymer-Coated Optical Fibers Irradiated in a Nuclear Fission Reactor," *IEEE Trans. Nucl. Sci*., **49**, 2852, Dec. 2002.

66. S. Shikama, K. Toh, S.Nagata, and B. Tsuchiya, "Optical Dosimetry for Ionizing Radiation Fields by Infrared Radioluminescence," *Measure. Sci. Technol.*, **17**, 1103, 2006.

67. G. Cheymol, J.F. Villard, A. Gusarov, B. Brichard, "Fibre optic extensometer for high radiation and high temperature nuclear applications," *Proceedings of the Second International Conference on Advancements in Nuclear Instrumentation, Measurement Methods and their Applications (ANIMMA2011)*, Ghent, Belgium, June 2011.

68. G. Cheymol, A. Gusarov, S. Gaillot, C. Destouches and N. Caron, "Dimensional Measurements under High Radiation with Optical Fibre Sensors based on White Light Interferometry - Report on Irradiation Tests," Paper 1208, *proceedings of the 2013 Conference on Advancements in Nuclear Instrumentation, Measurements Methods (ANIMMA 2013),* June 23-27, 2013 Marseilles, France.

69. B. Brichard, A. F. Fernandez, H. Ooms, and F. Berghmans, "Fibreoptic Gamma-Flux Monitoring in a Fission Reactor by Means of Cerenkov Radiation," *Measure. Sci. Technol.*, **18**, 3257, 2007.

70. B. Aarset, "In-reactor Instrumentation for Fuel Behavior Studies at the OECD Halden Reactor Project," *Proceedings from the Conference on Fast, Thermal, and Fusion Reactor Experiments*, p 1-85 through 1-96, April 12-15, 1982, Salt Lake City, Utah.

71. O. Aarrestad and H. Thoresen, "Fuel Rod Performance Measurements and Re-Instrumentation Capabilities at the Halden Project," *In-core instrumentation and core assessment: proceedings of a Specialists' Meeting,* Mito-shi, Japan, 14-17 October, 1996.

72. C. Vitanza, "On-line fuel rod performance measurements and fuel inspection applications," *Kerntechnik,* **56**, 1991, pp 124-130.

73. S. Solstad, HRP, email to J. Rempe, INL, February 6, 2008.

74. R. Van Nieuwenhove and S. Solstad, "In-Core Fuel Performance and Material Characterization in the Halden Reactor," *presented at ANIMMA,* Int. Conf., Marseille, France, June 7–10, 2009.

75. W. Wiesenack, "Experimental Techniques and Results Related to High Burn-up Investigations at the OECD Halden Reactor Project, *Proceedings of a Technical Committee Meeting held in Pembroke,* Ontario, Canada, April 28 - May 1, 1992, IAEA-TECDOC-697, p. 118.

76. P. Bennett, "In-core Measurements of Fuel-Clad Interactions at the Halden Reactor," *IAEA Technical Meeting on Fuel Rod Instrumentation and In-Pile Measurement Techniques,* Halden, Norway, 3-5 September 2007.

77. P. Bennett and T. Karlsen, "In-core Corrosion Monitoring in the Halden Test Reactor," *Energy Materials: Materials Science and Engineering for Energy Systems,* **3,** 2, June 2008, pp. 81-90.

78. S. Solstad and R. Van Nieuwenhove, "Instrument Capabilities and Developments at the Halden Reactor Project," *Nucl. Technol.,* **173**, 78 (2011).

79. O. Aarrestad, "Instrumentation Capabilities at Halden," I*FE/HRP Report HWR-351*, February 1993.

80. W. Wisenack, "Overview of the Halden Reactor Project," *presented at IAEA Technical Meeting - In-pile Testing and Instrumentation for Development of Generation IV Fuels and Materials, Halden*, Norway, 21-24 August 2012.

81. R. Van Nieuwenhove, "Development and Testing of Instruments for Generation IV Fuel and Materials Research at the Halden Reactor Project," *presented at IAEA Technical Meeting - In-pile Testing and Instrumentation for Development of Generation IV Fuels and Materials, Halden*, Norway, 21-24 August 2012.

82. P.A. C. Raynaud, *Fuel Fragmentation, Relocation, and Dispersal during the Loss-of-Coolant Accident,* NUREG-2121, March 2012.

83. US NRC, "NRC Information Notice 2009-21 Supplement 1: Nuclear Fuel Thermal Conductivity Degradation," October 26, 2012.

84. T.M. Karlsen, "Halden Reactor Materials Testing Techniques and Selected Results," *presented at IAEA Technical Meeting - In-pile Testing and Instrumentation for Development of Generation IV Fuels and Materials, Halden*, Norway, 21-24 August 2012.

85. K. Tsuchiya, "Irradiation Technology Development in JMTR" and "New JMTR," presentation and handouts provided to J. Rempe at JAEA meeting, September 29, 2009, Oarai, Japan.

86. M. Narui, T. Shikama, M. Yamasaki, and H. Matsui, "Development of High-Temperature Irradiation Techniques Utilizing the Japan Materials Testing Reactor," *Basic Studies in the Field of High Temperature Engineering, Second Information Exchange Meeting,* Paris, France, 10-12 October, 2001, pp. 145-152.

87. T. Shibata, T. Kikuchi, S. Miyamoto, K. Ogura, and Y. Ishigaki, "Development of the I-I TYpe Irradiation Equipment for the HTTR," *Basic Studies in the Field of High Temperature Engineering, Second Information Exchange Meeting,* Paris, France, 10-12 October, 2001, pp. 191-199.

88. T. Shikama, M. Narui, T. Kakuta, M. Ishitsuka, K. Hayashi, T. Sagawa, and T. Hoshiya, "Application of Optical Diagnostics in High-Temperature Gas-Cooled Systems," *Basic Studies in the Field of High Temperature Engineering, Second Information Exchange Meeting,* Paris, France, 10-12 October, 2001, pp. 153-160.

89. C. Mori, A. Uritanit, T. Kakuta, M. Katagiri, T. Shikama, M. Naikazawa, T. Iguchi, J. Kawarabayashi, I. Kimura, H. Kobayashi, and S. Hayashi, "Measurement Method of In-core Neutron and Gamma-Ray Distributions with Scintillator Optical Fibre Detector and Self -Powered Detector," *Basic Studies in the Field of High Temperature Engineering, Second Information Exchange Meeting,* Paris, France, 10-12 October, 2001, pp. 161-196.

90. H.Hanakawa, A. Shibata, H. Nagata, N. Kimura, N. Ohtsuka, M. Tanimoto, T. Saito, J. Nakamura and K. Tsuchiya, "Development of Instrumentation for Fuel and Material Irradiation Tests in JMTR," *presented at IAEA Technical Meeting - In-pile Testing and Instrumentation for Development of Generation IV Fuels and Materials, Halden*, Norway, 21-24 August 2012.

91. T. Soga, W.Itagaki, Y.Kihara, Y.Maeda, "Endeavor to Improve In-pile Testing Techniques in the Experimental Fast Reactor JOYO," *presented at IAEA Technical Meeting - In-pile Testing and Instrumentation for Development of Generation IV Fuels and Materials, Halden*, Norway, 21-24 August 2012.

92. J. Sackett, "Measurements of Thermal-hydraulic Parameters in Liquid-me1al-cooled Fast-breeder Reactors," *presented at the International Center for Heat and Mass Transfer Symposium: Measurement Techniques in Power Engineering,* August 29 - September 3, 1983, Beograd, Yugoslavia.

93. J. Markgraf, D. Perry, and J. Oudaert, "LWR Fuel Rod Testing Facilities in High Flux Reactor (HFR) Petten for Investigation of Power Cycling and Ramping Behavior," *Res Mechanica*, **13**, 1985, 187-210.

94. Email from K. Bakker, NRG, to J. Rempe, INL, dated December 11, 2007.

95. K. Bakker, NRG, discussions with J. Rempe, INL, at Petten, Netherlands, October 2008.

96. P. Blanchard, P. May, and H. Scheurer, "A Machine for the Fatigue Testing of CT type samples in the HFR," *Fusion Technology 1982, Proceedings of the 12th Symposium*, **2**, pp 749-752, 1983.

97. M. A. Fütterer, et al., "Next generation fuel irradiation capability in the High Flux Reactor Petten," Journal of Nuclear Materials," **392**, 2009, pp 184-191.

98. M. Laurie, M.A. Fütterer, K.H. Appelman, J.-M. Lapetite, A. Marmier, S. Knol, J. Best, "On-Line Fission Gas Release Monitoring System in the High Flux Reactor Petten," Paper 1076, *proceedings of the 2013 Conference on Advancements in Nuclear Instrumentation, Measurements Methods (ANIMMA 2013),* June 23-27, 2013 Marseilles, France.

99. B. G. Kim, et al., "Status and Perspective of Material Irradiation Tests in the HANARO, *paper and presentation from the 1st International Symposium on Materials Testing Reactors*, JAEA-Oarai, Japan, July 2008.

100. B. G. Kim, K-N Choo, J. M. Sohn, S. J. Park, K.Kim and Y. J. Kim, "Instrumentations for Materials Irradiation Tests in HANARO," *Proceedings of the ANS NPIC HMIT 2009 Topical Meeting on Nuclear Plant Instrumentation, Controls, and Human Machine Interface Technology,* Knoxville, TN, April 2009.

101. B.G. Kim, J. M. Sohn, and K-N Choo, "Development Status of Irradiation Devices and Instrumentation for Material and Nuclear Fuel Irradiation Tests in HANARO," *Nuclear Engineering and Technology*, **42**, 2, pp 203-210, April 2010.

102. S.H. Ahn, J.T. Hong, C.Y. Joung, and S.J. Park, "An Instrumentation and Control for Loop Test," *presented at IAEA Technical Meeting - In-pile Testing and Instrumentation for Development of Generation IV Fuels and Materials, Halden*, Norway, 21-24 August 2012.

103. J. L. Rempe, D. L. Knudson, J. E. Daw, T. Unruh, B.M. Chase, K. Davis, A. J. Palmer, and R. S. Schley, "Advanced In-pile Instrumentation for Materials Testing Reactors," ***invited paper*** *for ANIMMA 2013 Special Edition, IEEE Transactions on Nuclear Science, submitted July 2013.*

104. J. Rempe, D. Knudson, J. Daw, T. Unruh, B. Chase, and K. Davis, "Enhanced In-pile Instrumentation at the Advanced Test Reactor," *invited paper for ANIMMA 2011 Special Edition*, I*EEE Transactions on Nuclear Science,* **59**, Issue 4, Part:2, August 2012, pp 1214 -1223.

105. J. L. Rempe, D. L. Knudson, K. G. Condie, J. E. Daw, H. Ban, B. S. Fox, and G. E. Kohse, "New Sensors for the Advanced Test Reactor National Scientific User Facility" ***invited paper*** *from proceedings of the First International Conference on Advancements in Nuclear Instrumentation, Measurement Methods and their Applications (ANIMMA), Special Edition, IEEE Transactions on Nuclear Science*, **57**, No.5, pp 2653-2661, October 2010.

106. Standard Guide for Use of Melt Wire Temperature Monitors for Reactor Vessel Surveillance, E706 (IIE), ASTM E 1214-06, dated February 13, 2006.

107. K. L. Davis, D.L. Knudson, J.E. Daw, J.L. Rempe and A.J. Palmer, "Melt Wire Sensors Available to Determine Peak Temperatures in ATR Irradiation Testing," *Proceedings of the ANS NPIC HMIT 2012 Topical Meeting on Nuclear Plant Instrumentation, Controls, and Human Machine Interface Technology,* San Diego, CA, July 2012.

108. N. F. Pravdyuk, V. A. Nikolaenko, V. I. Kapuchin, V.N. Kusnetsov, in: Ed. D. J. Littler, *Proceedings of the Properties of Reactor Materials and the Effects of Radiation Damage,* Butterworths, 1962, p. 57.

109. L L. Snead, A. M. Williams, and A. L. Qualls, "Revisiting the use of SiC as a Post Irradiation Temperature Monitor," *Effects of Radiation on Materials,* ASTM STP 1447, M L. Grossbeck, Ed, ASTM International, West Conshohocken, PA, 2003.

110. L. L. Snead, "Revisiting the use of SiC as a Post Irradiation Temperature Monitor," *presented at the Int. Symp. Materials Test Reactors*, Idaho Falls, ID, September 28, 2009.

111. J. L. Rempe, K. G. Condie, D. L. Knudson, and L. L. Snead, "Comparison Measurements of Silicon Carbide Temperature Monitors," *IEEE Transactions on Nuclear Science,* **57**, No. 3, June 2010.

112. MacLean, H.J, and K. Sridharan, T. A. Hyde, "Irradiation Test Plan for the ATR National Scientific User Facility - University of Wisconsin Pilot Project," PNL-2784, Revision 1, Idaho National Laboratory, July 21, 2008.

113. J. L. Rempe, K. G. Condie, and D. L. Knudson, "Silicon Carbide Temperature Monitor Evaluation," PLN-3473, April 2010.

114. K. L. Davis, B. M. Chase, T. C.Unruh, D. L. Knudson, and J. L. Rempe, "Evaluations of University of Wisconsin Silicon Carbide Temperature Monitors 300 LO and 400 LO B," INL/EXT-11-24226, December 2011.

115. J. Rempe and M. Meyer, "ATR NSUF Instrumentation Enhancement Efforts," *Proceedings of the ANS NPIC HMIT 2009 Topical Meeting on Nuclear Plant Instrumentation, Controls, and Human Machine Interface Technology,* Knoxville, TN, April 2009.

116. J. L. Rempe, D. L. Knudson, K. G. Condie, and S. C. Wilkins, "Thermocouples for High-Temperature In-Pile Testing," *Nuclear Technology*, **156**, No. 3, December 2006, pp 320-331.

117. J. L. Rempe, D. L. Knudson, K. G. Condie, and S. C. Wilkins, "High Temperature Thermocouple Design and Fabrication," *US patent filed by Battelle Energy Alliance (IDR #BA-142) on behalf of DOE (Serial Number 11/678,901)*, published by US PTO as No. 2008/0205483 and issued January 18, 2011, Patent 7871198.

118. J. L. Rempe, D. L. Knudson, K. G. Condie, and S. C. Wilkins, "Long Duration Performance of High Temperature Irradiation Resistant Thermocouples," *Proceedings of the 2007 International Congress on Advances in Nuclear Power Plants (ICAPP'07)*, Nice, France, May 13-18, 2007.

119. J. Rempe, D. Knudson, K. Condie, J. Daw, and S. C. Wilkins, "New Sensors for In-Pile Temperature Detection at the ATR NSUF," *invited paper from the proceedings of the 13th International Topical Meeting on Nuclear Reactor Thermal-Hydraulics (NURETH13),* Kanazawa, Japan, October 2009. *NURETH13 Special Edition, Nuclear Technology*, **175**, September 2011, pp. 681-691.

120. D. L. Knudson, J. L. Rempe, K. G. Condie, S. C. Wilkins, J. E. Daw, and J. C. Crepeau, "High Temperature Irradiation Resistant Thermocouples - A Low Cost Sensor for In-Pile Testing at High Temperatures," Paper 8222, *Proceeding of the 2008 International Congress on Advances in Nuclear Power Plants (ICAPP '08)*, Anaheim, CA, June 8-12, 2008.

121. J. L. Rempe, D. L. Knudson, K. G. Condie, S. C. Wilkins, J. C. Crepeau, and J. E. Daw, "Options Extending the Applicability of High Temperature Irradiation Resistant Thermocouples," *invited paper for NURETH12 Special Edition, Nuclear Technology*, **167**, July 2009, pp 169-177.

122. J. E. Daw, J. L. Rempe, D. L. Knudson, S. C. Wilkins, and J. C. Crepeau, "High Temperature Irradiation-Resistant Thermocouple Performance Improvements," *ANS NPIC HMIT 2009 Topical Meeting on Nuclear Plant Instrumentation, Controls, and Human Machine Interface Technology,* Knoxville, TN, April 2009.

123. G. Kohse, "Summary Report of Irradiation of INL HTIR-TCs in the MITR," Draft report, December 2012.

124. H.A. Tasman, M. Campana, D. Pel, J. Richter, "Ultrasonic Thin-Wire Thermometry for Nuclear Applications," *Temperature: Its Measurement and Control in Science and Industry,* Vol. 5, Part 2, pp. 1191-1196, 1982.

125. R.J. Grossman, "Ultrasonic-Thermometry Development for In-Situ Measurement of Nuclear-Fuel Temperatures (AWBA Development Program)," KAPL-4160, General Electric Company Knolls Atomic Power Laboratory, 1982.

126. E.P. Papdakis, L.C. Lynnworth, D.R. Patch, E.H. Carnevale, "Ultrasonic Thermometry in LMFBR Systems," Final Report NYO-3906-13, Panametrics Inc. 1972.

127. M. Laurie, D. Magallon, J. Rempe, S. Wilkins, J. Pierre, C. Marquié, S. Eymery, and R. Morice, "Ultrasonic High Temperature Sensors: Past Experiments and Prospective for Future Use," *International Journal of Thermophysics*, **31** (8-9): 1417-1427 Special Issue, September 2010.

128. J. Daw, J. Rempe, and S. C. Wilkins, "Ultrasonic Thermometry for In-Pile Temperature Detection," *7th International Topical Meeting on Nuclear Plant Instrumentation, Control, and Human Machine Interface Technologies (NPIC&HMIT 2010),* Las Vegas, NV, November 7-11, 2010.

129. J. Rempe, J. Daw, D. Knudson, R. Schley, L. Bond, J. Coble, M. Good, and R. Meyer, *In-pile Instrumentation to Support Fuel Cycle Research and Development - FY11 Status Report,* FCRD-FUEL-2011-000307 (also issued as INL/EXT-11-23119), September 2011.

130. J. Rempe, J. Daw, D. Knudson, R. Schley, T. Unruh, and B. Chase, *In-pile Instrumentation to Support Fuel Cycle Research and Development - FY12 Status Report,* FCRD-FUEL-2012-000282, September 2012.

131. J. Rempe, J. Daw, R. Schley, K. Davis, D. Knudson T. Unruh, B. Chase, and J. Palmer, *In-pile Instrumentation to Support Fuel Cycle Research and Development - FY13 Status Report,* FCRD-FUEL-2012-000237, September 2013.

132. J. Daw, J. Rempe, and S. C. Wilkins, "Ultrasonic Thermometry for In-Pile Temperature Detection," *7th International Topical Meeting on Nuclear Plant Instrumentation, Control, and Human Machine Interface Technologies (NPIC&HMIT 2010),* Las Vegas, NV, November 7-11, 2010.

133. Y. S. Touloukian, et al., *Thermophysical Properties of Matter*, IFI/Plenum Publishing, New York, New York, 1973.

134. S.A. Chavez, G.E. Korth, D.M. Harper, and T.J. Walker, "High-temperature tensile and creep data for Inconel 600, 304 stainless steel and SA106B carbon steel," *Nuclear Engineering and Design,* **148**, pp. 351-363, 1994.

135. R. Syre, "Niobium, Molybdenum, Tantalum and Tungsten: a Summary of Their Properties with Recommendations for Research and Development," *AGARDograph,* **50**, 1961.

136. J.E. Daw, et al., "High Frequency Magnetostrictive Transducer for Waveguide Applications," Idaho National Laboratory Invention Disclosure Record 2257, Rev. 1, submitted August 8, 2012. Elected by the BEST Committee for Battelle Energy Alliance to pursue a patent on behalf of DOE, August 1, 2013.

137. M.J. Roberts, D.E. Holcomb, and R.A. Kisner, "Signal Processing Algorithm Implementation for In Vessel Level Measurement," https://inlportal.inl.gov/portal/server.pt/gateway/PTARGS-0-2-3310-277-2604-43/http%3B/inlpublisher%3B7087/publishedcontent/publish/communities/inl-gov/about-inl/gen-iv-technical-documents/signal-processing-algorighm.pdf, September 2006.

138. F. Honarvar, H. Sheikhzadeh, M. Moles and A. N. Sinclair, "Improving the time-resolution and signal-to-noise ratio of ultrasonic NDE signals," *Ultrasonics*, **41**, pp. 755-763, 3, 2004.

139. B. Fox, H. Ban, J. Rempe, D. Knudson, and J. Daw, "Development of an In-pile Technique for Fuel Thermal Conductivity Measurement," *Proceedings of the ANS NPIC HMIT 2009 Topical Meeting on Nuclear Plant Instrumentation, Controls, and Human Machine Interface Technology*, Knoxville, TN, April 2009.

140. B. Fox, H. Ban, J. Rempe, J. Daw, K. Condie, D. Knudson, "In-Pile Thermal Conductivity Measurement Method for Nuclear Fuels," Thermal Conductivity 30/Thermal Expansion 18, Daniela S. Gaal and Peter S. Gaal (Editor), DEStech Publications Inc., p 886, October 2010.

141. B. Fox, H. Ban, J. Daw, K. Condie, D.Knudson, and J. Rempe, Evaluation of Candidate In-Pile Thermal Conductivity Techniques, INL/EXT-09-16039, May 2009.

142. B. Fox, H. Ban, J. Rempe, J. Daw, K. Condie, and D. Knudson, "In-Pile Thermal Conductivity Measurement Method for Nuclear Fuels," *30th International Thermal Conductivity Conference and 18th International Thermal Expansion Symposium,* Pittsburgh, PA, August 29-September 2, 2009.

143. J. Daw, J. Rempe, K. Condie, D. Knudson, S. C. Wilkins, B. Fox, and H. Ban, "Hot Wire Needle Probe for In-Pile Thermal Conductivity Detection," *7th International Topical Meeting on Nuclear Plant Instrumentation, Control, and Human Machine Interface Technologies (NPIC&HMIT 2010)*, Las Vegas, NV, November 7-11, 2010.

144. "Needle Probe for In-Pile Thermal Conductivity Detection," Patent filed by DOE on October 10, 2012 (ID 13648502, Application S-122190). Inventors: Keith G. Condie, Joy L. Rempe, Darrell L. Knudson, Joshua E. Daw, S. Curtis Wilkins, Brandon S. Fox, and Heng Ban.

145. A. L. E. F. Schleirmacher, Vher die Warmeleitungder gase, *Weidemann Ann. Phys.* 34, p. 625, 1988.

146. Standard Test Method for Determination of Thermal Conductivity of Soil and Soft Rock by Thermal Needle Probe Procedure, ASTM D 5334-05, May 27, 2008.

147. M. S. Baghe-Khandan, Y. Choi, and M. R. Okos, "Improved Line Heat Source Thermal Conductivity Probe," *Journal of Food Science,* 45, p 1430-1432, 1981.

148. J.J. Healy, J. J. de Groot, and J. Kestin, "The Theory of the Transient Hot-Wire Method for Measuring Thermal Conductivity," *Physica*, 82C, pp 392-408, 1976.

149. X-G Liang, "The Boundary Induced Error on the Measurement of Thermal Conductivity by Transient Hot Wire Method," Measurement Science Technology, 6, pp 467-471, 1995.

150. K.Manohar, D. W. Yarbrough, and J. R. Booth, "Measurement of Apparent Thermal Conductivity by the Thermal Probe Method," Journal of Testing and Evaluation, September 2000.

151. P. Prelovsek and B. Uran, "Generalized Hot Wire Method for Thermal Conductivity Measurements," J. Phs. E: Sci. Instrum., 17, 1984.

152. M. Ichikawa, M. Uchida, K Yanagisawa, J. Nakamura and T. Nakajima, "Irradiation Studies of JAERI's Fuel at Halden Reactor," *Journal of Nuclear Science and Technology*, **25** [8], pp.609-614, August 1988.

153. M. Ichikawa, T. Fujishiro and S. Kawasaki, "LWR Fuel Safety Research with Particular Emphasis on RIA/LOCA and Other Conditions," *Journal of Nuclear Science and Technology,* **26**(1), pp. 118~125 (January 1989).

154. B. G. Kim, J. Rempe, D. Knudson, K. Condie, and B. Sencer, "An In-situ Creep Testing Capability for the Advanced Test Reactor," *submitted to Nuclear Technology*, MS 10-58, accepted October 24, 2011.

155. B. G. Kim, J. L. Rempe, D. L. Knudson, K. G. Condie, and B. H. Sencer, "Development of an In-situ Creep Testing Capability for the Advanced Test Reactor," *7th International Topical Meeting on Nuclear Plant Instrumentation, Control, and Human Machine Interface Technologies (NPIC&HMIT 2010),* Las Vegas, NV, November 7-11, 2010.

156. D. L. Knudson and J. L. Rempe, "LVDT Evaluations for ATR Irradiations," *Proceedings of the ANS NPIC HMIT 2009 Topical Meeting on Nuclear Plant Instrumentation, Controls, and Human Machine Interface Technology*, Knoxville, TN, April 2009.

157. D. Knudson and J. Rempe, "Recommendations for use of LVDTs in ATR High Temperature Irradiation Testing," *7th International Topical Meeting on Nuclear Plant Instrumentation, Control, and Human Machine Interface Technologies (NPIC&HMIT 2010)*, Las Vegas, NV, November 7-11, 2010.

158. D. L. Knudson and J. L. Rempe, "LVDT-Based Elongation Measurements in Advanced Test Reactor High Temperature Irradiation Testing," *Measurement Science and Technology, Measurement Science and Technology,* Vol. 23, 025604, January 2012.

159. B.G. Kim, J.L. Rempe, D.L. Knudson, K.G. Condie, and B.H. Sencer, "In-Situ Creep Testing Capability for the Advanced Test Reactor," *Nuclear Technology,* Vol. 179, No. 3, pp.417-428, September 2012.

160. D. Knudson and J. Rempe, "Recommendations for Use of LVDTs in ATR High Temperature Irradiation Testing," *7th International Topical Meeting on Nuclear Plant Instrumentation, Control, and Human Machine Interface Technologies (NPIC&HMIT 2010),* Las Vegas, NV, Nov. 7-11, 2010.

161. J. Rempe, J. Daw, R. Schley, K. Davis, D. Knudson T. Unruh, B. Chase, and J. Palmer, *In-pile Instrumentation to Support Fuel Cycle Research and Development -FY13 Status Report,* FCRD-FUEL-2012-000237, September 2013.

162. D.L. Knudson, K.L. Davis, K.G. Condie, and J.L. Rempe, "Qualification of an LVDT-Based Creep Test Rig for Use in ATR Loop 2A," INL/LTD-12-26173, Idaho National Laboratory, August 2012.

163. P. Moilanen, S. Tähtinen, B.N. Singh, and P. Jacquet, "In-Situ Investigation of the Mechanical Performance and Life Time of Copper: Final report on Design, Construction, and Calibration of Test Module for In-Reactor Tensile Tests in BR2 Reactor," VTT Report BTUO 76-031127, October 27, 2004.

164. N. Singh, S. Tähtinen, P. Moilanen, P. Jacquet, and J. Dekeyser, "In-Reactor Uniaxial Tensile Testing of Pure Copper at a Constant Strain Rate at 90 °C," Journal of Nuclear Materials, 320, pp.299–304, 2003.

165. K. L. Davis, et al., *A Variable Load LVDT-Based Creep Test Rig for Use in ATR Loop 2A,* INL EXT-13-29551, Idaho National Laboratory, July 2013.

166. to://www.americanpiezo.com/

167. Toacsan, M. I., Ioachim, A., Nedelcu, L. and Alexandru, H. V., "Accelerated ageing of PZT-type ceramics," *Progress in Solid State Chemistry* **35**, 531-537 (2007).

168. Broomfield, G. H., "The effect of low-fluence neutron irradiation on silver-electrode lead-zirconate-titanante piezoelectric ceramics," *J of Nuclear Materials* 91, 23-34 (1980).

169. R. Bratton, "AGC-1 Irradiation Experiment Test Plan," INL/EXT-06-11102, May 2006.

170. K. Totsu, Y. Haga and M. Esashi, "Ultra-miniature fiber-optic pressure sensor using white light interferometry," *J. Micromech. Microeng*. **15** (2005) 71-75.

171. R. Schley, J. Rempe, and D. Knudson, "Fiber Optic Elongation/Displacement Sensor," Idaho National Laboratory Invention Disclosure Record BA-725, 2219, Rev. 1, submitted February 29, 2012.

172. A. Joseph Palmer, Kurt L Davis, Joy L. Rempe, Sebastien P. Teysseyre, Gordon Kohse, Yakov Ostrovsky, and David M. Carpenter, "Adaptation of Crack Growth Detection Techniques to US Material Test Reactors," *Proceedings of the 2014 International Conference on Advances in Nuclear Power Plants (ICAPP 2014)*, Charlotte, USA, April 6-9, 2014.

173. ASTM Standard E399-2012,"Standardd Test Method for Linear-Elastic Plane-Strain Fracture Toughness KIc of Metallic Materials," *ASTM International*, West Conshohocken, PA, 2012.

174. Standard Test Method for Measuring Neutron Fluence Rates by Radioactivation of Cobalt and Silver, ASTM E481-03, February 2003.

175. Troy Unruh, Benjamin Chase, Joy Rempe, David Nigg, George Imel, Jason Harris, Todd Sherman, and Jean-Francois Villard, "In-core Flux Sensor Evaluations at the ATR Critical Facility," *Nuclear Technology*, MS NTECH-S-13-00170, accepted December 9, 2013.

176. T. Unruh, B. M. Chase, and J. L. Rempe, *ATRC Neutron Detector Testing Quick Look Report*, INL/EXT-13-29896, August 2013.

177. T. Unruh, J. Rempe, D. Nigg, P. Hart, G. Imel, J. Harris, and E. Bonebrake, "Flux Sensor Evaluations at the ATR Critical Facility," 7*th International Topical Meeting on Nuclear Plant Instrumentation, Control, and Human Machine Interface Technologies (NPIC&HMIT 2010)*, Las Vegas, NV, November 7-11, 2010

178. D.W. Nigg and K A. Steuhm, *Advanced Test Reactor Core Modeling Update Project Annual Report for Fiscal Year 2011*, INL/EXT-11-23348, September 2011.

179. W. P. Poenitz, D. W Maddison, J. M. Gasidlo, S. G. Carpenter, and R. J. Armani, "^{235}U(n,f), ^{238}U(n,γ), ^{238}U(n,f), and ^{239}Pu(n,f) Reaction Rate Measurement Calibrations at ZPPR", ANL Internal Document, ANL-87-5.

180. J. Rempe, B. Chase, P. Murray, and J. Palmer, "The Importance of Instrumentation in Advanced Test Reactor Irradiation Experiments," *2013 Conference on Advancements in Nuclear Instrumentation, Measurements Methods (ANIMMA 2013),* June 23-27, 2013 Marseilles, France.

181. M.F. Ohmes, D.S. McGregor, J.K. Shultis, P.M. Whaley, A.S.M. Sabbir Ahmed, C.C. Bolinger, T.C. Pinsent, "Development of Micro-Pocket Fission Detectors (MPFD) for Near-Core and In-Core Neutron Flux Monitoring," *Proc. SPIE*, Vol. 5198 (2003) pp. 234-242.

182. D.S. McGregor, J.K. Shultis, M.F. Ohmes, A.S.M.S. Ahmed, R. Ortiz, K Hoffert, "Micro-Pocket Fission Detectors (MPFD) for Near-Core and In-Core Neutron Flux Monitoring," *ANS 4th Topical Meeting NPIC & HMIT*, Columus, Ohio, September 19-22, 2004.

183. D.S. McGregor, M.F. Ohmes, R.E. Ortiz, A.S.M.S. Ahmed, and J.K. Shultis, "Micro-Pocket Fission Detectors (MPFD) for In-Core Neutron Flux Monitoring," *Nuclear Instruments and Methods,* A554 (2005) pp. 494-499.

184. M.F. Ohmes, D.S. McGregor, J.K. Shultis, A.S.M.S. Ahmed, R. Ortiz, R.W.Olsen, "Recent Results and Fabrication of Micro-Pocket Fission Detectors," *Proc. SPIE*, 6319 (2006) pp. 1P1 - 1P9.

185. D.S. McGregor, "Near-Core and In-Core Neutron Radiation Monitors for Real Time Neutron Flux Monitoring and Reactor Power Levels Measurements," NERI Final Report 2002-174, 2006

186. M. F. Ohmes, J. K. Shultis, D. S. McGregor, "3D Real-Time in-Core Neutron Flux Mapping with Micro-Pocket Fission Detectors (MPFD)," *IEEE Nuclear Science Symposium*, Waikiki, Hawaii, Oct. 28-Nov. 3, 2007.

187. C. Jammes, P. Filliatre, B. Geslot, L. Oriol, F. Berhouet, J.-F. Villard, et L. Vermeeren, "Research Activities in Fission Chamber Modeling in Support of the Nuclear Energy Industry," *IEEE Transactions on Nuclear Science,* 2010.

188. B. Geslot, F. Berhouet, L. Oriol, S. Bréaud, C. Jammes, P. Filliatre, et J.F. Villard, "Development and manufacturing of special fission chambers for in-core measurement requirements in nuclear reactors," *Advancements in Nuclear Instrumentation Measurement Methods and their Applications (ANIMMA)*, 2009.

189. N. Tsoulfanidis, *Measurement and Detection of Radiation*, 2nd Ed. Taylor & Francis, Washington, D.C., 1993.

190. Kansas State University, "Electronics Design Laboratory" http://www.k-state.edu/ksuedl/, Accessed August 15, 2012.

191. Kansas State University, "TRIGA Mark II Reactor Facility" http://www.mne.ksu.edu/research/centers/reactor/, Accessed August 15, 2012.

192. Kansas State University, "SMART Laboratory" http://www.mne.ksu.edu/research/centers/SMARTlab/mission, Accessed August 15, 2012.

193. P. Murray, "Thermal Analysis of Irradiation Experiments in the ATR", INL/CON-12-26307 Preprint, September 2012.

194. W. H. Todt, Sr., "Characteristics of Self-Powered Neutron Detectors Used in Power Reactors," OECD-NEA Proceedings of a Specialists' Meeting On In-Core Instrumentation and Core Assessment, Mito-Shi, Japan, October 1996.

195. O. Aarrestad, Instrumentation Capabilities at Halden, HWR-351, February 1993.

196. R.H. Leyse and R.D. Smith, "Gamma Thermometers for Light Water Reactors," *IEEE Transactions on Nuclear Science*, NS-26, pp.934-943, February 1979.

197. R. Van Nieuwenhove, IFE/HRP, personal communication with J. Rempe, INL, Halden, Norway, August 2012.

198. D. Ensminger, and L. J. Bond, *Ultrasonics: Fundamentals, Technologies, and Applications,* CRC Press, 2012.

199. K. Phani, et. al, "Estimation of Elastic Properties of Nuclear Fuel Material Using Longitudinal Ultrasonic Velocity - A New Approach," *J. Nucl. Mat.*, 366, 2007, pp. 129-136.

200. J. F. Villard, et. al.,"Acoustic Sensor for In-Pile Fuel Rod Fission Gas Release Measurement," *IEEE Transactions on Nuclear Science*, 58, 2011, pp. 151-155.

201. L.C. Lynnworth, "Ultrasonic Measurements for Process Control: Theory, Techniques, and Applications," Academic Press, 1989.

202. *MITR Users Guide Rev. 3 July 2012,* Massachusetts Institute of Technology (2012).

203. N. Gopalsami, A.C. Raptis, "Acoustic Velocity and Attenuation Measurements in Thin Rods with Application to Temperature Profiling in Coal Gasification Systems," *IEEE Transactions on Sonics and Ultrasonics*, SU-31, 1984, pp. 32-39.

204. K. E. Holbert, S. Sankaranarayanan, S. S. McCready, "Response of Lead Metaniobate Acoustic Emission Sensors to Gamma Irradiation," *IEEE Transactions on Nuclear Science*, vol. 52, no. 6, 2005, pp. 2583-2590.

205. Kulikov, et al., "Computer simulation of ferroelectric property changes in PLZT ceramics under neutron irradiation," *Proceedings of SPIE*, 4348, 2001, pp. 264-269.

206. H. Shea, "Radiation sensitivity of microelectromechanical system devices," *J. Micro/Nanolith.,* 8, 2009, pp. 1-11.

207. Wittels & Sherrill, "Fast Neutron Effects in Tetragonal Barium Titanate," J*ournal of Applied Physics*, 28 [5], 1957, pp. 606-609.

208. W. Primak, T. Anderson, "Metamimictization of Lithium Niobate by Thermal Neutrons," *Nuclear Technology*, 23, 1975, pp. 235.

209. T.K. Bierney, "Instrumentation for the Measurement of Vibration in Severe Environments Such as Nuclear Reactors," Endevco Technical Paper 272, 1976, pp. 1-8.

210. J. Daw, J. Rempe, P. Ramuhalli, R. Montgomery, H.T. Chien, B. Tittmann, B. Reinhardt, NEET In-Pile Ultrasonic Sensor Enablement-FY 2012 Status Report, INL/EXT-12-27233, September 2012.

211. J. Daw, J. Rempe, J. Palmer, P. Ramuhalli, R. Montgomery, H.T. Chien, B. Tittmann, B. Reinhardt, and G. Kohse, *NEET In-Pile Ultrasonic Sensor Enablement - FY 2013 Status Report,* INL/EXT-13-29144, September 2013.

212. D.A. Parks, B. R. Tittmann. "Ultrasonic NDE in a Reactor Core," *Presented at Review of Progress in Quantitative Nondestructive Evaluation*, July 17-22, Burlington, VT, 2011.

213. L.C. Lynnworth, E.H. Carnevale, M.S. McDonough, S.S. Fam, "Ultrasonic Thermometry for Nuclear Reactors," IEEE Transactions on Nuclear Science, Vol. NS-16, pp. 184-187, 1968.

214. L.C. Lynnworth, "Nuclear Reactor Thermometry," US Patent Application 3,597,316: 3 Aug 1971.

215. S.C. Rogers, G.N. Miller, "Ultrasonic Level, Temperature, and Density Sensor," IEEE Trans. on Nuclear Science, 29 (1), 1982, pp. 665-668.

216. J. Daw, J. Rempe, S. Taylor, J. Crepeau, and S.C. Wilkins., "Ultrasonic Thermometry for In-Pile Temperature Detection," Proceedings of NPIC&HMIT 2010, 2010.

217. R. Kazys, V. Voleisis, R. Sliteris, B. Voleisiene, L. Mazeika, and H. Abderrahim, "Research and Development of Radiation Resistant Ultrasonic Sensors for Quasi-Image Forming Systems in a Liquid Lead-Bismuth," *Ultragarsas (Ultrasound)*, 62(3),2006, pp. 7-15.

218. N. D. Patel and P. S. Nicholson, "High Frequency - High Temperature Ultrasonic Transducers," *NDT International*, pp. 262-266, 1990.

219. D. Stubbs, and R. Dutton, "High-Temperature Ultrasonic Sensor for in Situ Monitoring of Hot Isostatic Processing," *SPIE*, 1996, pp. 164-172.

220. K. Trachenko, "Understanding resistance to amorphization by radiation damage," *Journal of Physics: Condensed Matter*, 16(49), 2004, pp. R1491-R1515.

221. T. Yano, K. Inokuchi, M. Shikama, and J. Ukai, "Neutron irradiation effects on isotope tailored aluminum nitride ceramics by a fast reactor up to $2 \cdot 10^{26}$ n/m^2," *Journal of Nuclear Materials*, 2004, pp. 1471-1475.

222. Y. Ito, et al., "Radiation Damage of Materials Due to High Energy Ion Irradiation," *Nuclear Instruments and Methods in Physics Research*, 530, 2002.

223. Y. P. Meleshko, S. G. Karpechko, G. K. Leont'ev, V. I. Nalivaev, A. D. Nikiforov, and V. M. Smirnov, "Radiation Resistance of the Piezoelectric Ceramics TrsTS-21 and TNV-I," Translated from *Atomnaya Energiya*, 1986, pp. 50-52.

224. K. Trachenko, "Understanding resistance to Amorphization by Radiation Damage," *Journal of Physics Condensed Matter*, 16(49), 2004, pp. R1491-R1515.